Investigating the genome of Anaplastic Lymphoma Kinase-positive Anaplastic Large Cell Lymphoma

Hugo Larose

Department of Pathology
University of Cambridge
Gonville & Caius College

This Dissertation is submitted for the degree of
Doctor of Philosophy

October 2019

Preface

This dissertation is the result of my own work and contains nothing which is the outcome of work done in collaboration except as declared in the Declaration of Assistance Received (page 5) and specified in the text.

This dissertation is not substantially the same as any that I have submitted, or is being concurrently submitted for a degree or diploma or other qualification at the University of Cambridge or any other University or similar institution except as declared in the Preface and specified in the text. I further state that no substantial part of my dissertation has already been submitted, or, is being concurrently submitted for any such degree, diploma or other qualification at the University of Cambridge or any other University of similar institution except as declared in the Preface and specified in the text.

I have published the majority of Chapter 1 as a peer-reviewed review article (Larose, H., *et al.*, 2019, From bench to bedside: the past, present and future of therapy for systemic paediatric ALCL, ALK+. *British Journal of Haematology*, **185,** 1043–1054).

This dissertation does not exceed the prescribed word limit set by the Degree Committee for the Faculty of Biology.

The research in this thesis was carried out under the supervision of Dr. Suzanne D. Turner at the Division of Cellular and Molecular Pathology, Department of Pathology, University of Cambridge, between October 2015 and October 2019.

Abstract

Dissertation Title: Investigating the genome of Anaplastic Lymphoma Kinase-positive Anaplastic Large Cell Lymphoma

Name: Hugo Larose

Anaplastic Large Cell Lymphoma (ALCL) is a T cell Non-Hodgkin Lymphoma, mainly presenting in paediatric and young adult patients. The majority of cases express a chimeric fusion protein resulting in hyperactivation of Anaplastic Lymphoma Kinase (ALK) as the consequence of a chromosomal translocation. Patients diagnosed with ALCL are still treated with toxic multi-agent chemotherapy and as many as 25-50% of patients relapse. It is clear that continued adaption of current therapies will likely not improve these statistics and for progress to be made, integration of biology with the design and implementation of future clinical trials is required.

To understand disease pathology and to uncover novel targets for therapy, Whole-Exome Sequencing (WES) of ALK+ ALCL was performed, as well as Gene-Set Enrichment Analysis. This revealed that the Notch pathway was the most enriched in mutations. In particular, variant T349P of Notch1, which confers a growth advantage to cells in which it is expressed, was detected in 12% of ALK+ and ALK- ALCL patient samples. Furthermore, we demonstrate that the nucleophosphomin 1-Anaplastic lymphoma kinase (NPM-ALK) chimeric protein promotes Notch1 expression through binding of Signal Transducer and Activator of Transcription 3 (STAT3) upstream of *notch1*. Moreover, inhibition of Notch1 with γ-secretase inhibitors (GSI) or silencing by shRNA leads to apoptosis; co-treatment *in vitro* with the ALK inhibitor crizotinib led to additive/synergistic anti-tumour activity suggesting this may be an appropriate combination therapy for future use in the circumvention of ALK inhibitor resistance. Indeed, crizotinib-resistant and sensitive ALCL cells were equally sensitive to GSIs. In conclusion, we show a variant in the extracellular domain of Notch1 that provides a growth advantage to cells and confirm the suitability of the Notch pathway as a second-line druggable target in ALK+ ALCL.

Declaration of Assistance Received

The following list discloses and details the only experiments performed not by myself but by collaborators or service providers;

1. Department of Biochemistry, University of Cambridge – DNA (Sanger) Sequencing. Plasmids to be sequenced/validated were sent to the Department of Biochemistry.

2. Washington State University Core Facility – Whole Exome Sequencing. Patient DNA samples were sent to the Washington State University Core Facility for quality control, library preparation, and whole exome sequencing. All bioinformatic processing was done by myself.

3. BBSCR NIHR Cell Phenotyping Hub – Cell sorting. When cells needed sorting (co-cultures; CRISPR knock-down system), NIHR Hub technicians performed the sorting. I performed all fluorescence-activated cell cytometry assays myself.

4. Nina Prokoph - CRISPR knock-down and CRISPR overexpression. My colleague in the lab developed the ALCL cell lines with appropriate Cas9 plasmids to obtain CRISPR-enabled cell lines. Preparation of sgRNA expression plasmids and transduction of plasmids into CRISPR-enabled cells was done by myself, as were all downstream applications.

5. Ali Alsulami and Tom Blundell, Department of Biochemistry, University of Cambridge – Molecular Dynamics. Our collaborators developed the predictive model of the Notch1 mutation tertiary structure and processed the Gibbs-free energy calculation.

6. Michaela Schlederer and Sandra Högler – Immunohistochemistry and clinical correlation. Our collaborators Michaela and Sandra stained the Tissue Microarray and quantified the staining using the histoscore.

“Imagination is not only the uniquely human capacity to envision that which is not, and therefore the fount of all invention and innovation In its arguably most transformative and revelatory capacity, it is the power that enables us to empathize with humans whose experience we have never shared ”

- Joanne Rowling

Acknowledgments

This thesis is dedicated in loving memory to my grand-father, whose curiosity and scientific mind have always been an inspiration. He followed my studies and research with great interest, painstakingly translating essays and papers into French so that he may read and understand them. He passed in 2019 after a long, peaceful and happy life, giving me one more reason to work on cancer research.

My work and research over the last four years, culminating in this thesis would not have been possible without support from every quarter. First, to my dear colleague and friend Nina, for invaluable help and collaboration but most importantly for helping me stay motivated throughout. Thanks also to the rest of my colleagues, past and present – in particular Sorcha, Stephen, Lidiya, Ricky and Shubha in the office for their help and companionship. I would also like to thank my supervisor, Dr. Suzanne Turner and my mentor, Prof. Du Ming for their guidance throughout my project.

I would also like to acknowledge Gonville & Caius College, for hosting and supporting me; and give thanks to all the staff who run the place and make the College such a lively place. I would also like to thank Lucy for being my partner over a year at the helm of the Caius MCR.

Thank you also to all my friends for making the last four years an unforgettable experience, full of joy and happiness. In particular I would like to thank Marta and Alessandro for their unfailing support as well as Valerio, Jilles, Jakob, Cameron, Alberto, Steven, Paulina, Lauriane, Claudia, Lander, Caitlin, Sebastian and Dominika. To my dear friends at the Graduate Union, Sofia, Nikita, Darshana, Ben, and Ellie, thank you for being my militant friends. To my friends at the World Health Organisation, Elisabeth, Yousra, Chris, Gabby, Nini, Vero, Milena, Gabriel and Sebastian thank you for three amazing months – and to Donna and Snezhana, for being inspiring mentors and teaching me as much as you did.

My heartfelt thanks to the patients who kick-started this research and without whose help none of the data in this thesis could have been collected.

Last but certainly not least, thank you to my parents, grand-parents, and the rest of my family without whom I would never have gotten this far.

Abbreviations

ABVD	Doxorubicin, Bleomycin, Vinblastine, Dacarbazine
ADAM	A Disintegrin and Metalloprotease
ALCL	Anaplastic Large-Cell Lymphoma
ALK	Anaplastic Lymphoma Kinase
α-MEM	α-Minimum Essential Medium
AML	Acute Myeloblastic Leukaemia
ANK	Ankyrin
AP-1	Activator Protein 1
apc	*adenomatous polyposis coli*
APO	Doxorubicin, Vincristine and Prednisone
AV	Annexin V
BAD	BCL2-Associated Agonist of Cell Death
BAM	Binary Alignment Map
BATF	Basic Leucine Zipper ATF-like Transcription Factor
BCL2	B-Cell Lymphoma 2
BED	Browser Extensible Data
BLAST	Basic Local Alignment Search Tool
BRCA	Breast Cancer (gene)
BSA	Bovine Serum Albumin
BV	Brentuximab Vedotin
CAR-T	Chimeric Antigen Receptor T-cell
CCG	Childrens' Cancer Group
CDK	Cyclin-Dependent Kinase
cDNA	complementary DNA
ChIP	Chromatin Immunoprecipitation
CHOEP	Cyclophosphamide, Doxorubicin, Vincristine, Etoposide and Prednisone
CHOP	Cyclophosphamide, Doxorubicin, Vincristine and Prednisone
COG	Childrens' Oncology Group
COSMIC	Catalogue Of Somatic Mutations In Cancer
CRISPR	Clustered Regularly Interspaced Short Palindromic Repeats
CSL	CBF1, Suppressor of Hairless, Lag-1
ctbp2	*c-terminal binding protein 2*
ddPCR	digital droplet PCR
defb132	*Defensin-β 132*
DLL1	Delta-Like Canonical Notch Ligand 1
DMEM	Dulbecco's Modified Eagle Medium
DMSO	Dimethyl Sulfoxide
dnmt1	*DNA methyltransferase*
dNTP	Deoxynucleoside Triphosphate
DSL	Delta-Serrate-LAG2 domain
DTT	Dithiothreitol
dtx1	*deltex E3 ubiquitin ligase 1*
EDTA	Ethylenediaminetetraacetic Acid
EFS	Event-Free Survival
EGF	Epidermal Growth Factor
EGFR	Epidermal Growth Factor Receptor
EICNHL	European Inter-Group for Childhood Non-Hodgkin Lymphoma
ERK	Extracellular-Signal-Regulated Kinase
EV	Empty Vector
FACS	Fluorescence-Activated Cell Sorting

FBS	Foetal Bovine Serum
FDA	Food and Drug Administration
FFPE	Formalin-Fixed Paraffin-Embedded
gab2	*grb2-associated binding protein*
gapdh	*glyceraldehyde 3-phosphate dehydrogenase*
(E) GFP	(Enhanced) Green Fluorescence Protein
gng2	*g-protein sub-unit γ2*
GPCR	G-Protein-Coupled Receptor
grb2	*growth factor receptor-bound protein 2*
GSEA	Gene-Set Enrichment Analysis
GSI	γ-Secretase Inhibitor
HDC	Heterodimerization Domain: C-Terminal
HDD	Heterodimerization Domain
HDN	Heterodimerization Domain: N-terminal
HEK293FT	Human Embryonic Kidney 293
hes	*hairy and enhancer of split 1*
hey	*hairy and enhancer of split related with YRPW motif 1*
HL	Hodgkin's Lymphoma
HRP	Horseradish Peroxidase
HSP90	Heat Shock Protein 90
IC50	Half-maximal Inhibitory Concentration
ICN	Intracellular Domain of Notch1
IGFR	Insulin Growth Factor Receptor
IgG	Immunoglobulin G
IHC	Immunohistochemistry
InDel	Insertions/Deletions
IRF4	Interferon Regulatory Factor 4
Jag	Jagged Canonical Notch Ligand 1
JAK	Janus Kinase
JNK	c-Jun N-terminal Kinase
K299	Karpas 299
kcnj18	*potassium voltage-gated channel subfamily member 18*
LB	Lysogeny Broth
LNR	Lin-12/Notch Repeat
MAPK	Mitogen-Activated Protein Kinases
MDD	Minimal Disseminated Disease
MDM2	Mouse Double Minute 2 Homolog
miRNA	micro RNA
MOPP	Mechlorethamine, Vincristine, Procarbazine and Prednisone
MRD	Minimal Residual Disease
mTOR	Mammalian Target Of Rapamycin
MTT	3-(4,5-dimethylthiazol-2-yl)-2,5-diphenyltetrazolium
NCOR2	Nuclear Receptor Corepressor 2
NEXT	Notch Extracellular Truncation
NFκB	Nuclear Factor κ-light-chain-enhancer of Activated B Cells
NGS	Next Generation Sequencing
NHL	Non-Hodgkin Lymphoma
NHL-BFM	Non-Hodgkin Lymphoma-Berlin-Frankfurt-Münster group
NPM-ALK	Nucleophosphomin-Anaplastic Lymphoma Kinase
NRR	Negative Regulatory Region
NS	Not Significant
NSCLC	Non-Small Cell Lung Cancer
NT	Non-Targeting
OS	Overall Survival

PBS	Phosphate-Buffered Saline
(q) PCR	(quantitative) Polymerase Chain Reaction
PD1	Programmed cell Death protein 1
PDGFR-β	Platelet-Derived Growth Factor Receptor-β
PDL-1	Programmed cell Death protein Ligand 1
PE	Phycoerythrin
PEST	Proline-Glutamate-Serine-Threonine rich sequence
PI	Propidium Iodide
PI3K	Phosphoinositide 3-Kinase
PKC	Protein Kinase C
PLC-γ	Phospholipase C-γ
POG	Paediatric Oncology Group
ppia	*peptidylprolyl isomerase a*
psph	*phosphoserine phosphatase*
PTEN	Phosphatase and Tensin Homolog
RAM	RBPJ-Association Molecule
RBP-Jκ	Recombination Signal Binding Protein for Immunoglobulin Jκ Region
RIPA	Radioimmunoprecipitation Assay
RPMI	Roswell Park Memorial Institute medium
SAM	Sequence Alignment Map
SCT	Stem-Cell Therapy
SDS	Sodium Dodecyl Sulphate
sgRNA	short-guide RNA
sh2	*src homology region 2*
shp2	*sh2-containing protein tyrosine phosphatase 2*
shRNA	short-hairpin RNA
siRNA	small interfering RNA
SNP	Single Nucleotide Polymorphism
SNV	Single Nucleotide Variant
SOC	Super Optimal broth with Catabolite repression
ssODN	single-stranded donor Oligonucleotide
STAT3	Signal Transduced and Activator of Transcription
TAD	Transactivation Domain
T-ALL	T-cell Acute Lymphoblastic Leukaemia
TCR	T-Cell Receptor
tfg	*trk-fused gene*
TKI	Tyrosine Kinase Inhibitor
tpm3	*tropomycin 3*
traf1	*tnf-receptor-associated factor 1*
TYK2	Tyrosine Kinase
tyro3	*protein tyrosine kinase 3*
tyw1b	*trna-yw synthesizing protein 1 homolog β*
VCF	Variant Call Format
VEGF	Vascular endothelial growth factor
WES	Whole Exome Sequencing
WHO	World Health Organization
wnt	*wingless-type*

List of Figures and Tables

Table of Contents

1. Introduction

1.1 The history of ALCL

The history of Hodgkin Lymphoma (HL) can be traced back to the 17th century with a report from 1666 (Malpighi, 1666), though it took until the 19th century for Thomas Hodgkin to publish his now famous paper on "Some morbid appearance of the absorbent glands and spleen" (Hodgkin, 1832), where he detailed historical clinical mentions of a similar disease and his own findings. In 1865, Sir Samuel Wilks further characterized the disease and named it in his paper "Cases of Enlargement of the Lymphatic Glands and spleen (or Hodgkin's Disease) with Remarks" (Reviewed by Bonadonna, 2000). This was followed by large amounts of research on the characterization of the different tumour types throughout the 20th century (Reviewed in Bonadonna, 2000; Lakhtakia & Burney, 2015a; Canellos *et al*, 2014). There were a number of attempts to standardize classification of Hodgkin's Lymphomas and other tumour types (including Non-Hodgkin Lymphomas), but the differentiation between Hodgkin and Non-Hodgkin Lymphoma (NHL) only crystallized in 2001 with the publication of the World Health Organisation (WHO) Classification of Tumours of Haematopoietic and Lymphoid Tissues (WHO, 2001; Lakhtakia & Burney, 2015b; Bonadonna, 2000).

The path to the identification of Anaplastic Large Cell Lymphoma (ALCL) as a distinct lymphoma entity began in 1982, with the discovery by Stein and colleagues of the antigen CD30 (also called Ki-1 or Berh-H2) consistently expressed on Hodgkin Reed-Sternberg cells (Stein *et al*, 1982; Schwab *et al*, 1982). Reed-Sternberg cells are giant cells, often derived from B-lymphocytes, named after Dorothy Reed Mendenhall and Carl Sternberg, who in the early 20th century observed and described the microscopic feature of HL, before publishing these findings for the first time (Sternberg, 1898; Reed Mendenhall, 1902). CD30 expression was seen not only on Reed-Sternberg cells of HL but also on cells within tumours showing an unusually large morphology. The tumours in which these cells resided were initially named Ki-1-positive Large Cell Lymphomas due to this unique, unusually large morphology. The name Anaplastic Large Cell Lymphoma itself was used in a number of publications (Krc *et al*, 1987), but was not widely adopted until the end of the 1980s (Pallesen & Hamilton-Dutoit, 1988; Rimokh *et al*, 1989; Herbst *et al*, 1989; Le Beau *et al*, 1989; Delsol *et al*, 1988).

In 1988, a cell line shown to carry the t(2;5)(p23;q35) translocation was established from a Ki-1-positive tumour (Fischer *et al*, 1988; Rimokh *et al*, 1989; Le Beau *et al*, 1989). In 1994, Morris and colleagues reported the results of cloning and identification of the t(2;5) translocation breakpoints seen in ALCL samples from patients; the gene involved was named *anaplastic lymphoma kinase* (*alk*), a gene with sparse expression outside of the brain or developmental tissue (Morris *et al*, 1994). The catalytic domain of ALK was found to be transposed next to the amino terminus of *nucleophosphomin 1* (*npm1*). NPM-ALK has since been characterised as an 80 kDa protein, present in both the cytoplasm and the

nucleus of ALCL tumour cells (Pulford *et al*, 1997). NPM-ALK homodimerizes via the NPM oligomerization domains, mimicking ligand binding, which in turn activates the ALK catalytic domain. NPM-ALK can also dimerize with wild-type NPM1, a protein involved in cellular trafficking, which is thought to explain the dual cytoplasmic/nuclear localization of the chimeric protein (Mason *et al*, 1998).

Not every patient presents with an ALK-encoding translocation, however, leading to a distinction between cases presenting with the ALK chimera and those without (Bitter *et al*, 1990; Lamant *et al*, 1996; Yee *et al*, 1996; Benharroch *et al*, 1998). As such, there are two recognised subtypes of systemic ALCL, ALK+ or ALK-, which are listed in the revised 2008 WHO classification as distinct tumour types (WHO, 2008). While *npm1* is the most common partner with *alk* in children with ALCL (70-75% of cases), a number of alternative partner genes besides *npm1* have also since been identified in ALK+ ALCL, such as *tropomycin 3* (*tpm3*), *atic*, *trk-fused gene* (*tfg*), *cltc*, *alo17* or *tnf-receptor-associated factor 1* (*traf1*) (Lamant *et al*, 1999; Rosenwald *et al*, 1999; Liang *et al*, 2004; Trinei *et al*, 2000; Cools *et al*, 2002), but NPM-ALK remains the predominant translocation product, as it is present in three quarters of ALCL, ALK+ cases (Brugières *et al*, 2009).

The 2008 WHO Classification also lists five histomorphology subtypes of ALK+ ALCL: common, small-cell, lymphohistiocytic, Hodgkin-like and composite morphologies (WHO, 2008). As the name indicates, common patterns are the most frequently observed, in over half of ALCL cases. The lymphohistiocytic sub-type represents about a tenth of ALCL cases, and are identified by the presence of histiocytes which may sometimes mask tumour cells (Pileri *et al*, 1990). Small-cell patterns, represent less than a tenth of ALCL cases and are identifiable by the presence of small anaplastic cells with irregular nuclei and clear cytoplasm (Kinney *et al*, 1993). Hodgkin-like patterns of ALCL are so similar to HL that the two are easily confused, but represent just 3% of ALCL (Vassallo *et al*, 2006).

1.2 NPM-ALK

The ALK protein is sparsely expressed in healthy human tissues, mostly concentrated in neural and endothelial cells, although *alk* mRNA is seen in a few other organs (Morris *et al*, 1994; Bilsland *et al*, 2008). ALK itself is a receptor tyrosine kinase with an extracellular ligand-binding domain, a transmembrane domain and an intracellular tyrosine kinase domain (Iwahara *et al*, 1997), although its function remains largely unclear. However, some of ALK's ligands have recently been described (Guan *et al*, 2015). The subcellular localization of the chimeric ALK in ALCL depends on its fusion partner. NPM-ALK in particular is distributed between the cytoplasm and nucleus; this is due to the ability of NPM-ALK to form complexes with wild-type NPM1 which contains a nuclear localization motif (Bischof *et al*, 1997).

NPM1 is a ribonucleic shuttle protein ubiquitously expressed at high levels in healthy cells, and has been shown to promote cell growth, but also to act as an oncogene in some contexts (Jiang & Yung, 1999; Zeller *et al*, 2001; Feuerstein *et al*, 1988; Lim & Wang, 2006). Since *alk* is expressed at low levels in human tissues, it is thought that *npm*'s constitutively activated promoter is the driver behind aberrant *npm-alk* expression in ALCL. NPM1 has also proven to be the reason for NPM-ALK's constitutive activation, while both NPM1 and ALK's intracellular tyrosine kinase domain are required for downstream signalling (Bischof *et al*, 1997).

NPM-ALK activates numerous downstream signalling pathways: it recruits the SH2 domain of PI3K, which in turn activates the Akt pathway (Bai *et al*, 2000). The Akt pathway is well-known for promoting cell growth and survival, and for being oncogenic if constitutively activated. PI3K also phosphorylates p27 (also called Kip1), targeting it for degradation, which mediates the downstream cell growth observed (Slupianek & Skorski, 2004; Rassidakis *et al*, 2005). In addition, NPM-ALK has been shown to recruit the SH2 domain of PLC-γ, which along with PI3k/Akt, is thought to be responsible for the mitogenic phenotype observed in NPM-ALK positive cells (Bai *et al*, 1998). Finally, Signal Transducer and Activator of Transcription 3 and 5 (STAT3 and STAT5) are also important targets of NPM-ALK, protecting NPM-ALK positive cells from apoptotic inducers (Zhang *et al*, 2007; Nieborowska-Skorska *et al*, 2001; Zamo *et al*, 2002). Numerous other proteins may be involved in signalling downstream of NPM-ALK, such as Shp2, Grb2, grb2-associated binding protein (Gab2) and Src, to name but a few, but the major signalling pathways downstream of NPM-ALK thought to lead to oncogenesis are summarised in **Figure 1.1**; indeed the targets of NPM-ALK signalling have been extensively reviewed (Chiarle *et al*, 2008; Lim & Wang, 2006; Webb *et al*, 2009).

It should be said, however, that the aforementioned genes are but the main mitogenic pathways which are influenced by the NPM-ALK chimera and lead to the anaplastic phenotype observed in ALCL. Indeed, research groups, including our own, have shown NPM-ALK to be sufficient for the development of Lymphomas in NPM-ALK transgenic mice (Chiarle *et al*, 2003; Jäger *et al*; Turner *et al*, 2003, 2006). In addition to this, cloning NPM-ALK into primary cells leads to aberrant proliferation, invasiveness and transformation, as observed in ALCL (Zhang *et al*, 2013)**.**

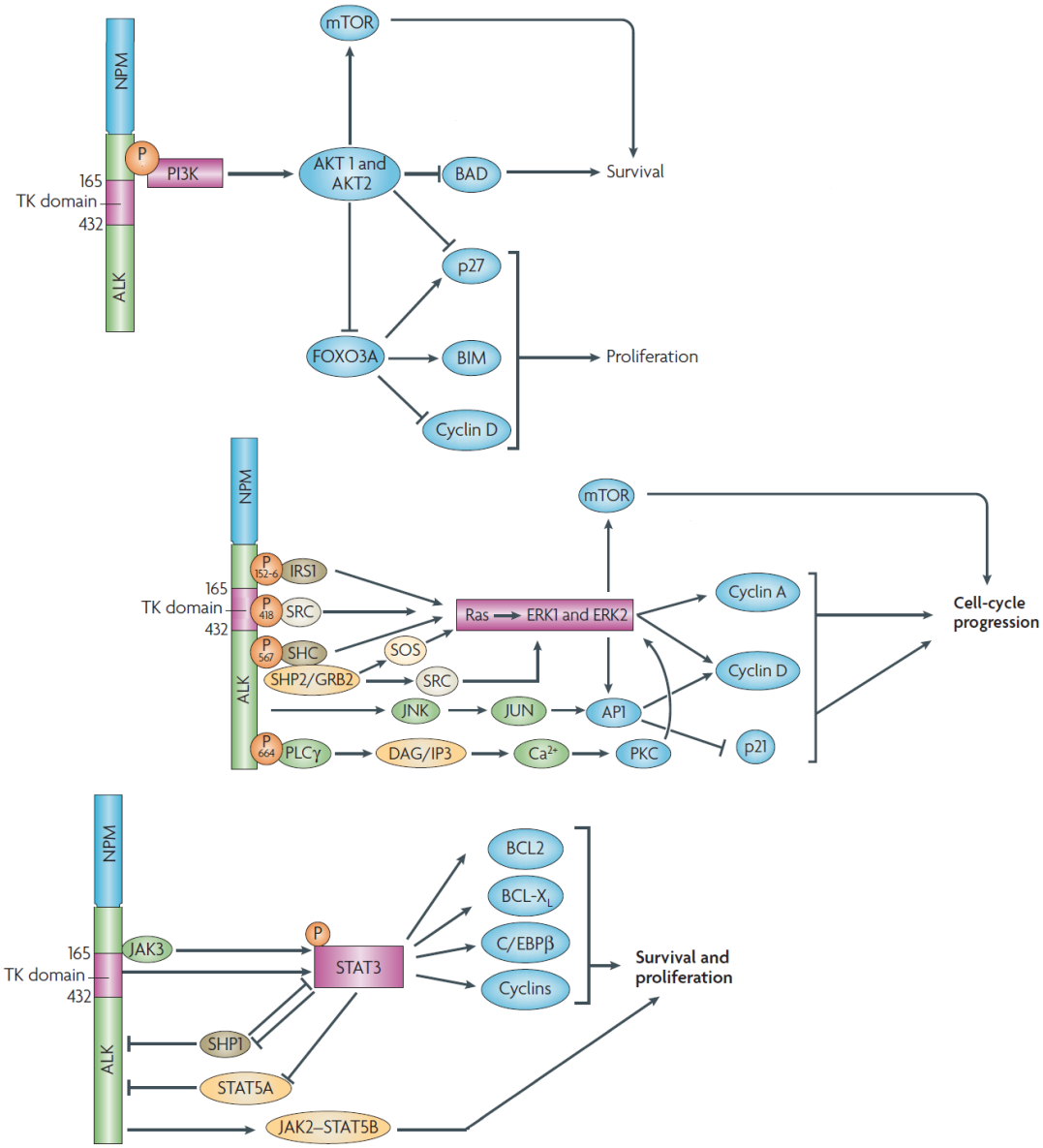

Figure 1.1: Major signalling pathways downstream of NPM-ALK. There are three main signalling pathways downstream of NPM-ALK: (1) Phosphoinositide 3-kinase (PI3K) and the Akt pathway, (2) the Ras/Extracellular signal-regulated kinase (ERK)-Mitogen Activated Protein Kinase (MAPK) pathway, and (3) the STAT3 pathway. (1) NPM-ALK recruits PI3K, which activates Akt1 and Akt2; this leads to enhanced survival and proliferation of NPM-ALK positive cells, by increased mammalian Target of Rapamycin (mTor) and B-cell lymphoma 2 (BCL2)-Associated Agonist of Cell Death (BAD) activity, as well as decreased Cyclin p27 activity. (2) NPM-ALK can also promote Ras activity by recruiting proteins such as Src homology region 2 (SH2)-containing protein tyrosine phosphatase (Shp2), Src and Growth factor receptor-bound protein 2 (Grb2). Ras then activates the Ras/MAPK pathway, leading to increased proliferation by activation of Cyclins. In parallel, NPM-ALK recruits Phospholipase C-γ (PLC-γ), which activates the Protein Kinase C pathway (PKC). The PKC pathway overlaps with Ras/MAPK and leads to the same increase in cellular proliferation. (3) Finally, NPM-ALK activates STAT3 directly and via Janus Kinase 3 (JAK3). STAT3 activates downstream effectors which inhibit apoptosis and ensure cell survival. Parallel to this, the JAK2/STAT5 pathway has a similar effect, and is also activated by NPM-ALK (Modified from Chiarle et al, 2008).

1.3 Treatment options

Discovered by Wilhelm Röntgen (Röntgen, 1896), X-rays were quickly put to good use: anecdotal evidence suggesting their involvement in cancer therapy as early as 1896 (News of Science, 1957). Indeed already in 1902 was radiation therapy reportedly used on a HL patient; this is the first published evidence of non-symptomatic cancer treatment (Pusey, 1902). Radiotherapy was refined through trial and error throughout the 20th century, particularly by Gilberts and colleagues first, in France, and Peters and her colleagues in Toronto (Gilbert & Babaiantz, 1931; Peters, 1950). The advent of chemical warfare in the two World Wars led to the discovery of chemotherapy (starting with the discovery of mustard gas' properties as a potent haematopoiesis suppressor), and in the 1970s radiation therapy was combined with chemotherapeutic agents for the first time (Mechlorethamine, Vincristine, Procarbazine and Prednisone, or MOPP protocol; Rosenberg & Kaplan, 1975; Devita *et al*, 1970). These efforts were greatly helped by the fact that Hodgkin Lymphoma's Reed-Sternberg cells are unusually sensitive to both radiotherapy and chemotherapy. Due to the toxicity of the first iteration of chemotherapy regimens, a number of alternative drug combinations were trialled, and the protocols CHOP (Cyclophosphamide, Doxorubicin, Vincristine and Prednisolone) or CHOEP (CHOP plus Etoposide) were determined to be the best options for NHL, as less toxic yet as effective (Fisher *et al*, 1993).

Several trials attempted to refine the chemotherapy regimen, first for B- and T-cell NHL, and then specifically for ALCL. ALCL, not initially being recognised as an independent entity, as explained earlier, was treated as B- or T-cell NHL until the 1990s - indeed, retrospective studies have shown that a number of ALCL cases were treated within the B- and T-cell NHL trials (all these trials have been extensively reviewed in Prokoph *et al*, 2018). Some of the best results for ALCL were obtained by the NHL Berlin-Frankfurt-Münster (NHL-BFM) working group, which recommended the use of methotrexate along with the CHOP backbone (Seidemann *et al*, 2001). Unfortunately, this was associated with a number of serious short-term adverse events, hence the NHL-BFM95 study attempted shorter doses with short-pulses, and found this to be not inferior but less toxic (Woessmann *et al*, 2005).

The European Inter-group for Childhood NHL (EICNHL) led the first and largest international ALCL-specific clinical trial initiated in 1999 for patients under the age of 22: ALCL99 (NCT00006455), which recruited 352 children in 11 European countries and Japan. (Mori *et al*, 2014; Attarbaschi *et al*, 2011). The protocol's objectives were to test two different methods of delivering methotrexate and to test the efficacy of the addition of vinblastine in high risk patients. Indeed, CHOP was still seen as too toxic, particularly in the paediatric setting, and so the search remained for less aggressive alternatives. Vinblastine, originally extracted from the Madagascar periwinkle (Brown, 1965), had been investigated as part of the ABVD backbone (Adriamycin, Bleomycin, Vinblastine, Dacarbazine), and was found to be

significantly less toxic than MOPP (Santoro *et al*, 1987; Bonadonna *et al*, 1975). ALCL99 used the recommended NHL-BFM90 protocol, with either a 24-hour methotrexate infusion (with intrathecal injection), or a higher 3-hour dose of methotrexate without intrathecal injections respectively for arms MTX1 or MTX3 (1g/m^2 over 24 hours with intrathecal injections versus 3g/m^2 over 3 hours without injections). These protocols were then supplemented with weekly Vinblastine for randomized high-risk patients, followed by Vinblastine weekly, on its own for 52 weeks, as a maintenance treatment. Maintenance could be given on an outpatient basis, thereby greatly improving quality of life.

The Event-Free Survival (EFS) for patients on the trial were not significantly improved over those obtained in previous trials, though it did demonstrate that 3g/m^2 short-pulse methotrexate without intrathecal injections was less toxic than the alternative arm. The trial reported a 2-year Overall Survival (OS) of 92%, and a 2-year EFS of 74%; ALCL99 as a front-line regimen has since become the gold standard for paediatric ALK+ ALCL (Brugières *et al*, 2009; Seidemann *et al*, 2001; Wrobel *et al*, 2011). The addition of Vinblastine for high-risk patients showed no improvement in the 2-year EFS compared to patients who did not receive vinblastine, although these data suggest that the 1-year maintenance phase delays relapse (Le Deley *et al*, 2010). Whilst OS using this trial protocol is excellent, EFS remains sub-optimal and acute toxicity remains significant, with 60% of patients reporting grade 4 neutropenia, 20% with weight gain and 15% mucositis (Wrobel *et al*, 2011).

In North America, different chemotherapeutic backbones were used. The Paediatric Oncology Group (POG) and the Children's Cancer Group (CCG; later combined into the Children's Oncology Group; COG) ran two concurrent studies: POG9315 and CCG5941. POG9315 trialled a year-long regimen based on the APO chemotherapy backbone (Adriamycin, Prednisone and Vincristine) (Laver *et al*, 2005), while CCG5941 tested one year of chemotherapy (Vincristine, Prednisone, Cyclophosphamide, Daunomycin, Asparaginase for induction, along with 6-thioguanine, cytarabine and methotrexate for consolidation and maintenance) designed to treat T lymphoblastic lymphoma (Lowe *et al*, 2009). The trials found similar results to the European trials, with a 4-year EFS of 72% for the POG trial, versus a 5-year EFS of 68% for the CCG trial. It should be noted that only advanced stage III and IV patients were included in both of these trials, as opposed to the European trials which were open to all ALCL patients possibly accounting for the lower OS observed. Later came COG trial ANHL0131 which assessed the efficacy of vinblastine when combined with the APO regimen of POG9315. The trial led the COG to the same conclusion as the EICNHL, with a similar 3-year EFS of 76% and no benefit to the addition of vinblastine (Alexander *et al*, 2014). Currently, both APO and ALCL99 could be considered standard chemotherapy for children with ALCL. That said, as ALCL99 has potentially less long-term toxicity (especially cardiac) than APO and in order to facilitate wider international collaboration, the ALCL99 backbone was adopted by the COG in their current clinical trial.

Due to the relatively small number of relapsed or refractory patients, it has been difficult to design and conduct a trial for this group of patients. Instead, a number of retrospective studies by European and Japanese groups assessed the success with which small cohorts of patients had been treated, using either allogeneic or autologous Stem Cell Transplantation (SCT). There is some evidence to show that allogeneic SCT yields better outcomes for relapse patients, yet there is no consensus on this, nor on the type of conditioning which should be used, although radiotherapy seems to be the most common option (Reviewed in Prokoph *et al*, 2018). Some of the more recent trials, however, have shown promise. Perhaps most interestingly, the EICNHL trial ALCL-Relapse (NCT00317408) has shown that allogeneic SCT yields a higher survival rate for relapsed patients but is inconclusive as far as refractory patients are concerned. In addition, single-agent vinblastine achieved high remission rates for both relapsed and refractory patients (Woessmann *et al*, 2012; Ruf *et al*, 2015). Hence, vinblastine is a potential option as a single-agent therapy, although only with a low-dose, long-term regimen (Woessmann *et al*, 2012).

1.4 A ceiling has been hit - the need for biomarkers and prognostic factors

The success of prior trials with OS varying from 80-92% has in itself resulted in difficult ethical considerations for trialling new drugs, particularly for low risk patients (Minard-Colin *et al*, 2015). This, combined with the relatively low incidence of ALCL, which represents just 15% of childhood and young adult NHL presents dilemmas in the design and conduct of new trials. Indeed, data from British Columbia suggests an incidence of diagnosed ALCL cases of under 4 per million children and young adults (Alessandri *et al*, 2002). In Europe, this represents fewer than 100 new cases per year (Shiramizu *et al*, 2016). In contrast to OS rates, EFS rates are lower, ranging from 59-76%, depending on the treatment protocol used (Prokoph *et al*, 2018; Minard-Colin *et al*, 2015). Unfortunately, this means that not only do 10-15% of children not survive a diagnosis of ALCL, but many survivors suffer from the late effects of intensive therapies and/or transplantation required to cure them. Therefore, there is a clear need for new therapies facilitated by bench-side biological research into ALCL and the development of predictive biomarkers. Targeted therapies, for instance, may well prove significantly less toxic than the current gold standards, as often having less off- or un-intended targets, and hence fewer side-effects.

What is clear is that some children respond well to treatment and have a low risk of relapse, whilst others fail therapy and/or suffer multiple relapses. It is therefore likely that we are over-treating some children and as a consequence exposing them to unnecessary toxicities. In order to identify these children, biomarkers are required that are clinically actionable. Some clinical factors such as visceral or mediastinal disease and bone marrow involvement initially showed promise as predictors of treatment failure (Lamant *et al*, 2011; Mussolin *et al*, 2005; Le Deley *et al*, 2008). Other potential

biomarkers such as circulating tumour cells in bone marrow or peripheral blood may have prognostic value (Damm-Welk *et al*, 2007). Tumour cells in peripheral blood, or minimal disseminated disease (MDD) has gained traction in recent years as a biomarker for ALCL. Indeed, studies have shown significant differences in progression-free survival when retrospectively stratified using a combination of MDD and anti-ALK autoantibody titres, the latter being another promising biomarker for ALCL (Mussolin *et al*, 2013). Anti-ALK autoantibodies can be identified and quantified in a majority of patients, and may on their own help to predict risk of relapse (Ait-Tahar *et al*, 2010; Knörr *et al*, 2018). Other potential biomarkers for relapse risk are microRNA (miRNA) detected in exosomes within the peripheral blood of patients. In particular, miR-103a-3p and miR-223-3p when detected in exosomes are predictive or relapse, potentially because they are thought to increase the invasiveness of ALCL (Lovisa *et al*, 2018).

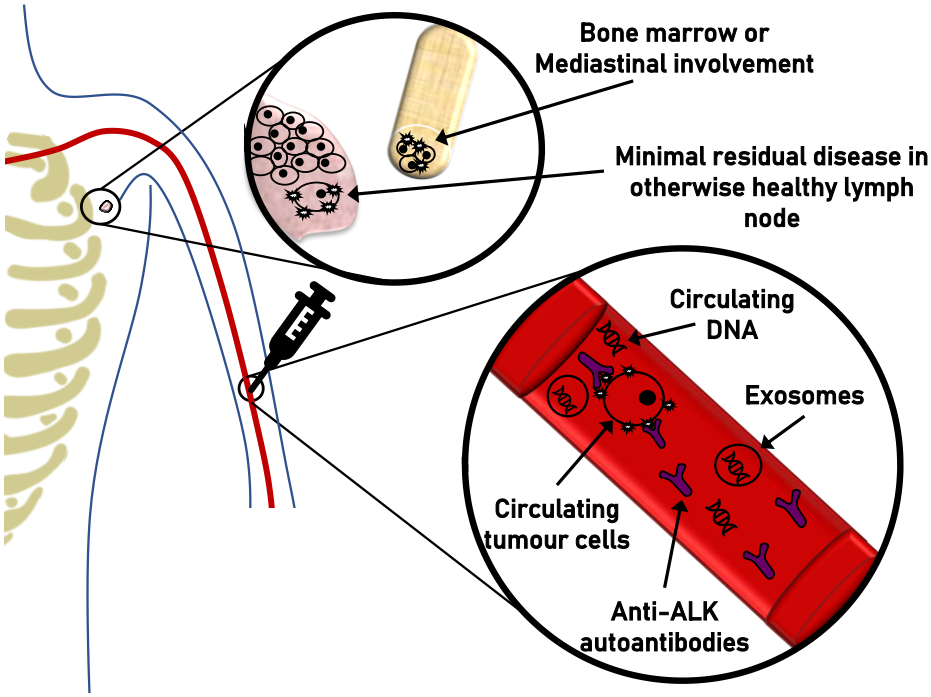

Figure 1.2: Main biomarkers thought to be predictive of relapse risk or prognosis in ALCL. The most obvious prognostic biomarkers are of a clinical nature, including bone-marrow or mediastinal involvement. Minimal residual disease is also a predictive biomarker. More recent liquid biopsy-based biomarkers show promise, though have yet to be validated in prospective clinical trials, these include exosomes (and miRNA profiles), circulating tumour cells (MDD), circulating DNA and anti-ALK autoantibodies. A combination of these may yet prove to be sufficient to predict ALCL prognosis or relapse.

Studies have also shown MDD and minimal residual disease (MRD) to be a potential combination to stratify ALCL patients according to risk, although MDD may be a valid prognostic factor on its own when employing the highly sensitive technique of digital droplet PCR (Damm-Welk *et al*, 2018). However, it remains to be seen whether prognostic markers predicting response to established chemotherapy schedules will apply to therapeutic protocols involving new targeted agents. The potential of biomarkers based on liquid biopsies is immense, yet all require validation in prospective clinical studies (**Figure 1.2**). MDD and ALK autoantibody titres may be predictive of response to therapy with the ALK inhibitor crizotinib or the anti-CD30 drug conjugate brentuximab vedotin (BV) when given in combination with an ALCL99 backbone although full results are not expected until 2019 and 2022 (Rolland *et al*, 2018; Lowe, 2018).

1.5 Current avenues for treatment - breaking the ceiling

A number of different chemotherapy regimens have been trialled, but none have been able to breach an OS of 90% and 70% EFS (Prokoph *et al*, 2018; Lowe & Lim, 2013). It is therefore unlikely that modifying current trial protocols further will improve these statistics, but modifications could improve the acute side-effects of therapy. EICNHL therefore aims to launch a trial of single-agent vinblastine as a front-line therapy for standard-risk patients, to test whether this could replace ALCL99 and thus drastically reduce toxicity, though whether this will improve OS or EFS remains to be seen. In addition, although a prolonged course of vinblastine is a significant commitment for parents and their families, the fact that this can be given as an outpatient may significantly improve the patients' qualify of life. High risk patients (defined using a biomarker yet to be determined) would continue to receive the current standard of care.

Progression on therapy carries an extremely negative prognosis, with only 25% of these patients estimated to survive, even when given aggressive salvage therapies (Woessmann *et al*, 2006, 2011). This is a salient issue, particularly given the lack of consensus on the treatment of relapsed or refractory ALCL. Latent toxicity is also an issue, as methotrexate has a number of side-effects, not to mention possible long-term effects for the survivors (Oeffinger *et al*, 2006). Indeed, long-term morbidity for survivors of NHL is significantly higher than healthy controls - survivorship and long-term follow-up should be kept in focus when developing new therapies (Burkhardt & Woessmann, 2018; Ehrhardt *et al*, 2018). Consequently, novel trial designs are required incorporating bench-side research to risk-stratify patients towards dose reduction for low risk patients, while the introduction of novel, targeted agents is needed for high risk children - but also to facilitate a better distinction between children more likely to suffer an event from those for whom therapy will be curative.

ALK is arguably the ideal target for ALK-positive diseases due to tumour addiction to its expression – inhibition of NPM-ALK alone in cell and murine models leads to tumour regression - and its near-absent expression in healthy tissue. Unfortunately, the rarity of ALCL has meant little interest from pharmaceutical companies in developing a small molecule inhibitor for this indication. Indeed, only after being identified in Non-Small Cell Lung Cancer (NSCLC) did interest peak in ALK as a therapeutic target and in 2008, Pfizer launched a phase I trial for crizotinib, an ALK/cMet/ROS1 inhibitor – and was awarded breakthrough approval in 2011 for the treatment of NSCLC (Camidge *et al*, 2012). Other ALK inhibitors have since been developed, although none have so far been approved for use in paediatric ALCL. However, their use is starting to be trialled in a number of settings, including ALCL (Reviewed in Prokoph *et al*, 2018). Results are promising, particularly for refractory adult ALCL patients, for whom odds of survival have improved significantly from 30% to 73% (Gambacorti Passerini *et al*, 2014). Recent data in a paediatric setting have also shown encouraging outcomes, with response rates for refractory and relapse ALCL patients of between 80 and 90% depending on dosage (Mossé *et al*, 2017). Unfortunately, trial data on the use of ALK Tyrosine Kinase Inhibitors (TKIs) as a front-line treatment for ALCL is so far missing, although trials are in progress (Prokoph *et al*, 2018). Unfortunately, given the objectively high OS rates observed in ALCL patients, clinicians are understandably wary to trial ALK TKIs as a stand-alone therapy, and therefore these trials have started by combining ALK TKIs with standard therapy – rather than to facilitate dose-reduction of chemotherapy. The COG trial ANHL12P1 (NCT01979536) is currently testing the addition of BV or crizotinib to ALCL99 chemotherapy for newly diagnosed patients with ALCL. The trial also includes prospective analysis of MDD, MRD and ALK autoantibodies, to assess whether these have prognostic value. Patients have been randomized to receive either BV (1.8 mg/m² once per cycle), or crizotinib (165 mg/m² for 21 days each cycle) along with the ALCL99 backbone. The trial opened in November 2013 in 135 institutions and is reaching accrual as of time of writing. As a change to previous COG trials, the current one includes stage II patients, who have been shown to have similar outcomes to those of stages 3-4 in previous trials. A further phase II trial of crizotinib combined with vinblastine could provide a further option for treatment of relapsed and refractory ALCL (CRISP trial**,** ITCC053).

As with other TKIs, resistance is expected, and has indeed been observed, sometimes with aggressive relapses in isolated cases (Gambacorti-Passerini *et al*, 2016; Sharma *et al*, 2018). It may be that ALK TKIs should be given on a long-term basis, possibly on a metronomic schedule to improve control of tumour progression (Amin *et al*, 2015). It may also be that combination therapies could alleviate the risk of relapse, indeed recent data in experimental settings show synergies between either Notch inhibitors and ALK TKIs (Larose *et al*, 2018), or ALK TKIs and BV (Hudson *et al*, 2018). Combination approaches require further study, although the latter combination demonstrating synergy is somewhat surprising given the fact that inhibition of NPM-ALK leads to downregulation of CD30 expression, thus robbing BV of its target (Hsu *et al*, 2006). In addition, it has been reported that

chemotherapeutic drugs such as doxorubicin may act antagonistically to crizotinib (Hudson *et al*, 2018).

An alternative target for the treatment of ALCL - regardless of ALK status - is CD30, which is consistently present on ALCL cells, and which expression is restricted to activated T and B-cells under homeostatic conditions, thereby limiting the risk of off-target effects. Early attempts at developing antibody-based drug delivery of toxins such as saporin-6 or pseudomonas exotoxin A, or radioisotopes such as iodine-131 to CD30-positive cells proved too toxic for the paediatric setting (Pasqualucci *et al*; Klimka *et al*, 1999; Schirrmann *et al*, 2014; Schnell *et al*, 2005). The arrival of the anti-CD30 antibody SGN-30 conjugated to the anti-microtubule agent monomethyl auristatin E (BV, or SGN-35), which targets CD30-positive cells and delivers the antimitotic drug has shown promise. BV was approved by the Food and Drug Administration (FDA) in 2011, but only for use in chemo-resistant, relapsed adult ALCL patients (FDA, 2011). A number of adult HL and NHL trials have since published their results, including some incorporating adolescent and young adult patients (Sekimizu *et al*, 2018), but it wasn't until 2012 that a paediatric-specific phase I/II trial for relapsed or refractory ALCL patients began (NCT01492088). Early results from this study have recently been reported, and are disappointing; only 53% of ALCL patients achieved an overall response, and all patients on the study experienced adverse events, with 44% suffering at least one grade 3 or worse treatment-related side-effect (Locatelli *et al*, 2018). In addition, questions remain as to how to treat patients failing BV, as this has been shown to be associated with a very poor outcome (Chihara *et al*, 2018). An alternative therapy targeting CD30 may be Chimeric Antigen Receptor T (CAR-T) cells (cells engineered with an ectopic T-cell receptor targeting a specific antigen). A number of trials are planned for adult relapsed CD30-positive lymphoma, but no data for the paediatric setting has yet been published.

The importance of the immune response to ALCL has been highlighted by the role of anti-ALK autoantibodies in treatment outcome. However, tumour cells also evade the immune response by downregulating CD48, thereby promoting immune evasion, a process that is reversed by inhibiting ALK (Wu *et al*, 2018). Immune evasion is also facilitated by NPM-ALK-induced expression of Programmed Cell-Death Ligand 1 (PDL-1) on the surface of ALCL cells, which has been confirmed in patient tumours (Yamamoto *et al*, 2009; Marzec *et al*, 2008). Given the role of PDL-1, PDL-2 and receptor PD-1 in tumour-driven immune suppression of T-cells, immunotherapy holds potential promise for the treatment of ALCL. Following case reports of adolescent or young adult patients with relapsed ALCL responding to nivolumab (anti-Programme cell Death protein-1 or PD-1; which also reported minimal toxicity) (Rigaud *et al*, 2018; Hebart *et al*, 2016), the checkpoint inhibitor was entered into clinical trials for both adult and paediatric relapsed and refractory ALK+ ALCL (NCT03703050, trial 'Nivo-ALCL'). Perhaps the main caveat for check-point inhibitors such as nivolumab, is the lack of agreed biomarkers. Studies have shown that strength of expression of PDL-1 does not predict response to treatment; not

only do patients with strong PDL-1 not necessarily respond, but some patients without strong PDL-1 expression have shown excellent responses (Grigg & Rizvi, 2016).

As depicted in **Figure 1.3**, the timespan between bench-side discoveries and development at the bedside has accelerated in recent years, though unfortunately is mostly driven by developments to treat adult patients. These new targets, along with therapies and trials have all been summarized in **Table 1.1**.

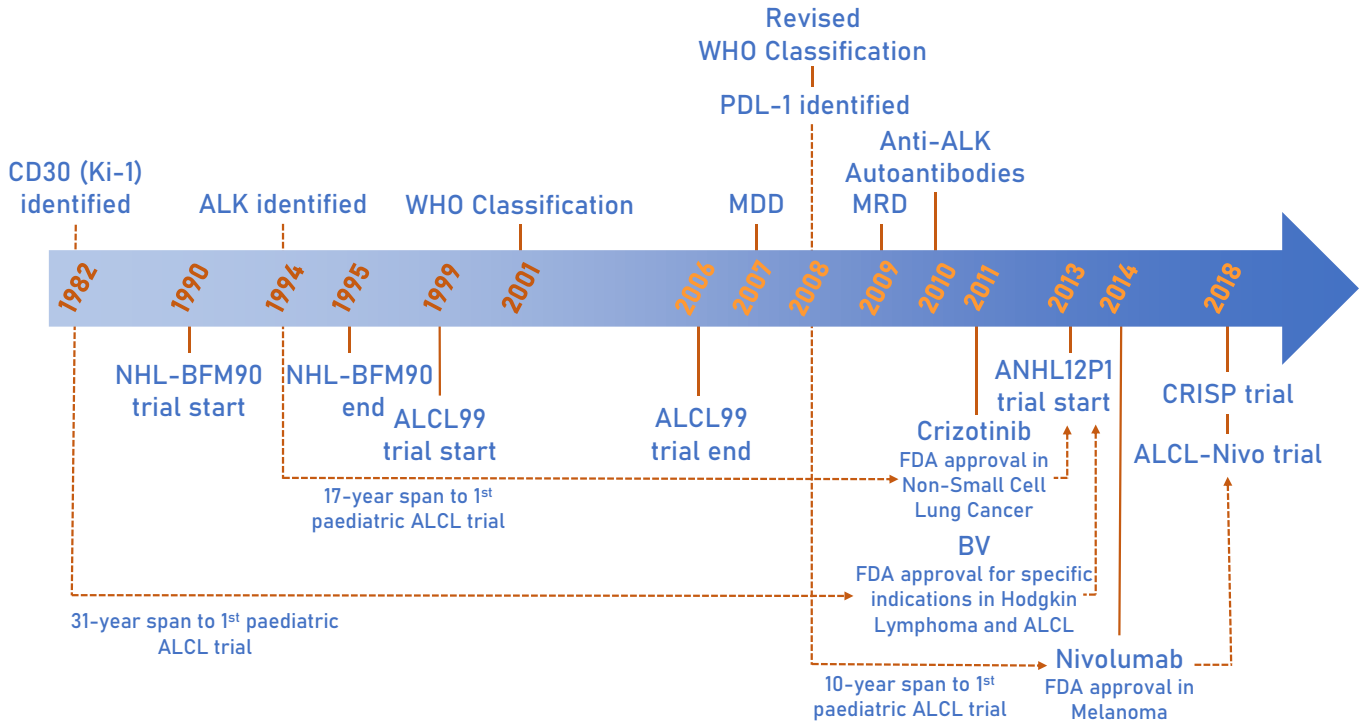

Figure 1.3: Timeline of the main discoveries relevant to ALCL. The most ground-breaking bench-side studies of ALCL are depicted in the timeline and point to, where relevant, the main clinical trials involving said discoveries in ALCL patients. The major bedside advances in ALCL are depicted below the timeline.

Target	Therapy	Trial	Phase	Patients	Schedule	Dose	Notes
ALK	**crizotinib**	NCT00939770	I/II	Relapsed/Refractory	Orally, twice daily	Determining RP2D	
		NCT01606878	I	Relapsed/Refractory	Oral solution, daily	Determining RP2D	Combination with standard chemotherapy
		UMIN000028075	I/II	Relapsed/Refractory	Orally, twice daily	Determining RP2D	
		ITCC053	I-B	Relapsed/Refractory	Twice Daily	Determining RP2D	Combination with VBL
		NCT01979536	II	Frontline stages II-IV	Orally, twice daily	Unknown	Combination with standard chemotherapy
		NCT02034981	II	All patients	Orally, twice daily	165mg/m2 for patients under 18	
	alectinib	UMIN000016991	II	Relapsed/Refractory	Orally, twice daily	300mg, except for patients <35kg, who got 150mg for at least one year	
	ceritinib	NCT02729961	I/II	Frontline	Orally, once daily after first week	Determining RP2D	Combination with BV
CD-30	**BV**	NCT02729961	I/II	Frontline	IV (30 mn) every three weeks for 18 weeks	Determining RP2D	Combination with ceritinib
		NCT01492088	II	Relapsed/Refractory	IV (30 mn) every 3 weeks	Range of 1.4-1.8mg/kg, determining RP2D	
		NCT01979536	II	Frontline stages II-IV	IV (30 mn) every three weeks for 18 weeks	Unknown	Combination with standard chemotherapy
	SGN-30	NCT00354107	I/II	Relapsed	IV, weekly for 8 weeks	Determining RP2D	Combination with standard chemotherapy
PD-1	**nivolumab**	NCT03703050	II	Relapsed	IV, every 2 weeks for 8 weeks, then every 4 weeks for 25 doses	3mg/kg	
PDGFR-β	**imatinib**	NCT02462538	I/II	Relapsed/Refractory patients of at least 18 years of age	Orally, for up to 48 weeks	200 mg daily, up from 100 mg	Combination with BV

Table 1.1: Targets for which therapies exist along with corresponding current trials. The treatment protocols and doses for the targeted agents are also detailed (BV: Brentuximab Vedotin, VBL: Vinblastine, IV: Intra-venous, RP2D: Recommended Phase-II Dose).

1.6 Developing our understanding of the biology of ALCL to identify novel therapeutic targets

A number of potential therapeutic targets have been identified in the laboratory, but most have yet to make headway at the bedside. For example, the signalling pathways active in ALCL have been extensively studied and documented providing multiple potential targets for therapy. The PI3-Kinase, Akt, Mouse double minute 2 homologue (MDM2), c-Jun N-terminal Kinase (JNK), STAT3 and PLCγ pathways are all activated by NPM-ALK and have been shown to drive cell survival in experimental settings (Bai *et al*, 1998, 2000; Turner & Alexander, 2006; Slupianek & Skorski, 2004; Chiarle *et al*, 2005; Leventaki *et al*, 2007; Marzec *et al*, 2007; Turner *et al*, 2007; Zhang *et al*, 2002; Cui *et al*, 2009). Perhaps more advanced in its clinical progress is the platelet derived growth factor receptor beta (PDGFR β) which has been shown to be a promising therapeutic target in the treatment of ALCL both at the bench and bedside (in adult patients; Laimer *et al*, 2012; Garces de los Fayos Alonso *et al*, 2018a). PDGFRβ expression in ALCL is mediated by MAPK, in particular the Activator Protein (AP-1) transcription factors Jun and JunB (Garces de los Fayos Alonso *et al*, 2018b; Leventaki *et al*, 2007). Indeed, AP-1 transcription factors themselves are attractive therapeutic targets in ALCL since patient tumours express high levels of the transcription factors *basic leucine zipper ATF-like transcription factor* (*batf* and *batf3*) (Liang *et al*, 2018).

Overall, the limitations to conducting paediatric ALCL trials are not the science and discovery of new targets, but clinical development, which requires intelligent trial design to develop protocols with small patient number, lower toxicities and higher EFS rates. The road from the bench to the bedside for ALCL has been slower than for many cancers. Indeed, seventeen years separate the discovery of NPM-ALK and the approval of the first drug targeting it – and still we are waiting for its approval for the treatment of paediatric ALCL. CD30 is a similar story, with nineteen years spanning its first description in ALCL and the FDA approval of a targeted agent. Indeed, while in many cancers academics may struggle to keep up with the rate of new clinical trials and drug development, at least in the paediatric setting the reverse is often seen, as access to new agents is more difficult.

Fortunately, there is movement from regulatory agencies to facilitate treatment for children with ALCL. In the USA, legislation such as the RACE for Children Act, signed into law as part of the FDA Reauthorization Act of 2017 may yet change the equation by requiring paediatric trials for drugs of interest already being trialled in adults (Walden, 2017). In Europe, the ACCELERATE platform, formed in 2013 as part of the European Network for Cancer research in Children and Adolescents is steered by a number of representatives from patient advocacy groups, academia, industry and regulatory bodies. The platform aims to identify bottlenecks and hurdles to speed up the arrival of drug at the patient bedside (Pearson *et al*, 2016; Vassal *et al*, 2015). Laboratory research into ALCL has greatly improved our understanding of the oncogenic nature of the disease (Reviewed in Larose *et al*, 2019). We hope that this extensive knowledge coupled with the cooperation of clinicians, researchers, pharmaceutical

companies and regulatory agencies will allow all children who develop ALCL to be cured with minimal toxicity in the very near future.

1.7 The Notch pathway

One pathway thought to be important for the biology of ALCL is the Notch pathway (Larose *et al*, 2018). The *notch* gene was stumbled upon while studying Drosophila melanogaster just over a century ago, when Morgan and colleagues observed notches on flies following genetic mutations leading to loss of function of the *notch* gene (Morgan, 1917). This family of genes have since been found to encode large (300 KDa) proteins. Notch proteins are transmembrane receptors made up a number of different domains; the main extracellular ones are the 36 epidermal growth factor (EGF)-like repeats and the Negative Regulatory region (NRR) which, in wild-type setting, prevents ligand-independent activation of the receptor, though mutations to the *notch* family of genes may override this. The intracellular domains are made up of a Recombination Signal Binding Protein Jκ (RBP-Jκ)-Association Molecule (RAM), 6 Ankyrin repeats (ANK; which contain the two nuclear localization signals), a Transactivation (TAD; also known as Heterodimerization) domain and a sequence rich in Proline, Glutamic Acid, Serine and Threonine (PEST) as depicted in **Figure 1.4A**.

Members of the Notch family of receptors are activated by one of five ligands; Jagged1 or 2, Delta-like1, 3 or 4 (Jag1, Jag2, DLL1, DLL3 and DLL4), which leads to cleavage of the intracellular domain of Notch (ICN) by γ-secretase (a protease complex which cleaves proteins with an intramembrane domain). The ICN then is transported to the nucleus where changes in gene expression are effected by binding of ICN to RBP-Jκ, displacing corepressors and thus preventing RPB-Jκ from inhibiting Notch target genes (Reviewed in Borggrefe & Oswald, 2009 and summarized in **Figure 1.4B**) – though it should be noted that there is also evidence for signalling outside the RBP-Jκ pathway (Reviewed in Heitzler, 2010).

A number of genes are directly targeted, but the main ones include the *hairy enhancer of split* family (*hes* and *hey*), the *hes-related repressor protein* family (*herp*), *ptcra*, *nrarp*, *deltex E3 ubiquitin ligase 1* (*dtx1*) and *cyclin-dependent kinase* (*cdk*)-related genes involved in cell cycle regulation (Davis & Turner, 2001; Iso *et al*, 2003; Rangarajan *et al*, 2001; Krebs *et al*, 2001; Deftos *et al*, 2000; Reizis & Leder, 2002). Some of the main pathways effected by Notch include Nuclear factor kappa-light-chain-enhancer of activated B cells (NFκB), Akt/mTOR and Wingless-type (Wnt) (Reviewed in Ayaz & Osborne, 2014). The Notch pathway regulates a number of key biologic functions (Reviewed in Greenwald, 1998), one of which is haematopoiesis and T-cell development. Indeed, Notch1 expression in bone marrow lymphoid progenitors instruct these cells to adopt a T cell fate: inactivation of the protein or of RBP-Jκ leads to the termination of T cell development (absence of Notch1 seems to lead to a default B cell fate, as

seen by a significant increase in the amount of B cells present in the thymus) - and constitutive activation of Notch has the opposite effect (Wilson *et al*, 2001; Pui *et al*, 1999; Kawamata *et al*, 2002). There is yet no overarching consensus as to the exact role Notch has to play in T cell differentiation beyond this (the topic has been extensively reviewed in Amsen *et al*, 2015; and Radtke *et al*, 2013).

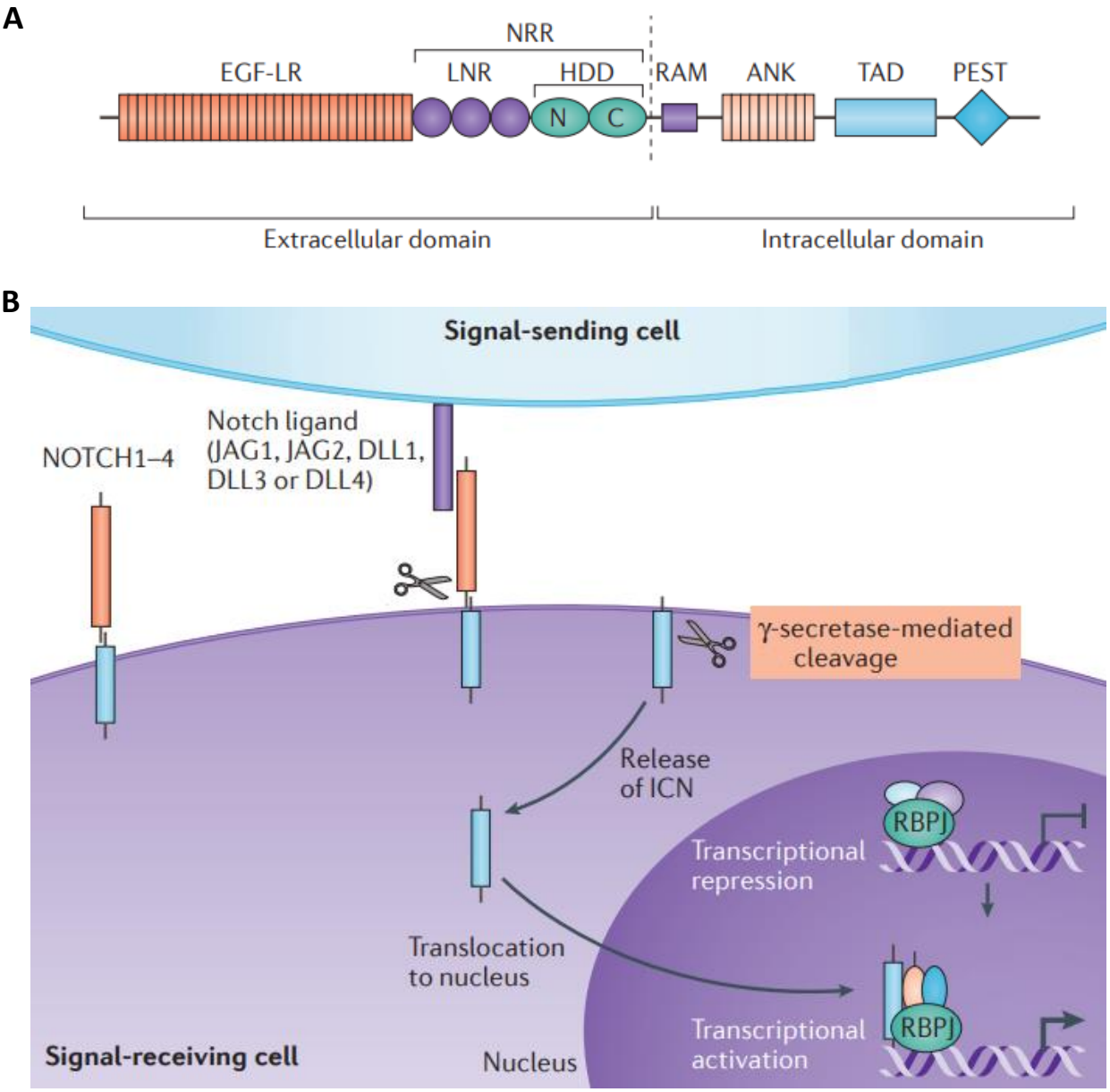

Figure 1.4: The Notch protein structure. ***(A)*** *Structure of the Notch1 receptor. EGF-like repeats (EGF-LR), Negative Regulatory Region (NRR), LIN12/Notch Repeats (LNR), Heterodimerization Domain (HDD), RBP-Jκ Association Molecule (RAM), Ankyrin Repeats (ANK), Nuclear Localization Signals (NLSs), Transactivation Domain (TAD), Polypeptide enriched in proline, glutamate, serine and Threonine (PEST).* ***(B)*** *Schematic Notch signalling cascade including Notch ligand families Jag and DLL, release of the ICN and the involvement of RBP-Jκ to effect transcription (Modified from Nowell & Radtke, 2017).*

As far as cancers are concerned, the evidence is mixed; indeed in some cell types, Notch has an oncogenic role (T cell acute lymphoblastic leukaemia, or T-ALL, for example), while in others (Acute myeloblastic leukaemia, AML, for example) a tumour suppressor effect has been observed (Reviewed in Hernandez Tejada *et al*, 2014). A number of lymphoma and leukaemia have also shown Notch mutations driving cancer, including paediatric T cell lymphoma (Grabher *et al*, 2006) – the role of Notch in ALCL will be detailed in subsequent chapters.

1.8 Next-Generation Sequencing and the ALCL genomic landscape

The genetics and epigenetics of ALCL have been sparsely studied. Evidence shows that the genome of ALCL is relatively stable, although there are indications that a higher frequency of chromosomal imbalances may be indicative of a poorer prognosis (Youssif *et al*, 2009; Salaverria *et al*, 2008; Eckerle *et al*, 2009). Some genetic events of ALCL, ALK- have also recently been identified, such as the involvement of the JAK/STAT pathway, or miRNA-155 overexpression, but there is still only limited data as to the therapeutic applications of these findings (Crescenzo *et al*, 2015; Merkel *et al*, 2010, 2015). Whilst the above described data provide obvious targets for therapy, delving deeper into the biology of ALCL can provide more findings not immediately apparent as therapeutic targets. Indeed, other molecules can regulate cell survival in ALCL including, for example, non-coding RNAs. The miRNA profile of ALCL tumours is highly dependent on NPM-ALK expression levels (Garbin *et al*, 2018) suggesting that some might be regulated directly by NPM-ALK activity, for example, miRNA-150 has been shown to be silenced in ALCL and that restoring expression hinders tumour cell growth (Hoareau-Aveilla *et al*, 2015).

It is not clear whether miRNA-150 is silenced in an NPM-ALK-dependent manner, but there is evidence that NPM-ALK affects the epigenome of ALCL, which in turn may explain downstream signalling despite a stable genome. Indeed, NPM-ALK has been shown to epigenetically silence a whole raft of genes, by signalling through STAT3, for instance (Ambrogio *et al*, 2009). Indeed, STAT3 has been shown to induce *dna methyltransferase* (*dnmt1*) expression, an important epigenetic silencer (Zhang *et al*, 2006, 2005). Some examples of genes silenced in ALCL include *stat5a* and *il-2r* whose rescue has been shown to inhibit NPM-ALK expression in a manner which is tumour suppressive (Zhang *et al*, 2007, 2011). NPM-ALK is also increasingly thought to be the cause of a number of epigenetic changes (Reviewed in Ducray *et al*, 2019). This has led to new potential therapeutic avenues by reactivating silenced genes; there already exists proof-of-concept evidence for this approach *in vitro* (Hassler *et al*, 2012). A number of these epigenetic changes are thought to be mediated by modulating CpG island methylation; studies show that ALCL cell lines have increased methylation at such islands (Eberth *et al*, 2010; Piazza *et al*, 2013; Watanabe *et al*, 2008; Nishikori *et al*, 2003). Long non-coding RNA have also recently been

implicated in ALCL, such as LINC01013, which has been shown to promote invasiveness of ALCL cells (Chung *et al*, 2017).

NGS is increasingly used to understand the genetics of tumours and identify risk factors. The genetics of ALCL for example have revealed a multitude of ALK fusion partners (Reviewed in Ducray *et al*, 2019). This has also been helpful in ALK- ALCL, some subtypes of which have been identified, as mentioned. Two main types of analyses are being employed to identify driver mutations; either examining driver genes by looking for frequently mutated genes (at varying positions), or by looking for specific point mutations, deletions and insertions that are mutated in a constant manner in several different tumours. The former technique is mostly employed to identify driver oncogenes or lost tumour suppressors, or genes consistently indicative of poor prognosis (Lasorsa *et al*, 2016). However the latter technique has been used to identify a number of mutations involved in malignancy (Ho *et al*, 2013; Wang & Armstrong, 2007). Not only do these Single Nucleotide Polymorphism (SNP) chips or panels lead to intriguing cancer detection possibilities by DNA sequencing, they also pave the way for prognosis prediction.

1.9 Aims of this study

As explained, second-line treatment and combination therapies for relapse patients are still required – as well as predictive markers to allow dose de-escalation for patients who would react well to the current gold-standard, often children who could benefit from a less toxic treatment than ALCL99. Many breakthroughs in other cancer types have come from the study of the genome of these malignancies, by identifying oncogene addiction or driving mutations and/or pathways. Since relatively little is known of the genomic profile of ALCL, this necessarily limits both our understanding of the biology of ALCL, and our ability to posit about new therapies and predictive biomarkers.

This thesis describes work conducted performing whole exome sequencing (WES) of ALK+ ALCL, pooling different cohorts together, analysing a total of 25 ALK+ ALCL tumours genomes, further validating the variants identified in another 78 cases of ALCL to understand disease pathology and to uncover novel targets for therapy. The main mutated pathways in ALCL were then assessed, along with the genomic profile more broadly, in the context of what is known of paediatric cancer genomes. Gene Set Enrichment Analysis (GSEA) is employed here to enable pathway analyses, combining results from different algorithms to form robust conclusions. The biological significance of any identified and validated variant or significantly mutated pathway is then analysed to both improve our understanding of ALCL biology and to uncover new potential treatment options, as well as to look for prospective predictive biomarkers of either relapse or poor prognosis.

2. Materials and Methods

2.1 Cell culture

Routine culture and passaging

The cell lines HEK293FTs, ALK+ ALCL cell lines (Karpas 299, SU-DHL1, SUP-M2, DEL), ALK- ALCL lines (MAC2A, FEPD), an acute T-cell leukaemia cell line (CD4 and CD8 negative Jurkat), and mouse feeder cell lines (wild-type or DLL-1 expressing OP9) were cultured in a humidified 37^{o} C incubator, at 5% CO_2. ALK+ ALCL and Jurkat cell lines were obtained from the DSMZ, while FEPD were obtained from Annarosa Del Mistro at the University of Padua, and Mac2A were obtained from Olaf Merkel at the Medical University of Vienna. OP9 cells were obtained from Alison Michie, in Glasgow, and HEK293FT were obtained from Nick Coleman, at the University of Cambridge.

HEK293FT is an adherent line grown in Dulbecco's Modified Eagle's Medium (DMEM; ThermoFisher Scientific, Cat# 11995065) supplemented with 10% Fetal Bovine Serum (FBS, Sigma-Aldrich, Cat# F9665) and 1% Penicillin-Streptomycin (Sigma-Aldrich, Cat# P4333). ALCL cell lines are all suspension cell lines and were cultured in Roswell Park Memorial Institute (RPMI) 1640 (ThermoFisher Scientific Cat# 21875091) medium supplemented with 10% FBS and 1% Penicillin-Streptomycin. OP9 cells were transduced to express the Notch1 ligand DLL-1 (expressed using the pMIGR-1 plasmid, see chapter 2.6). OP9 cells are adherent and were grown in α-Modified Eagle's Medium (α-MEM) medium (ThermoFisher Scientific, Cat# 12561056), supplemented with 20% FBS.

Every two to three days, suspension cells were collected by centrifugation at 100 g for 5 min at room temperature and were seeded to reach either a density of 100,000 cells per mL, or to the density required for the subsequent experiment. Every 6 months, cell lines were tested for Mycoplasma, using an EZ-PCR Mycoplasma test kit (Geneflow, Cat# 20-700-20), according to the manufacturers' instructions. Every two to three days, adherent cell lines were detached by incubating in 0.05% Trypsin-Ethylenediaminetetraacetic acid (Trypsin-EDTA; ThermoFisher Scientific, Cat# 2530054) for 5 min in a cell culture incubator. Cells were then collected by centrifugation at 100 g for 5 min at room temperature, before diluting cells to reach a confluency of 20%, or were seeded to a confluency depending on the needs of the subsequent experiment.

OP9-DL1 co-culturing

OP9-DL1 cells were seeded at 20% confluency as described above. Two days later, the media was removed and replaced with either media containing HEK293FTs, which were also seeded at 20% confluency, or ALCL cells which were seeded at a density of 100,000 cells/mL. Cells were left in co-culture for 48 hours. HEK293FTs were first stably transduced to express Green Fluorescence Protein

(GFP) using pJLM1-GFP (Addgene, Cat# 19319) and Puromycin selected at 1 µg/mL, as detailed in chapter 2.6. HEK293FTs were then trypsinised and sorted for GFP-positive cells (GFP was co-transduced into HEK293FTs along with the Notch1 plasmid), following co-culturing with the OP9-DLL1 cell line, while ALCL cells were then washed off and processed for downstream assays.

Deriving crizotinib-resistant ALCL cell lines

Crizotinib-resistant Karpas 299, SUP-M2, SU-DHL-1 and DEL cells were established as described previously (Ceccon *et al*, 2013). Briefly, ALCL cells were seeded at approximately 0.5 x 10^6 cells/mL. Crizotinib (see **Table 2.1**) was added at a starting concentration of 50 nM, and cells were maintained in fresh drug containing medium changed every 48-72 hours. After every two passages at a given concentration of drug, the concentration of crizotinib was increased in half-log intervals.

2.2 KRAB-dCas9 Knock-down and Activation

Two Clustered Regularly Interspaced Short Palindromic Repeats (CRISPR) systems were used: an overexpression system (transcriptional activation) and a knock-down system (transcriptional inhibition).

CRISPR Activation

With respect to transcriptional activation, cells were transduced to express plasmids dCas9-VP64_Blast (Addgene, Cat# 61425) and MS2-P65-HSF1_Hygro (Addgene, Cat# 61426), before being selected with Blasticidin and Hygromycin (concentrations in **Table 2.1**, as described in chapter 2.6). Cells were then transduced with plasmid sgRNA(MS2)_Zeo (Addgene, Cat# 61427) containing the appropriate oligonucleotides (as described in chapter 2.9) and selected with Zeocin (concentrations in **Table 2.1**).

CRISPR Knock-down

With respect to transcriptional inhibition, a lentiviral-based two plasmid system was used: pHR-SFFV-KRAB-dCas9-P2A-mCherry (Addgene Cat# 60954), and doxycycline-inducible FgH1tUTG (Addgene Cat# 25307932). DEL, Karpas 299 and SUP-M2 cell lines were transduced (as described in chapter 2.6) to express pHR-SFFV-KRAB-dCas9-P2A-mCherry and cells were sorted for expression of mCherry (chapter 2.8). To knockdown *notch1*, 2 guide sequences per candidate gene were designed using the Broad Institute short guide RNA (sgRNA) Designer (*https://portals.broadinstitute.org/gpp/public/analysis-tools/sgrna-design-crisprai*) and introduced into FgH1tUTG using Golden-Gate assembly (as described in chapter 2.9). Cells were then transduced to express the cloned FgH1tUTG (chapter 2.6), and cells positive for eGFP were collected by Fluorescence-Activated Cell Sorting (FACS) following sorting for GFP expression (chapter 2.8). FgH1tUTG transduced cells were cultured with tetracycline-free FBS and sgRNA expression induced with 1 µg/mL doxycycline for 24 to 96 hours.

Reagent	Category number	Concentration	Application
GSI 1	Abcam, Cat# ab145891	Variable	Therapeutic
BMS-906024	Sigma-Aldrich, Cat# 0018	Variable	Therapeutic
PF-03084014	Sigma-Aldrich, Cat# PZ0298	Variable	Therapeutic
Zeocin	ThermoFisher Scientific, Cat# 100687010	DEL (100 µg/mL) Karpas 299 (100 µg/mL) SU-DHL1 (80 µg/mL) SUP-M2 (100 µg/mL)	Selection marker
Blasticidin	ThermoFisher Scientific, Cat# R21001	DEL (10 µg/mL) Karpas 299 (10 µg/mL) SU-DHL1 (5 µg/mL) SUP-M2 (10 µg/mL)	Selection marker
Hygromycin	Invivogen, Cat# ant-zn-1	DEL (200 µg/mL) Karpas 299 (200 µg/mL) SU-DHL1 (125 µg/mL) SUP-M2 (200 µg/mL)	Selection marker
Puromycin	Sigma-Aldrich, Cat# 8833	DEL (500 ng/mL) Karpas 299 (1 µg/mL) SU-DHL1 (1 µg/mL) SUP-M2 (1 µg/mL)	Selection marker
Methotrexate	Sigma-Aldrich, Cat# A6770	Variable	Therapeutic
crizotinib	Sigma-Aldrich, Cat# PZ0191	Variable	Therapeutic
ceritinib	MedChem Express, Cat# HY-15656	Variable	Therapeutic
DMSO	Sigma-Aldrich, Cat# D8418	Volume equivalent to compound tested	Vehicle control

Table 2.1: Compounds used in this thesis. Drugs were obtained lyophilized from the manufacturer and reconstituted in the appropriate diluent at the maximum tolerated concentration before being aliquoted in appropriate volumes and kept at temperatures recommended by the manufacturer to minimize freeze/thaw cycles.

2.3 Drug treatments & Growth assays

ALCL cell lines were treated with various drugs (**Table 2.1**). Drug treatments were conducted in 96-well plates for proliferation assays, whereby drugs were diluted to 10 times the final concentration in RPMI, and 10 µL of the diluted drug was added to 90 µL of cells seeded in a 96-well plate. For other assays, the stock solution of drug or antibiotic was added directly to the well at the appropriate volume.

Cell proliferation was mostly measured using a tetrazolium dye (MTT) assay (Sigma-Aldrich, Cat# M5655). Cells were seeded at 100,000 cells/mL in 100 µL (or 90 µL for drug treatments, as described above) in a 96-well plate (ThermoFisher Scientific, Cat# AB-2396). After a suitable incubation period,

Thiazolyl Blue Tetrazolium Bromide was added to a final concentration of 1 mg/mL. After a further 4 hours of incubation at 37°C, Sodium Dodecyl Sulphate (SDS) in suspension (Sigma-Aldrich, Cat# 75746) was added to a final concentration of 10% w/v to dissolve the formazan crystals that have formed. Cells were incubated for 4 hours at 37°C, before absorbance was measured at 570 nm using a SpectraMax i3 plate reader. Samples were analysed in technical and biological triplicates.

Alternatively, cell proliferation was measured using the RealTime-Glo kit (Promega, Cat# G9711) to measure more than one time-point. Reagents were first incubated at 37°C before cells were seeded at 100,000 cells/mL in a 96-well plate, following which Real-Time Glo reagents were added to a final concentration of 1X following the manufacturer's instructions. Luminescence was then measured using a SpectraMax i3 plate reader at 24, 48 and 72 hours, following the manufacturer's instructions. Samples were analysed in technical and biological triplicates.

2.4 Apoptosis and Cell Cycle Assays

Apoptosis assay

1 million cells were harvested by centrifugation at 100 g for 5 min at 4°C. Cells were washed in Annexin V (AV) Binding Buffer (ThermoFisher Scientific, Cat# V13246), before being resuspended in 100 µL of AV solution (Annexin V (Biolegend, Cat# 640920) diluted 1:20 in AV Binding Buffer). Cells were incubated in the solution for 30 min at room temperature, in the dark, before being washed with AV Binding Buffer. Finally, cells were resuspended in 250 µL of Propidium Iodide (PI) (Propidium Iodide (Sigma-Aldrich, Cat# P4864) diluted 1:1000 in AV Binding Buffer). Stained cells were then immediately analysed using FACS, with a BDBioscience FACSCalibur. Samples were analysed in technical and biological triplicates.

Cell cycle assay

To assess the fraction of cells in each stage of the cell cycle, 1 million cells were washed in cold Phosphate-Buffered saline (PBS) and collected by centrifugation at 100 g for 5 min at 4°C before resuspension in 400 µL 70% ethanol, by adding the ice cold ethanol dropwise, while vortexing the cells at high speed before a final incubation on ice for 45 min. Cells were then washed once in PBS after being collected by centrifugation at 2000 g for 5 min at 4°C. Finally, cells were resuspended in a PI solution (PI diluted 1:1000, supplemented with 100 µg/mL RNAse A (Sigma-Aldrich, Cat# 10109142001)) and incubated 10 min at room temperature before immediately being analysed using a BDBioscience FACSCalibur. Samples were analysed in technical and biological triplicates.

2.5 siRNA and shRNA expression silencing

siRNA Nucleofection

ALCL cell lines were nucleofected with small interfering RNA (siRNA) (siRNA Silencer Select, ThermoFisher Scientific, Cat# 4392420, Assay # 108983, or Cat# AM4611 for scrambled siRNA) using Amaxa Solution V (Lonza, Cat# VCA-1003), according to the manufacturer's instructions, using an Amaxa Nucleofector. Samples were analysed in biological triplicates.

ALCL cell lines were cultured in 12-well plates in 2 mL of medium to reach a density of 0.5 million cells/mL. Cells were collected by centrifugation at 90 g for 10 min at room temperature, and were resuspended in 100 µL of Amaxa Solution V (Lonza, Cat# VCA-1003), before transfer to an Amaxa cuvette (Lonza, Cat# VCA-1003) along with 30 pmol siRNA suspended in 2 µL RNAse-free water (siRNA Silencer Select, ThermoFisher Scientific, Cat# 4392420, Assay # 108983, or Cat# AM4611 for scrambled siRNA), and nucleofection with an Amaxa Nucleofector (Lonza, Cat# AAB-1001) using programme A-030. Cells were then resuspended in 1 mL of RPMI medium, in a 12-well plate. Subsequent experiments were conducted 24 hours post Nucleofection.

shRNA silencing

ALCL cell lines were transduced with shRNA constructs (detailed in chapter 2.6, constructs are in **Table 2.2**), and cells successfully transduced were selected on incubation in media containing the relevant antibiotic (**Table 2.1**). Following 96 hours of selection, RNA was extracted as detailed in Chapter 2.7 to verify gene silencing, following which cells were cultured in fresh, antibiotic-free media for downstream applications.

2.6 Lentiviral production & Transductions

HEK293FTs were seeded at 50% confluency 1 day before transfection. The plasmid of interest was co-transfected with plasmids pMD2.G (Addgene Cat# 12259, kind gift from Didier Trono), and psPAX2 (Addgene Cat# 12260, kind gift from Didier Trono) using TransIT-293 (MirusBio Cat# MIR 2700). A mix of 19.2 µL TransIT-293, 1.52 µg of envelope plasmid PMD2.G (Addgene, Cat# 12259), 2.38 µg of packaging plasmid psPAX2, and 2.7 µg of the expression plasmid (see **Table 2.2**) was first prepared in 500 µL of Opti-MEM medium (ThermoFisher Scientific, Cat# 31985062), and incubated at room temperature for 15 min. The mix was then added to cells.

Supernatant was collected 54 hours after transfection; the media was harvested, and cell debris was removed by centrifugation at 100 g for 5 min. The virus-containing media was then frozen down at -80^{o}C until required or used immediately for transduction.

ALCL cell lines were cultured in T25-flasks (Corning, Cat# 430641) in 5 mL of medium, to a density of 0.5 million cells/mL. Cells were then treated with medium containing viral particles at a MOI of less than 0.7. Following transduction (24 hours), cells were either selected by adding antibiotic to the media for 4 days (See **Table 2.1**) or sorted based on expression of the relevant fluorescent protein. In any case a negative control of untransduced cells helped to confirm that the transduction was successful.

Plasmid	Addgene Reference (if applicable)	Selection protein/antibiotic
psPAX2	12260	-
PMD2.G	12259	-
FgH1tUTG	70183	EGFP
dCas9-VP64_Blast	61425	Blasticidin
MS2-P65-HSF1_Hygro	61426	Hygromycin
sgRNA(MS2)_Zeo	61427	Zeocin
pHR-SFFV-KRAB-dCas9-P2A-mCherry	60954	mCherry
pLJM1-EGFP-Notch1	-	Puromycin
LentiCas9-Blast	52962	Blasticidin
LentiGuide-Puro	52963	Puromycin
MISSION® shRNA for Notch1	Sigma-Aldrich, Cat# SHCLNG-NM_017617 (TRCN0000003362, TRCN0000350253, TRCN0000350254)	Puromycin
MISSION® shRNA for STAT3	Sigma-Aldrich, Cat# SHCLNG-NM_003150 (TRCN0000020840, TRCN0000020842)	Puromycin
NPM-ALK shRNA	Obtained from Roberto Chiarle (Piva *et al*, 2006)	-
pIND_puro_ALK	Obtained from Liam Lee	Puromycin

Table 2.2: Plasmids used in this thesis. EGFP = Enhanced GFP.

Name	F/R	Application	Sequence
NOTCH1: sequencing of the whole cDNA	Forward	Sanger sequencing	CTCTGCCTGGCGCTGCTG
	Forward	Sanger sequencing	GGAAACAACTGCAAGAACGGG
	Forward	Sanger sequencing	TGTGCCAGTACGATGTGGAC
	Forward	Sanger sequencing	ATGACCAGTGGCTACGTGTG
	Forward	Sanger sequencing	CAATGAGTGCGACTCACAGC
	Forward	Sanger sequencing	GCGTCAATGACTTCCACTGC
	Forward	Sanger sequencing	ACTGCAAGGACCACTTCAGC
	Forward	Sanger sequencing	AAAGTGTCTGAGGCCAGCAA
	Forward	Sanger sequencing	AACAACAGGGAGGAGACACC
	Forward	Sanger sequencing	CTGCAGCATGGCATGGTAGG
	Forward	Sanger sequencing	CAGGGCCGACCAGAGGAG
	Forward	Sanger sequencing	TGCACCCATGGTACCAATCA
	Forward	Sanger sequencing	ATTCCACGTCTCCGACTGG
	Forward	Sanger sequencing	ATGCCAAAAAGCTCCTGGG
	Forward	Sanger sequencing	CCAGATGCGTCCCAAGATGT
U6	Forward	Sanger sequencing	AATGACTATCATATGCTTACCG
F1	Forward	Sanger sequencing	TCGCTATGTGTTCTGGGAAA
CMV_F	Forward	Sanger sequencing	CGCAAATGGGCGGTAGGCGTG
SP6	Forward	Sanger sequencing	CGATTTAGGTGACACTATAG
NOTCH1	Forward	qPCR	TACAAGTGCGACTGTGACCC
NOTCH1	Reverse	qPCR	ATACACGTGCCCTGGTTCAG
JAG1	Forward	qPCR	GCCGAGGTCCTATACGTTGC
JAG1	Reverse	qPCR	CCGAGTGAGAAGCCTTTTCAA
CAS9	Forward	qPCR	CCTGCGGCTGATCTATCTGG
CAS9	Reverse	qPCR	AGCTGGTTGTAGGTCTGCAC
HEY1	Forward	qPCR	GTTCGGCTCTAGGTTCCATGT
HEY1	Reverse	qPCR	CGTCGGCGCTTCTAATTATTC
HES1	Forward	qPCR	TCAACACGACACCGGATAAAC
HES1	Reverse	qPCR	GCCGCGAGCTATCTTTCTTCA
PPIA	Forward	qPCR	GCTTTGGGTCCAGGAATG
PPIA	Reverse	qPCR	AGAAGGAATGATCTGGTGGTTAAG
GAPDH	Forward	qPCR	CTGGGCTACACTGAGCACC
GAPDH	Reverse	qPCR	AAGTGGTCGTTGAGGGCAATG
NOTCH1_1	Forward		AAACCCCGGGCCCGGCTCCGCGCCC

NOTCH1_1	Reverse	CRISPR Overexpression	CACCGGGCGCGGAGCCGGGCCCGGG
NOTCH1_2	Forward		AAACCACAGCGCCGCCAGCCAGCCCC
NOTCH1_2	Reverse		CACCGGGCTGGCTGGCGGCGCTGTG
NOTCH1_1	Forward	CRISPR Knock-down	TCCCCCGCGCTCGCCGCACGAGGT
NOTCH1_1	Reverse		AAACACCTCGTGCGGCGAGCGCGG
NOTCH1_2	Forward		TCCCGCGGCGGCATGCCTCCCCAC
NOTCH1_2	Reverse		AAACGTGGGGAGGCATGCCGCCG
NOTCH1	Forward	PCR for cloning	ATATATACCGGTATAGCGCGTGTGCGTCCCAGCCC
NOTCH1	Reverse	PCR for cloning	CTCTCATTCGAATCAGCGCCGTTTACTTGAAGGCC
NOTCH1_645	Forward	Site-Directed Mutagenesis	GGTCATGGCAGGGGCGCCGTGGAA
NOTCH1_645	Reverse	Site-Directed Mutagenesis	TTCCACGGCGCCCCTGCCATGACC
NOTCH1_759	Forward	Site-Directed Mutagenesis	GTGTTGTGGCAGGGCCCGCCGTTCTGG
NOTCH1_759	Reverse	Site-Directed Mutagenesis	CCAGAACGGCGGGCCCTGCCACAACAC
MYC	Forward	qPCR	GGCTCCTGGCAAAAGGTCA
MYC	Reverse	qPCR	CTGCGTAGTTGTGCTGATGT
DTX1	Forward	qPCR	GACGGCCTACGATATGGACAT
DTX1	Reverse	qPCR	CCTAGCGATGAGAGGTCGAG
STAT3	Forward	qPCR	CAGCAGCTTGACACACGGTA
STAT3	Reverse	qPCR	AAACACCAAAGTGGCATGTGA
JAG1	Forward	qPCR	GTCCATGCAGAACGTGAACG
JAG1	Reverse	qPCR	GCGGGACTGATACTCCTTGA
DLL1	Forward	qPCR	GATTCTCCTGATGACCTCGCA
DLL1	Reverse	qPCR	TCCGTAGTAGTGTTCGTCACA
NPM-ALK	Forward	qPCR	CTGTACAGCCAACGGTTTCCC
NPM-ALK	Reverse	qPCR	GGCCCAGACCCGAATGAGG
NOTCH1	Forward	ChIP	ATCAACCTGTTCCTCCCCTG
NOTCH1	Reverse	ChIP	TTCCCGACTACAAGCGGACT
IRF4	Forward	ChIP	CTCTAAACACCGCGGAGAGG
IRF4	Reverse	ChIP	CTTTGCAGAGCGTGTAACGG
Control	Forward	ChIP	ATTCCACCTTGTCCAGCCCT
Control	Reverse	ChIP	GGTTTTATCCCTCTCCCCGAC

Table 2.3: Oligonucleotides used in this thesis. ChIP = Chromatin Immunoprecipitation

2.7 RNA extraction & Reverse-Transcription-quantitative Polymerase Chain Reaction (qPCR)

RNA extraction

TRI reagent (0.5 mL, Sigma-Aldrich, Cat# T9424) was used to thoroughly resuspend cell pellets, in which they were incubated for 5 min at room temperature. Chloroform (200 µL) was then added to samples before mixing vigorously and another 5 min incubation at room temperature. The different cellular components of the samples were then separated by centrifugation at 16000 g for 15 min at 4°C, and the aqueous phase was transferred to a new Eppendorf tube.

Nucleic acids were then precipitated in 300 µL Isopropanol and collected by centrifugation at 16000 g for 30 min at 4°C, followed by a wash in 500 µL 70% ethanol, and finally allowed to air dry to evaporate any remaining alcohol. TURBO DNAse (ThermoFisher Scientific, Cat# AM1907) was then used to degrade DNA contaminants according to the manufacturer's instructions, and the reaction was stopped by adding the provided Inactivation Buffer.

Reverse Transcription

First, a mix of 500 µM deoxynucleotide triphosphate (dNTPs) (ThermoFisher Scientific, Cat# R0191), 50 ng of random hexamers (ThermoFisher Scientific, Cat# SO142), and up to 13.2 µL RNA, such that all reverse transcription reactions had the same amount of input RNA, as measured by nanodrop, were incubated at 65°C for 5 min. First-Strand Buffer diluted to 1X (ThermoFisher Scientific, Cat# 18080-093), 50 µM Dithiothreitol (DTT), 50 units of RNAse OUT (ThermoFisher Scientific, Cat# 10777019), and 60 units of SuperScript III Reverse Transcriptase (ThermoFisher Scientific, Cat# 18080-093) were then added before incubation in a thermocycler for 5 min at 25°C, 1 hour at 50°C and 15 min at 70°C (for inactivation). A control sample lacking template was included. Finally, 10 µg/mL RNAse A (ThermoFisher Scientific, Cat# EN0531), was used to degrade all the RNA using a 20 min incubation at 37°C before the products were diluted 1:10 for quantitative PCR.

qPCR

The following mix was prepared: Forward and Reverse primer (**Table 2.3**) each at 500 nM, PowerUp SYBR Green Master Mix (ThermoFisher Scientific, Cat# A25741) diluted to a 1X concentration, DNA (varying concentrations depending on the assay), supplemented with nuclease-free water up to a total volume of 10 µL. Samples was incubated in an QuantStudio 6 Flex System PCR machine, using the following programme: 2 min at 50°C, followed by activation for 10 min at 95°C, then 40 cycles of 15 seconds at 95°C and 1 min at 60°C; computing the melting curve then consisted of ramping up the temperature from 60°C to 95°C and measuring fluorescence at every 0.1 °C increment. The quantity of fragments was measured in both biological and technical triplicates. Where possible, primers were selected from Primer Bank *(https://pga.mgh.harvard.edu/primerbank/*) as these have already been validated. In other cases, primers were designed using Primer Blast

(*https://www.ncbi.nlm.nih.gov/tools/primer-blast/index.cgi*). SYBR-Green qPCR analysis was then performed using the QuantStudio™ 6 Flex Real-Time PCR System in accordance with the manufacturer's protocol. Transcription levels were normalized to expression of the average of *glyceraldehyde 3-phosphate dehydrogenase* (*gapdh)* and *peptidylprolyl isomerase A (ppia)* expression.

2.8 Fluorescence-Activated Cell Sorting

Cells were separated using the NIHR Cambridge BRC Phenotyping Hub's BDBioscience's BD FACSARIA (AriaIII and Aria-Fusion). OP9 cells were labelled with a fluorescently tagged antibody detecting DLL-1 to sort for OP9 cells expressing this protein (for antibodies see **Table 2.4**) in 100 µL FACS Buffer (PBS supplemented with 1% BSA) for 30 min at 4^{o}C, before being washed twice in FACS Buffer collecting cells by centrifugation at 200 g for 5 min at 4°C. In the case of CRISPR, cells were separated according to positivity for GFP or mCherry expression, while for and HEK293FT/OP9-DL1 co-cultures, cells were stained for Notch1 using a PE-conjugated antibody (see **Table 2.4**).

A FACSCalibur (BD) was used to analyse cells stained either for AV-PI or intracellular PI. Cells were first plotted by Side-Scatter vs Forward-Scatter to gate on the live cells, followed by Forward-Scatter-Height vs -Area to gate on singlets. Cells were then plotted either on an AV vs PI plot to determine the ratio of cells which were AV and PI negative, AV positive and PI negative, AV and PI positive, AV negative and PI positive, using an unstained control sample to determine the AV and PI negative population. Samples were analysed in technical and biological triplicates.

In the case of Intracellular PI, cells were directly plotted on PI-intensity vs number of events to determine the ratio of cells in Sub-G0, G0, G1, S and M phases. Samples were analysed in technical and biological triplicates.

2.9 Golden Gate Assembly

sgRNAs were cloned into the sgRNA expression vector FgH1tUTG (Addgene Cat# 70183, kind gift from Marco Herold) as previously described (Joung *et al*, 2017). Briefly, a pair of 25 nt oligonucleotides (See **Table 2.3**) containing 4-bp overhangs for the forward (TCCC) and complementary reverse (AAAC) sequences were designed and generated to enable cloning into the Bsmb-I site following their phosphorylation and annealing.

To clone oligonucleotides into sgRNA backbones, Golden Gate assembly was used. Oligonucleotides were first annealed and phosphorylated, by mixing 10 µM each of the Forward and Reverse oligonucleotides, 10 Units T4 Polynucleotide Kinase (ThermoFisher Scientific, Cat# EK0031), and T4 Ligation Buffer diluted to 1x (NEB, Cat# M0202), topped up with nuclease-free water to a total volume of 10 µL. The mixture was incubated in a thermocycler for 30 min at 37^{o}C, then 5 min at 95^{o}C, before

the temperature was decreased to 25°C at 5°C per min. Products were diluted 1:10 for golden gate assembly. The Golden Gate assembly itself consisted 1 mM DTT (ThermoFisher Scientific, Cat# R0861), 0.1 mg/mL Bovine Serum Albumin (BSA, ThermoFisher Scientific, Cat# AM2616), T4 Ligase Buffer diluted to 1X, 1 ng/µL of the backbone plasmid, 10 units of BsmBI (NEB, Cat# R0580), 400 units of T4 DNA Ligase (NEB, Cat# M0202), and 1 µL of the diluted, annealed oligonucleotides as described above, topped with up nuclease-free water to a total volume of 25 µL. The mix was cycled in a thermocycler for 15 cycles of 5 min at 37°C followed by 5 min at 20°C before 2 µL of the product was transformed (as detailed in 2.12) and sequenced to verify that the oligonucleotides were cloned as expected using a H1-Tet primer.

Name	Provenance	Application	Quantity used
PE-conjugated DLL-1	ThermoFisher Scientific, Cat# 12-5767-80	FACS	0.2 µg
Notch1	BioLegend, Cat# 629105	FACS	0.4 µg
Notch1	Biolegend, Cat# 629101	Western Blot	1:500
α-tubulin	Sigma-Aldrich, Cat# T9062	Western Blot	1:2500
HRP anti-rabbit IgG	CiteAb, Cat# P0161	Western Blot	1:10000
HRP anti-mouse IgG	CiteAb, Cat# P0448	Western Blot	1:10000
phospho-ALK (Tyr1278)	Cell Signaling Technology, Cat# 6941S	Western Blot	1:1000
ALK	Cell Signaling Technology, Cat# 3633S	Western Blot	1:1000
STAT3	Cell Signaling Technology, Cat# 4904SS	Western Blot	1:1000
STAT3	Cell Signaling Technology, Cat# 9139	ChIP	3 µg
GFP	Abcam, Cat# ab290	ChIP	3 µg
Notch1	eBioscience, Cat#14578581	IHC	1:80

Table 2.4: Antibodies and concentrations used in this thesis. IHC = Immunohistochemistry, IgG = Immunoglobulin G

2.10 *notch1* Cloning & Site-Directed Mutagenesis

notch1 plasmid cloning

The full-length *notch1* complementary DNA (cDNA) was obtained from the Aster lab (Harvard Cancer Center), already cloned into the backbone pCDNA3 plasmid (Addgene, Cat# 2092).

To clone the *notch1* gene into the viral vector-containing plasmid pLJM1-EGFP, 1 µg of pLJM1-EGFP (Addgene, Cat# 19319) was digested with 10 units of AgeI-HF (NEB, Cat# R3552) and 10 units of BstBI (NEB, Cat# R0519) in 1X CutSmart Buffer (NEB, Cat# R3552 or R0519) in a total volume of 25 µL in nuclease-free water for 4 hours at 37^{o}C. The product was then loaded into a 1% Agarose gel, the relevant band excised and purified using a Monarch DNA Gel purification kit (NEB, Cat# T1020S) according to the manufacturer's instructions.

Second, the *notch1* cDNA fragment was amplified from the pcDNA3 plasmid vector using the following mix: 1 unit Q5 Polymerase (NEB, Cat# M0491S), 1X Q5 Polymerase Buffer, 1X GC enhancer 200 µM dNTPs, 500 nM of each forward and reverse primer, 1 ng of the *notch1*-containing plasmid, and nuclease-free water to a total volume of 50 µL. The mix was incubated in a thermocycler using the following programme: 30 seconds at 98^{o}C followed by 35 cycles of 7 seconds at 98^{o}C and 8 min at 72^{o}C, followed by a final extension of 10 min at 72^{o}C. The products were separated by gel electrophoresis and purified as described above. The forward and reverse primers (see **Table 2.3**) were designed to include the first and last 20 nucleotides of the *notch1* cDNA respectively, with the 6 nucleotide recognition sites of AgeI and BstBI at each end, followed by 6 nucleotides randomly chosen to optimize the primer melting temperature (so as to reach the lowest melting temperature possible, while achieving similar melting temperatures for both oligonucleotides).

Finally, the ligation mix of 25 ng of digested pLJM1-EGFP, 100 ng of the *notch1* fragment, 10 units of T4 DNA Ligase (NEB, Cat# M0202) in 1X T4 Ligation Buffer, nuclease-free water up to a total volume of 20 µL was incubated at 16^{o}C overnight. The ligated products were then transformed as described in 2.12.

Site-Directed Mutagenesis

Primers for site-directed mutagenesis were designed using Agilent's online tool (*https://www.genomics.agilent.com/primerDesignProgram.jsp*) and are detailed in **Table 2.3**. A mix of 100 ng of the plasmid vector, 2 units Pfu turbo DNA Polymerase (ThermoFisher Scientific, Cat# EP0571), DNA Polymerase Buffer diluted to 1X (ThermoFisher Scientific, Cat# EP0571), 125 ng of each forward and reverse primer and 200 µM dNTP mix, with nuclease-free water up to a total volume of 50 µL was prepared.

The mix was incubated in a thermocycler at 95°C for 30 seconds, then for 14 cycles of 30 seconds at 95°C, 1 min at 55°C, and 24 min at 68°C. After the cycle was completed, 10 units of DpnI (ThermoFisher Scientific, Cat# FD1703) was added, and the reaction mix was incubated at 37°C for 1 hour, to digest the parental plasmid. The product (2 µL) was then transformed into XL-10 Gold bacteria (Agilent, Cat# 200314) as described in 2.12, after which the plasmid DNA extracted and sequenced to verify the presence of the desired mutation. For sequencing primers used, see **Table 2.3**. The concept for site-directed mutagenesis is sketched out in **Figure 2.1**.

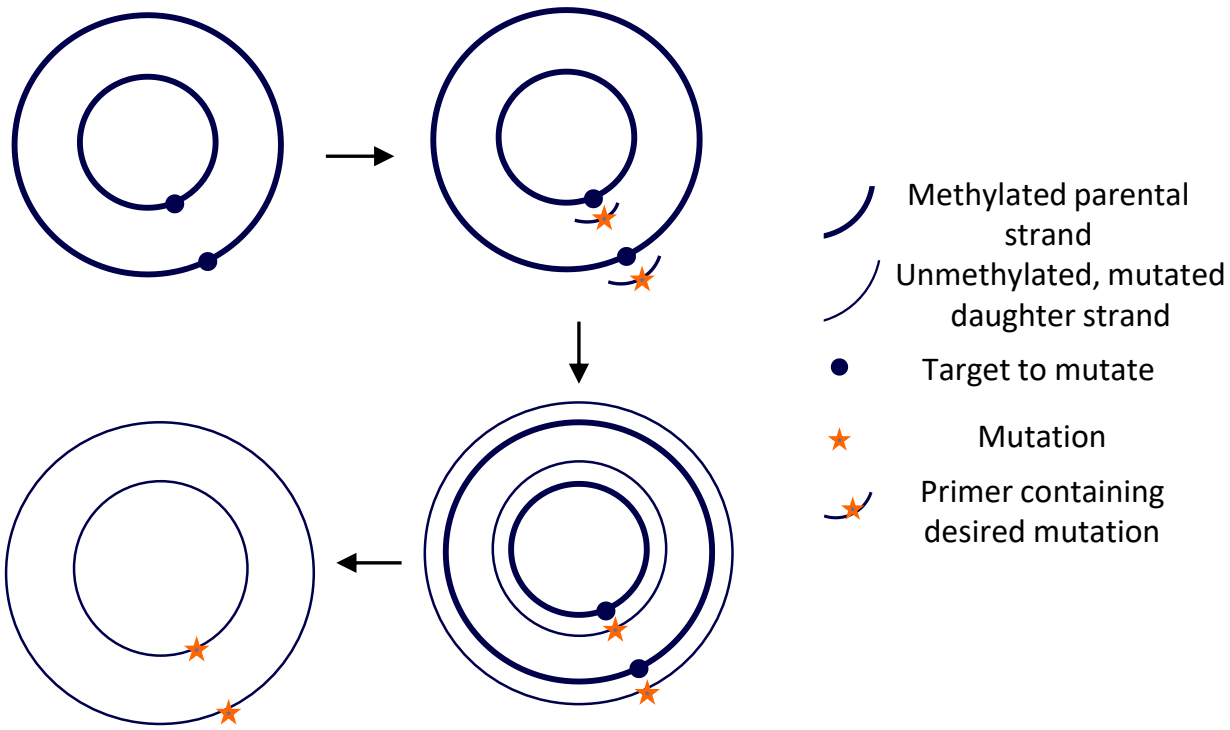

Figure 2.1: Site-Directed Mutagenesis methodology. The parental strain containing the nucleotide to be mutated is replicated using primers containing the mutation, before the methylated parental strand is digested to leave only the unmethylated, mutated daughter plasmid.

2.11 droplet digital PCR

Fractional abundance of mutations was analysed using BioRad's ddPCR suite of machines: the QX200 Droplet Generator, the PX1 PCR Plate Sealer, the C1000 Touch Thermal Cycler, and the QX200 Droplet Reader.

First, 70 µL of Droplet Generation Oil for Probes (Biorad, Cat# 1863005), and a mix of 1X ddPCR mix for Probes (no dUTP) (Biorad, Cat# 1863023), 1X of Fam/Hex ddPCR Mutation Assay (Biorad, Cat# 10049047, Assay # dHsaMDS123542085), made up to a final volume of 20 µL with nuclease-free water was added to a DG8 cartridge (Biorad, Cat# 1864008). Cartridges were sealed with a DG8 Gasket

(Biorad, Cat# 1864008), and loaded into the droplet generator before 40 µL of the droplet mix was transferred into a 96-well plate, which was sealed with a pierceable foil seal (Biorad, Cat# 181404), and sealed using the Plate Sealer. Plates were then loaded into the Thermal Cycler, and incubated using the following cycle: 10 min at 95°C, 40 cycles of 30 seconds at 94°C, 1 min at 53°C, followed by a 10 min inactivation step at 98°C.

Plates were then loaded into the Droplet Reader, and samples were read. Results were analysed using the Biorad QuantaSoft Analysis Pro software. Samples were analysed in technical duplicates. Controls included a no template control, and both positive and negative controls for each of the two probes.

2.12 Transformation & Plasmid Extraction

Plasmids were transformed using NEB Stable E. coli (NEB, Cat# C3040), with the following protocol – except for transformation of the full-length *notch1* cDNA-containing plasmid which was conducted using Agilent's XL10-Gold Ultracompetent cells (Agilent, Cat# 200314), using the manufacturer's protocol.

NEB stable E. coli (50 µL) were incubated for 30 min on ice with 2 µL of the DNA to be transformed. The mix was then subject to a heat-shock at 42°C for exactly 30 seconds, before incubating for 5 min on ice. The mix was then supplemented with 200 µL of Super Optimal Broth with Catabolite repression (SOC) medium (ThermoFisher Scientific, Cat# S1797), before incubating at 30°C, on a shaking plate (220 rpm) for 1 hour. The bacteria were then plated on 100 µg/mL Ampicillin (ThermoFisher Scientific, Cat# A9518)-containing Lysogeny Broth (LB) agar plates and incubated overnight at 30°C.

A single colony was then isolated from the agar plate and propagated in LB supplemented with 100 µg/mL Ampicillin overnight at 30°C, on a shaking plate (220 rpm). The plasmids were then extracted from the bacteria using Qiagen's Plasmid Mini or Maxi Kit depending on the output amount required (Cat# 12123 and 12162, respectively), following the manufacturers' instructions. Samples were then sent of sequencing at the University of Cambridge Department of Biochemistry using the oligonucleotides listed in **Table 2.3**.

2.13 Oligonucleotides

Oligonucleotides were ordered from Sigma-Aldrich suspended in water at a concentration of 100 µM. Sequencing primers were designed using the Primer Basic Local Alignment Search Tool (BLAST) online tool (Y*e et a*l, 2012). For a complete list of primers used, see **Table 2.3**. Sequencing primers were designed to obtain PCR products approximately 500-800 base pairs in length. Primer GC content was restricted to 40-60%, and primer length was 17-22 base pairs. Primers for qPCR were primarily taken from the Primer Bank database of validated primers (Spandidos *et al*, 2010). See relevant Methods sections for the design of other oligonucleotides.

2.14 Western Blotting & Antibodies

Cells were collected by centrifugation at 100 g for 5 min at 4^{o}C before washing once in cold PBS, and resuspending in Pierce Radioimmunoprecipitation Assay (RIPA) buffer (Thermo Scientific, Cat# 89900) supplemented with Halt Protease and Phosphatase Inhibitor Cocktail (Thermo Scientific, Cat# 78441), and incubated on ice for 30 min. Centrifugation was then conducted at 16000 g for 10 min at 4^{o}C to remove cell debris. The protein content in the supernatant was determined using a Qubit protein assay (ThermoFisher, Cat# Q33211), according to the manufacturers' instructions. Finally, samples were diluted in Laemlli Buffer (10% SDS, 50% Glycerol, 25% β-Mercaptoethanol, 0.03% Bromophenol Blue and 200 mM Tris at pH 7) to generate solutions containing equivalent concentrations of proteins, before boiling at 100^{o}C for 5 min.

Samples were loaded onto a TGX 10% Acrylamide Gel (Bio-Rad Cat# 161-0173), prepared according to the manufacturer's instructions (incorporating 0.1% TEMED (National Diagnostics, Cat# EC503), and 0.03% Ammonium Persulfate (Bio-Rad, Cat# 161-700)) along with 2 µL of protein ladder (ThermoFisher Scientific, Cat# 26619). The gel was immersed in Running Buffer (25 mM Tris-HCl at pH 7, 200 mM Glycine, 0.1% SDS) at 70 V until the dye front reached the bottom of the gel. Proteins were transferred onto a 0.45 µm nitrocellulose membrane (Immobilon, Cat# IPVH00010) in 1X Transfer Buffer (Bio-Rad, Cat#10026938) using the Bio-Rad Trans-Blot Turbo system (7 min at 25 V and 1.3 A). The membrane was then incubated in 5% BSA (Acros Organics, Cat# 240405000) w/v in Wash Buffer (50 mM Tris-HCl at pH 7, 150 mM NaCl and 0.1% Tween-20) for 1 hour at room temperature. Membranes were then exposed to primary antibody overnight at 4^{o}C in 3% BSA w/v in Wash Buffer (antibodies are detailed in **Table 2.4**). The membrane was then washed in Wash Buffer three times for 10 min, before being exposed to HRP-conjugated secondary antibody in 3% BSA w/v in Wash Buffer (see antibodies and concentrations in **Table 2.4**) for 1 hour at room temperature. The membrane was again washed in Wash Buffer three times for 10 min. Finally, proteins were visualised following exposure to HRP substrate (Millipore, Cat# WBKLS0500) using a LAS4000 imager. Samples were analysed in biological triplicates.

2.15 Patient samples

Patient tumour tissues and matched peripheral blood DNA were obtained following informed patient/parental consent according to both the Declaration of Helsinki and local guidelines from the following institutions; Children's Cancer and Leukaemia Group tissue bank, Nottingham, UK; Institut Universitaire du Cancer Toulouse, France; University Hospital Brno, Czech Republic; Biobank of the Medical University of Graz, Austria; Belarusian Centre for Paediatric Oncology, Hematology and Immunology, Minsk, Belarus; Justus-Liebig University, Giessen, Germany; Our Lady's Children's Hospital, Crumlin, Ireland (**Table 2.5**). All tissues were obtained and processed with full ethical approval (NHS Research ethics committee reference numbers 07/Q0104/16, 06/MRE04/90 and 08/H0405/22+5).

Only samples from patients presenting with systemic ALCL (not cutaneous, for e.g.) were used for this study. **Table 2.5** summarizes the clinical data.

Characteristic	Subgroup	Number of patients
Gender	**Male**	20
	Female	25
	Unknown	58
Age at diagnosis	**0-15**	42
	16-25	11
	26-40	4
	>40	29
	Unknown	17
ALK Status	**+**	80
	-	23
Matched blood	**Yes**	23
	No	87
Follow-up known?	**5-year EFS known**	79
	5-year OS known	63
	No	24
Provenance	**UK**	50
	Crescenzo et al; SRP044708	7
	France	19
	Czech Republic	10
	Giessen	6
	Ukraine	8
	Graz	5

Table 2.5: Patient data.

2.16 Immunohistochemistry

Immunohistochemistry was performed on formalin-fixed paraffin-embedded (FFPE) sections with the conventional avidin–biotin–peroxidase method (Vector Laboratories, Cat# SP2001). In brief, heat antigen retrieval was performed using citrate buffer at pH 6.1. Endogenous peroxidases were quenched by incubating sections in 3% H_2O_2 in PBS for 10 min. Sections were incubated in primary antibodies diluted in 1% BSA in PBS at 4°C (**Table 2.4**) overnight followed by incubation with biotin-conjugated secondary antibodies at room temperature for 1 hour. Sections were then incubated with Horseradish Peroxidase (HRP) using IDtect Super Stain System–HRP (following the manufacturer's protocol; Empire Genetics, Cat# ID851007) and developed under visual control using the AEC substrate kit (BD Pharmingen, Cat# 551015). Hemalaun counterstaining was performed before mounting coverslips with AquaTex (Merck, Cat# 108562). Sections were washed with PBS 3 times for 20 min at room temperature between every step. Stained slides were assessed by an experienced pathologist (blindly with respect to clinicopathological parameters and patient outcome). Quantification of the slides was determined using the histoscore system: stained slides were scored for both the intensity and percentage of positively staining cells (0 negative, 1+ weak, 2+ moderate and 3+ strong staining). Positive staining was considered 2+ if present in >1% of cells. The Histoscore was then calculated by multiplying the intensity by the percentage of positively stained cells. The Kaplan-Meier method was used to compute the EFS or OS, while the statistical differences between patient groups was derived using the log-rank test using the PRISM software.

2.17 DNA extraction & Sanger sequencing

DNA Extraction

To extract DNA from cell lines, frozen or FFPE tumour samples, the Qiagen's DNeasy Blood & Tissue Kit (Cat# 69504) was used according to the manufacturers' instructions. The only modification on the manufacturer's protocol was the elution of DNA (in 20 µL of DNAse-free water) three times consecutively into separate Eppendorf tubes to ensure all DNA had been eluted from the column.

Sanger Sequencing

DNA fragments were amplified using a solution of 5 units of DeamTaq polymerase (ThermoFisher Scientific, Cat# EP0702), Polymerase Buffer diluted to 1X, 100 µM dNTP mix (ThermoFisher Scientific, Cat# R0191), 200 nM of each Forward and Reverse primers (**Table 2.3**), and 1 ng of template DNA (where PCRs failed due to poor quality DNA, input amount was increased to 20 ng), topped up with nuclease-free water to a total volume of 25 µL. The programme used was; 1 min at 95°C, followed by 35 cycles of 30 seconds at 95°C, 30 seconds at 64°C, and 45 seconds at 72°C, followed by a final extension of 10 min at 72°C.

Primer dimers and other contaminants were removed from the reactions using 0.5 µL ExoSAP-IT (ThermoFisher Scientific, Cat# 78200.200), 3.5 µL of 10X GeneAmp PCR Buffer II (ThermoFisher Scientific, Cat# N8080010), and 1.5 µL of the PCR product as detailed above. This mix was incubated for 15 min at 37°C, followed by 15 min at 80°C.

PCR products were then labelled using the BigDye Terminator v3.1 Cycle Sequencing Kit (ThermoFisher Scientific, Cat# 4337455), using a mix of 0.35 µL of BigDye, 1.75 µL of the provided sequencing buffer, 0.4 µM of the Forward primer, and 2 µL of nuclease-free water, which, added to the previous 5.5 µL of ExoSAP-IT product, led to a total volume of 10 µL. This mix was incubated in a thermocycler for 1 min at 95°C, followed by 25 cycles of 20 seconds at 96°C,15 seconds at 50°C, 1 min at 60°C, before a one-off 4 min incubation at 25°C.

Samples were then purified prior to sequencing using the Dynabead Sequencing clean-up kit (ThermoFisher Scientific, Cat# 66101) whereby 13 mL of 96% Ethanol was added to a fresh bottle of Dynabeads before 20 µL of Dynabead solution was added to each sequencing reaction. Samples were mixed and incubated at room temperature for 5 min. The samples were then collected by centrifugation at 500 g for 10 seconds before placing on a magnetic plate (ThermoFisher Scientific, Cat# 12331D) for 1 min, before being subject to centrifugation upside-down at 100 g for 10 seconds to remove supernatant. Next, 100 µL of 85% ethanol was added to wash the samples before incubating at room temperature for 5 min. Samples were then collected by placing on a magnetic plate for 1 min before being subject to centrifugation upside-down again. The samples were allowed to air-dry for 10 min before adding 30 µL of nuclease-free water and mixing thoroughly, incubating at room temperature for 5 min and placing on the magnetic plate for 1 min. Finally, 25 µL of the eluant was transferred to a MicroAmp sequencing plate (ThermoFisher Scientific, Cat# N8010560). Samples were sequenced using a 48 capillary ABI 3730 DNA sequencer (ThermoFisher Scientific). Sanger traces were analysed using the SeqScanner 2 software (Applied Biosystem).

2.18 Whole Exome Sequencing

DNA was extracted from patient tissue or blood (chapter 2.17). Only samples of fresh frozen tissue with a high tumour content (>90%) as determined by a histopathologist were sent for exome sequencing. Samples were sent either to the University of Ha'il (Kingdom of Saudi Arabia), or to the Washington State University sequencing core (United States) for library preparation and whole exome sequencing in two different batches (see **Table 2.6**). Sequencing files are available online at the Sequence Read Archive (*https://www.ncbi.nlm.nih.gov/sra*) under accession PRJNA491296.

Source	Library Prep Kit	Sequencing machine	Matched blood available	ALK status	Number of samples
Crescenzo et al; SRP044708	SureSelect 50 Mb All Exon kit	Illumina HiSeq 2000	Yes	+	7
New samples, from UK tissue bank	Nextera Rapid Capture Exome	Illumina HiSeq 2500	Yes for 4 of 5	+	5
Samples from ALCL99 sequenced previously, from UK tissue bank	Nextera Rapid Capture Exome	Illumina MiSeq	No	+	13

Table 2.6: WES Sequencing and library preparation detail from fresh frozen tumour tissue.

2.19 Bioinformatic analysis (full pipeline detailed in Chapter 3)

Briefly, reads were analysed using FastQ, before quality trimming was performed to remove any base pair at the end of each read with a quality score below 30. Reads from these and the 18 *de novo* sequenced samples were aligned to a reference genome (version hg38) using Burrows-Wheeler Alignment ('bwa-mem' version 0.7.12-5) employing default settings; duplicates were marked and removed using Picard (version 2.5.0). SNVs (Single-Nucleotide Variants) were called using CaVEMan (Turinsky et al, 2008) (version 1.9.5) and InDels (Insertions and Deletions) using Pindel (Ye et al, 2009) (version 0.2.5b8), following which SNVs and InDels were annotated using Annovar (Wang et al, 2010). Variants contained in any of the 11 matched peripheral blood samples were filtered out from all samples. Variants identified as present in the population at a frequency of > 0.1% as determined by dbSNP (build 148) and the 1000 Genome project (phase 3 release) were also filtered out. Variant Effect Prediction scores were compiled using prediction software CADD (Kircher et al, 2014), FATHMM (Shihab et al, 2013), LRT (Chun & Fay, 2009), MutationAssessor (Reva et al, 2011), MutationTaster (Stenson et al, 2009), SIFT (Vaser et al, 2016), PROVEAN (Choi et al, 2012) and Polyphen (Ramensky et

al, 2002). Variants predicted to be benign based on this compiled score and the MetaLR/MetaSVM databases were filtered out.

Mutational signatures were derived with the 'deconstructSigs' R package (Rosenthal *et al*, 2016).

2.20 Chromatin Immunoprecipitation-sequencing & ChIP-qPCR

Browser Extensible Data (BED) files were downloaded from the GSE archive (accession GSE117164 (Menotti *et al*, 2019) for STAT3 ChIP-seq, GSE104261 (Choi *et al*, 2017) and GSE29600 (Wang *et al*, 2011a) for NOTCH1 and NOTCH3). Files were sorted using BEDTools ('sort'), then converted into BEDGraph using BEDTools ('genomecov'), and then into BigWig track files using UCSC's 'bedgraphToBigWig'. The genome browser tracks were visualized in IGV (v2.3.92).

ChIP-qPCR analysis for Notch1 was performed with 10 million ALCL cells per sample using an anti-STAT3 (Cell Signalling, Cat# 9139) or anti-GFP antibody (Abcam, Cat# ab290). Following treatment with 1 µM crizotinib or dimethyl sulfoxide (DMSO) for 3 hours suspended in RPMI 1640 supplemented with 10% FBS, 1 x 10^7 cells were fixed with 0.75% formaldehyde for 15 min using orbital shaking at room temperature. Subsequently, glycine was added to a final concentration of 125 nM and cells were incubated for 5 min at room temperature. Next, cells were washed twice with cold PBS, collected by centrifugation at 100 g for 5 min at 4°C and flash frozen using liquid nitrogen and stored at -80 °C until use. Cell pellets in which DNA had been cross-linked as detailed above were lysed in 650 µL ChIP lysis buffer (50 mM HEPES-KOH pH 7.5, 140 mM NaCL, 1 mM EDTA pH8, 1% Triton X-100, 0.1% Sodium Deoxycholate and 0.1% SDS) supplemented with cOmplete™ Mini EDTA-free Protease Inhibitor Cocktail (Roche, Cat# 11836170001) at the manufacturer's indicated concentration, followed by sonication for a total of 10 min using 30 seconds on/off pulses. Immunoprecipitation reactions were performed overnight with 3 µg STAT3 or GFP antibodies rotating at 4 °C. Next, antibodies and chromatin were captured on 50 µL of Protein G Dynabeads (Thermo Scientific, Cat# 10004D) for 2 hours at 4 °C. Following capture, the bead-chromatin complexes were washed three times in Low Salt Buffer (0.1% SDS, 1% Triton X-100, 2 mM EDTA, 20 mM Tris-HCL pH 8.0, 150 mM NaCL), followed by three washes in High Salt Buffer (0.1% SDS, 1% Triton X-100, 2 mM EDTA, 20 mM Tris-HCl at pH 8, 500 mM NaCL), two washes in Lithium Chloride Buffer (0.25 M LiCL, 1% NP-40, 1% Sodium Deoxycholate, 1 mM EDTA, 10 mM Tris-HCl at pH 8) and two final washes in TE Buffer (10 mM Tris pH 8.0, 1 mM EDTA). DNA was eluted into 200 µL elution buffer (1% SDS, 100 mM $NaHCO_3$), RNA was digested using 2 µL RNase A (10 mg/mL, Roche, Cat# 10109169001) at 37 °C for 30 min, before reversing cross-linking by incubating at 65°C for 2 hours with 2 µL proteinase K (20 mg/mL, Thermo Scientific, Cat# EO0491). De-cross-linked DNA was purified with a Zymo DNA Clean and Concentrator-5 kit (Zymo research, Cat# D4003) according to the manufacturer's instructions. ChIP and input DNA were analysed by SYBR-Green qPCR performed using a QuantStudio™ 6 Flex Real-Time PCR System in accordance with the

manufacturer's protocol using qPCR primers (**Table 2.3**) from a published ChIP-seq dataset (Menotti *et al*, 2019).

2.21 Microarray analysis

Microarray files were downloaded from the GSE archive (accession GSE5827 (Sanchez-Martin *et al*, 2017), GSE104261 (Choi *et al*, 2017) and GSE29600 (Wang *et al*, 2011a)) and analysed using NCBI's GEO2R online pipeline (Wilhite & Barrett, 2012), by creating a group for samples treated with vehicle control (DMSO), and another for samples treated with GSI. The top 250 hits (according to adjusted p-values) were then extracted from GEO2R; hits present in at least two of the three datasets were retained for display on a heatmap.

2.22 Statistical analyses and Graphing

All experiments were executed in biological triplicates. The MTT, RealTimeGlo, Apoptosis, Cell Cycle and qPCR assays were additionally conducted in technical triplicates. Unless indicated otherwise, all plots are representative of the mean of the biological replicates, while the error bars represent the standard deviation. Two-tailed t-tests were used to calculate the p-value when comparing two samples (multiple comparisons were corrected using the Holm-Sidak method); when comparing more than two samples, two-way ANOVA was used (again, multiple comparisons were corrected using the Holm-Sidak method). The log-rank test was used to compute the statistical difference between sub-groups of patient EFS or OS. All statistical tests were conducted using GraphPad PRISM 8 (GraphPad).

3. DNAseq analysis of 25 ALK+ ALCL patient samples

3.1 Introduction

ALK fusion proteins induce the activation of several downstream signalling pathways involved in the oncogenesis of ALCL. Beyond this however, as mentioned previously, no published study has shown further significant genetic abnormalities in ALK+ ALCL. Indeed, there is little literature about the genomics of ALCL beyond the papers published by Youssif *et al.*, Salaverria *et al.*, and *Crescenzo et al*. Youssif, Salaverria and colleagues performed array comparative genomic hybridization on ALK+ ALCL and recorded a few gains and losses, though by and large found the genome to be stable, as large-scale studies of paediatric cancers have also shown (Gröbner *et al*, 2018). Some years later, Crescenzo and colleagues looked at the genome of ALK- ALCL in more detail, performing WES, and showed that a sub-section of ALK- ALCL patients presented with mutations of the JAK/STAT3 pathway, as well as chimeras involving transcription factors NFκB2 and Nuclear Receptor Corepressor 2 (NCOR2), and tyrosine kinases ROS1 and Tyrosine Kinase 2 (TYK2). Indeed, these discoveries proved to have potential therapeutic implications, as inhibition of the JAK/STAT3 pathway was shown to inhibit cell growth both in ALK- ALCL cell lines and mouse models. This chapter presents data regarding the genome of ALK+ ALCL from 18 tumours sequenced within this project combined with data from 7 samples of published cases of ALK+ ALCL (Crescenzo *et al*, 2015). The bioinformatic processing and the results we obtained from this analysis are presented in this chapter.

3.2 Whole Exome Sequencing

The genomic data analysed in this thesis is composed of three separate datasets (**Table 2.6**); sequencing data for the first set of samples, composed of 7 adult ALK+ ALCL with matched peripheral blood, were retrieved from an online repository as detailed in chapter 2 (Crescenzo *et al*, 2015). Two further datasets were produced from patient samples, which were sequenced in individual batches resulting in a range of read lengths and coverage (**Figure 3.2.1**, **Table 3.1**). These two batches of samples were derived from tumour tissue banked within the CCLG paediatric cancer tissue bank, most isolated from children entered into the ALCL99 trial (**Table 2.5, Table 2.6**) and therefore receiving a consistent therapeutic protocol.

Sample Name	Average number of reads	Average Length of reads (bp)	Coverage
S1	4.96E+07	75	176.7
S2	1.60E+07	75	57.2
S3	4.68E+07	75	156.0
S4	1.69E+07	75	59.7
S5	4.20E+07	75	149.9
S7	4.26E+07	75	152.4
S9	2.21E+07	75	73.6
S11	2.45E+07	75	87.3
S12	5.48E+07	75	195.3
S13	2.32E+07	75	82.5
S14	4.96E+07	75	176.7
S15	1.33E+07	75	44.3
S16	4.96E+07	75	176.7
S18	6.41E+07	100	284.8
S23	3.68E+07	100	163.4
S23B	8.05E+07	100	357.9
S26B	6.06E+07	100	269.39
S26	4.21E+07	100	187.02
S28B	6.96E+07	100	309.39
S28	5.73E+07	100	156.00
S28n	5.69E+07	100	252.9
S28nB	6.53E+07	100	290.2
S31	3.87E+07	100	172.1
S31B	5.99E+07	100	266.1
S32	4.21E+07	100	187.0
S32B	3.70E+07	100	164.3
S57B	5.29E+07	100	235.07
S57	5.14E+07	100	228.53
S67B	5.38E+07	100	156.00
S67	5.03E+07	100	223.40
S71B	5.17E+07	100	229.95
S71	5.44E+07	100	241.77
S75B	5.08E+07	100	225.83
S75	4.74E+07	100	210.48
S90B	3.80E+07	100	156.00
S90	2.07E+07	100	92.04

Table 3.1: Initial WES output. Detail of the number of reads, read length and coverage obtained for each sample processed by WES.

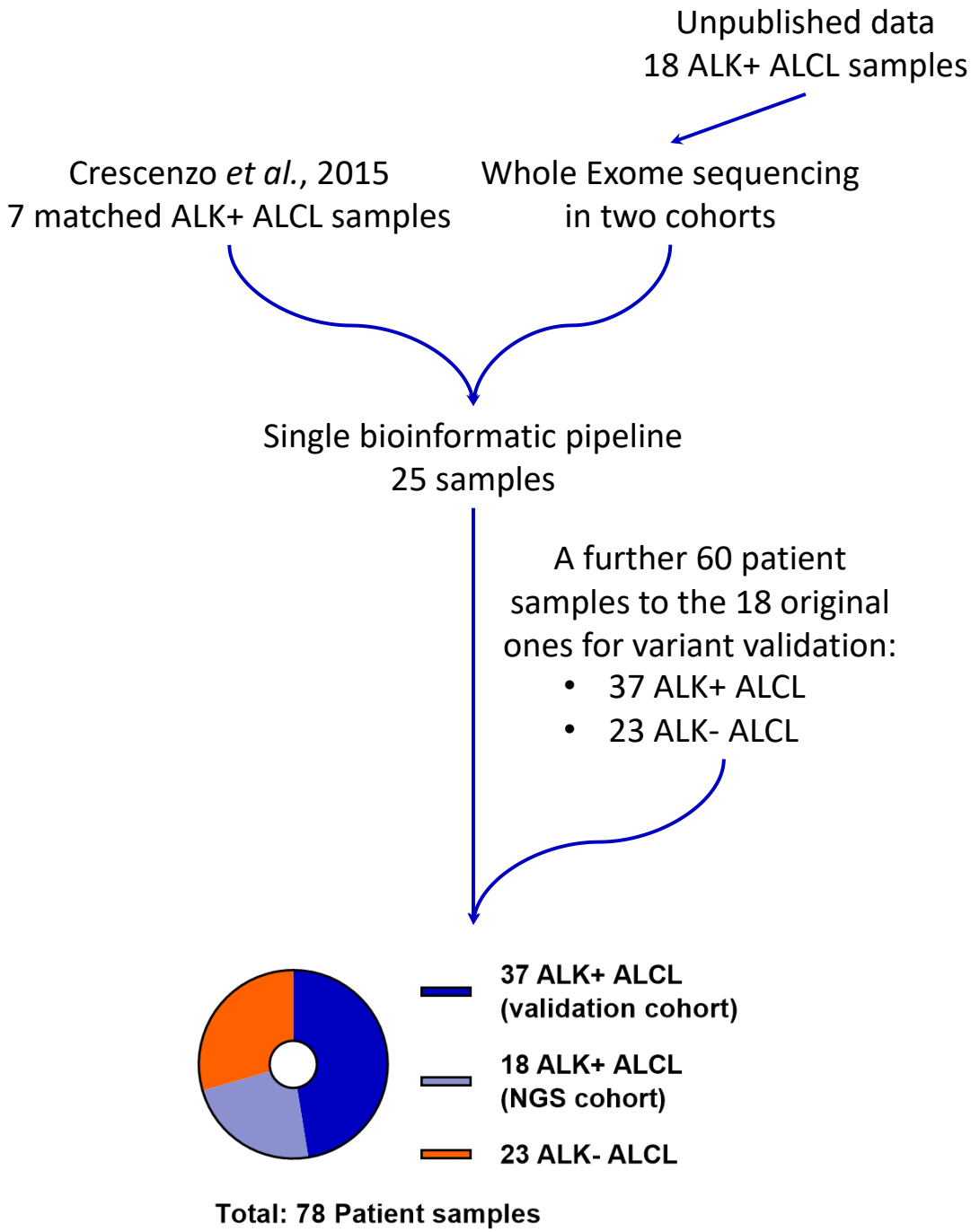

Figure 3.2.1: Schematic of the patient samples used in this study. This includes not only the patient samples analysed by WES but also the patient samples then used for validation of the variants as detailed in Chapter 3.6.

3.3 Bioinformatic processing

Following sequencing, the FastQ files were analysed using FastQC for quality control; a representative samples' read length distribution is shown (**Figure 3.3.1A**), with a vast majority of reads along the expected size (as detailed in **Table 3.1**), and a long tail of shorter reads. Some of the reads were of too low a quality to process further (as defined by an average quality score under 30; **Figure 3.3.1B**). Reads were therefore trimmed using 'fastx_quality_trimmer', by removing all calls with individual quality scores inferior to 30, starting from the end of the read, until reaching a call with a score of 30 or above. The result of this quality trim is displayed (**Figure 3.3.2**), which had the main effect of increasing the mean, and upper and lower quartile quality scores of the end of the reads. Trimming also caused an increase in the average quality score (by both decreasing the amount of reads with a low-quality score and increasing the amount of reads with a high score; **Figure 3.3.3**). The shortest reads were also removed (any reads under 50 nucleotides in length were removed).

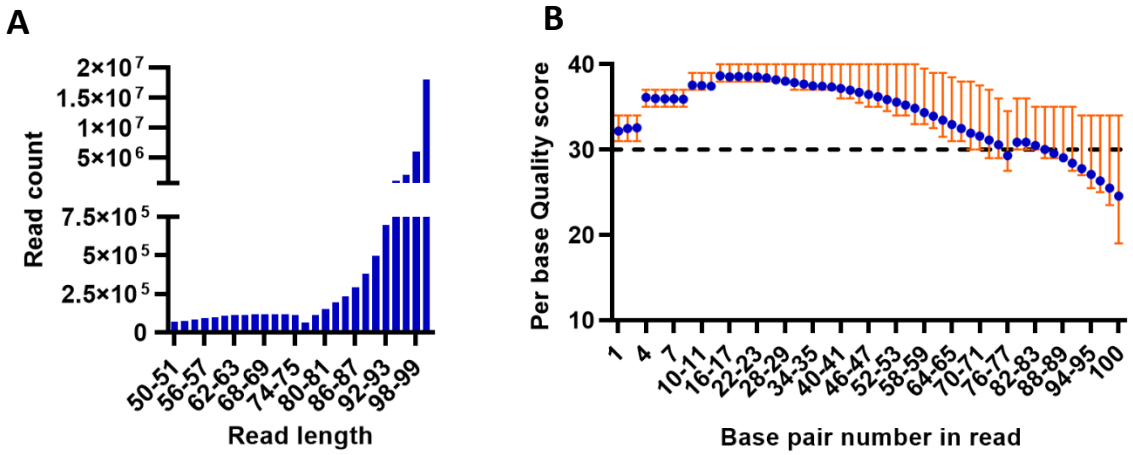

*Figure 3.3.1: Make-up of a representative read obtained from WES. Read length distribution **(A)** and Average, upper and lower quartile Quality scores **(B)** for each individual call.*

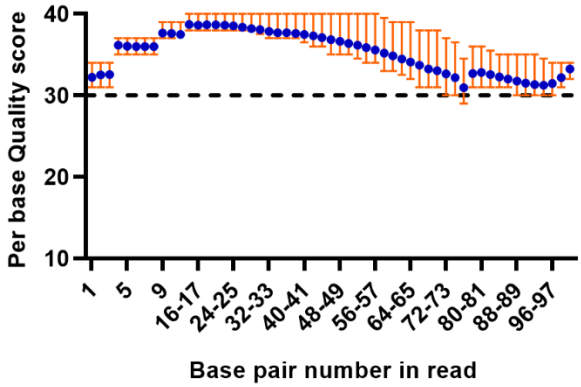

Figure 3.3.2: Post-trim average, upper and lower quartile Quality scores for each individual call.

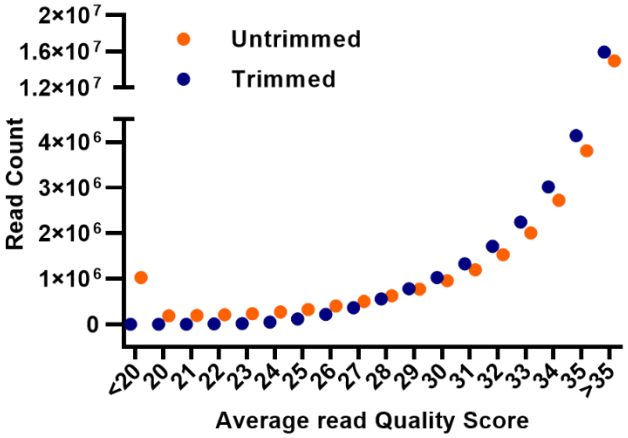

Figure 3.3.3: Number of reads for a given average read quality score.

The Burrows-Wheeler Alignment algorithm (Li & Durbin, 2009) ('bwa mem' version 0.7.12-5) was used to align reads to the reference sequence of the human genome (version hg38), which was indexed using the Burrows-Wheeler alignment tool, using default algorithm settings. The output of this was a collection of aligned files in the SAM format ('Sequence Alignment Map') which were translated into the BAM format ('Binary-compressed SAM file') using SAMtools (Li *et al*, 2009) to optimize storage space and speed up downstream processing of aligned files. These aligned files were then sorted and indexed (still using SAMtools), after which duplicate reads were removed and reads around known Insertion and Deletion (InDel) loci were realigned (using Picard's 'MarkDuplicates', 'RealignerTargetCreator' and 'IndelRealigner'), again using default algorithm settings (McKenna *et al*, 2010).

The coverage of the human exome was computed for each aligned file thus obtained. The average coverage for each file is presented (**Table 3.1**). There was relatively wide disparity between file coverage, though this is to be expected as the libraries and sequencing have different sources, and since the input DNA was of varying quality (some having derived from FFPE tissues; **Table 3.1**). However, coverage of the exons is satisfying, as shown using the example of the *notch1* gene of one representative patient sample (**Figure 3.3.4**).

InDels and SNVs were then called using two separate software packages; Pindel (Ye *et al*, 2009) and CaVEMan (Turinsky *et al*, 2008). With respect to Pindel, InDels on all chromosomes were called, and the same reference genome as above was used. A configuration file containing the required data (sample type and insert size) was required, as detailed in the software's manual. The output was then translated to the VCF format ('Variant Call Format') for downstream processing. All files were called in parallel to increase call accuracy – the output for all samples is saved in a single VCF file containing all sample information.

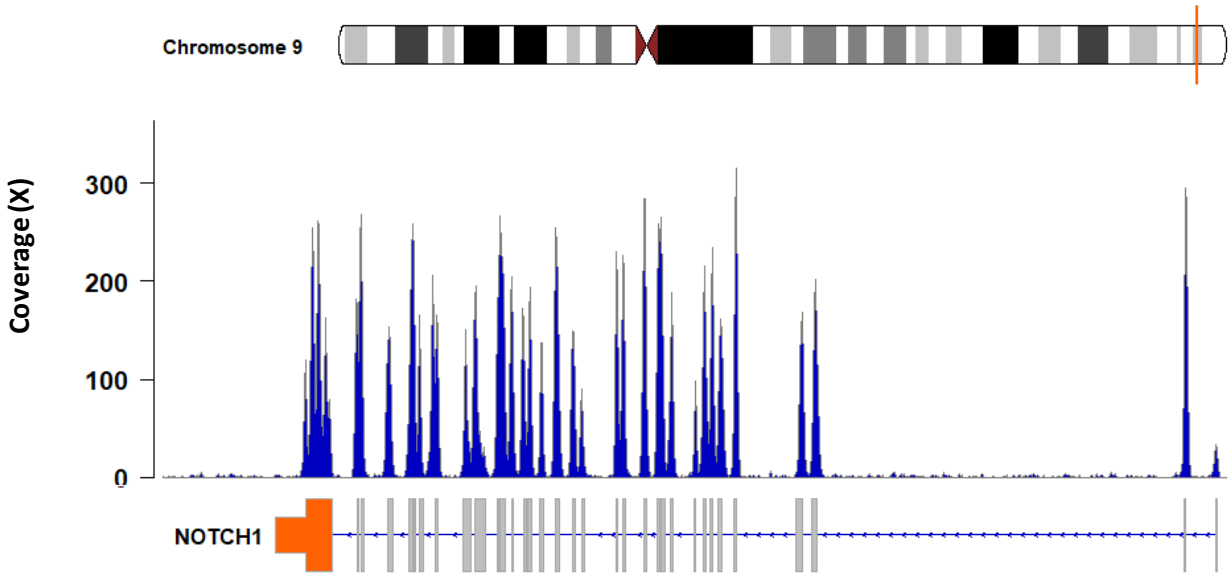

Figure 3.3.4: Coverage of a representative sample. Coverage is displayed for the gene notch1, for which exons are indicated in grey and UTR in orange.

With respect to CaVEMan, samples were called (where possible) against their peripheral blood counterparts to screen out germline variants (though each peripheral blood sample was called for SNVs using CaVEMan as well to analyse germline variants). CaVEMan requires the same reference genome, along with BED file ('Browser Extensible Data') defining non-exonic regions to be ignored. A file was compiled using all the intergenic regions as determined by the University of California Santa Cruz Genomics Institute. As opposed to Pindel, CaVEMan requires a number of steps for variant calling; setup, splitting (the files to be called into segments to be analysed), creating files for each segment and merging these, before finally calling variants. The resulting output was also in the VCF format, with one file per segment. Files were concatenated into a single file along with the corresponding result file for Pindel. As expected, a number of variants were found, for example those found in the locus of *notch1* (**Figure 3.3.5**).

These results were annotated using Annovar (Wang *et al*, 2010). The VCF files were converted to the Annovar input format using 'convert2annovar.pl', separating out all samples of the Pindel results file, and each of the CaVEMan results files. For each sample, the Pindel and CaVEMan results files were concatenated so each sample could be annotated individually. Annovar's 'table_annovar.pl' function was then used to annotate variants (both single nucleotide and indels), against the human genome (build hg38) as a reference. The variants were annotated against the refGene (build 77) (San Lucas *et al*, 2012), Catalogue of Somatic Mutations in Cancer (COSMIC, build 78) (Tate *et al*, 2019), AVSNP (build 147) and dbSNP (build 148) databases – while refGene was used as an Annovar gene-based annotation to describe the genes on which each variant was identified, the remaining databases were all filter-based variant annotation databases. Variants were also annotated against a number of variant

prediction databases: SIFT (Vaser *et al*, 2016), Polyphen (Ramensky *et al*, 2002), LRT (Chun & Fay, 2009), MutationTaster (Stenson *et al*, 2009), MutationAssessor (Reva *et al*, 2011), FATHMM (Shihab *et al*, 2013), PROVEAN (Choi *et al*, 2012), MetaSVM and MetaLR (Dong *et al*, 2015), CADD (Kircher *et al*, 2014), dbSNP (Sherry, 2001), 1000Genome (phase 3 release) (The 1000 Genomes Project Consortium, 2015), ExAc (Lek *et al*, 2016) and Clinvar (Landrum *et al*, 2016).

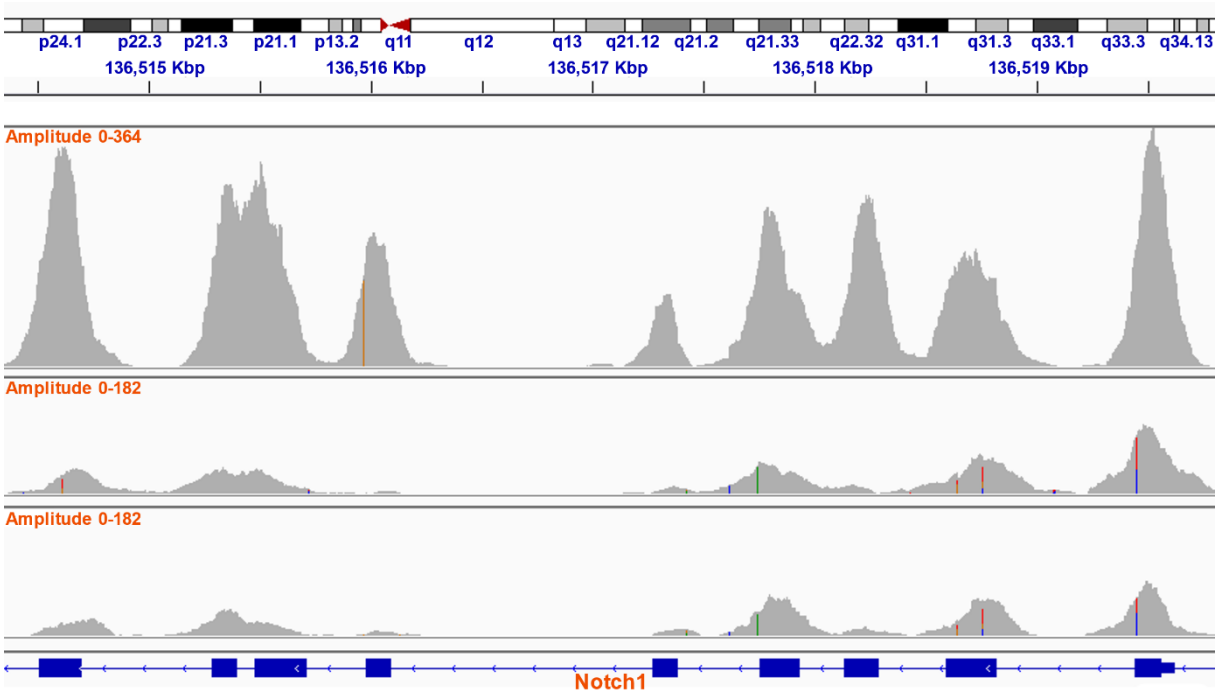

Figure 3.3.5: Variants in a locus of the notch1 gene in three representative samples. Coverage is indicated on a scale of 0 to 364X by the amplitude, representing the number of reads covering a particular locus. Colourful stacks of lines represent potential variants identified throughout the stack of reads at a certain locus. Coverage varied by sample as displayed here.

Variants identified as part of intronic, intergenic, untranslated regions or immediately upstream or downstream of a gene were filtered out, as none of the variant databases contained sufficient information to annotate these – particularly in terms of likelihood of them being pathogenic. Synonymous single nucleotide variants were also filtered, as unlikely to produce any significant biological changes. Highly variable genes with a low likelihood of pathogenicity were also screened out at this stage using published literature (Shyr *et al*, 2014). Following this, variants identified in any of the 11 matched peripheral blood samples were removed from all the other samples, to exclude germline variants.

Variants were then screened based on pathogenicity, using annotated variant effect prediction scores. Variants were filtered in two sets; those present in the MetaSVM and/or MetaLR databases, and those present in neither. Indeed, MetaSVM and MetaLR collate data from eleven function prediction

algorithms, three conservation prediction algorithms and four ensemble scores (Details can be found in Dong *et al*, 2015). Variants predicted to be damaging both by MetaSVM an MetaLR were retained, while others were filtered out. For variants not in the MetaSVM/MetaLR databases, custom scores combining 8 Variant Effect Prediction software programmes (SIFT, Polyphen, LRT, MutationTaster, MutationAssessor, FATHMM, PROVEAN, CADD) were derived: scores from each were translated to a 0-1 scale and averaged out, following which only variants with scores in the 10th most damaging percentile or above were retained.

The final filter eliminated SNPs identified as present in 0.1% or more of the population, as determined by dbSNP, the 1000 Genome and ExAc databases (variants annotated as present in the general population at a frequency of > 0.1% in any of the three databases were removed). A list of variants identified in at least 10% of our ALCL cohort is presented in **Appendix I**.

3.4 The ALCL genome: first insights

Having obtained a list of variants, the first step was to mine the data for insights as to the genomic make-up of ALCL. First, the average number of mutations per sample for each of the three sequencing cohorts was analysed, but no significant difference was found (as determined by One-way Anova; **Figure 3.4.1**), thereby eliminating the possibility of batch effects. However, there was a slight correlation between patient age and the number of mutations, whereby adult patients had more mutations than paediatric patients (**Figure 3.4.2A**). In fact, there is a small difference in the average number of mutations between the two groups (**Figure 3.4.2B**). This is in line with published literature: meta-analysis of paediatric cancers have consistently shown fewer somatic mutations than in adult cancers (Gröbner *et al*, 2018). Copy-number variations were also studied (only in samples for which we held matched peripheral blood; data not shown), but not copy-number variant (greater than 10000 bp) were found in more than one sample, in keeping with published literature (Youssif *et al*, 2009).

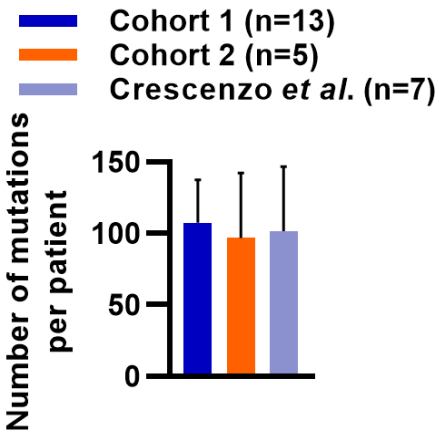

Figure 3.4.1: Number of mutations per patient for each sequencing cohort.

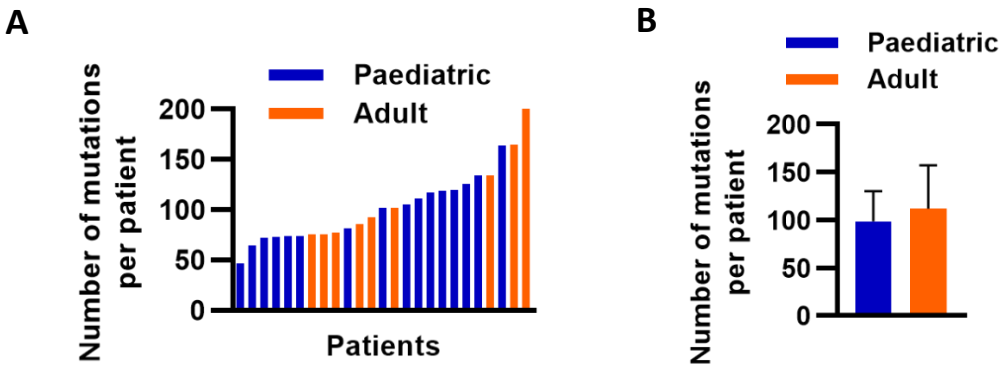

Figure 3.4.2: Correlation between number of mutations and patient age. ***A.*** *Number of mutations for each patient, in order from the highest to the lowest number of variants identified per patient, colour-coded by age (paediatric < 19, adult ≥ 19).* ***B.*** *Average and standard deviation of the number of mutations per patient for the paediatric (n=16; age <19) and adult (n=9; age 19 and over) cohorts (***p<0.0001; unpaired Student's T-test).*

Across all patients, the distribution of variants per chromosome is far from linear, though it correlates very closely with the number of genes per chromosome (**Figure 3.4.3**). This suggests a relatively silent genome, without high mutational loads on particular genes or loci since variants are spread evenly across chromosomes and are not specifically targeted at a few loci. Interestingly the distribution of somatic and germline variants per chromosome varies (**Figure 3.4.4**).

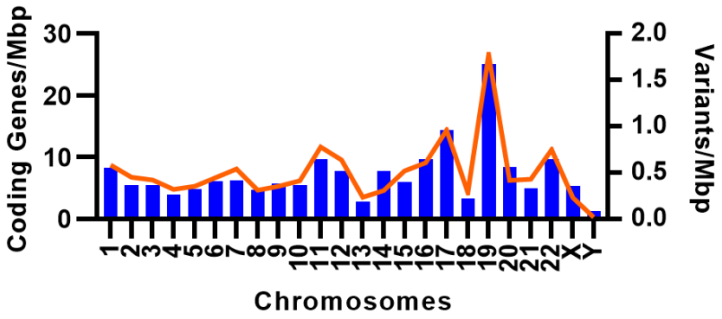

Figure 3.4.3: Mutational load per chromosome. Correlation between the number of genes per chromosome and the mutational burden per chromosome (expressed as the number of mutations per million base pairs).

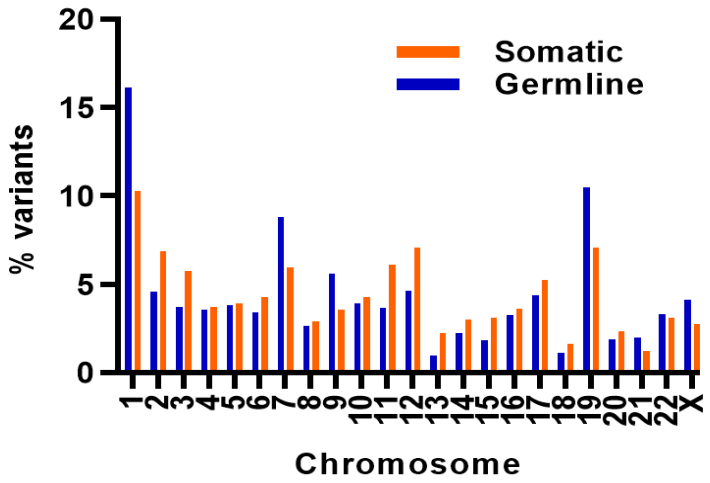

Figure 3.4.4: Mutational load per chromosome of germline and somatic samples.

3.5 Genomic signatures indicative of relapse risk

Considering the types of variants detected across all patients, 39.4% were non-synonymous SNPs, followed by frameshift and non-frameshift deletions, and splice variants (24.1%, 10.8% and 10.6% respectively) (**Figure 3.5.1A**). The distribution of variant types found in germline patients is markedly different, with a vast majority of non-synonymous SNVs (89.3%) crowding out all other types of variants (**Figure 3.5.1B**). Since frameshift variants almost invariably lead to loss of function of a protein, as opposed to non-frameshift deletions, this chimes with the ability of germline cells to avoid major mutational events, as opposed to cancer cells, which would have lost replication quality control.

Our analysis compares favourably with other studies of the paediatric and adult germline genomic landscape (Huang *et al*, 2018; Zhang *et al*, 2015): of the published pathogenic variants identified both adult and paediatric patients, one was identified in the eleven matched germline DNA samples analysed; a non-synonymous SNV in *adenomatous polyposis coli* (*apc)* (identified by Zhang *et al.* in a paediatric cohort) on Chromosome 5. Both studies identified similar variant rates in cancer patients (8.5% for Zhang et al and 8% for Huang et al), which fits with our small study of one variant in eleven patients.

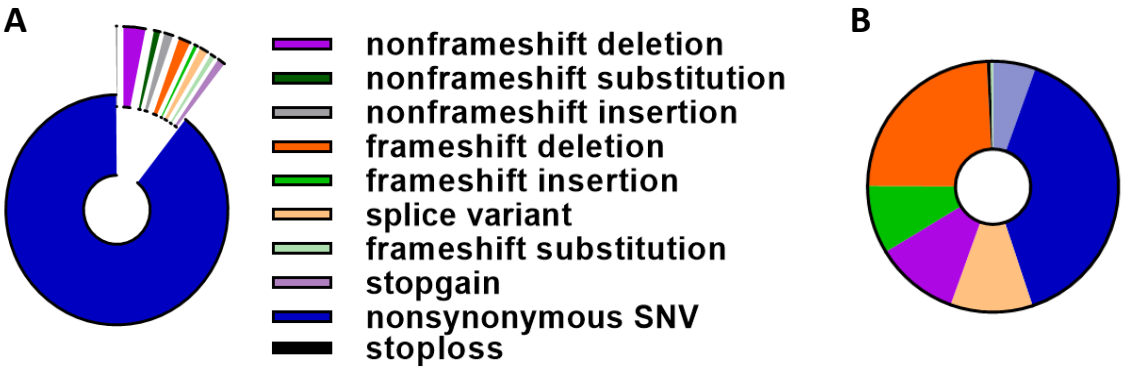

*Figure 3.5.1: Distribution of variant types for the somatic mutations identified. Data are divided into variants identified in germline **(A)** or somatic **(B)** samples. Distribution of variant type averaged for somatic samples (n=25) and germline samples (n=11).*

Looking at the types of variants identified amongst patient samples reveals great variance (**Figure 3.5.2**) – looking at the three sequencing cohorts again eliminates any batch effects (**Figure 3.5.3**). Interestingly, patients that are known to have relapsed (n=9) have a significantly higher proportion of non-synonymous SNVs than patients who did not (n= 9; $p<0.0001$), suggesting that the genetic make-up of patients may reveal differences in terms of prognosis (**Figure 3.5.4**). Unfortunately, NGS is not quite yet a suitable biomarker, as its cost is still high on a per-patient basis, and it remains a time-intensive technique that still lacks in the way of standardization of protocol and bioinformatic processing, which can lead to large differences in the results observed. Nonetheless, it remains interesting that the genomic constitution of patient tumours may correlate with the likelihood of relapse, and in this case may underscore the oncogenic relevance of cumulating single-nucleotide polymorphisms, as opposed to InDels.

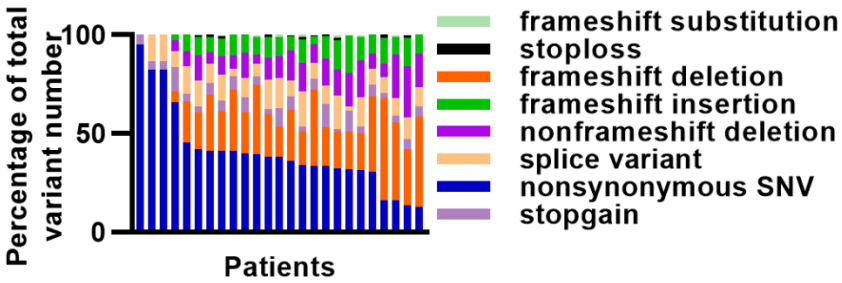

Figure 3.5.2: Proportion of each variant type for each patient tumour DNA sequenced.

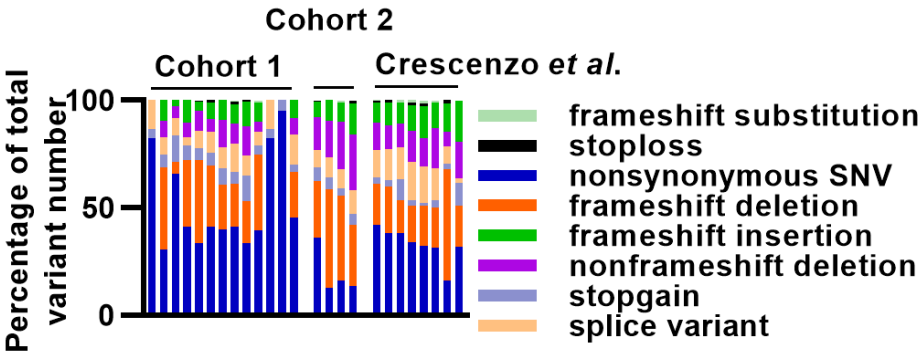

Figure 3.5.3: Proportion of each variant per patient, by sequencing cohorts. Three sequencing cohorts are separated out: the two sequencing cohorts processed in this study, and the sequencing files retrieved online from the paper by Crescenzo and colleagues.

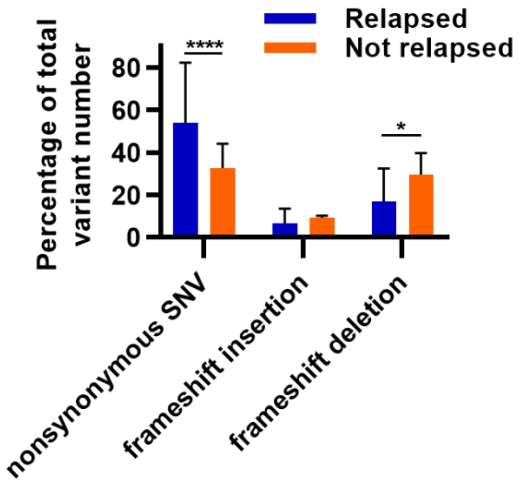

*Figure 3.5.4: Proportion of each variant type according to relapse occurrence. Average and standard deviation of the proportion of variant type per patient, separated out between patients who did (n=9) or did not (n=9) relapse (****p<0.0001; T-tests corrected for multiple testing using the Holm-Sidak method) (in both cases this includes only patients for whom we hold clinical follow-up to compute the 5-year EFS).*

3.6 Mutational Signatures of ALCL

Different mutational processes lead to unique patterns of mutations, and the advent of large-scale genomic data has allowed the identification of a growing number of these so-called 'mutational signatures' (Alexandrov *et al*, 2013). The mutational signature of the eleven paediatric samples for which sequenced matched peripheral blood DNA was analysed using the R package 'deconstructSigs', looking for matches with published mutational signatures (Alexandrov *et al*, 2013). The fraction for each of the 96 variant types for the eleven samples in this cohort is shown (**Figure 3.6.1**). The fractions were used to derive the contribution from each signature, an example of which is presented (**Figure 3.6.2**).

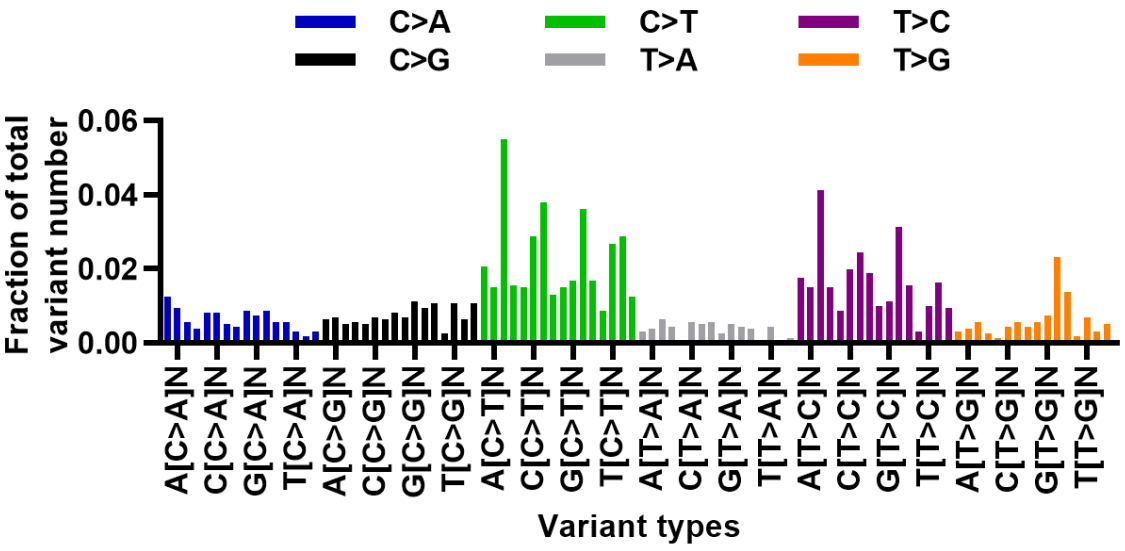

Figure 3.6.1: Prevalence of variant types for patient S57.

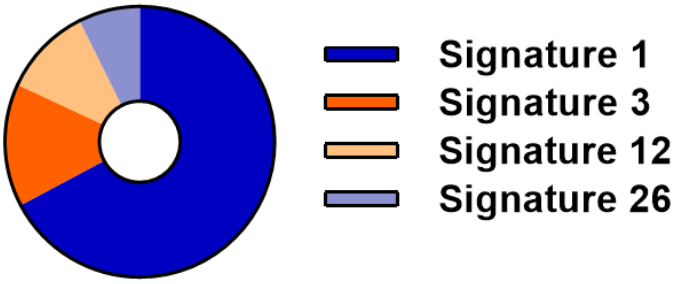

Figure 3.6.2: Mutation signature for patient S57. These were derived from the variant types displayed in Figure 3.8.1.

Analysis of data generated from the eleven patient tumours (**Figure 3.6.3**) showed that signature 1 alone contributes to at least half of the identified somatic mutations (Alexandrov *et al*, 2013). Interestingly, signature 1 is based on the prevalence of C>T transitions at NpCpG trinucleotides and is associated with spontaneous deamination of 5-methyl-cytosine (Helleday *et al*, 2014). Signature 3 has its roots in homologous recombination DNA double strand break repair deficiency (Alexandrov *et al*, 2013) and is usually associated with *breast cancer 1* and *2* (*brca1* and *brca2*) mutations in ovarian, breast and pancreatic cancers, so its manifestation in ALCL is more surprising. Signature 26 is also associated with a DNA repair mechanism, although in this case DNA mismatch repair, hinting that a breakdown in DNA repair mechanisms in ALCL could account for disease pathogenesis, which fits well with the fact that Signature 1 is associated with an increasing tumour burden with age. The aetiology of Signature 12 is as yet unknown. There was no difference between adult and paediatric patient mutational signatures suggesting common mechanisms.

Comparable patterns were found when comparing signatures to the COSMIC signature database (Tate *et al*, 2019) (data not shown). Our analysis compares with other pan-paediatric cancer studies which have also found signature 1 in a majority of samples, and signature 3 in some samples (Gröbner *et al*, 2018; Ma *et al*, 2018).

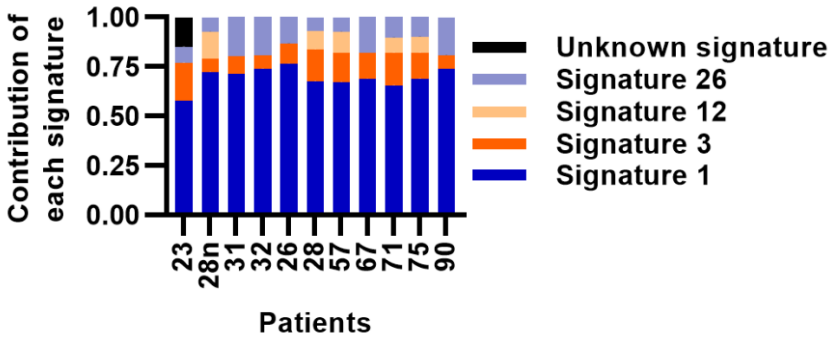

Figure 3.6.3: Main mutation types detected in the 11 samples analysed.

3.7 Identification of the most prominent variants

Beyond these insights into the constitution of the genome of ALCL, variants and mutated genes themselves were also analysed (**Figure 3.7.1**). These data show that the most commonly identified variants in both adult and paediatric cases are found in the following genes: *trna-yw synthesizing protein 1 homolog b* (*tyw1b*), *potassium voltage-gated channel subfamily member 18* (*kcnj18*), *mir1-1hg* and *defensin-β 132* (*defb132*) while the most frequently mutated genes are *kcnj18*, *protein tyrosine kinase 3* (*tyro3*), *phosphoserine phosphatase* (*psph*), *pde3dip* and *notch1*.

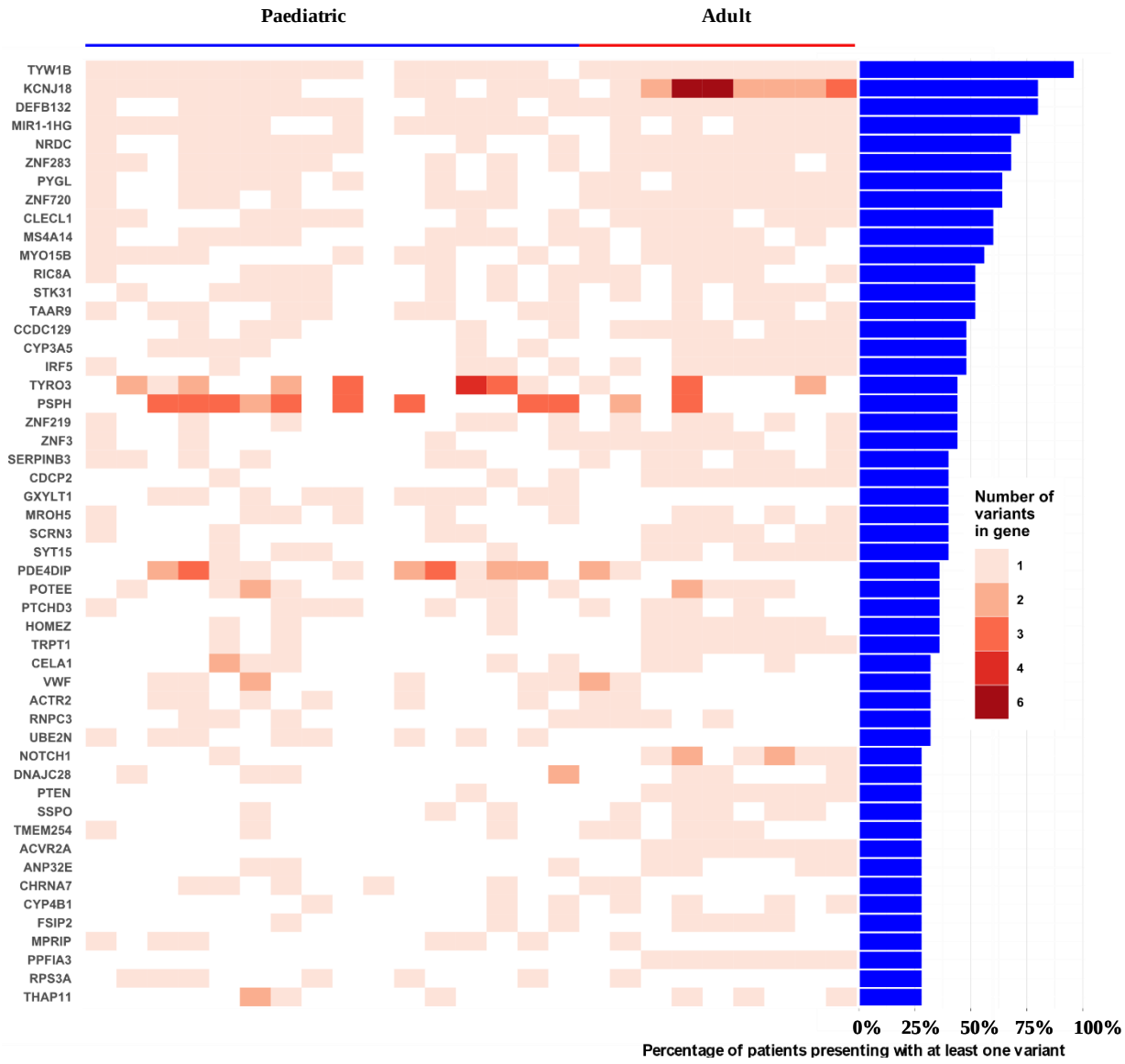

Figure 3.7.1: Heatmap of the most commonly mutated genes detected. Individual results for each patient presented as a heatmap for genes found to be mutated in at least a quarter of patients. The right-hand side panel shows the percentage of patients presenting with at least one variant of the indicated gene. Paediatric and adult patients are separated and ordered from youngest to oldest (at date of diagnosis).

Voltage-gated potassium ion channels, such as that encoded by *kncj18* have received increasing interest as a therapeutic target, in cancers particularly, although their roles are still controversial and ill-defined (Reviewed in Serrano-Novillo *et al*, 2019). Little is known about the role of *mir1-1hg*, a microRNA precursor gene. The other variants detected, *tyw1b* and *defb132* are equally understudied but are thought to encode proteins that hypermodify the guanosine component of the tRNA complex and a defensin involved in the immunological response to microorganisms respectively (Noma *et al*, 2006; Hollox & Armour, 2008).

Phosphodiesterase biology has been implicated in cancers before, starting with lymphocytes in leukemic mice in the 1980s (Weiss & Winchurch, 1978), to its role in angiogenesis and the interplay between lymphomas and the microenvironment more recently (Suhasini *et al*, 2016), which may explain the frequent mutations found in genes of this pathway such as *pde3dip*. Other metabolic pathways such as serine biosynthesis are implicated here, as exemplified by frequent mutations in *psph*, a gene and pathway which has also previously been implicated in T-cell malignancies (Kampen *et al*, 2019).

Perhaps the least surprising hits identified in this study are the frequent mutations in *tyro3*, a receptor tyrosine kinase and emerging oncogene of which the signalling cascade shows extensive cross-talk with pathways important to ALCL pathobiology such as PI3K, Akt and JAK/STAT (Reviewed in Smart *et al*, 2018), as well as *notch1*, which has been implicated in ALCL pathogenesis previously (see Chapter 1.7).

In order to further define identified mutations in genes that may be important towards the pathogenesis of ALCL, pathway analysis was conducted.

3.8 Gene Set Enrichment Analysis: The Notch pathway

To further investigate the likelihood of pathways being of systemic importance to ALCL, Reactome network clustering was conducted (Fabregat *et al*, 2018). **Figure 3.8.1** illustrates the main interactions of mutated genes in the dataset. Clear nodes appear around *tp53, g-protein sub-unit γ2 (gng2)* as well as small clusters around *notch1* and *c-terminal binding protein 2* (*ctbp2),* indicating proteins that interact with a number of the other mutated genes. *tp53* is not unexpected as p53 has been reported to play a key role in ALCL pathogenesis (Cui *et al*, 2009). As mentioned previously, the Notch pathway is of marked importance in T-cell biology (Osborne & Minter, 2007) particularly in the developing thymus which is proposed as the origin of ALK+ ALCL (Malcolm *et al*, 2016), and has previously been implicated in the pathogenesis of ALCL (Jundt *et al*, 2002). GNG2 is another node which given the central importance of G-proteins and the centrosome in cellular biology is not an unexpected finding: many proteins interact with these sub-units. Clearly the most frequently affected pathways in this dataset are very different from those presented previously (**Figure 3.7.1**), suggesting that the main mutated genes may not be the ones that are of the most systemic importance in ALCL (**Figure 3.8.1** and **Figure 3.8.2**). However, genes such as *tp53* or *gng2* are neither frequently mutated nor presenting with frequent variants (**Figure 3.7.1**), indicating that mutation of pathways may be more relevant than individual genes.

The main mutated nodes were cross-checked by Gene-Set Enrichment Analysis (GSEA), which could help identify vital pathways in ALCL, since biologically relevant pathways should be enriched more heavily with variants than others (**Figure 3.8.2**). All genes which were mutated in at least a tenth of the 32 patients were included in the GSEA. Two different software programmes were used; DAVID (Huang *et al*, 2009) for protein domains, and Reactome (Fabregat *et al*, 2018) for pathway analysis. Reactome analysis combined 5 different databases: IPA (Qiagen), PantherDB (Mi *et al*, 2017), KEGG (Goto *et al*, 1997), the National Institute for Health's Protein Interaction Database and Reactome's own database. Analysis of protein domains with DAVID used four different databases, GO (The Gene Ontology Consortium, 2019), Seq-Feat (National Centre for Biotechnology Information, US), SMART (Letunic & Bork, 2018) and InterPro (Mitchell *et al*, 2019). The number of databases in which each pathway or domain was found to be enriched are displayed along with *p*-values and the number of genes in the pathway, plotted using ggplot2 in R (**Figures 3.8.2** and **Figure 3.8.3**).

This analysis showed the gene set to be enriched in T-cell Receptor (TCR) signalling pathway genes across all five databases used, along with genes of the Notch pathway (**Figure 3.8.2**). The TCR signalling pathway is perhaps not surprising, as it is one of the main signalling pathways in T-cell biology; it has previously been shown that NPM-ALK can substitute for key TCR-induced distal signalling pathways and silencing of proximal proteins has been shown in ALCL (Ambrogio *et al*, 2009; Turner *et al*, 2007). Other less significant hits such as the G-protein-coupled receptor (GPCR) signalling pathway, calcium

signalling or neurotransmission are also unsurprising considering the hits already identified in *kcnj18* (a calcium-regulated potassium synaptic channel), *gng2* (part of the G-protein complex) and others.

Analysis of domains frequently present in the mutated genes revealed an enrichment in proteins with EGF-like or Calcium ion binding domains (**Figure 3.8.3**), two features of the Notch protein. Interestingly, 3 of the 4 identified *notch1* variants are found within the EGF-like calcium binding domain of Notch1 (also the extracellular ligand-binding domain of the protein).

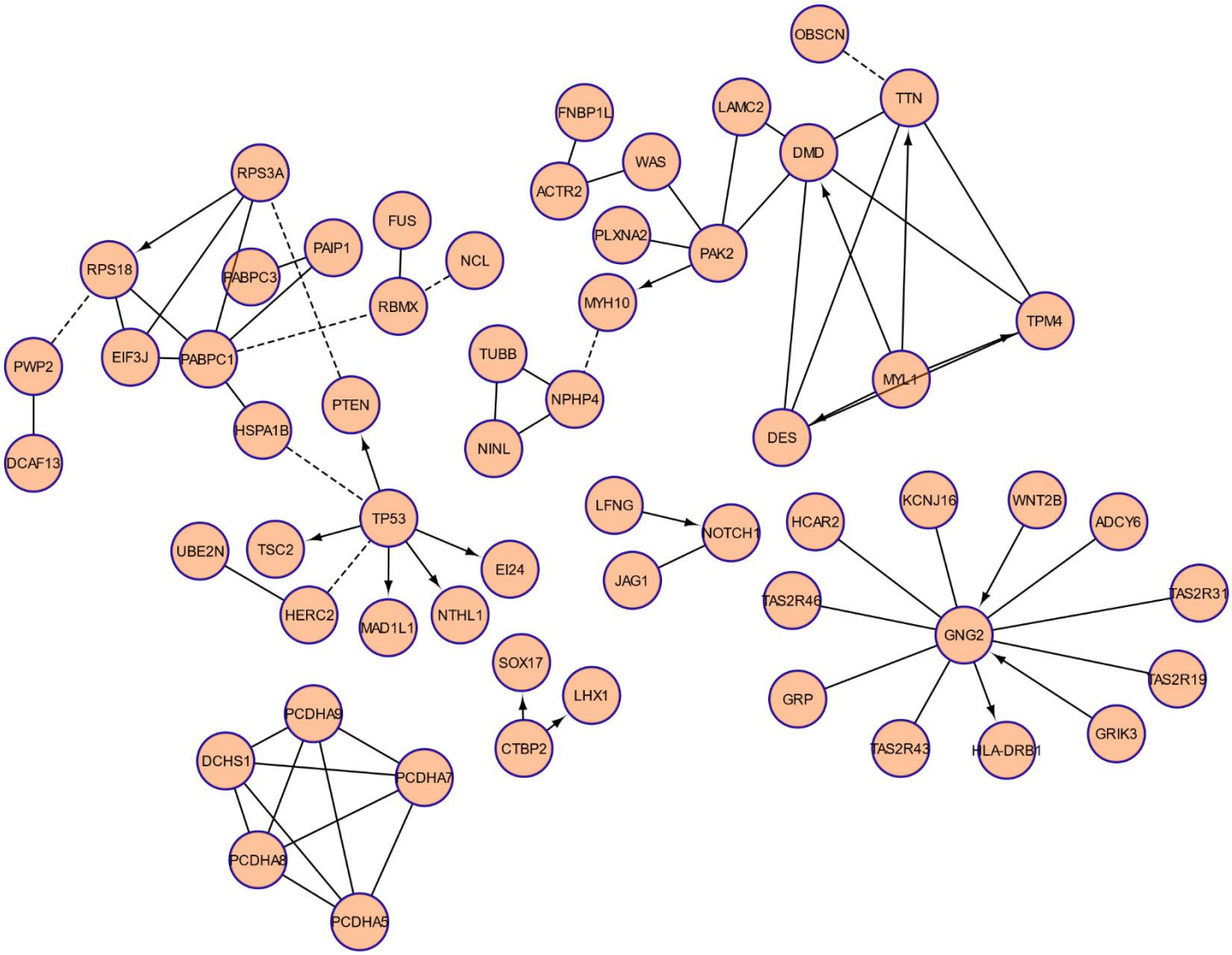

Figure 3.8.1: Reactome Network Clustering Analysis. Nodular interaction plot showing connections between variants. The plot was designed using Reactome. Arrows indicate activating interactions, dotted lines indicate hypothesised interactions, lines ending with a perpendicular bar indicate inhibition.

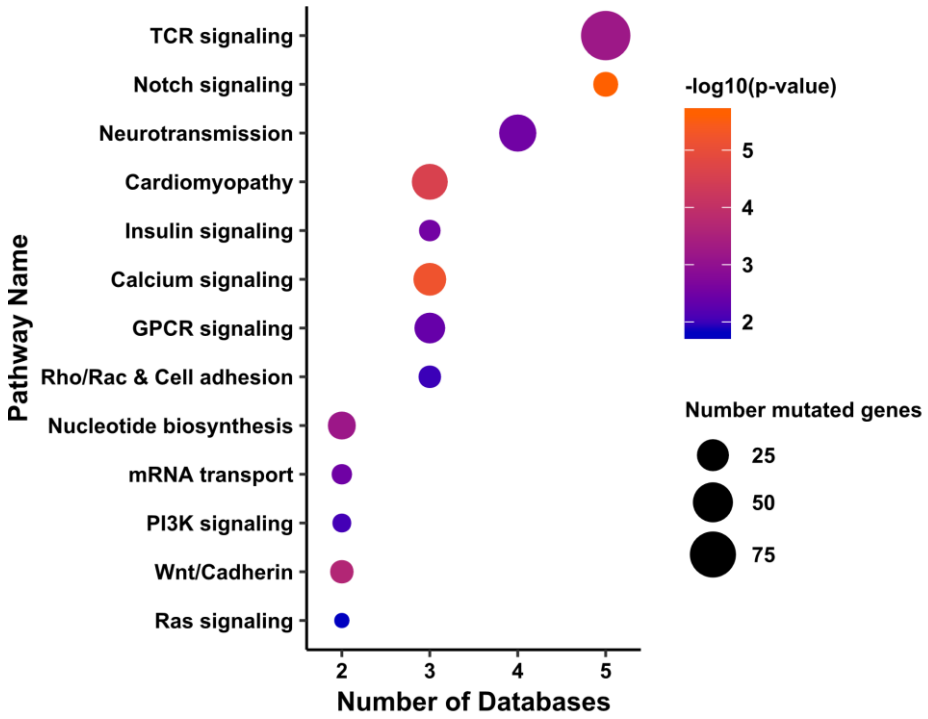

Figure 3.8.2: GSEA of the mutated genes using Reactome and five databases. Scatter plots of the pathways found to be enriched in the dataset, displaying the number of databases in which each hit was found to be enriched, along with the (-)log$_{10}$ of the p-value of the software in which each hit is found to be most enriched, and the corresponding number of genes involved.

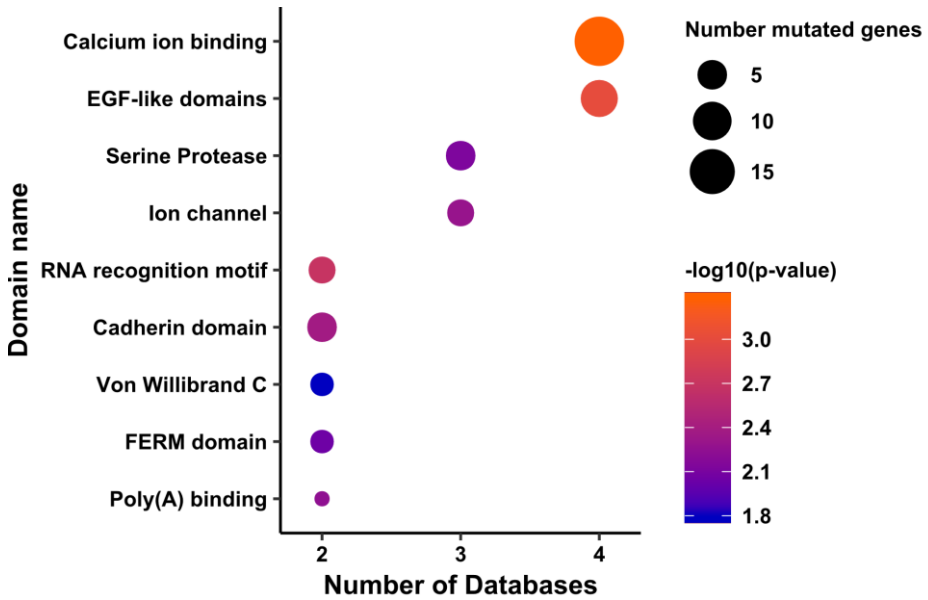

Figure 3.8.3: GSEA of the mutated gene domains using DAVID and four databases. Scatter plots of the domains found to be enriched in the dataset, displaying the number of databases in which each hit was found to be enriched, along with the (-)log$_{10}$ of the p-value of the software in which each hit is found to be most enriched, and the corresponding number of genes involved.

3.9 Hit validation in a larger cohort of patient tumours

Given the importance of the Notch pathway to T cell biology, the most frequent variants detected in *notch1* (T349P and T311P) were validated in a larger patient cohort (**Table 2.5**).

Of the 25 ALK+ ALCL tumour samples analysed by WES, 24% presented with Notch1 variant T349P while 12% had Notch1 variant T311P. Of the extended cohort of 78 samples (including 18 of the samples previously analysed by WES with a total of 55 ALK+ ALCL, and 23 ALK- ALCL as described in **Figure 3.2.1**); the variant T349P was validated in 12% of patients (n=78; 15% of ALK- patients and 9.3% of ALK+ patients) (**Figure 3.9.1**). Variant T311P was found in 7.6% of patients (n=78; 10.2% of ALK+ patients, none in ALK- patients) (**Figure 3.9.2**). Interestingly, the overall incidence of patients with at least one mutation of the EGF-like domain in which these variants were found is cumulatively 18% (14 of 78 patients).

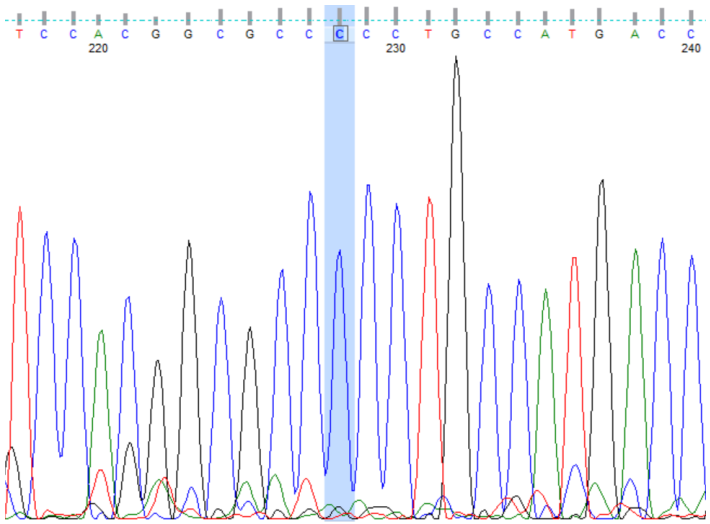

Figure 3.9.1: Sanger chromatogram for notch1 variant T349P.

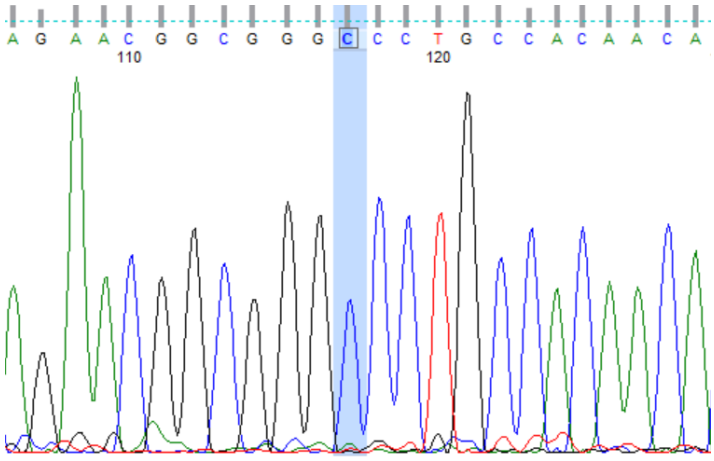

Figure 3.9.2: Sanger chromatogram for notch1 variant T311P.

There was therefore no significant difference in incidence of Notch1 mutations between ALK+ ALCL or ALK- ALCL, nor was there a significant difference between adult and paediatric ALCL patients (Table 3.9). Overall, there is a slight difference in the 5-year OS and EFS between patients that are wild-type for T349 and T311, and those that present with at least one of the two mutations (a difference of just over 9 months and 6 months, respectively for OS and EFS). Interestingly, the difference is much more significant for adult and ALK- ALCL patients, though generally patient number prevents a more solid analysis of this data, which therefore remains largely anecdotal.

	All patients		Adult patients		Paediatric patients		ALK+ ALCL patients		ALK- ALCL patients	
	WT NOTCH1	NOTCH1 T349P and/or T311P	WT NOTCH1	NOTCH1 T349P and/or T311P	WT NOTCH1	NOTCH1 T349P and/or T311P	WT NOTCH1	NOTCH1 T349P and/or T311P	WT NOTCH1	NOTCH1 T349P and/or T311P
# Patients	n = 57	n = 11	n = 13	n = 3	n = 27	n = 5	n = 45	n = 8	n = 12	n = 3
OS (years)	4.4	3.6	4.2	1.7	4.4	2.9	4.5	4.3	4.5	1.7
EFS (years)	2.6	2.1	4	1.7	4.2	3.2	2.3	2.2	3.6	1.7
Death (%)	25%	36%	38%	67%	26%	20%	18%	25%	50%	67%
Relapse (%)	61%	55%	38%	0%	52%	60%	67%	75%	42%	0%

Table 3.9: Detail of the Notch1 status of our validation cohort. The Notch1 mutation status at T311 and T349 (WT: Wild-Type) of the patients in our validation cohort is detailed here, broken down by ALK+ and ALK- ALCL patients, and adult and paediatric ALCL patients. In addition, the assorted clinical data is detailed, with the 5-year Overall Survival (OS), 5-year Event-Free Survival (EFS), and proportion of patients who died or relapsed.

3.10 digital droplet PCR

Finally, we investigated the possible presence of sub-clonal T349P mutations using digital droplet PCR technology, which first uses a lipid-based technology to separate out different clones of a sample of DNA (one per droplet), before PCR-amplifying the clone contained in each droplet using two different fluorescently-tagged probes, corresponding either to the wild-type or mutated allele of the variant studied (in this case, T349P). This technology requires a certain amount of optimisation, to determine the optimal amount of input DNA, the optimal PCR cycle (and melting temperature). This optimisation manifested itself in the total number of droplets (though the manufacturer claims that up to 20,000 droplets can be generated and created, we achieved an average of around 15,000 after optimisation, though some runs were far less successful; **Figure 3.10.1**), and the difference in amplitude between droplets negative or positive for either of the probes (this helps determine the count of positive or negative droplets; see examples of poor runs in **Figure 3.10.1** and better ones in **Figure 3.10.2** and **Figure 3.10.3**).

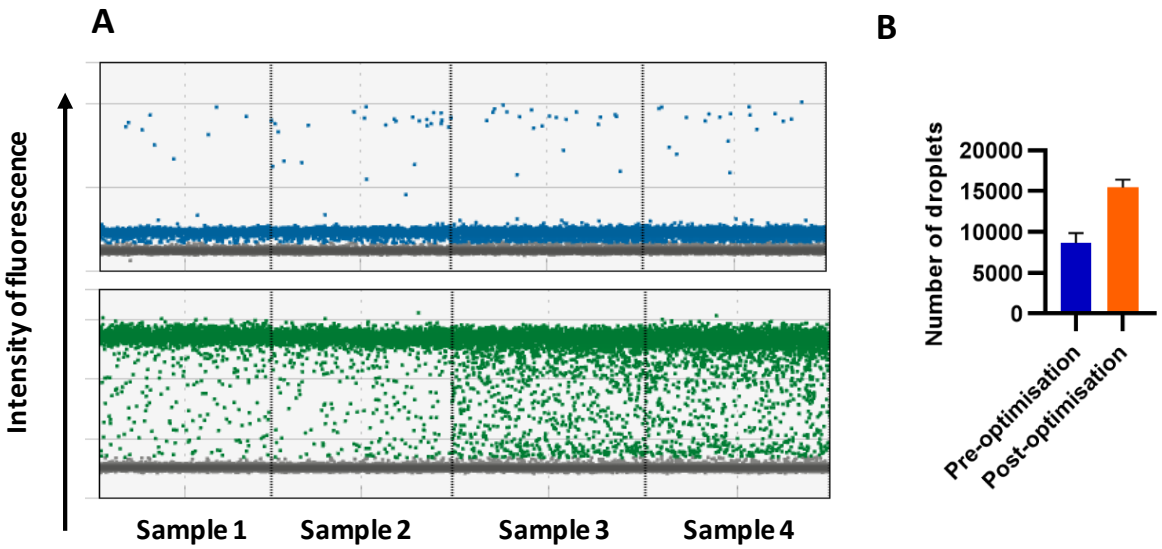

Figure 3.10.1: Optimisation. ***(A)*** *ddPCR plot of clones expressing the wild-type (green) or T349P mutated allele (blue) – droplets negative for the fluorophore measured are coloured grey, for four different samples, before protocol optimisation. Each dot represents one droplet (one clone), and its position on the Y-axis represents the intensity of fluorescence that emanates from the droplet.* ***(B)*** *Number of droplets before and after protocol optimisation, as measured by Fluorescence-Activated droplet sorting – bars represent the mean of the 16 samples contained in one run, error bars represent standard deviation.*

We were able to use the wild-type and mutated Notch1 cDNA plasmids as negative and positive controls to verify that the probes worked as intended (**Figure 3.10.2**). Though the technology is in theory capable of detecting as little as one clone, it is generally accepted that at least three positive droplets are required to rule out false positives. Our data (**Figure 3.10.3**) however shows that we did not need to test the limit of detection of the technology, as our patient samples were clearly either positive or negative for mutation T349P, and none of the samples we tested (n=60) appeared to present with sub-clonal mutations of T349P.

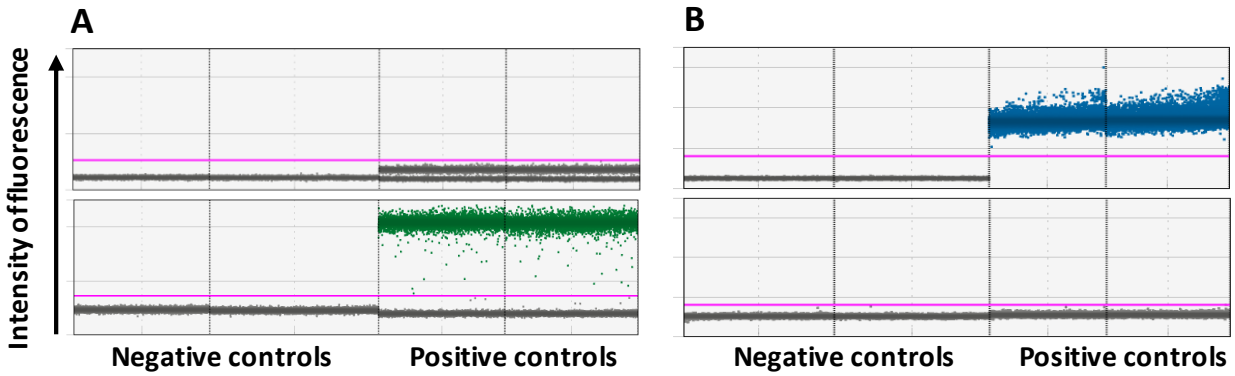

*Figure 3.10.2: Positive and negative controls. ddPCR plot of clones expressing the wild-type (green) or T349P mutated allele (blue) – droplets negative for the fluorophore measured are coloured grey, for four samples, showing two negative controls and two positive controls for the Wild-type **(A)** and mutated **(B)** allele. Each dot represents one droplet (one clone), and its position on the Y-axis represents the intensity of fluorescence that emanates from the droplet. The pink line is the threshold for droplets determined to be positive for the allele investigated.*

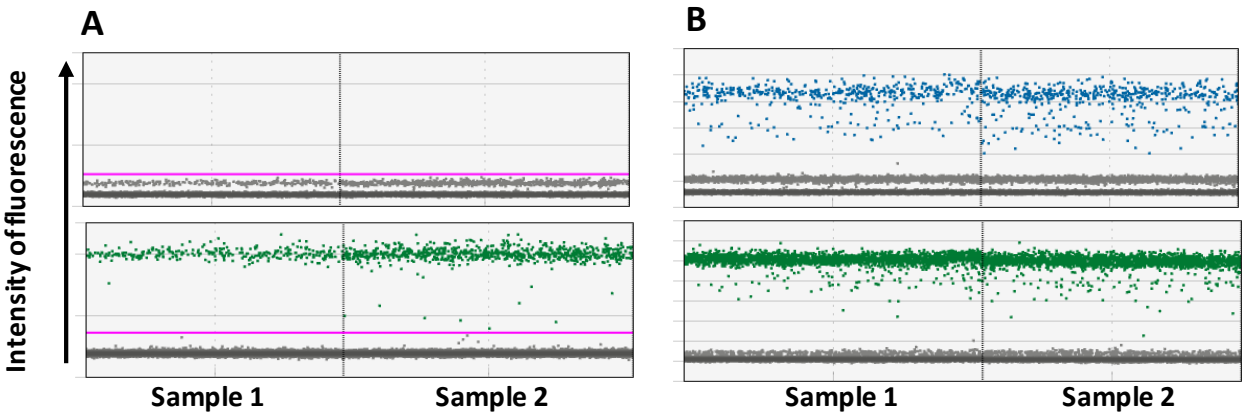

*Figure 3.10.3: Example of samples showing a lack of sub-clonal mutations. ddPCR plot of clones expressing the wild-type (green) or T349P mutated allele (blue) – droplets negative for the fluorophore measured are coloured grey, for four samples, showing two samples each with a Wild-type **(A)** and mutated **(B)** allele. Each dot represents one droplet (one clone), and its position on the Y-axis represents the intensity of fluorescence that emanates from the droplet. The pink line is the threshold for droplets determined to be positive for the allele investigated.*

3.11 Discussion

In this chapter, DNA extracted from 18 ALK+ ALCL patient samples was assessed by WES and analysed alongside 7 previously published samples, using a custom-designed bioinformatic pipeline. The genomic constitution of the ALCL DNA, both paediatric and adult was analysed, and it was determined that, as suggested by a larger meta-analysis, paediatric tumours on average present with slightly less variants than adult tumours – although it is unusual to be able to study this in a cancer that manifests in both adults and children. The genome of ALCL patients remains fairly silent, with an absence of consistent copy-number variations or large InDels, and largely absent frequent mutations and hyper-mutated genes, bar those described in this chapter.

It would be interesting to ask whether the trend is similar for germline mutations, which could be expected to bear more of the responsibility for tumourogenesis in paediatric patients compared to adults – although research so far has shown little difference (Huang *et al*, 2018; Zhang *et al*, 2015). Indeed, though we did not find any significant insertions, deletions or copy-number variations in our eleven matched peripheral blood patient samples, our analysis was fine-tuned for the detection of somatic mutations, and thus it would be worth analysing these samples using a more targeted bioinformatic pipeline. Nonetheless, comparing the germline variant list we obtained with published large-scale studies points to probable pathogenic variants in the germline of three patients: S23, S66 and S74, presenting with a non-synonymous SNP in *tp53* (SNP ID rs1042522) and another two in *brca2* (SNP ID COSM4984873 and rs80359165) respectively (Zhang *et al*, 2015).

Looking at tumour signatures, signatures 1, 3, 12 and 26 were the most common in our analysis, with Signature 1 by far the biggest contributor. Our analysis compares with other pan-paediatric cancer studies which have also found signature 1 in a majority of samples, and signature 3 in some samples (Gröbner *et al*, 2018; Ma *et al*, 2018). The fact that signature 1 (based on the prevalence of C>T transitions at NpCpG trinucleotides associated with spontaneous deamination of 5-methyl-cytosine) is associated with age might explain the slight correlation we found between mutational burden and age, as also shown by Gröbner *et al*. Signature 3 was also detected in all 11 patient samples, a signature with its roots in homologous recombination DNA double strand break repair deficiency (Alexandrov *et al*, 2013). This suggests that DNA damage repair mechanisms might be impaired in these children, predisposing them to ALCL, perhaps through germline mutations. Interestingly, this signature is strongly associated with germline and somatic *brca1*/2 mutations, of which we found two potential pathogenic ones in our patients (along with other germline *brca1* and *brca2* mutations in other patients, less likely to be pathogenic). Signatures 12 and 26 are both consistent with repair by transcription-coupled nucleotide excision repair, and though the aetiology of Signature 12 remains

unknown, that of signature 26 is linked with defective mismatch repair – all in all, pointing to an increased likelihood of DNA damage, and possibly defective repair mechanisms, which may or may not lead to an accumulation of mutational burden with age, as signature 1 and our data may suggest.

While we also attempted to correlate some of the genetic features back to clinical outcomes and markers, our sample size is too small to be able to conclusively determine much that can be taken forward. Indeed, it is possible that the effect we see, correlating relapse with the type of variants found is merely a by-product of another mechanism, such as a particular type of DNA damage or repair defect. Nonetheless, the fact that we found this correlation is important as it indicates that, at the genomic level, there is a significant difference between patients who relapse, versus those who don't. It may be that the larger proportion of non-synonymous SNPs cluster in certain genes or loci, for example, which we were not able to analyse with the facilities available.

The biologic importance of some of the mutated genes and affected pathways were then identified by GSEA and other methods. The two signalling pathways most significantly enriched in variants are the T-cell receptor signalling and Notch signalling pathways. These findings are somewhat unsurprising, given the importance of both these signalling pathways in T cell biology – indeed, there is increasing evidence suggesting cross-talk between the two pathways in T cells (Steinbuck *et al*, 2018). In addition to this, deregulation of Notch signalling has been identified as heavily prominent in several leukaemia and lymphomas (Gain-of-function mutations in Notch1; perhaps most so in T-ALL, where 50 to 60% of patients present with such mutations (Weng *et al*, 2004; Breit *et al*, 2006; Aster *et al*, 2011)). All this evidence suggested to us that *Notch1* and the signalling pathway in which it resides is likely to be of importance to ALCL.

Indeed, two of the main mutations detected in *notch1* (of four mutations identified by WES) were validated in a wider cohort of almost 80 patients, whereby a fifth of the samples presented with at least one of the Notch1 variants. We described a novel gain-of-function mutation in the extracellular EGF-like domains of Notch1. Though in other cancers most of these mutations are in the intracellular domains of the protein, some are also found in the extracellular domain: cutaneous and lung squamous cell carcinoma patients also present with Notch1 mutations, a number of which are located in the extracellular EGF-like domains, though only one of these has been studied in any level of depth, and is predicted to lead to loss-of-function (Wang *et al*, 2011b). Indeed, T349P and T311P are thought to manifest in other tumour types, such as primary central nervous system lymphoma (Bruno *et al*, 2014), chronic myelomonocytic leukaemia (Mason *et al*, 2016), chronic lymphocytic leukaemia (Ljungström *et al*, 2016), T-ALL (Neumann *et al*, 2015), and squamous cell carcinoma (Martin *et al*, 2014). Though

none of these publications validate the presence of Notch1 T349P, it is unlikely for the variant to be present as an artefact or false-positive in all five publications. Finally, despite evidence suggesting that other Notch mutations have been found in cancers at sub-clonal frequencies (Minervini *et al*, 2016), we show that this was not the case for mutation T349P in ALCL.

We have therefore analysed the genome of ALCL, and found it to be fairly stable, as ALCL literature suggests. Having found evidence that the Notch pathway may be hypermutated and considering evidence from the literature concerning Notch1 in ALCL, we decided to validate the two main variants found in Notch1. Since we were able to prove that about 20% of patients present with at least one Notch1 variant in the extracellular domain of the protein, we then decided to investigate the functional impact of the mutation.

4. Investigating the functional impact of Notch1 mutations T349P and T311P

4.1 Introduction

In a wild-type state, members of the Notch family of receptors are activated by one of five ligands; Jag1, Jag2, DLL1, DLL3 or DLL4 (**Figure 4.1.1**). Notch activation is regulated by post-translational modification of both the Notch receptor and the Notch ligand – as well as proximity of the Notch-expressing cell and the ligand-expressing cell, which is why the tumour microenvironment, and the presence of ligand-expressing endothelial cells are increasingly understood to be significant when studying the role of Notch signalling in cancer (Reviewed in Meurette & Mehlen, 2018; Bray, 2016). Notch is a heavily conserved signalling pathway in most organisms, underscoring its biological importance – and mutations of the Notch family of genes is often associated with oncogenic events. Indeed both independent studies and the COSMIC database have shown that the negative regulatory region and the PEST sequence of the Notch family of proteins are the target of a large number of mutations, across many cancer types (Wang *et al*, 2011b; Forbes *et al*, 2008), though it has been noted previously that a number of mutations are also found in the EGF-like repeats, even though these have rarely been investigated for their functional consequences to the protein (Mutvei *et al*, 2015; Wang *et al*, 2011b; Rebay *et al*, 1991). In the previous chapter, two mutations in the extracellular EGF-like domain of Notch1 were detected in ALCL. The functional significance that these mutations may have on the activity of Notch1, and therefore the significance these mutations may have in ALCL biology are described here.

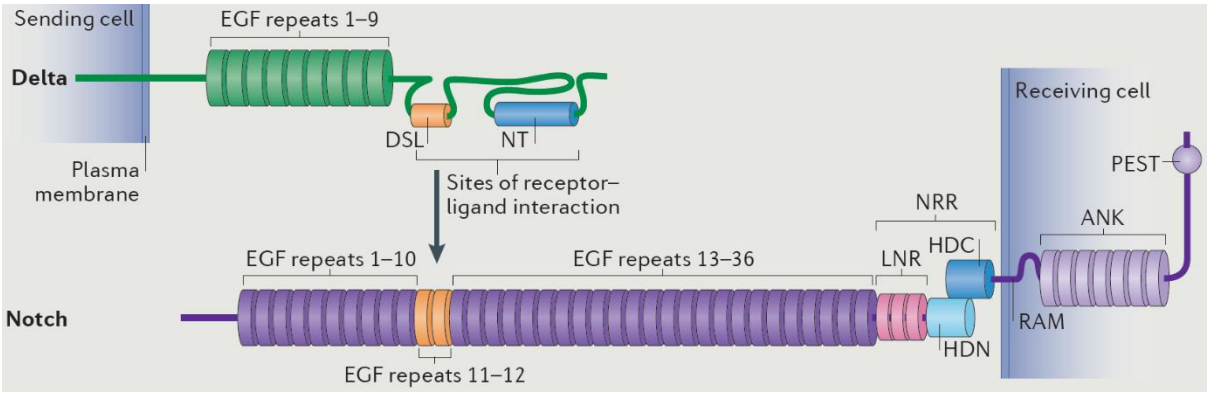

Figure 4.1.1: Schematic showing the interaction of Notch and its ligand. The Notch receptors are composed of the following domains; Epidermal Growth Factor-like repeats (EGF), Negative Regulatory Region (NRR), LIN12/Notch Repeats (LNR), Heterodimerization Domains (HDC and HDN), RBP-Jκ Association Molecule (RAM), Ankyrin Repeats (ANK), Polypeptide enriched in proline, glutamate, serine and Threonine (PEST) – and the Notch ligands (in this example, DLL) activate the Notch receptors using the Amino-Terminal (NT) and delta-Serrate-LAG2 (DSL) domains. (Modified from Bray, 2016).

4.2 Defining Notch1 mutations T349P and T311P

The most frequent *notch1* variant identified in this study, is at position 1045 of the *notch1* coding sequence, in the 6th of 34 exons, changing an Adenosine to a Cytosine, leading to a change in the 349th amino acid from Threonine into Proline. The 6th exon encodes one of the numerous EGF-like domains which make up the extracellular domain of Notch1. Notch1 T349P was predicted to be a function-altering mutation by variant effect prediction software including SIFT (which gave it a score of 0.01), Polyphen (which gave the variant a score of 0.999), FATHMM, LRT, MutationTaster, PROVEAN, and the MetaLR and MetaSVM databases (Adzhubei *et al*, 2010; Kumar *et al*, 2009; Chun & Fay, 2009; Schwarz *et al*, 2014; Choi *et al*, 2012). Similarly, the T311P variant was scored as being damaging by all the same software, except for Polyphen (which gave it a score of only 0.181 as opposed to 0.012 by SIFT).

Notably, the loss of Threonine leads to the potential loss of O-linked Glycosylation. O-linked Glycosylation or Fucosylation of Notch1's EGF-like domain has been demonstrated to promote Notch signalling and regulate binding to its ligand in some cases (Schneider *et al*, 2018; and reviewed by Stanley & Okajima, 2010 and; Pakkiriswami *et al*, 2016). In addition, Proline is one of the few extremely rigid amino acids known to force a change of confirmation in tertiary structure, and interestingly often forces a change in β-sheet structure (each EGF-like domain is made up of 4 β-sheets among other secondary structures). Molecular studies have shown specific EGF-like domains to be necessary but not sufficient for Notch-ligand binding in the presence of Calcium ions (Chillakuri *et al*, 2012), indicating that nearby calcium-binding is likely to be involved in ligand binding. To note, bioinformatic analysis identified two more variants in nearby EGF-like domains, and one in Lin12/Notch repeat domain 2. Notch1 variant T311P is also found in the 6th exon, at position 1193 of the coding sequence, with similarly an Adenosine mutated into a Cytosine leading to a change from Threonine into a Proline, resulting in a predicted loss of O-linked Fucosylation on one of the EGF-like domains of the extracellular portion of Notch1.

Furthermore, the COSMIC database shows that T311 and T349 are the two most frequently reported mutated amino acids at the presumed Notch1/Jag1 interface across a range of cancers (including chronic myelomonocytic leukaemia (Mason *et al*, 2016), chronic lymphocytic leukaemia (Ljungström *et al*, 2016), T-ALL (Neumann *et al*, 2015), rhabdomyosarcoma (Kohsaka *et al*, 2014) and squamous cell carcinoma (Martin *et al*, 2014)) (**Figure 4.2.1**). These two variants were also validated as present in a further patient cohort for which DNA was available as detailed in chapter 3.9.

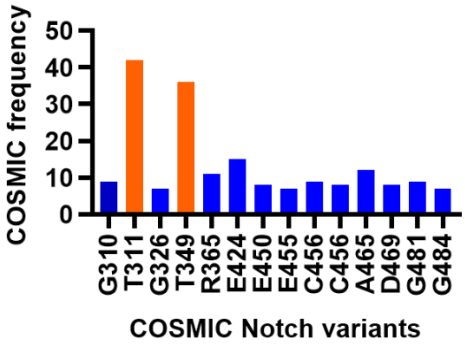

Figure 4.2.1: COSMIC variant frequencies. Frequency at which select Notch1 mutations at the Notch/ligand interface are reported in the COSMIC database.

4.3 Molecular Dynamics of Notch1 mutations

Since Notch1 amino residues T349 and T311 are present at the Notch/ligand interface, *in silico* modelling was performed to predict the effects of the mutation on protein conformation and ligand binding. The predicted conformational change was modelled using a combination of previously published structures of Notch1 and Jag1 and structural predictions using machine learning to predict structure and reconcile the various crystal structures used (**Figure 4.3.1**). Specifically using a structure of Notch1's extracellular EGF-like domains 8 to 12 bound to its ligand (Luca *et al*, 2017) (PDBID 5UK5) allowed detailed analysis of the Notch1/Jag1 interface (**Figure 4.3.2** and **Figure 4.3.3**).

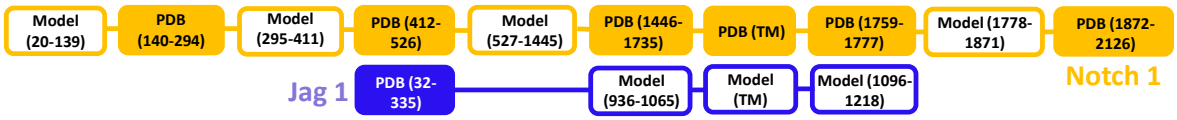

Figure 4.3.1: Detail of sources of protein conformation modelling. A mix of published datasets in the protein database (PDB) and predictions (Model) were used to compute the full Notch1 and Jag1 structures, the amino acids which were obtained from published datasets or models are detailed here. The transmembrane (TM) domains were not modelled.

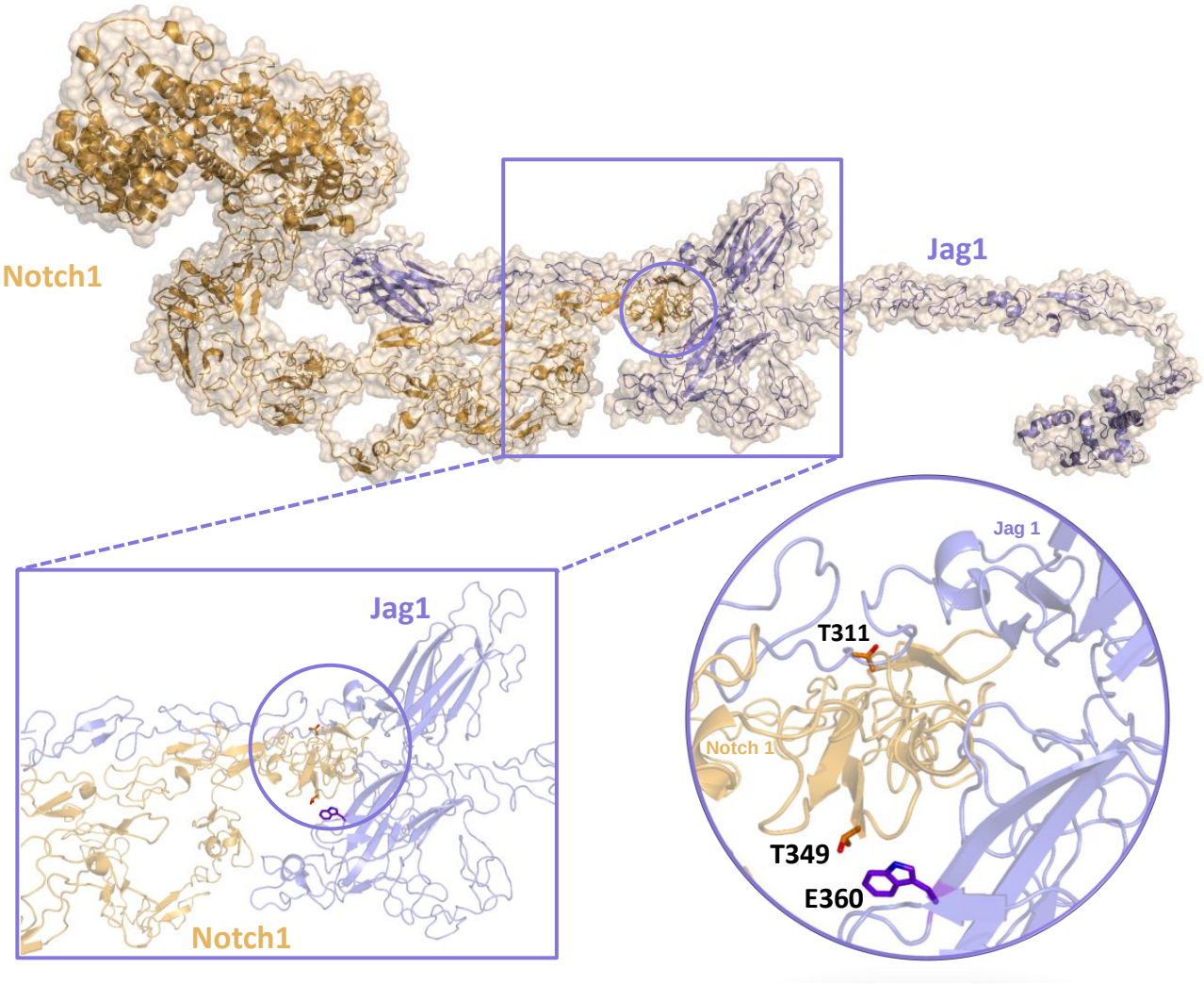

Figure 4.3.2: Full-length modelling of the Notch1 protein bound to Jag1. Binding of Notch1 to Jag1, showing enlarged images of amino acid residues T349 and T311. The molecules are presented in their secondary (spirals represent α-helices and arrows β-sheets) and tertiary conformations (the semi-transparent surface outline), with the side-chains of residues T311 and T349 presented as stick cartoons. The residue of Jag1 with which T349 is predicted to interact (E360) is also presented as a stick cartoon.

A cartoon representation of the Notch1 domain containing residues T349 and T311 is shown, displaying Hydrogen bonds in black, and a nearby Calcium ion as a sphere (**Figure 4.3.3**). The two β-sheets are anchored to each other by Hydrogen bonds, two of which are dependent on Threonine 349 and 311, and one of which will be lost when replaced by a Proline residue.

Mutations T349P and T311P are predicted to displace the β-sheets due to both the bulkier side-chain of Proline (as compared to Threonine) and due to the loss of a stabilizing Hydrogen bond (**Figure 4.3.4**). However, the remaining Hydrogen bonds seem sufficient to avoid a more drastic change in conformation. Superimposition of wild-type and mutated Notch1 (**Figure 4.3.5**) clearly show the displacement of the β-sheets that mediate ligand binding, and the possible displacement of the nearby Calcium ion as well. Although residues T349 and T311 are not in physical contact with the Notch1 ligand, a change in Notch1's conformation is still seen that may modulate ligand binding.

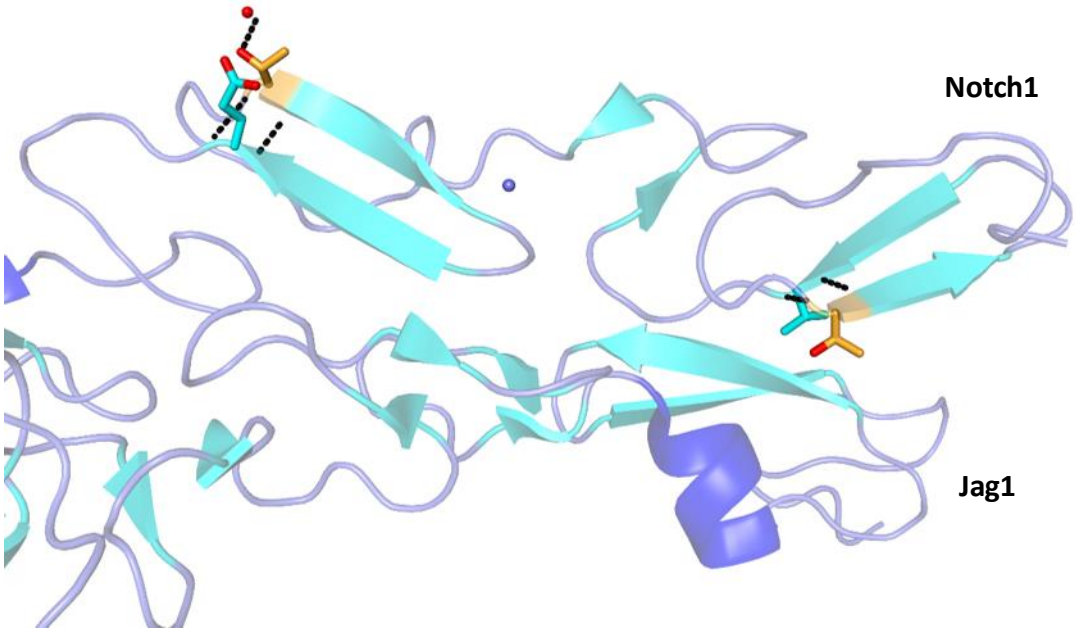

Figure 4.3.3: Enlarged locus of Notch1 residues T349 and T311 within the Notch1/Jag1 interface. The wild-type molecules are presented in their secondary (helices represent α-helices and arrows β-sheets) confirmation, with the side-chains of residues T311 and T349 presented as stick cartoons and Hydrogen bonds modelled as black dotted lines, while Calcium ions are purple spheres. Notch1 is the upper chain, while Jag1 the one below.

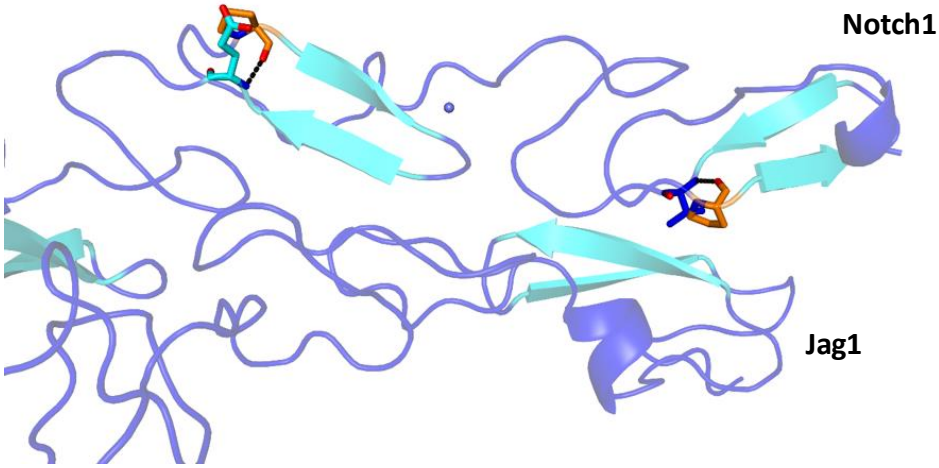

Figure 4.3.4: Detailed conformational changes at the Notch1/Jag1 interface. The molecules (wild-type Jag1 and mutated Notch1) are presented in their secondary (helices represent α-helices and arrows β-sheets) conformation, with the side-chains of residues T311 and T349 presented as stick cartoons and Hydrogen bonds modelled as black dotted lines, while Calcium ions are purple spheres. Notch1 is the upper chain, while Jag1 the is the lower.

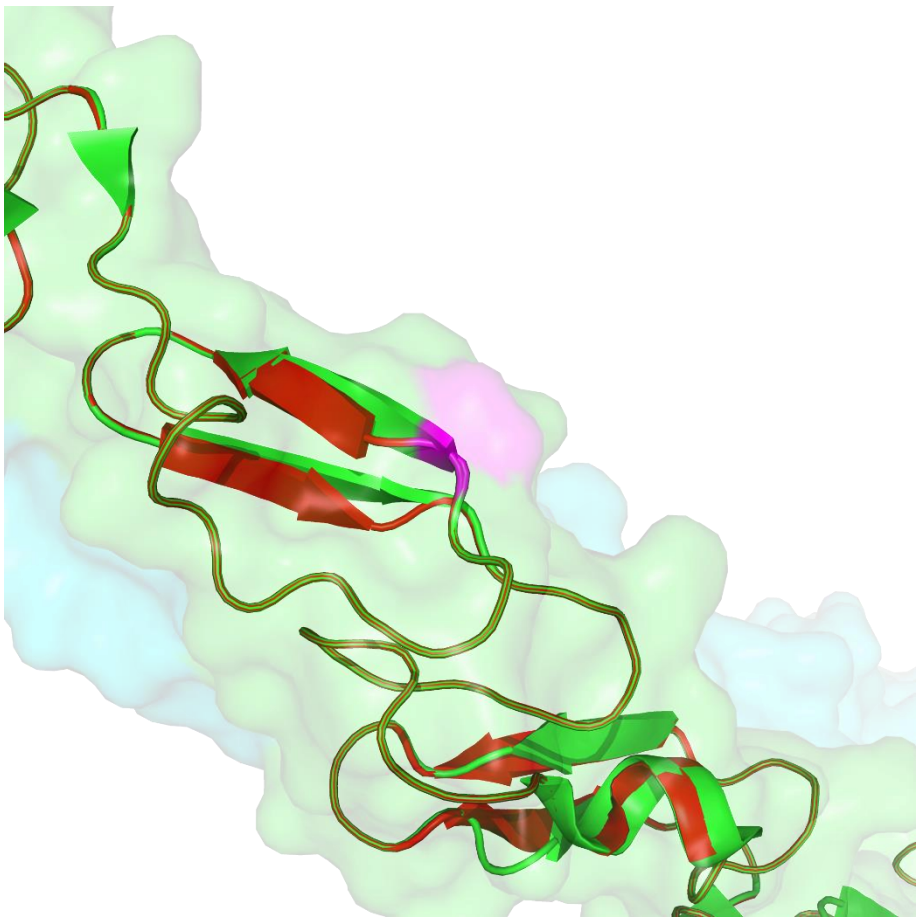

Figure 4.3.5: Superimposition of the Wild-type and mutated Notch1. Wild-type Notch1 is shown in green, the mutated chain in red, and T349 is shown in pink.

Changes in Gibbs-free energy created by the two variants were then computed in order to determine what impact the mutations are likely to have on protein folding. Defining $\mathbf{\Delta\Delta G}$ as the change in Gibbs-free energy and $\mathbf{\Delta G}$ as steady-state Gibbs-free energy, $\mathbf{\Delta\Delta G}$ was calculated as follows:

$$\mathbf{\Delta\Delta G = \Delta G(wildtype) - \Delta G(mutation)}$$

SDM (Pandurangan *et al*, 2017) and mCSM (Pires *et al*, 2014) analyses predicted that neither T311P and T349P would significantly change protein stability (|ΔΔG|<1; **Figure 4.3.6**); mCSM protein-protein interaction analysis predicts a negligible change in ΔΔG (|ΔΔG|<0.5 kcal/mol) of the Notch1-ligand binding interaction (**Figure 4.3.7**). Other online variant confirmation prediction software including DynaMut predicted similar negligible changes (stabilizing ΔΔG<1) (Rodrigues *et al*, 2018). These data suggest that since there is little quantifiable change in Gibbs-free energy caused by the two mutations, any functional effect seen may not be due to alterations in the Notch-ligand interaction.

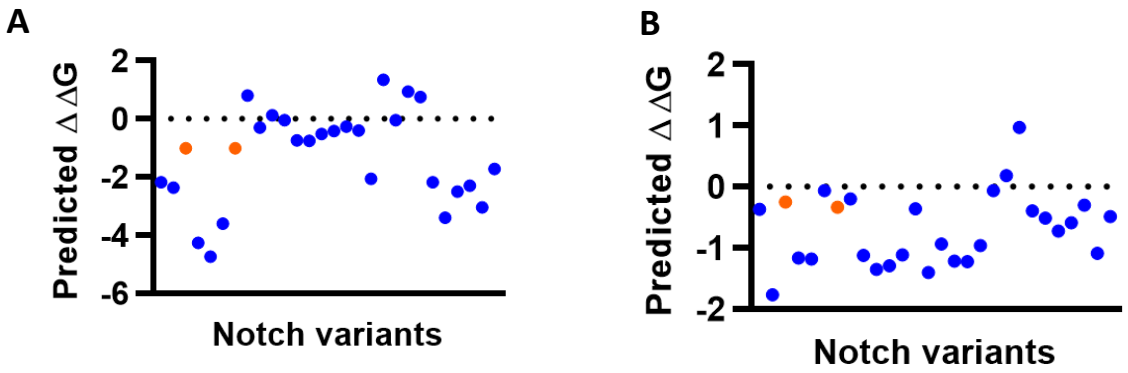

*Figure 4.3.6: Quantifying the changes in Gibbs-free energy released by T349P and T311P. Analyses by SDM **(A)** and mCSM-stab **(B)** for all the Notch1 variants found in COSMIC that are at the protein-ligand interface (T311P and T349P mutants are coloured orange).*

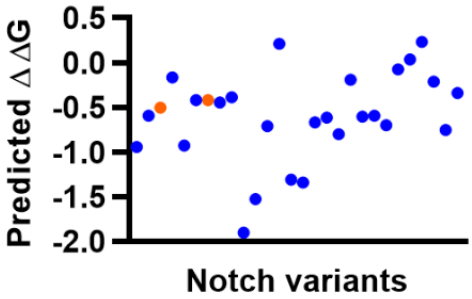

Figure 4.3.7: mCSM-protein-protein-interaction analysis. Analyses for all the Notch1 variants found in COSMIC that are at the protein-ligand interface (T311P and T349P mutants are coloured orange).

4.4 Investigating *in vitro* models to study Notch1 mutations

Notch1 is expressed at high levels in ALCL cell lines (Jundt *et al*, 2002), which fits with data showing that Notch1 is highly expressed in patient tumours (more on this in Chapter 5). However, of all the cell lines evaluated, none express the *notch1* variants detected in the patient samples (data not shown). Hence, in order to functionally evaluate the consequences of these mutations to the proteins encoded, attempts were made, using CRISPR-Cas9 technology, to engineer T349P and T311P Notch1 into ALCL cell lines. The Cas9 expression plasmid pSpCas9(BB)-2A-GFP (Addgene; Cat# 48138) was expressed into ALCL cell lines using nucleofection, after failed attempts to insert the plasmid into ALCL cell lines using the latest generation of Lipofectamine™; Lipofectamine 3000 (Thermo Fisher Scientific, Cat# L3000001; **Figure 4.4.1**). Indeed, previous experience has shown suspension T-cell derived lines to be resistant to liposome-based transfection technology, although we had hoped that the latest iteration of Lipofectamine™ may have overcome this issue, as the manufacturer's promotional material suggests.

Instead, we proceeded with electrical current-based nucleofection using Amaxa's Nucleofector™ (now owned by the Lonza Group). Optimisation suggested that programmes A030 and G016 produced the best results, in terms of balancing toxicity of the technique and electroporation of the plasmid into the cell lines. Sorting using the plasmid's GFP marker allowed to select for nucleofected cell lines expressing Cas9, protein and mRNA expression of which was verified using Western Blotting (**Figure 4.4.1** and **Figure 4.4.2**) and RT-qPCR (data not shown). Following this, single-stranded Donor Oligonucleotides (ssODN) and sgRNA were designed to mediate cleavage and homology-directed repair of the *notch1* gene to introduce the variants we identified. Unfortunately, it soon became clear that nucleofection of these oligonucleotides for transient expression was too toxic to ALCL cell lines already stressed by the expression of Cas9, and transfection had already proven to be impossible. Stable expression of the sgRNA and ssODN using viral transduction was investigated, but well-documented concerns for significant off-target mutations (Pattanayak *et al*, 2013) should cell lines stably express both Cas9 and sgRNA for the months required for downstream experiments led us to abandon this approach. Putting the off-target effects aside, ssODN could not, at the time, be transduced into cell lines, as they could not be expressed by a simple plasmid, and thus would require nucleofection regardless, which has proven both too toxic and to have too low a transfection efficiency for this approach to work – particularly since cells would have to be grown out from single clones to guarantee a homogeneous cell population.

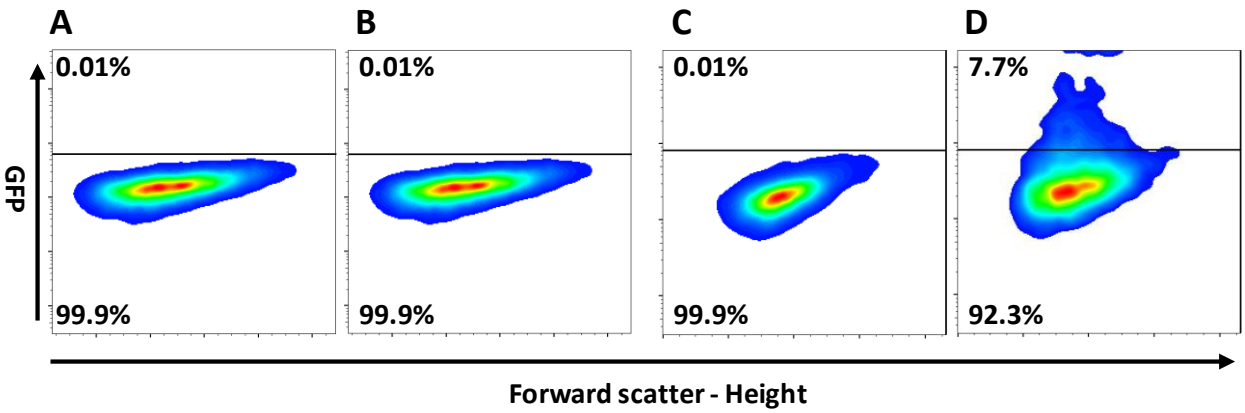

*Figure 4.4.1: FACS plots of Cas9 nucleofection and transfection. ALCL cell lines were transfected, using Lipofectamine, with either an empty vector **(A)** or a GFP-Cas9-expressing plasmid **(B)** or electroporated using Nucleofection, with the same empty vector **(C)** or GFP-Cas9 construct **(D)** and analysed for GFP expression using FACS (representative FACS plots are shown).*

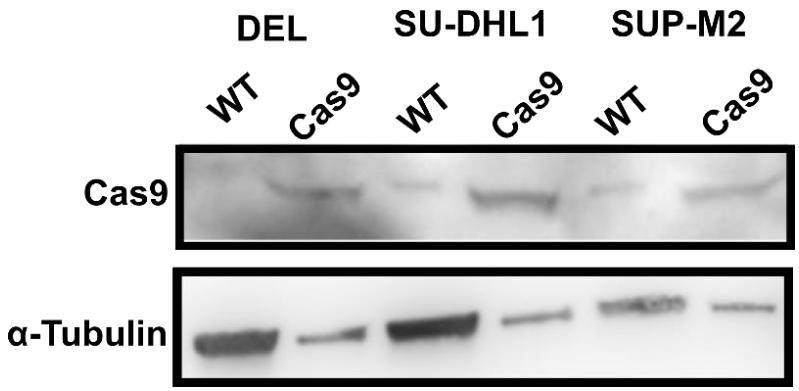

Figure 4.4.2: Validating Cas9 expression. Western Blot validating Cas9 protein expression in electroporated ALCL cell lines. Blots are representative of three biological replicates.

4.5 Notch1 T349P confers a proliferative advantage to cells in which it is expressed

An expression plasmid containing the whole length *notch1* cDNA (Li *et al*, 2008) was mutated by site directed mutagenesis to carry the variants T349P and T311P. Due to the high basal expression levels of Notch1 in ALCL cell lines, an alternative cell line was chosen in which to express the Notch1 mutants in order to assess their functional consequences.

Unfortunately, B- and T-cell lines all have high basal levels of *notch1*, as do many other cell lines and therefore the HEK233FT cell line, a well-characterized, easy-to-use, and easy-to-transfect with proven low-to-absent endogenous levels of *notch1* expression was employed (**Figure 4.5.1**) (Petit *et al*, 2002; Oh *et al*, 2010). Wild-type or mutated Notch1 plasmids were transfected into HEK293FT cells, and protein levels visualised by Western Blot to verify expression and activation of both full-length Notch1 and the activated ICN (**Figure 4.5.1**). In addition, mRNA expression levels of the proteins were assessed by RT-qPCR to verify that levels of expression were not significantly different between cells expressing the wild-type and mutated Notch1 plasmids (**Figure 4.5.1**).

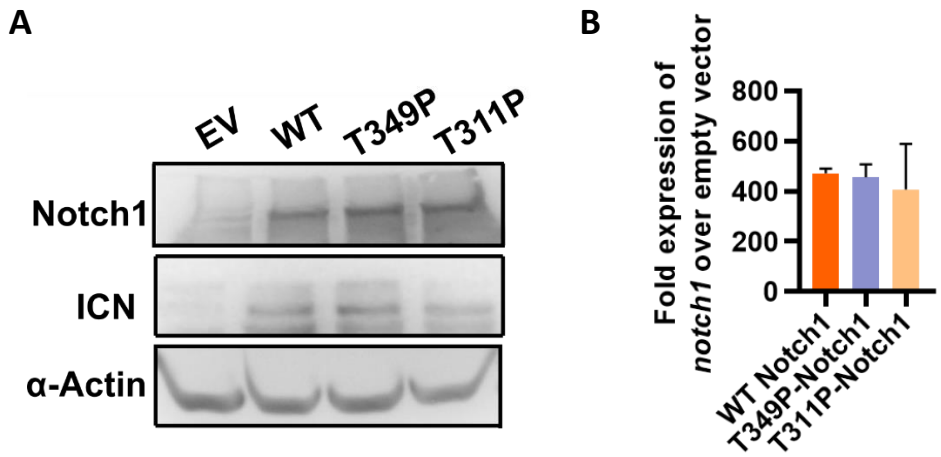

Figure 4.5.1: Validation of ectopic Notch1 expression in HEK293FTs following transfection. ***(A)*** *Expression of the indicated proteins according to Western Blot, blots are representative of three biological replicates. EV = Empty Vector, WT = Wild-type.* ***(B)*** *Fold expression of notch1 mRNA in HEK293FTs expressing either a Wild-Type (WT) or mutated Notch1 over an Empty Vector control, as measured using RT-qPCR.*

In order to assess the functional consequences of the mutations, Notch1 mutants T349P and T311P were expressed in HEK293FT cells and cell proliferation monitored by the RealTimeGlo assay (**Figure 4.5.2**). The T349P mutant led to a significant increase in cell proliferation at 72 hours, as compared to both the empty vector control and the HEK293FTs stably transfected with the wild-type cDNA of *notch1*. These data suggest that the T349P Notch1 mutant, confers a survival advantage to the cells in which it is expressed in the absence of exogenously-applied ligand.

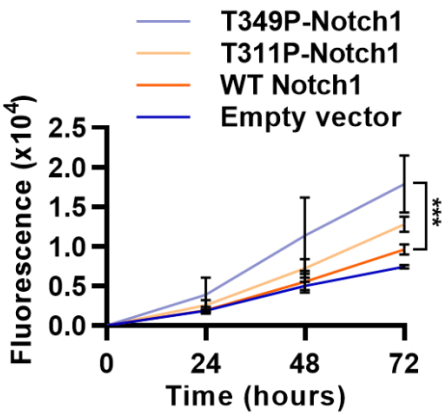

*Figure 4.5.2: Proliferative effect of the Notch1 mutations. Proliferation of HEK293FTs expressing either an Empty Vector, Wild-Type (WT) or mutated Notch1, as measured by the Real-Time-Glo assay (***p<0.001; n=3).*

In keeping with a proliferative advantage, cells expressing the mutant forms of Notch1 also showed increased transcript levels of the transcriptional targets of Notch1 activity, *hes1* and *hey1*, suggesting that Notch1 is transcriptionally active in these cells (**Figure 4.5.3**). These data confirm the previously detected increase in ICN expression observed in the cell lines expressing mutant forms of Notch1 (**Figure 4.5.1**).

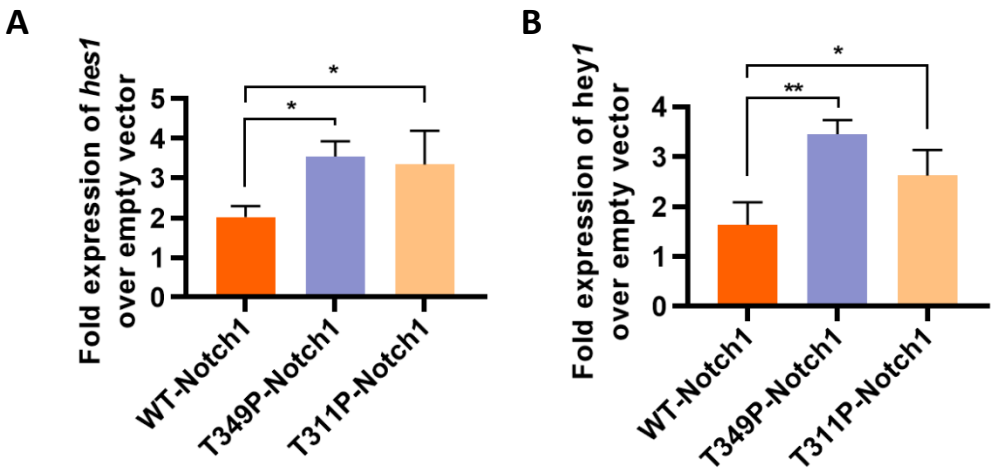

Figure 4.5.3: Expression levels of Notch1 downstream genes. Fold expression of hes1 ***(A)*** *or hey1* ***(B)*** *in HEK293FT cells expressing either Wild-Type (WT) or mutated Notch1 compared to an Empty vector, as measured by RT-qPCR (*p<0.05; **p<0.01; n=3).*

4.6 Interplay between Notch1 T349P and its ligand, DLL1

Since *in silico* modelling suggested that T349P and T311P could mediate binding to the Notch1 ligand, assays were conducted to determine whether the increase in cell proliferation observed was dependent on binding to the Notch1 ligand. HEK293FT cells expressing wild-type or mutant *notch1* were co-cultured with either the wild-type OP9 cell line or OP9 cells expressing the Notch1 ligand DLL1. The OP9-DLL1 system is a widely used as a means to activate Notch1 activity, often to promote differentiation of immune cells (Zúñiga-Pflücker, 2004; Holmes & Zúñiga-Pflücker, 2009). Here, OP9-DLL1 cells were used both to activate the exogenously expressed Notch receptor in HEK293FTs using a co-culture protocol followed by sorting on Notch1 (**Figure 4.6.1** and **Figure 4.6.2**) - or to activate the Notch1 receptor in ALCL cell lines endogenously expressing wild-type Notch1 (as described in Chapter 5).

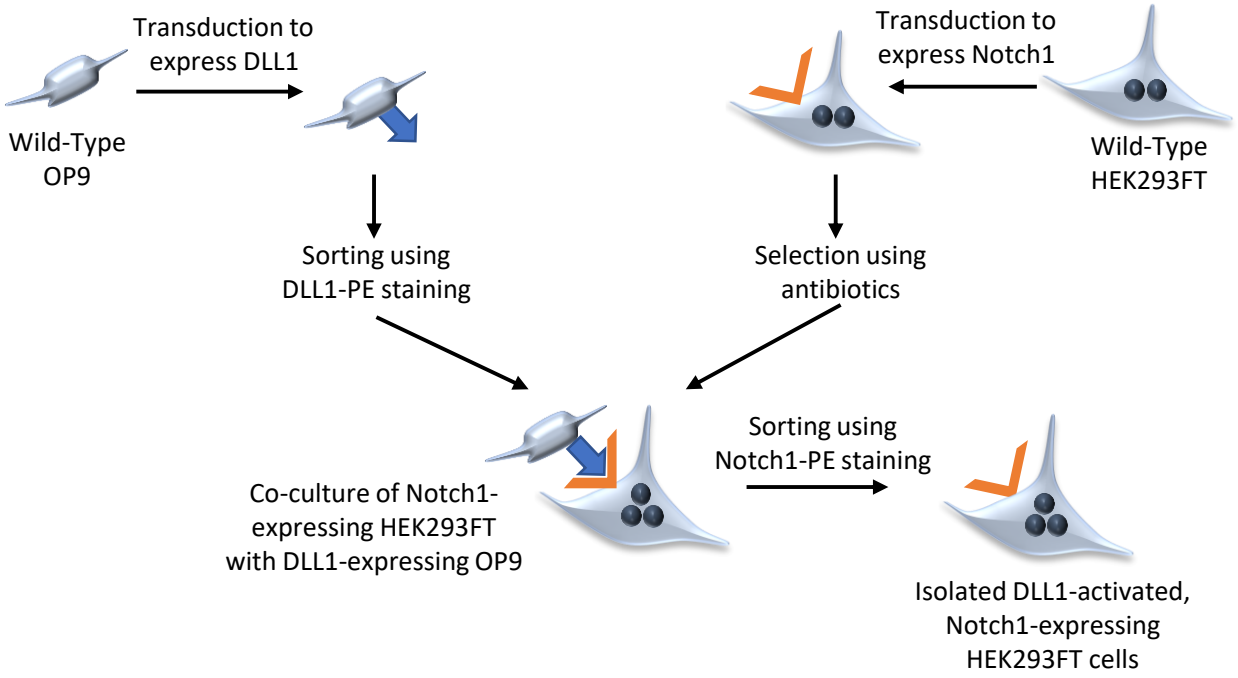

Figure 4.6.1: Summary of the co-culture method. This cartoon describes the method we used here to express DLL1 in the OP9 cell line, Notch1 (wild-type or mutated) in the HEK293FT cell line, and how the two cell lines were co-cultured to activate the Notch1 receptor using the DLL1 ligand.

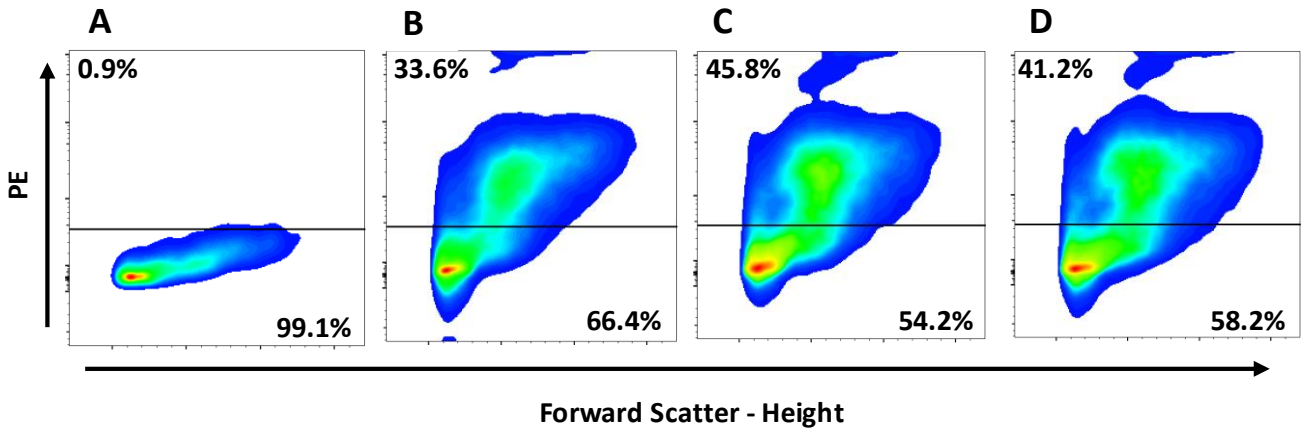

*Figure 4.6.2: Sorting of the OP9-DLL1 and Notch1-expressing-HEK293FT co-culture. HEK293FT cells transfected with an empty vector **(A)**, wild-type **(B)**, T349P-notch1 **(C)** or T311P-notch1 **(D)** were separated by flow cytometry according to Phycoerythrin (PE) staining (cells were stained using a Notch1-PE conjugated antibody). Plots are representative of three biological replicates.*

There was no discernible difference in proliferation between cells co-cultured with wild-type OP9, or OP9-DLL1 cells (**Figure 4.6.3**). In other words, while the Notch1 mutations T349P and T311P provided a growth advantage, the co-culture did not. In keeping with this observation, there was no increase in expression of the Notch1 downstream target genes *hes1* and *hey1* (**Figure 4.6.4**). This suggests that the co-stimulation using the OP9-DLL1 feeder cell line may not have worked.

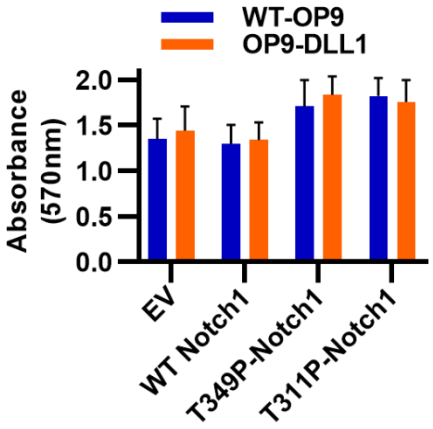

Figure 4.6.3: Cell proliferation upon co-culture with OP9 cells presenting the Notch1 ligand, DLL1. Proliferation of HEK293FTs expressing either an Empty Vector (EV), Wild-type (WT) or mutated Notch1, co-cultured with either wild-type (WT-OP9) or DLL1-expressing OP9 (OP9-DLL1) cells, as measured by an MTT assay. Representative of three biological and technical replicates

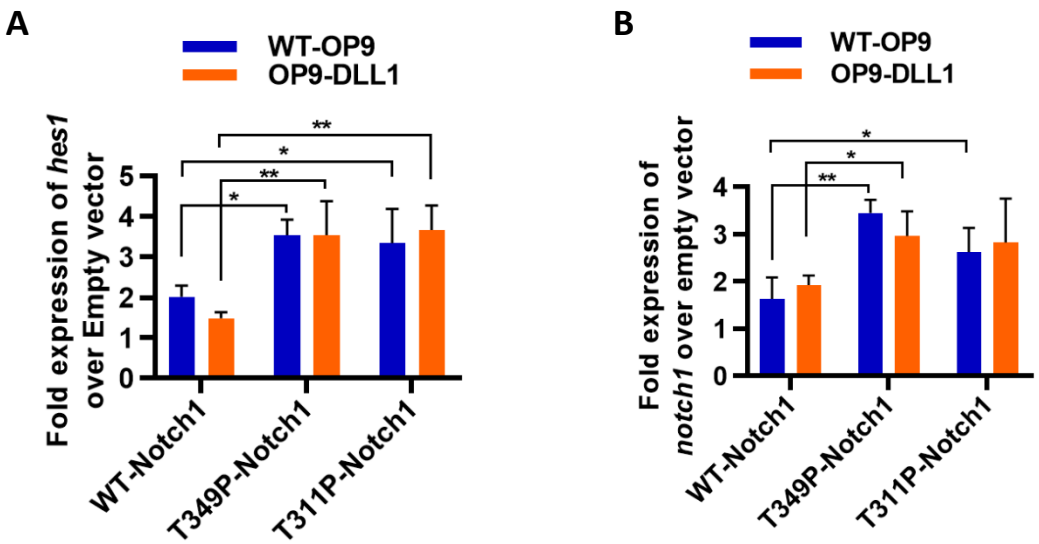

Figure 4.6.4: Expression levels of Notch1 target genes when co-cultured with OP9-DLL1 cells. Fold expression of hes1 ***(A)*** *and hey1* ***(B)*** *in HEK293FTs expressing either Wild-Type (WT) or mutated Notch1 over an Empty vector, when co-cultured with a Wild-Type (WT-OP9) or DLL1-expressing (OP9-DLL1) OP9 cell line as measured by RT-qPCR (*p<0.05; **p<0.01; n=3).*

Interestingly, increased transcription of endogenously-expressed DLL1 was observed on expression of the mutant forms of Notch1 compared to wild-type protein suggesting that the mutant proteins might themselves lead to transcription of ligand in an autonomous fashion (**Figure 4.6.5**). We did, as a positive control, test that presenting the Notch ligand to ALCL cells increased expression of Notch target genes and found that this was indeed the case (see chapter 6.6).

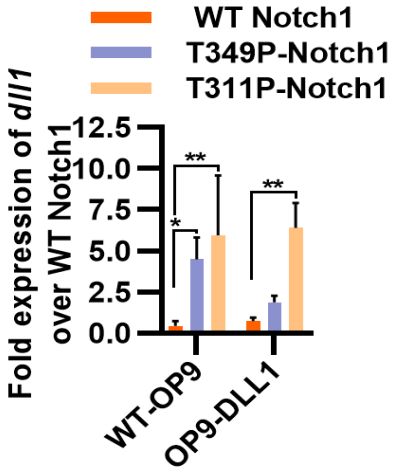

*Figure 4.6.5: Expression of the Notch ligand DLL1 in HEK293FT cells. Cells expressing either Wild-Type (WT) or mutated Notch1 compared to an Empty vector control, when co-cultured with either Wild-Type (WT-OP9) or DLL1-expressing (OP9-DLL1) OP9 cell lines as measured by RT-qPCR (*p<0.05; **p<0.01; n=3).*

4.7 Discussion

In this chapter the functional consequences of Notch1 mutants T349P and T311P were investigated: although these variants have previously been identified, they have never before been characterised. Threonine bases within the EGF-like domains are post-translationally modified by O-linked Glycosylation which is necessary for ligand-dependent Notch1 signalling (Stanley & Okajima, 2010; Pakkiriswami *et al*, 2016; Haines & Irvine, 2003). In contrast, Proline is one of the few extremely rigid amino acids, known to result in a change in tertiary structure, often forcing a change in β-sheet conformation (each EGF-like domain is made up of 4 β-sheets among other structures). To note, our bioinformatics analysis identified two more variants in EGF-like domains 8 and 31, as well as one in the Lin12/Notch repeat domain 2. In addition, it has been shown that EGF-like domains 8 to 12 are important for Notch1 binding to its different ligands (Luca *et al*, 2017; Rebay *et al*, 1991). Because of all this data and literature, we theorize that the variant identified here might modulate ligand binding.

In parallel, calcium signalling is thought to be dysregulated in ALCL (Rust *et al*, 2005), but studies have also shown that Calcium ions play an important role in Notch ligand binding (Rand *et al*, 2000). Indeed, binding of the Calcium ions may modulate the tertiary structure of Notch1 and thus effect ligand binding affinity (Cordle *et al*, 2008), thereby modulating Notch1 downstream signalling (Raya *et al*, 2004). In addition to this, we have shown through GSEA that not only are calcium signalling genes hypermutated, but that a number of proteins with calcium ion binding domains are mutated as well

(**Figure 3.8.2** and **Figure 3.8.3**). It therefore seems possible that calcium signalling and the presence of calcium ions for binding of Notch1 to its ligand is important in determining the effect of T349P and T311P. Indeed, it may be that these variants only modulate Notch ligand binding by effecting calcium ion binding, though unfortunately we did not have the facilities to test this hypothesis. Ultimately, it's likely that only such an assay as crystallography could verify this, though it remains questionable whether the biological question and implications are worth investing in such a time- and resource-intensive technique.

As explained then, we posited that these mutations in the extracellular EGF-like domains of the Notch1 receptor may modulate the binding of Notch1 with its ligands – however, *in silico* data did not suggest that these variants force conformational changes that lead to a significant change in Gibbs-free energy. While modelling the strength of ion binding is also a possibility, this would require a high-resolution crystal structure of the binding of the calcium ions to the relevant extracellular domains of Notch, which is not available, hence we could not proceed with such modelling. In addition, it should be said that crystal structures seldom feature post-translational modification, as the proteins are expressed ectopically in specialty strains of yeast or bacteria. As a result, the Notch1 and Jag1 proteins modelled here may well lack important modifications, including some notorious ones such as Glycosylation or Fucosylation, which would be lost in the mutated protein. Research has shown that these modifications are important to the interaction between Notch and its ligands – indeed removing certain Fucosylation sites inhibited Notch1 signalling (Schneider *et al*, 2018).

Since the computer modelling left us with little clues as to the functional consequences of variants T311P and T349P in ALCL, the variants were studied *in vitro* in both the presence and absence of Notch1 ligand. Full-length Notch1 was expressed in the HEK293FT cell line as it has low endogenous levels of expression compared to ALCL and other lymphoma cell lines. This replaced CRISPR-based protocols to engineer the variants into ALCL cell lines, for the reason delineated in this chapter. Ideally, we would have studied these mutations in ALCL, particularly since using an alternative non-T cell cancer cell line is too far removed from the model we would prefer to use. In particular, it's unclear whether the ectopic expression we induced would lead to the activation of the same pathways that Notch1 would signal through in ALCL. Among other reasons, this is due to the possible absence in HEK293FTs of pathways with which Notch1 cross-talks in ALCL, examples of which are given in Chapter 5. Overexpressing the Notch1 plasmid, wild-type or mutated, in ALCL, would leave the strong, endogenous wild-type Notch1 in place, and evidence from digital droplet PCR suggests that the fractional abundance of mutated Notch1 mRNA in such a system is below 25%, which we did not believe was sufficient to study the two Notch1 mutations. Furthermore, as detailed in Chapters 5 and

6, ALCL are addicted to Notch1 expression, so knocking out the *notch1* gene to then express the ectopic plasmid was not an option either, as cells would have died following knocking out of the endogenous copy of the gene.

Expression of the Notch1 T349P mutation led to an increase in cellular proliferation in this system, concurrent with increases in expression of *hes1* and *hey1*, two genes immediately downstream of Notch1. In keeping with the lack of effects on ligand-receptor interaction predicted *in silico*, activating the Notch1 receptor using the co-culture OP9-DLL1 system did not induce a growth advantage to T349P or T311P Notch1 mutant-expressing cells, although this may be because HEK239FT cells endogenously express Notch ligands (Mumm *et al*, 2000; Oh *et al*, 2010), or because the mutant Notch1 proteins promote expression of Notch ligands in HEK293FT cells. Our positive control, detailed in chapter 6.6, shows that presenting the Notch ligand to ALCL cells significantly increased expression of Notch1 target genes, indicating that the co-culture concept is viable, as suggested by the large amount of literature using this exact system. It is also possible that, as two sets of adherent cell lines, HEK293FTs and OP9-DLL1 cells may not grow close enough or at the right orientation for Notch1 and its ligand come into contact, as opposed to co-culturing OP9-DLL1 cells with suspension ALCL cells. However, growing both OP9-DLL1 and HEK293FT should provide sufficient confluency and coverage to ensure that a majority of the Notch1 receptors come into contact with their ligand – indeed it seems more likely, as the literature suggests, that HEK293FTs express the Notch ligand endogenously. If that is indeed the case, most of these experiments would need to be attempted using a different cell line than HEK293FTs, although few ubiquitous cell lines are documented as having low endogenous levels of Notch1, making this a difficult endeavour.

Therefore, it remains unclear whether the Notch ligand is in any way responsible for the functional effects of T349P and T311P. It remains a possibility that the Notch ligand expressed in HEK293FTs results in a perpetually activated Notch1 when exogenously expressed in HEK293FTs, a theory given credence by **Figure 4.5.1**, which shows the presence of activated, intracellular Notch1 in HEK293FTs cultured on their own. This is more likely than the possibility of T349P promoting ligand-independent activation of the Notch receptor, as such an effect would only really be expected by a loss-of-function mutation in the negative regulatory region of Notch1, responsible for exactly that: preventing ligand-independent activation of Notch1. Indeed, mutations have been observed in T-ALL doing just that: activating Notch1 by disrupting the activity of the negative regulatory region (Weng *et al*, 2004). Due to the apparent systemic importance of Notch signalling in ALCL, and since we show here that Notch1 can affect cell proliferation, we decided to investigate the importance and role of the Notch pathway in ALCL.

5. The Notch pathway in ALCL

5.1 Introduction

Binding of the Notch receptor to one of its ligands leads to proteolytic cleavage of Notch; first at a site in the Negative Regulatory Region (NRR) by the A-Disintegrin and Metalloprotease (ADAM) family of proteases, leading to Notch Extracellular Truncation (NEXT), which sheds the extracellular domain of Notch but leaves the intracellular domain tethered to the cell membrane. This first cleavage changes the conformation of Notch, rendering it a target for γ-secretases. Proteolysis by γ-secretase releases the ICN, except in cases where the PEST or Heterodimerization domains are mutated, in which case the ICN is cleaved without the required conformational change from the extracellular domains, as only observed in some malignancies. Mutations in the negative regulatory region meanwhile lead to ligand-independent activation of the receptor (Weng *et al*, 2004). In a healthy setting, signal transduction by the ICN is tightly regulated as demonstrated by its short half-life and the fact that it is quickly targeted for proteasomal degradation by an ubiquitin ligase (Tsunematsu *et al*, 2004; Fryer *et al*, 2004). The ICN is then transported to the nucleus by means so far unknown, where the ICN RAM and ANK domains bind to a CSL (CBF1, Suppressor of Hairless, Lag-1) transcription factor: RBP-Jκ (Lubman *et al*, 2007; Friedmann *et al*, 2008). This complex then displaces transcriptional repressors to promote expression of a number of target genes, though it is not altogether clear what promoter sequences the Notch/RBP-Jκ complex has a strong affinity for and therefore binds to.

While the role of Notch1 signalling is still hotly debated, particularly in developmental biology, it clearly has a key role to play in T cell biology, as laid out in chapter 1. It is therefore of no surprise that Notch1 has been shown to play an oncogenic role in a number of T cell malignancies, in particular in ALCL (Kamstrup *et al*, 2014). Indeed, recent evidence from our lab suggests that NPM-ALK may induce Notch1 expression in T cell development and tumour formation (Malcolm *et al*, 2016). Therefore, in this chapter the relevance of the Notch1 pathway in ALCL is investigated, as well as its relationship with NPM-ALK signalling.

To study this, we used widely accepted and used *in vitro* model cell lines derived from tumour tissue of ALCL patients, mostly from the most common sub-type (anaplastic, large-cell), they are Karpas 299 ('K299'), SU-DHL (more than one type exists; SU-DHL1 will be used in this thesis), SUP-M2 and DEL, indeed these are the cell lines used throughout this thesis to model ALCL tumours (Fischer *et al*, 1988; Barbey *et al*, 1990; Morgan *et al*, 1989; Epstein & Kaplan, 1974). These ALCL cells lines all present with the NPM-ALK translocation and are not significantly different from each other, safe for Karpas 299 which have been shown to behave differently on a biochemical level, probably due to additional mutations of the PTEN and p53 pathways (Turturro *et al*, 2001).

5.2 Silencing *notch1* in ALCL cell lines leads to a decrease in proliferation

We first attempted to silence the expression of *notch1* using siRNA. The effect was limited, though we still observed a statistically significant 8.3%, 10.4%, and 12.8% decrease in *notch1* expression, respectively in Karpas 299, DEL and SUP-M2 cell lines, as measured by qPCR (**Figure 5.2.1**). This led to a limited, though again statistically significant decrease in proliferation, as measured by MTT (**Figure 5.2.2**). However, as inhibition of gene expression was at the limit of detectability by qPCR, we decided to validate these data using another technique.

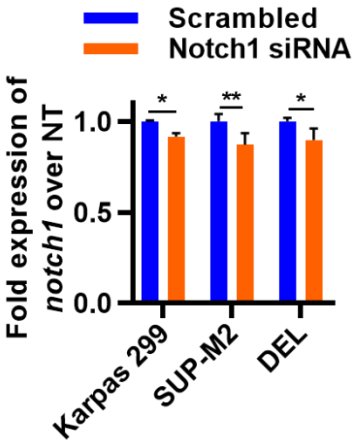

*Figure 5.2.1: notch1 expression in siRNA-treated ALCL cells, as measured by qPCR. Fold expression of notch1 in ALCL cells nucleofected with siRNA targeting notch1, calculated as fold scrambled siRNA, and measured by qPCR 48 hours following nucleofection (*p<0.05; **p<0.01; n=3).*

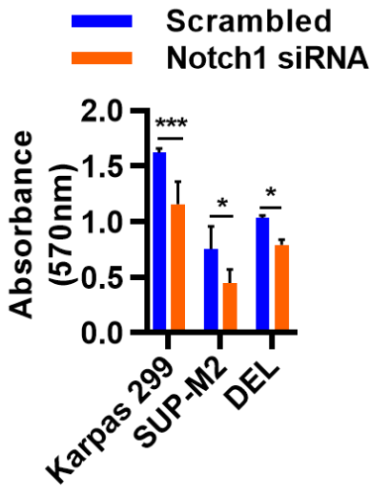

*Figure 5.2.2: Proliferation of ALCL cell lines under siRNA-mediated notch1 silencing. Proliferation of ALCL cells nucleofected with siRNA targeting notch1, measured by MTT at 48 hours following nucleofection of the siRNA, compared to scrambled siRNA (*p<0.05; ***p<0.005; n=3).*

We then attempted to confirm these results using a two-plasmid KRAB-dCas9 CRISPR inactivation construct (Gilbert *et al*, 2014). This protocol uses a sgRNA to direct dCas9 fused to a transcriptional repressor (KRAB) to the promoter of a particular gene; in this case *notch1*. The decrease in expression of *notch1* was greater than observed with siRNA; of two sgRNAs tested, the second showed statistically significant 31.6%, 41.4% and 30% decreases in *notch1* expression in DELs, Karpas 299s, and SUP-M2s respectively, as compared to a non-targeting sgRNA (**Figure 5.2.3**). This led to statistically significant decreases in proliferation of 19.6%, 19.5% and 28% at 48 hours, respectively in DEL, Karpas 299 and SUP-M2 cell lines (**Figure 5.2.4**).

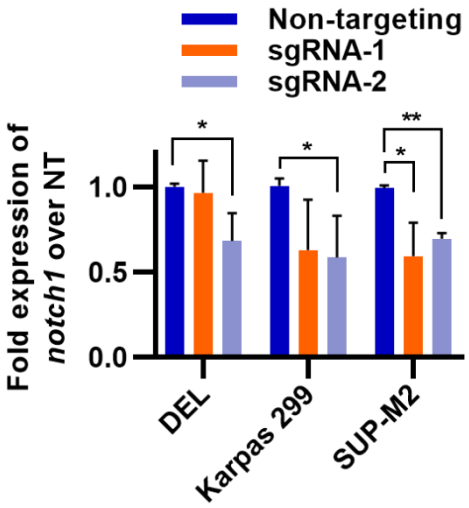

*Figure 5.2.3: CRISPR-inactivation of notch1 expression, as measured by qPCR. Fold expression of notch1 in ALCL cells transduced with Notch1-silencing sgRNA, calculated as fold change over non-targeting (NT) sgRNA, and measured by qPCR 48 hours following nucleofection (*p<0.05; **p<0.01; n=3).*

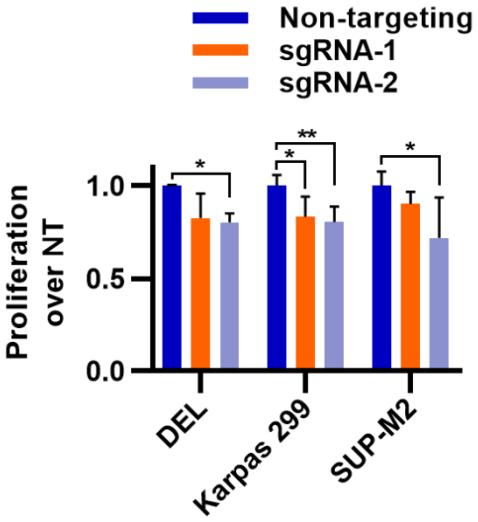

*Figure 5.2.4: The effect on proliferation of CRISPR-inactivation-mediated notch1 silencing. Proliferation of ALCL cells transduced with sgRNA targeting Notch1, measured by MTT 48 hours following nucleofection, calculated as fold-change over non-targeting (NT) sgRNA (*p<0.05; **p<0.01; n=3).*

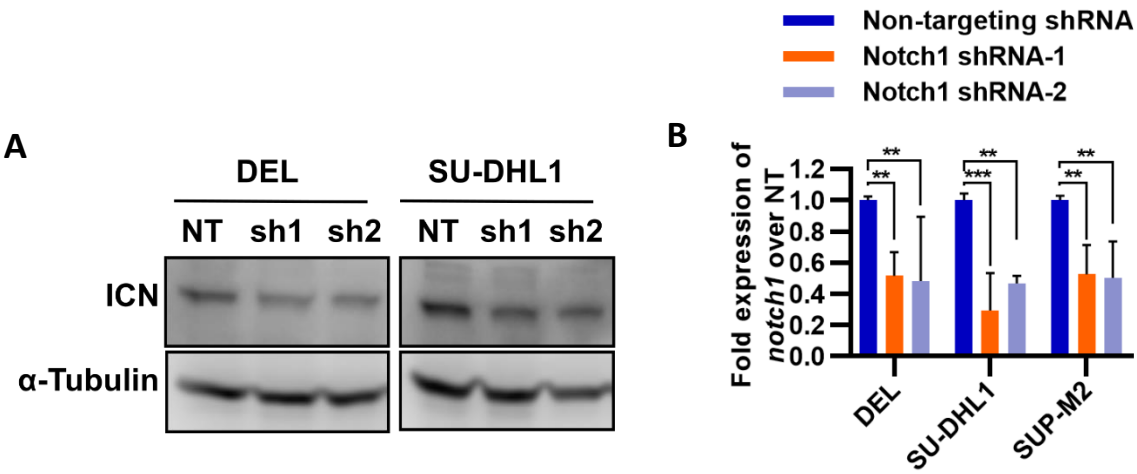

Figure 5.2.5: shRNA silencing of notch1 expression, as seen at the transcript and protein level. Cells were transduced with 2 shRNA targeting Notch1 or a non-targeting (NT) control shRNA. ***(A)*** *Western Blot showing decreased expression of the activated, ICN in ALCL cell lines. Blots are representative of three biological replicates.* ***(B)*** *Fold expression of notch1 in ALCL cells transduced with Notch1-silencing shRNA, calculated as fold change over non-targeting (NT) shRNA, and measured by qPCR (**p<0.005; ***p<0.0001; n=3).*

For added certainty, we proceeded with shRNA silencing of *notch1* expression using lentiviral expression plasmids, and were able to verify a decrease in expression of at least 50% across 2 shRNA and 3 cell lines at both transcript and protein levels (**Figure 5.2.5**). This in turn led to a significant decrease in cell proliferation at 48 hours, as measured by MTT in all 3 cell lines and for 2 shRNA (**Figure 5.2.6**). It is therefore clear that ALCL cell lines are addicted to *notch1* expression to proliferate.

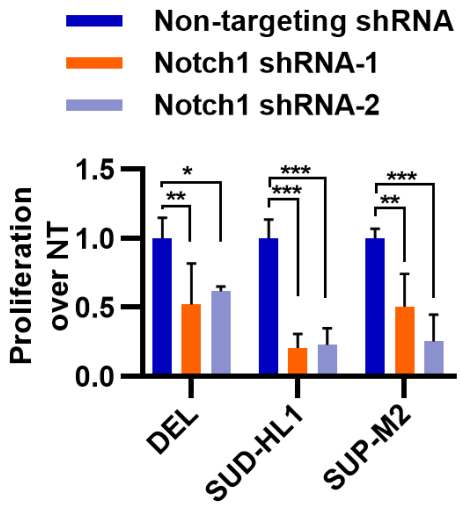

*Figure 5.2.6: Proliferation of ALCL cell lines under shRNA-mediated notch1 silencing. Proliferation of ALCL cells transduced with shRNA targeting Notch1, measured by MTT calculated as fold-change over non-targeting (NT) shRNA (*p<0.05; **p<0.005; ***p<0.0001; n=3).*

5.3 The decrease in proliferation observed upon *notch1* silencing is due to apoptosis.

To investigate the effect of silencing *notch1* in ALCL cell lines, we first measured the expression levels of Notch1's transcriptional targets *hes1* and *hey1*; they were also downregulated upon *notch1* silencing by shRNA (**Figure 5.3.1**). To identify the mechanics leading to decreased cell viability, apoptosis was assessed following staining of cells for AV and PI. A significant increase in the percentage of cells staining positive for Annexin V (AV) and/or Propidium Iodide (PI) was observed suggestive of cell death via apoptosis (**Figure 5.3.2**). Cells were also stained with intracellular PI to identify any changes in cell cycle. Representative FACS plots show the effect of *notch1* shRNA in SUP-M2: there is a significant shift to sub-G0, indicating that cells are entering apoptosis (**Figure 5.3.3**). This shift was quantified; a significant decrease in the G0-G2 population and a significant increase in the sub-G0 population is observed in all three cell lines when transfected with shRNA (**Figure 5.3.3**). We can therefore confidently conclude that ALCL cell lines are addicted to *notch1* expression, and that silencing this gene leads to cell death by apoptosis.

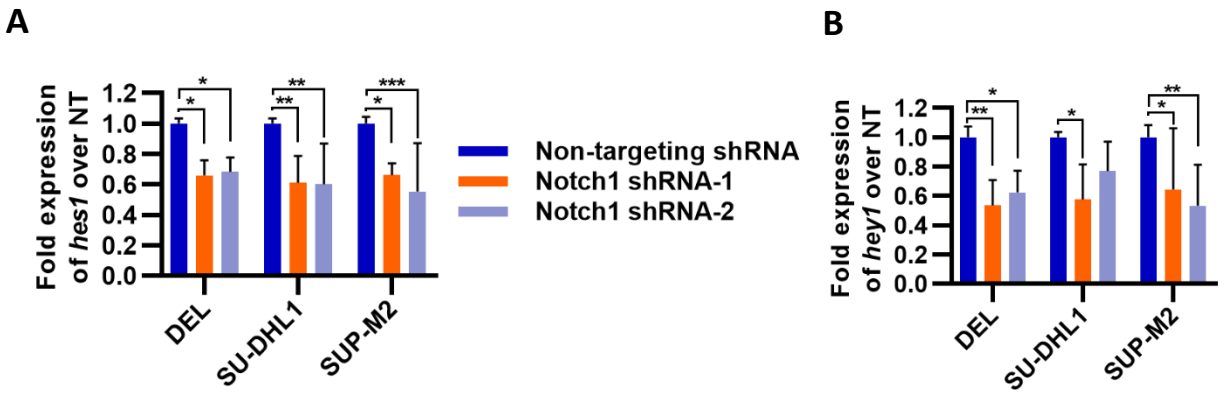

Figure 5.3.1: Expression of hes1 and hey1 upon shRNA silencing of Notch1. Fold expression of hes1 ***(A)*** *and hey1* ***(B)*** *in ALCL cells transduced with Notch1-silencing shRNA, calculated as fold change over non-targeting (NT) shRNA, and measured by qPCR (*p<0.05; **p<0.01; ***p<0.001; n=3).*

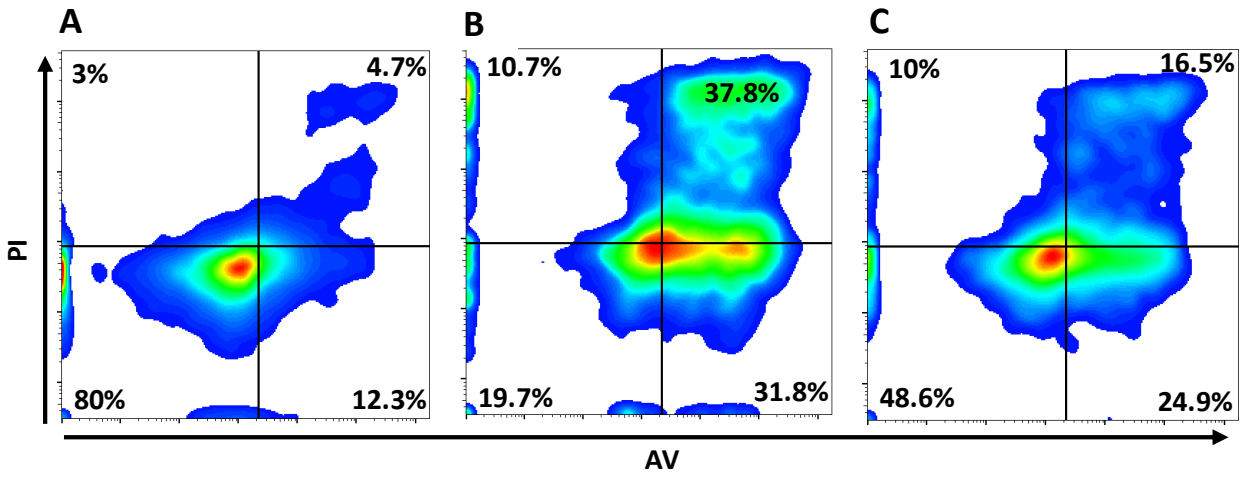

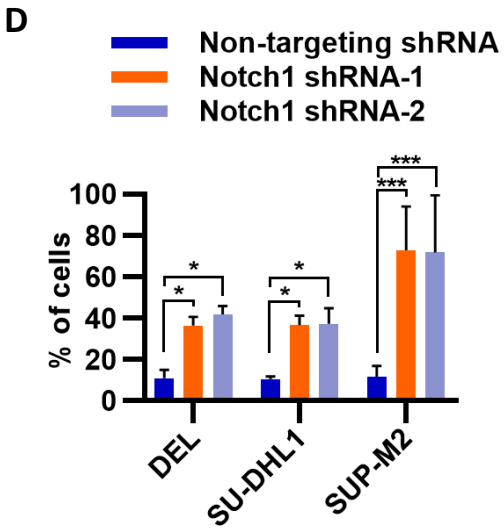

Figure 5.3.2: AV-PI staining of shRNA-transduced ALCL cell lines. Representative FACS plots of ALCL cells were transduced with a control non-targeting shRNA ***(A)*** *or a Notch1-targeting shRNA* ***(B-C)*** *and stained for AV and PI.* ***(D)*** *Quantification of cells staining for AV and/or PI (*p<0.05; ***p<0.0001; n=3).*

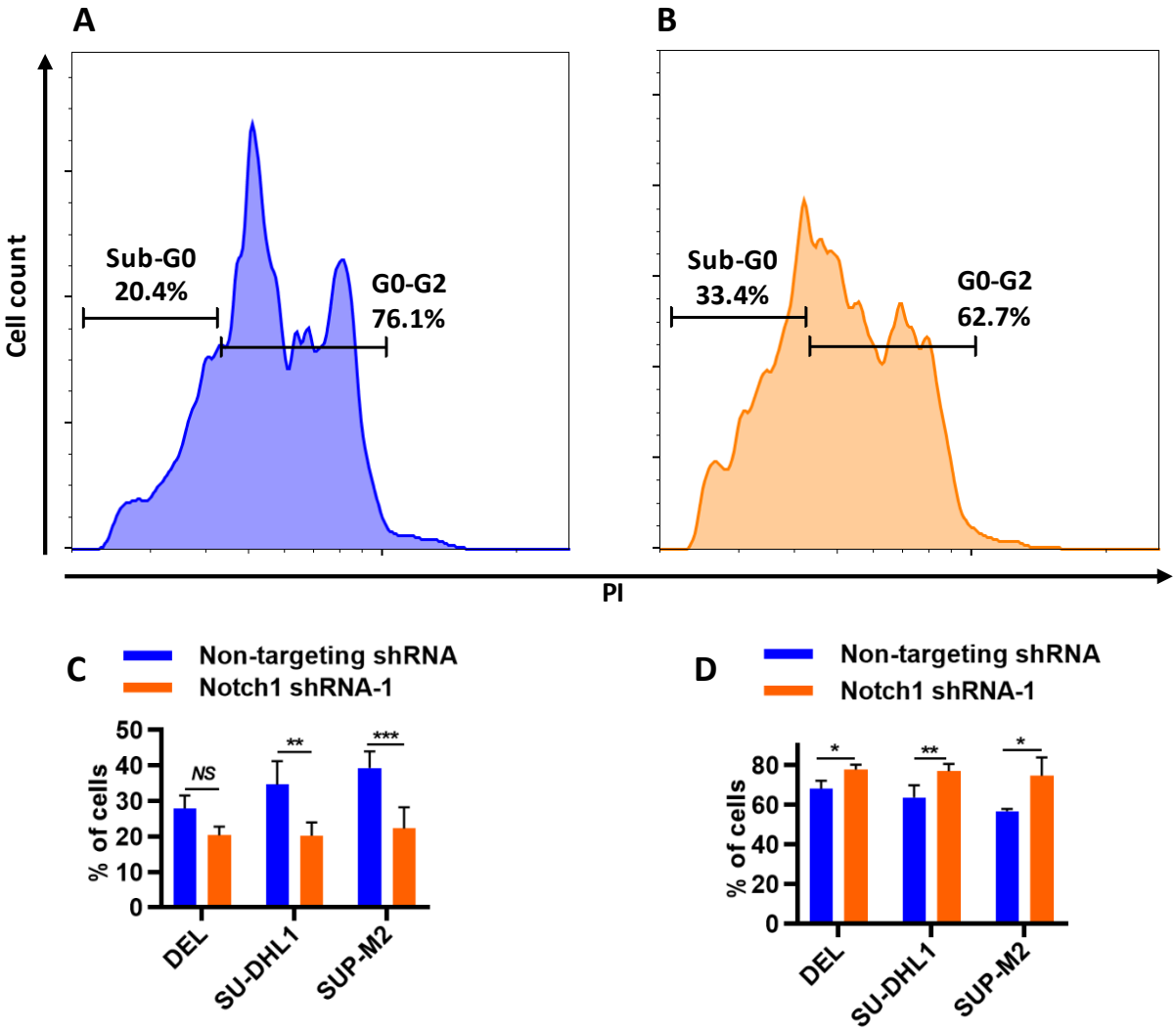

*Figure 5.3.3: Cell cycle analysis of ALCL cells after notch1 shRNA silencing. ALCL cells were transduced with a control non-targeting shRNA **(A)** or a Notch1-targeting shRNA **(B)**, permeabilised and stained for intracellular PI. FACS plots are representative of three technical and biological replicates. Quantification of cells in either G0 to G2 phases **(C)** or sub-G0 **(D)** (NS=not significant; *p<0.05; **p<0.01; ***p<0.0001; n=3).*

5.4 Notch1 promotes *myc* and *dtx1* expression in ALCL

To determine the signalling cascade downstream of Notch1, we made use of published microarray data of the T-ALL cell line CUTLL-1 that examines the effects of GSI treatment on gene expression (Choi *et al*, 2017; Sanchez-Martin *et al*, 2017; Wang *et al*, 2011a). The differential expression of the top hits present in at least two of three published datasets was computed - *hes1* and *hey1* are found, along with *dtx1*, a known regulator of the Notch pathway (suggesting a feedback mechanism), and other hits such as *myc* (**Figure 5.4.1**). Using qPCR, we confirm that, in ALK+, ALCL cell lines DEL, SU-DHL and SUP-M2, silencing *notch1* by shRNA leads to a significant decrease in both *myc* and *dtx1* signalling (**Figures 5.4.2**), suggesting that Notch1 in ALCL signals through a number of pathways beyond *hes1* and *hey1*, including *myc*, an important oncogenic signalling pathway in and of itself. Analysis of previously published ChIP-seq data of Notch1 and Notch3 in the CUTLL1 cell line (Choi *et al*, 2017; Wang *et al*,

2011a) confirms that Notch1 and 3 bind at these gene loci, binding which disappears upon GSI treatment (**Figure 5.4.3**). Unfortunately, no such dataset exists for ALCL.

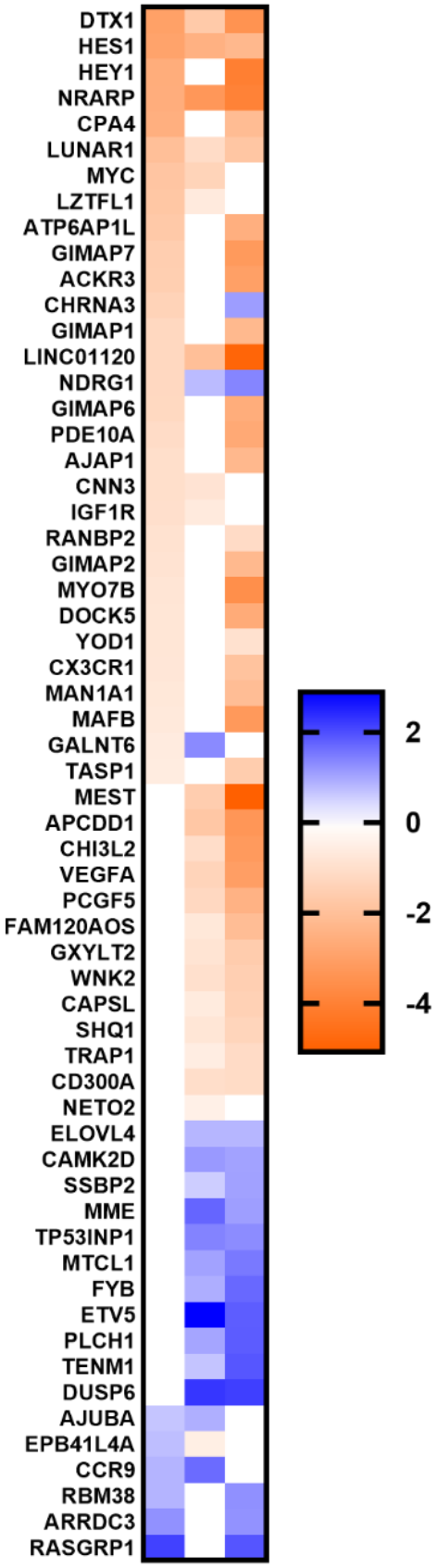

Figure 5.4.1: Microarray analysis of Notch1 downstream targets. Analysis of microarray data from three separate publications of the T-ALL cell line CUTLL-1, representing the fold-change in expression of the top 250 target genes (assessed by adjusted p-values) in the presence of GSI (over a vehicle control: DMSO); analysing previously published data (Choi et al, 2017; Sanchez-Martin et al, 2017; Wang et al, 2011a).

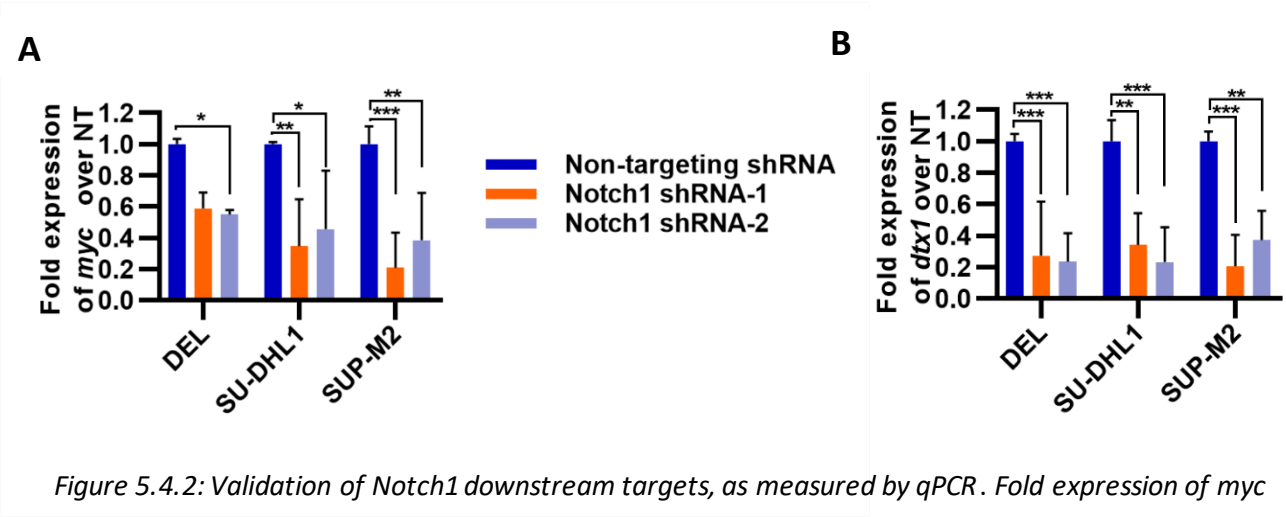

Figure 5.4.2: Validation of Notch1 downstream targets, as measured by qPCR. Fold expression of myc ***(A)*** *and dtx1* ***(B)*** *in ALCL cell lines transduced with Notch1-silencing shRNA, calculated as fold change over non-targeting (NT) shRNA, and measured by qPCR (*p<0.05; **p<0.01; ***p<0.0001; n=3).*

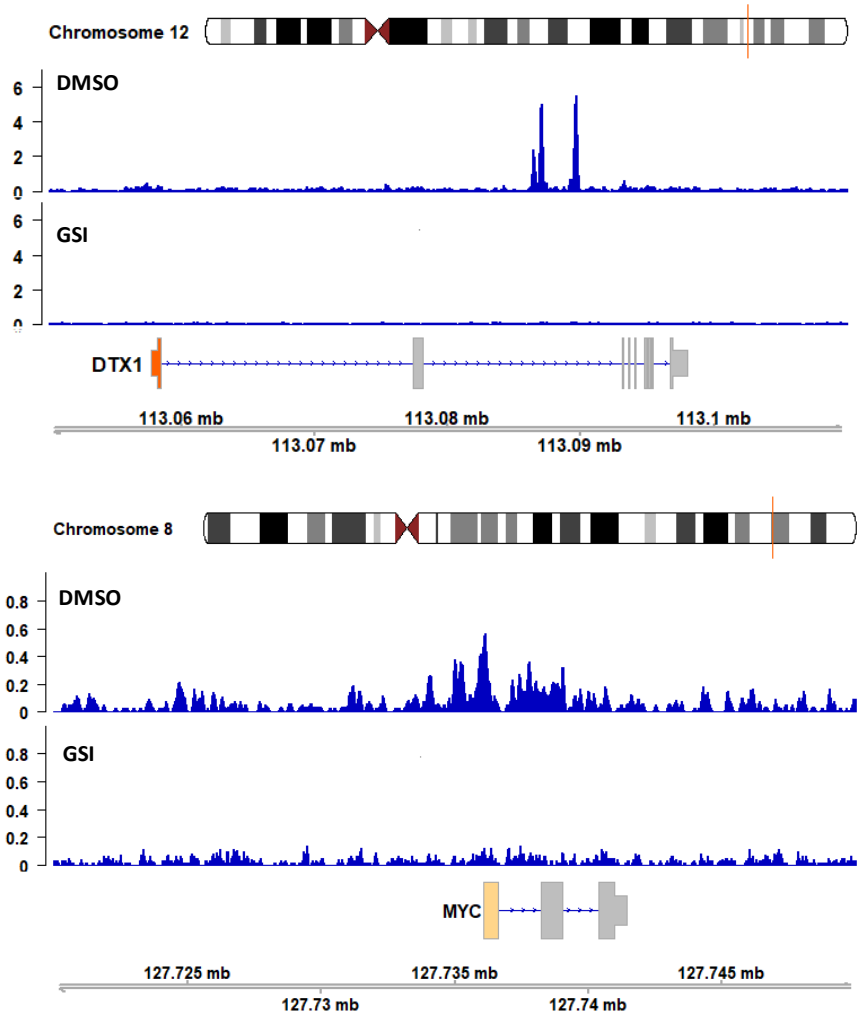

Figure 5.4.3: ChIP-seq data of Notch binding loci in T cell-derived malignancies. Analysis of published ChIP-seq data from two separate publications of the T-ALL cell line CUTLL1, looking at Notch1, and Notch1 binding at the loci of myc and dtx1, treated with vehicle control (DMSO; upper track) or GSI (lower track) (Choi et al, 2017; Wang et al, 2011a).

5.5 Inhibition of NPM-ALK leads to a decrease in *notch1* expression

To study the interplay between Notch1 and NPM-ALK in ALCL, we first attempted to determine whether NPM-ALK induces expression of Notch1. NPM-ALK activity was inhibited by incubation with the ALK/ROS/cMet inhibitor crizotinib (**Figure 5.5.1**) or expression silenced with a specific doxycycline-inducible shRNA (using a lentiviral expression plasmid; **Figure 5.5.3**). In both cases, a significant decrease in transcripts for Notch1 and its transcriptional targets *hes1* and *hey1* was observed (**Figure 5.5.2** and **Figure 5.5.4**), suggesting that Notch1 transcription is promoted by NPM-ALK expression and activity – indeed, in the case of NPM-ALK silencing by shRNA, the expression of *hey1* was completely inhibited (**Figure 5.5.4**).

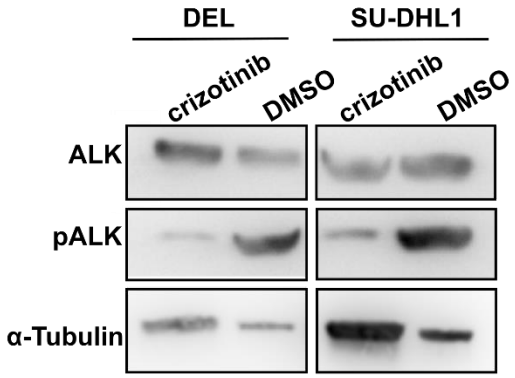

Figure 5.5.1: Validating crizotinib treatment using Western Blotting. ALCL cells were treated with 20nM crizotinib for 72 hours, and levels of the indicated proteins were measured by Western Blot. Blots are representative of three biological replicates.

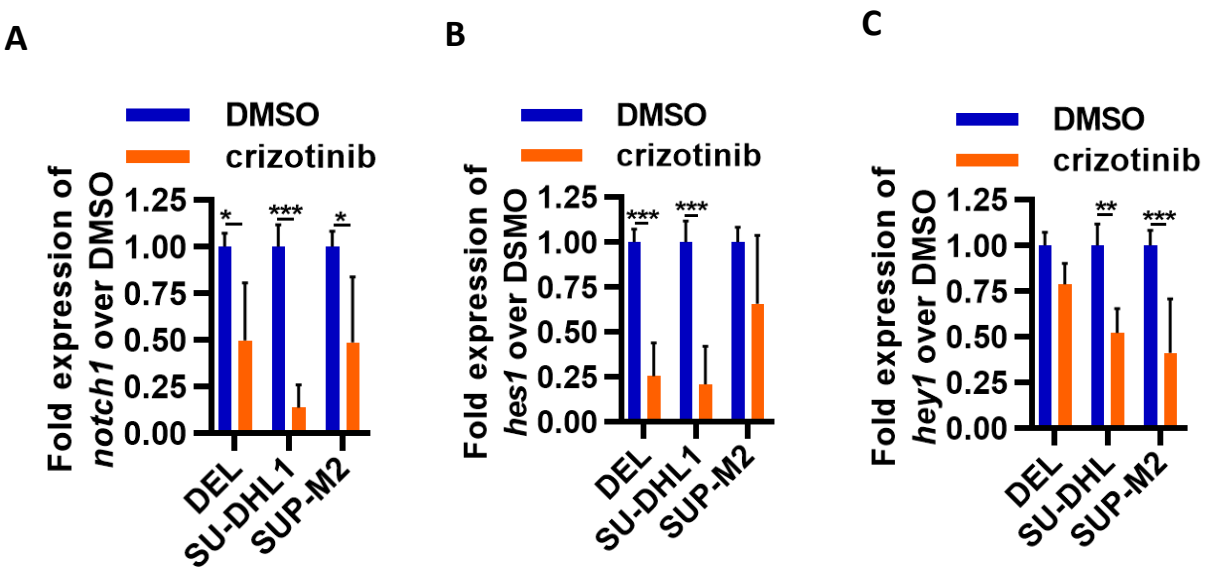

*Figure 5.5.2: The impact of crizotinib treatment on various genes, as measured by qPCR. ALCL cell lines were treated with 20nM crizotinib for 72 hours, and expression levels of notch1 **(A)**, hes1 **(B)** and hey1 **(C)**, calculated as fold change over vehicle control (DMSO), as measured by qPCR (*p<0.05; **p<0.01; ***p<0.0001; n=3).*

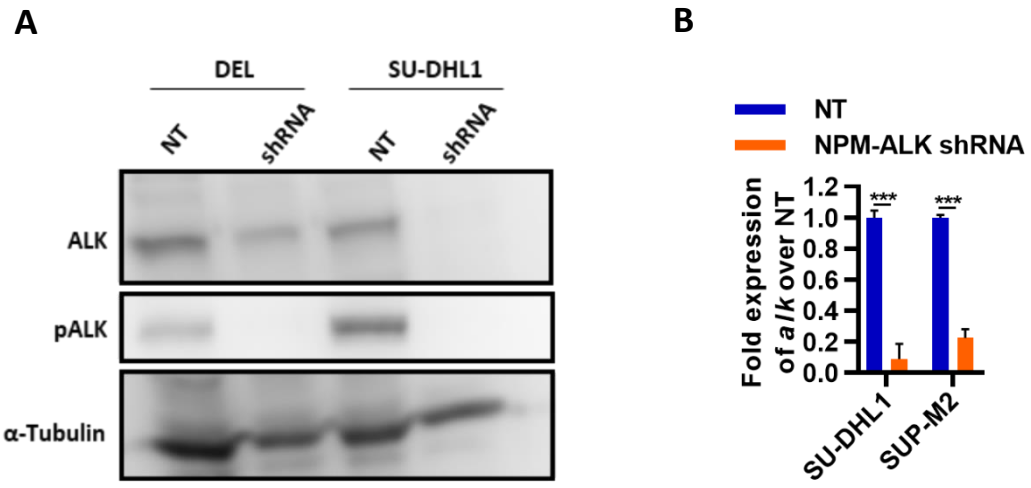

Figure 5.5.3: Validating NPM-ALK shRNA silencing. Cells were transduced with doxycycline-inducible shRNA targeting NPM-ALK or a non-targeting (NT) control shRNA and treated with 1 µM doxycycline for 48 hours. ***(A)*** *Western Blot validating silencing of NPM-ALK protein in ALCL cell lines. Blots are representative of three biological replicates.* ***(B)*** *Fold expression of npm-alk in ALCL cells transduced with NPM-ALK-silencing shRNA, calculated as fold change over non-targeting (NT) shRNA, and measured by qPCR (***p<0.0001; n=3).*

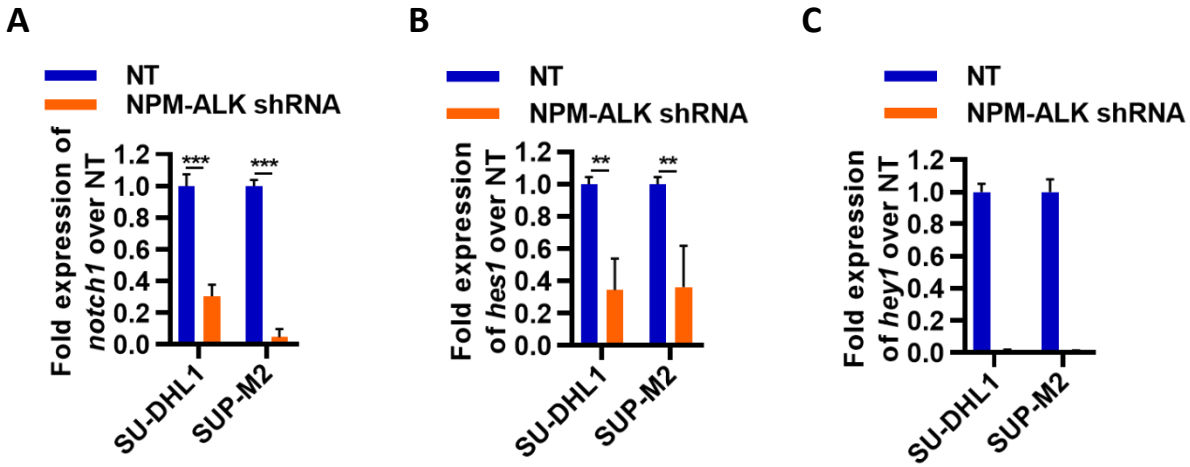

Figure 5.5.4: The impact of NPM-ALK silencing on various genes' expression. Cells were transduced with doxycycline-inducible shRNA targeting NPM-ALK or a non-targeting (NT) control shRNA and treated with 1 µM doxycycline for 48 hours. Fold expression of notch1 ***(A)****, hes1* ***(B)*** *and hey1* ***(C)*** *in ALCL cells, calculated as fold change over non-targeting (NT) shRNA, and measured by qPCR (**p<0.01; ***p<0.0001; n=3).*

5.6 Modest increases in *notch1* expression are observed on ectopic expression of *NPM-ALK*

NPM-ALK was expressed ectopically using plasmid pIND_puro_ALK in the HEK293FT cell line, and in ALK- ALCL cell lines Jurkat and Mac2A, and this was validated both at the protein and transcription level (**Figure 5.6.1**). An approximate two-fold increase in expression of *notch1* transcripts detected in HEK293FT, Jurkat and Mac2A cell lines ectopically expressing *npm-alk* was observed, with the highest levels seen in HEK293FT cells, which may be due to the already high basal levels of *Notch1* expression in Jurkat and Mac2A cell lines (**Figure 5.6.2**). These results are modest and were not tested at the protein level. We also investigated the effect of ectopic NPM-ALK expression on Notch1 targets *hes1* and *hey1*, but though we noticed a small increase, this did not reach significance (**Figure 5.6.3**).

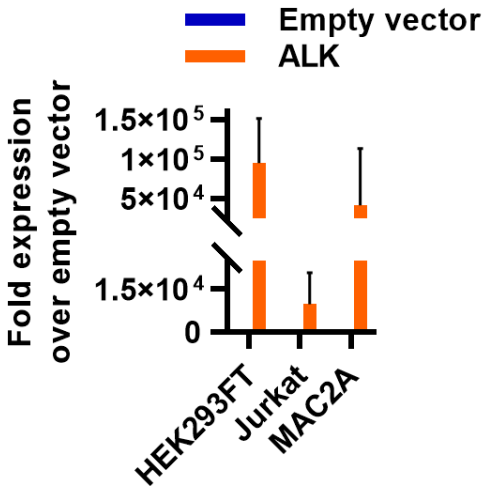

Figure 5.6.1: Validating ectopic NPM-ALK expression. Cells were transduced with an npm-alk expression plasmid or an empty vector control. Fold expression of npm-alk in various cell lines is presented, calculated as fold change over empty vector, and measured by qPCR (n=3).

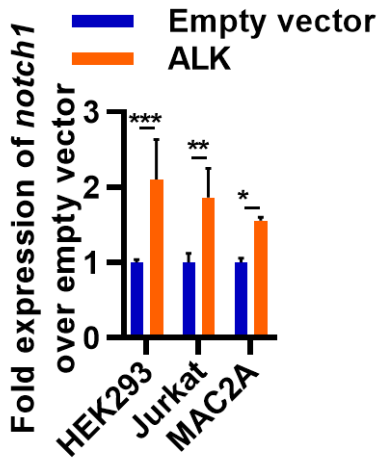

*Figure 5.6.2: The effect of ectopic NPM-ALK expression on Notch1. Cells were transduced with an npm-alk expression plasmid or an empty vector control. Fold expression of notch1 in various cell lines is presented, calculated as fold change over empty vector, and measured by qPCR (*p<0.05; **p<0.01; ***p<0.001; n=3).*

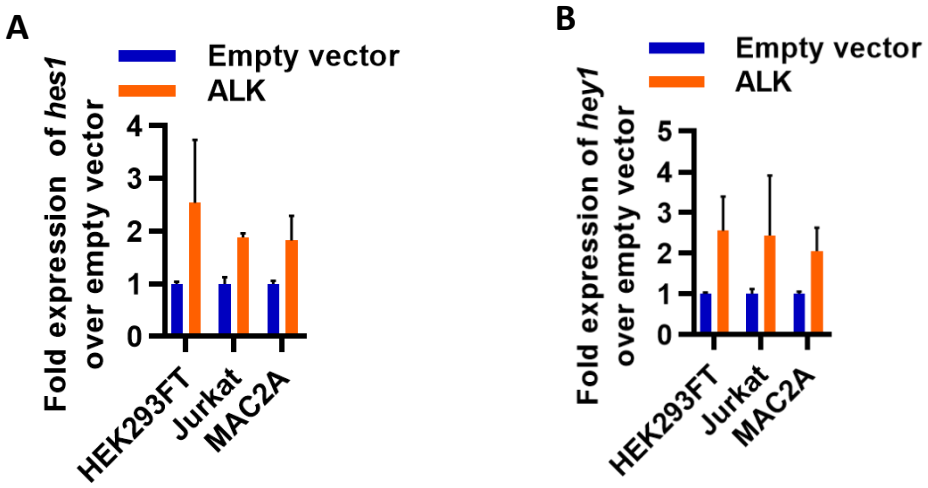

Figure 5.6.3: The effect of ectopic NPM-ALK expression on Notch1 targets. Cells were transduced with an NPM-ALK expression plasmid or an empty vector control. Fold expression of hes1 ***(A)*** *and hey1* ***(B)*** *in various cell lines is presented, calculated as fold change over empty vector, and measured by qPCR (*p<0.05; **p<0.01; ***p<0.001; n=3).*

5.7 ChIP-seq analysis reveals that NPM-ALK may regulate Notch1 through STAT3

A positive feedback loop has previously been described between Notch1 and STAT3 (Hildebrand *et al*, 2018). Since STAT3 is one of the major downstream signalling pathways of NPM-ALK activity, we investigated whether NPM-ALK-promoted expression of *notch1* was mediated through the STAT3 pathway. To do so, published ChIP-seq data (Menotti *et al*, 2019) of STAT3 binding sites in the ALCL cell lines SU-DHL1 and JB6 treated with either crizotinib or a vehicle control (DMSO) were analysed. These data show a significant decrease in binding of STAT3 at the *notch1* gene in crizotinib-treated cells as compared to vehicle control (DMSO)-treated cells (**Figure 5.7.1**). These data were validated by performing ChIP-qPCR; a significant decrease in binding of STAT3 at the *notch1* gene upon crizotinib treatment in SUP-M2 (**Figure 5.7.2**) and DEL (data not shown) cell lines was observed.

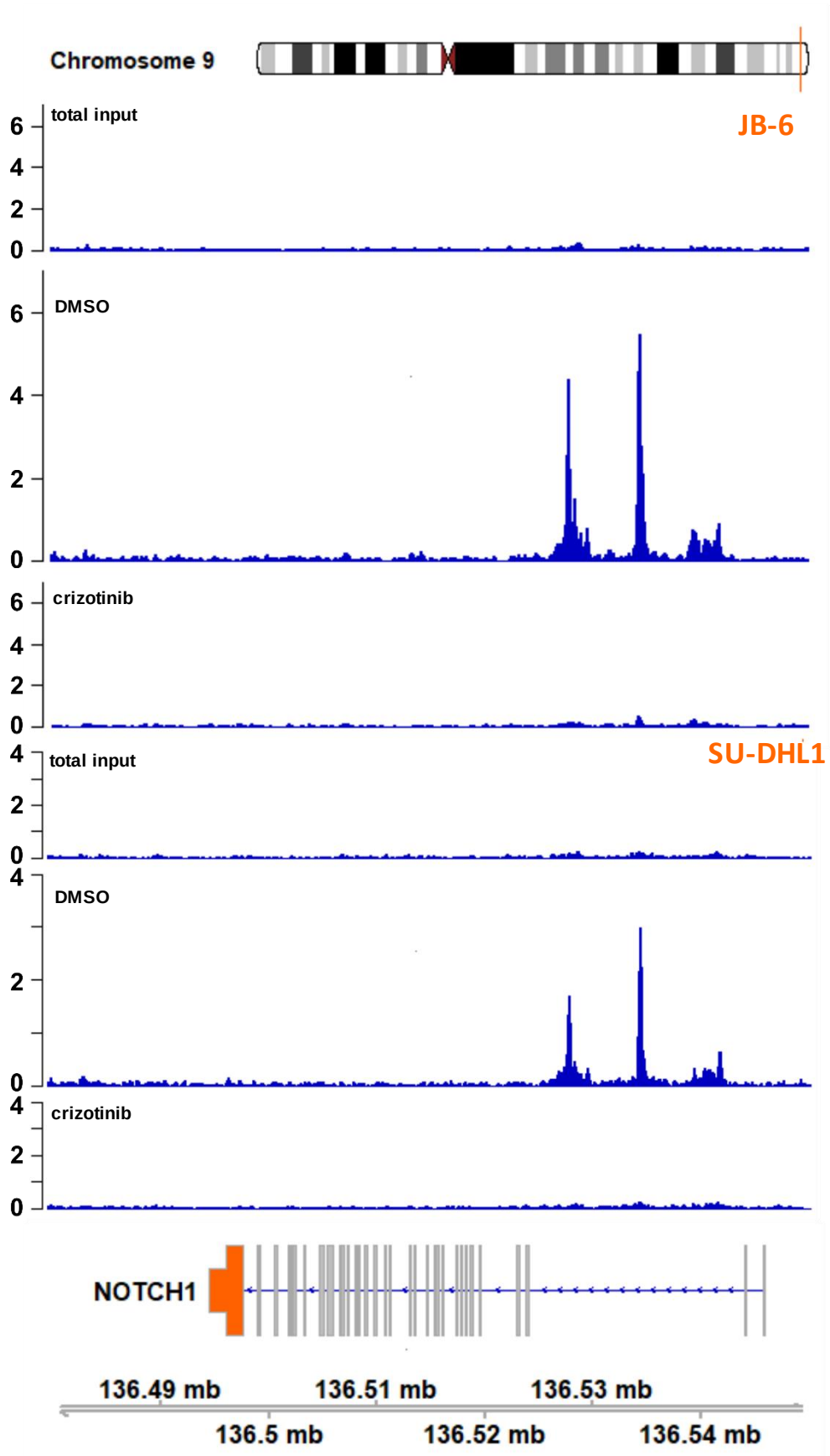

Figure 5.7.1: STAT3 binding at the Notch1 gene. Analysis of previously published ChIP-seq data, looking at binding of STAT3 to the notch1 gene in SU-DHL1 or JB-6 cell lines treated with a vehicle control (DMSO) or crizotinib; the upper track displays the total input for two separate cell lines (Menotti et al, 2019).

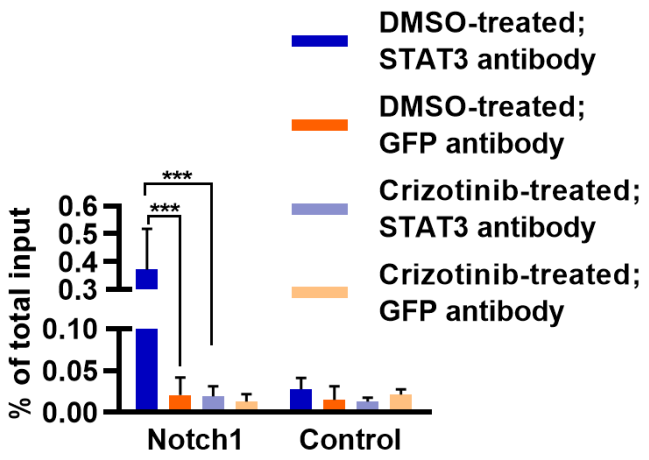

*Figure 5.7.2: ChIP-qPCR validation of the ChIP-seq analysis. ChIP-qPCR binding of STAT3 and GFP proteins at the notch1 gene, or at a negative control intergenic region, in SUP-M2 cells treated with either a vehicle control (DMSO) or crizotinib (300 nM) for 6 hours, as determined by qPCR (***p<0.0001; n=3), expressed as percentage of the total input.*

5.8 Silencing STAT3 leads to a decrease in *notch1* expression

To validate the hypothesis that STAT3 upregulates *notch1* expression, *stat3* was silenced employing specific shRNAs (using lentiviral expression plasmids) in ALCL cell lines. Knock-down in expression both at the transcript and protein levels were verified (**Figure 5.8.1**). As theorized, transcript levels of *notch1*, *hes1* and *hey1* (**Figure 5.8.2**) were all significantly downregulated as a result of *stat3* silencing.

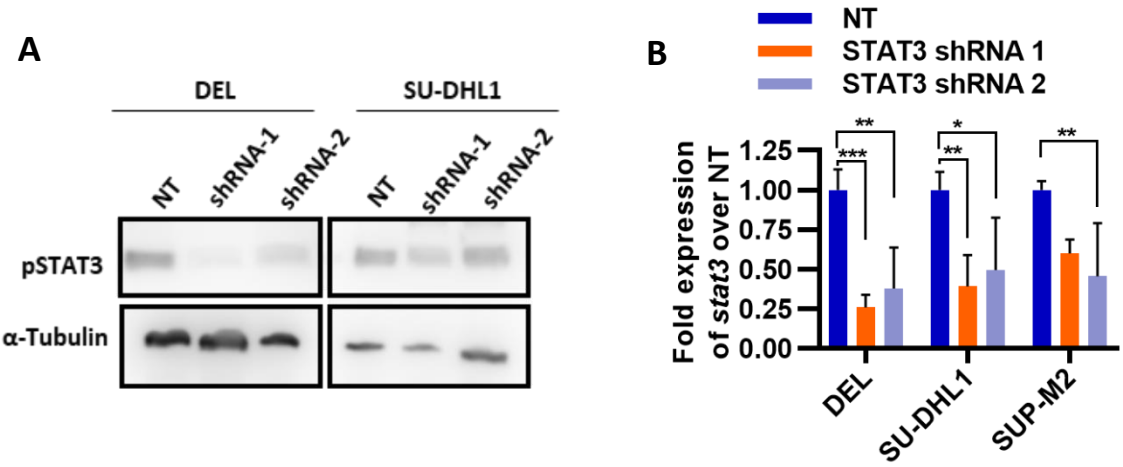

*Figure 5.8.1: STAT3 shRNA-mediated silencing in ALCL cell lines. Cells were transduced with 1 of 2 shRNA targeting STAT3 or a non-targeting (NT) control shRNA. **(A)** Western Blot validating silencing of STAT3 protein in ALCL cell lines. Blots are representative of three biological replicates. **(B)** Fold expression of stat3 in ALCL cells transduced with STAT3-silencing shRNA, calculated as fold change over non-targeting (NT) shRNA, and measured by qPCR (*p<0.05; **p<0.01; ***p<0.0001; n=3).*

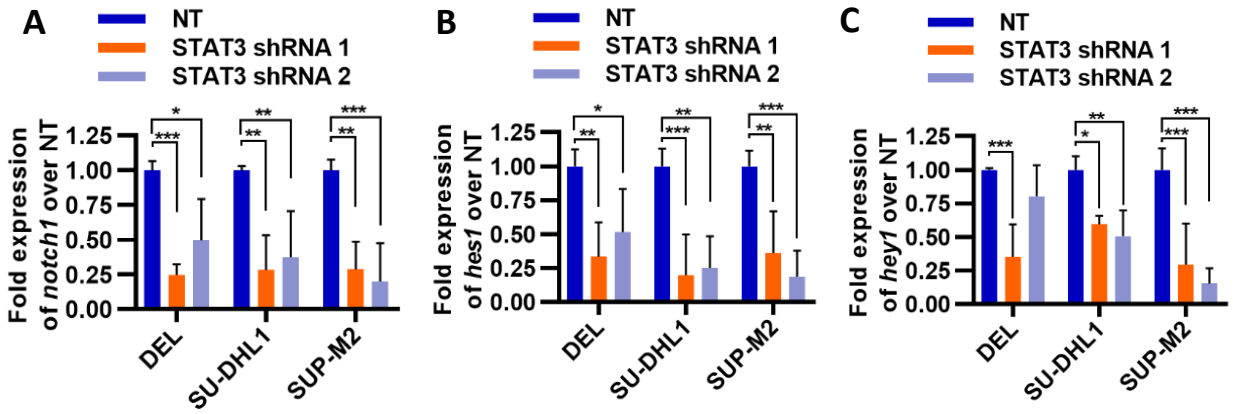

Figure 5.8.2: The effect of STAT3 silencing on the Notch pathway. Fold expression of notch1 ***(A)****, hes1* ***(B)*** *and hey1* ***(C)*** *in ALCL cells transduced with STAT3-silencing shRNA, calculated as fold change over non-targeting (NT) shRNA, and measured by qPCR (*p<0.05; **p<0.01; ***p<0.001; n=3).*

5.9 Discussion

As detailed previously, data informed our hypothesis that the Notch1 pathway is of systemic importance in ALCL, and that there is some cross-talk between Notch1 signalling and that of NPM-ALK, the driving oncogene in ALK+ ALCL. *notch1* expression was first silenced in ALCL cell lines, to determine the most essential functions of the signalling pathway. As laid out in the previous chapter, ALCL cell lines, suspension T-cells, are mostly impervious to lipid-based transfection, while electroporation-based technology such as Lonza's Nucleofection protocol is highly toxic to cells. Though we attempted to electroporate siRNA into ALCL lines – they are easier to electroporate than shRNA constructs due to their much shorter size, and at the time significantly cheaper than shRNA – we did not manage to find a satisfying balance between significant *notch1* silencing and toxicity of an intense electroporation protocol, which explains the very modest decrease in expression, stretching the limit of sensitivity of qPCR technology. CRISPR-based knock-down was the next step, as opposed to CRISPR knock-out, which is known to cause off-target mutations - and thus any effect seen using this technique is more likely to be due to Notch1 silencing rather than any off-target effect caused by knock-out CRISPR technology. Again unfortunately, the effect was relatively limited, with a <50% decreased of *notch1* expression, and only a relatively small effect on proliferation – and no other observable effect on cell physiology such as migration or morphology. Expression of *notch1* was therefore silenced using transduction of shRNA expression constructs into the genome of the cell lines using lentiviral-based technology, causing a significant decrease in proliferation, suggesting that ALCL cell lines depend on Notch1 signalling for growth. The expression of Notch1 target genes *hes1* and *hey1* was measured along with

notch1 as a proxy for Notch1 activity, to be certain that the effect seen at the transcriptional level translated to Notch1 activity at the protein level – though protein level of activated, intracellular Notch1 could have been assessed by western blotting, reverse-transcription quantitative PCR was used for its quantitative output and reliability.

We then showed that silencing Notch1 in ALCL triggers apoptosis, as seen by AV and PI staining, and the fact that cells were largely in the sub-G0 phase of the cell cycle. Caspase protein expression was not measured (another conclusive protocol to prove that apoptosis has been triggered), nor was Notch1 expression rescued to show that the effect is reversible and indeed due to Notch1 signalling, and not any off-target effect. However, considering that we silenced Notch1 by three different means, and proceeded with chemical inhibition of the receptor in Chapter 6, we deemed this evidence conclusive enough. These, instead, are all future experiments that would be worth undertaking – in particular rescuing Notch1 expression following silencing.

Looking at signalling downstream of Notch1 we hypothesize that two targets beyond *hes1* and *hey1* are *myc* and *dtx1*, expression of which is upregulated by Notch in T-ALL cell lines. Unfortunately, no such microarray data (in the presence and absence of Notch1) exists in ALCL, and so this is the closest data we could use to narrow down the potential list of downstream targets. Regardless, identifying *myc* and *dtx1* is not particularly surprising, as a multitude of studies have shown this in T-ALL or lymphoma (Weng *et al*, 2006; Gekas *et al*, 2016; Sharma *et al*, 2007). Indeed Notch mutations are known to induce *myc* expression in T-ALL (Chiang *et al*, 2016) raising the question of whether we should have looked at *myc* expression when studying Notch1 T349P. Equally, it is unclear whether these findings would translate into ALCL: not only are these data from T-ALL, but they were taken from cell lines treated with GSI, which is not a specific inhibitor. Indeed, GSIs are far from specific to the Notch pathway, with γ-secretases targeting a whole host of proteins for cleavages, including E-cadherin, VEGF, Type I Interferon Receptor and the Insulin Growth Factor Receptor (IGFR), as well as a number of Voltage-gated potassium channels, interestingly (Reviewed in Haapasalo & Kovacs, 2011)

To answer the first question, previous publications have shown c-myc to be of importance in ALCL pathobiology; indeed some cell lines are addicted to the *myc* oncogene (Lollies *et al*, 2018; Weilemann *et al*, 2015). We were able to validate these data, by showing a significant decrease in *myc* expression upon Notch1 silencing in ALCL cell lines suggesting that that these data are not simply due to off-target effects of GSIs. In other words, though Notch1 may well signal through more than one pathway, on its

own this evidence may explain why *notch1* silencing triggers apoptosis: Notch1 silences *c-myc*, itself necessary for ALCL cell survival (Weilemann *et al*, 2015).

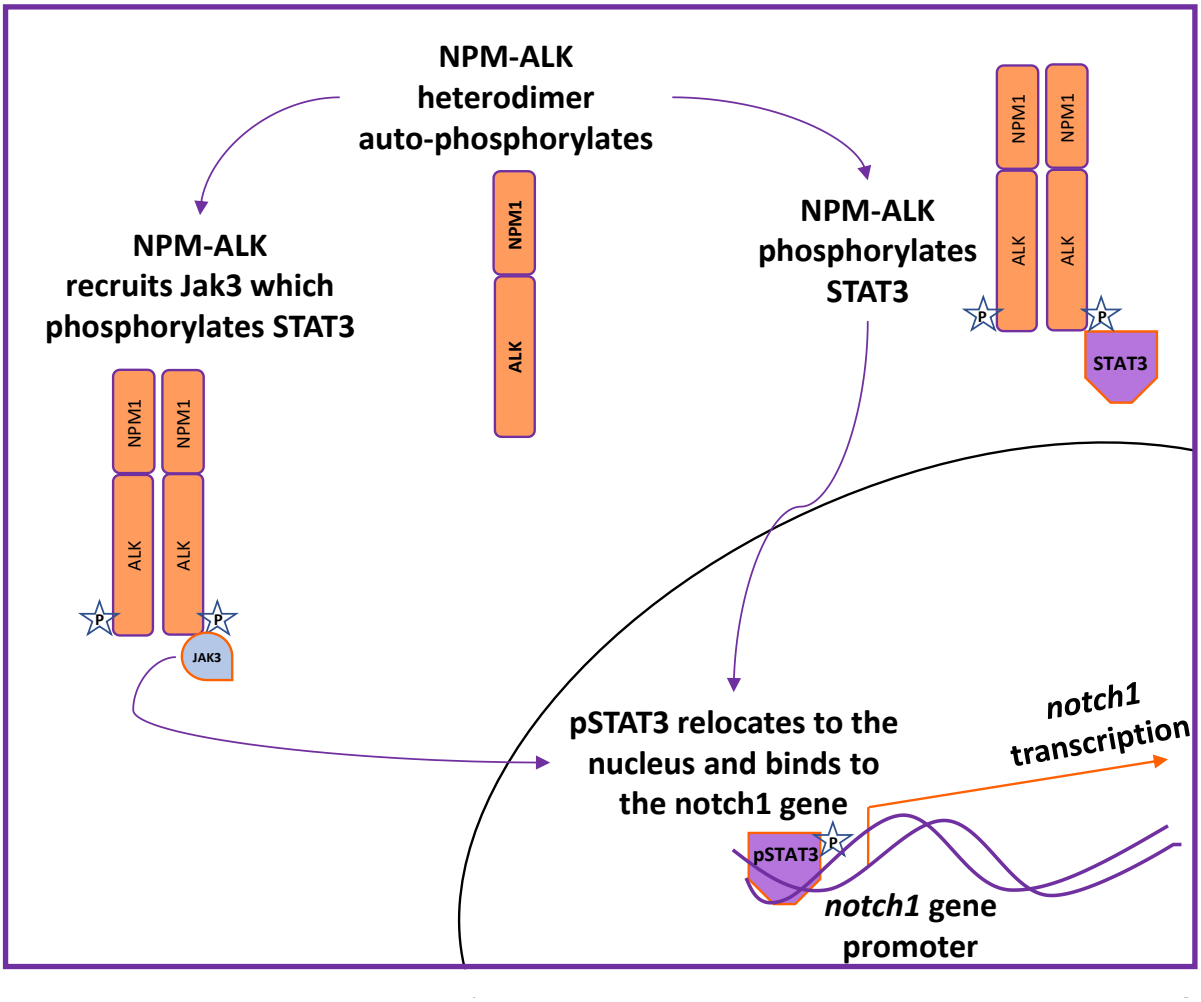

Figure 5.9.1: Schematic representation of our proposed model. We propose that NPM-ALK recruits JAK3, which phosphorylates STAT3, which in turn binds to and promotes expression of the *notch1* gene, although NPM-ALK can also by-pass JAK3 and phosphorylates JAK3 on its own.

Cross-talk between NPM-ALK and Notch signalling in ALCL was then studied. Silencing *npm-alk* led to a significant decrease in *notch1* expression, and this was equally true when chemically inhibiting NPM-ALK activity using the TKI crizotinib. Though less clear-cut, we also suggest that the opposite is true as well: increasing *npm-alk* expression upregulates *notch1* expression. Given that NPM-ALK is known to signal through a few well-established mediators such as JAK/STAT, PLC-γ, PI3K, Akt and ERK/MAPK, we hypothesized that one of these proteins was responsible for the cross-talk between NPM-ALK and Notch1. In particular, Notch1 and STAT3 signalling are known to interact (Wu *et al*, 2017) and indeed in different settings STAT3 upregulate *notch1* expression (Li *et al*, 2014). To test whether NPM-ALK effects *notch1* expression via STAT3 in ALCL, we looked at published ChIP-seq datasets in ALCL cell lines

treated with TKIs or vehicle controls and found STAT3 to bind at the *notch1* gene. We were able to validate this using ChIP-qPCR. We therefore show that STAT3 binds at the *notch1* gene, and that this binding can be modulated using small molecule inhibitors. Given that STAT3 is one of the major downstream signalling pathways of NPM-ALK, it is therefore very likely NPM-ALK upregulates *notch1* via STAT3 (proposed model depicted in **Figure 5.9.1**). In confirmation, silencing *stat3* expression led to a significant downregulation of *notch1* transcription as a result.

We are therefore confident that the Notch signalling pathway in ALCL is central to its pathobiology. We have identified cross-talk between Notch1 and NPM-ALK and elucidated its mechanism. The next logical step is to assess the therapeutic potential of the Notch pathway in ALCL; validate that the known anti-Notch1 drugs are as efficient as the literature suggests, study whether they are effective in an ALK+ ALCL setting, and study them in the context of the latest clinical developments.

6. Notch1 as a Therapeutic Target in ALCL

6.1 Introduction

Morgan discovered the notched wing phenotype in fruit flies more than a hundred years ago, in 1917 (Morgan, 1917). It took over half a century, until the late 1980s and early 1990s, for genomic translocations to be identified in T-cell malignancies, and to be implicated in the pathobiology of the diseases. Soon it became apparent that these translocations were mutating the human homolog of *notch*, first called *tan-1* (Raimondi *et al*, 1987; Ellisen *et al*, 1991). Nowadays, the Notch pathway is implicated in a number of different disorders (Reviewed in Andersson & Lendahl, 2014). A century on, there is therefore increasing interest in targeting the Notch pathway therapeutically, particularly as far as oncology is concerned.

γ-secretases are membrane-bound proteases formed of four proteins (Presenilin, Nicastrin, Pen2 and Aph1) which cleave a number of targets, including Notch (Reviewed in Selkoe & Wolfe, 2007). The existence of various isoforms of these component proteins points to the possibility of complex regulation of γ-secretases, thus adding another layer of fine-tuning to the already complex process of Notch activation. γ-secretases were the first molecules to be targeted as part of Notch therapies, with the first γ-secretase inhibitor (GSI; MK-0752) being trialled in 2006 in T-ALL patients in the USA (Deangelo *et al*, 2006). Despite evidence that the GSI MK-0752 was able to reduce tumour size, gastrointestinal toxicity was such that treatment had to be discontinued in this trial; and indeed, newer generation GSIs resulted in the same toxicity; they were not specific enough to target the γ-secretases expressed in T-cells. Nevertheless, they remain accessible and useful compounds for studies of Notch performed *in vitro*. In addition, promising new types of compounds targeting Notch itself, or its ligands, are being developed, leading to a renewed interest in using Notch as a therapeutic target. The existence of various isoforms of these component proteins suggest complex layers of regulation of γ-secretases, thus adding another layer of fine-tuning to the already complex process of Notch activation

In ALCL more specifically, a first publication showed that twelve ALCL patients presented with high levels of Notch1 expression (out of twelve tested), and that cells of the tumour microenvironment were expressing Jagged1, which drove Notch1 activity and, in turn, tumour growth (Jundt *et al*, 2002). The high expression of both Notch1 and Jagged1 was confirmed in a further twelve patients with primary cutaneous ALCL in a subsequent publication (Kamstrup *et al*, 2008). A final paper on this topic shows varying expression levels of Notch1 in 10 ALK+ ALCL and 9 ALK- ALCL patients, and suggested that inhibition of Notch1 by GSIs led to apoptosis in the ALCL cell line Karpas 299 (Kamstrup *et al*, 2014). In this chapter the utility of Notch1 as a therapeutic target in ALCL is investigated. In addition, the effectiveness of GSIs in ALK- ALCL is studied, using not only two ALK- ALCL cell lines, FEPD and Mac2A, derived from ALK- ALCL patient tumours (del Mistro *et al*, 1994; Davis *et al*, 1992), but also the

CD4 and CD8-negative T cell leukaemia cell line Jurkat (immortalization described in Schneider *et al*, 1977; followed by phenotyping in Gillis, 1980).

6.2 Chemical inhibition using γ-Secretase Inhibitors of Notch1

A number of small molecular inhibitors are available to target Notch1, hence cell lines were exposed to different Notch1 inhibitors starting with GSI I, which has been proven to inhibit growth of the ALCL cell line Karpas 299 (Kamstrup *et al*, 2014). The efficacy of GSI I was first verified by assessing the protein levels of ICN by Western Blot, to verify inhibition of Notch1 cleavage, and therefore activity (**Figure 6.2.1**). The effect of GSI I in ALK+ and ALK- ALCL cell lines was tested, both confirming the effects seen previously and showing that γ-secretase inhibitors targeting Notch1 have the same effect in ALK- ALCL cell lines (**Figure 6.2.2**). Staining cell lines for AV and PI demonstrated a significant increase in cells positive for both AV and PI when treating four different ALK+ ALCL and two different ALK- ALCL cell lines with GSI I for 48 hours (**Figure 6.2.3**) – indicating the pro-apoptotic effect of Notch1 inhibition. This result was verified by staining ALCL cell lines treated with GSI I with intracellular PI, to assess the proportion of cells in each phase of the cell cycle, and a significant increase in the proportion of cells in the sub-G0 fraction was detected, indicating again that the cells are dying (**Figure 6.2.4**). It should be said that the cell cycle analysis would have been improved had Bromodeoxyuridine been used.

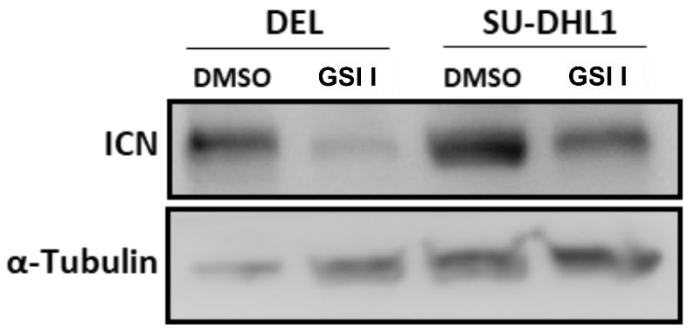

Figure 6.2.1: Validating the efficacy of GSI treatment in ALCL cell lines. Cells were treated with 1 µM GSI I or a vehicle control (DMSO) for 48 hours, and the protein levels of the activated, intracellular domain of Notch1 was measured by Western Blot. Blots are representative of three biological replicates.

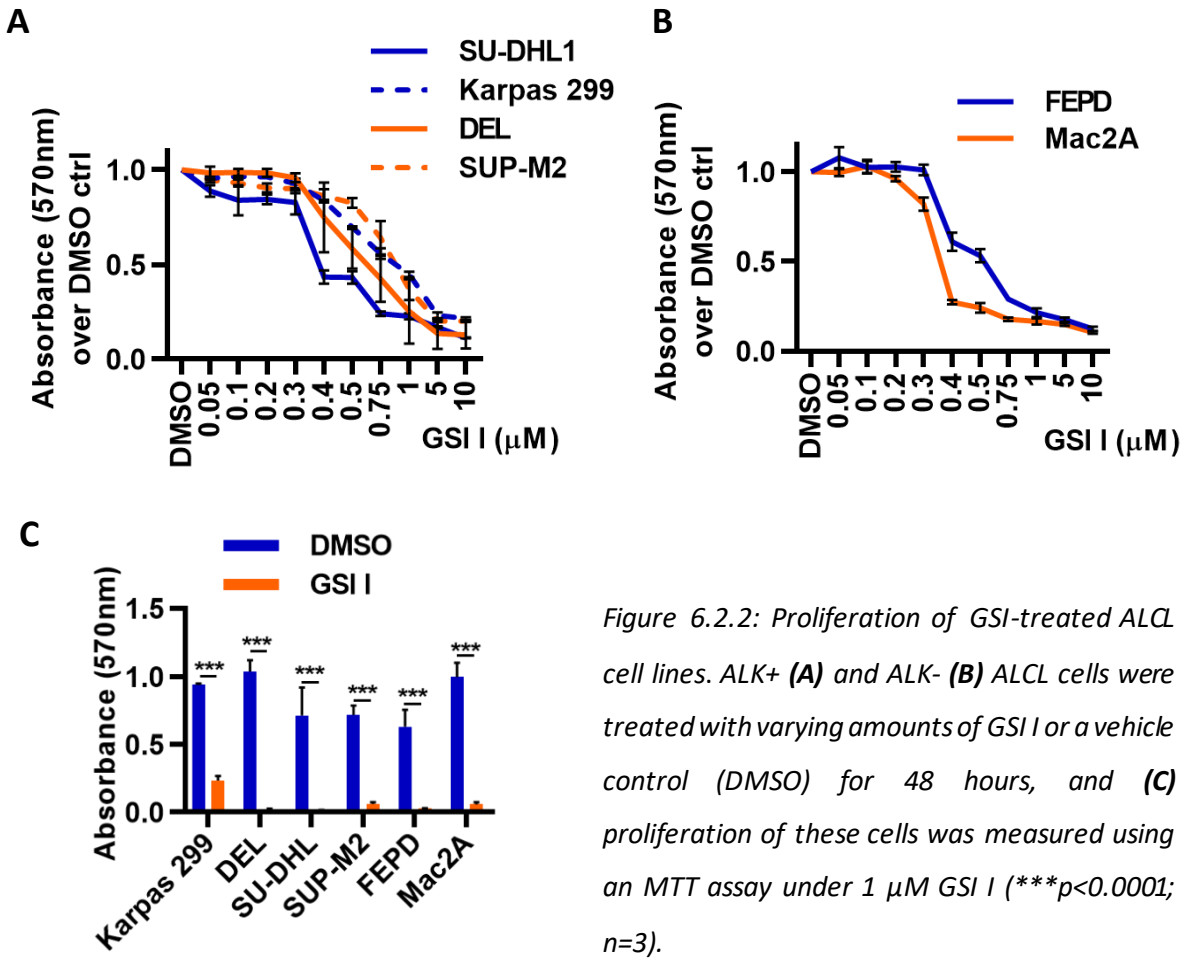

Figure 6.2.2: Proliferation of GSI-treated ALCL cell lines. ALK+ ***(A)*** *and ALK-* ***(B)*** *ALCL cells were treated with varying amounts of GSI I or a vehicle control (DMSO) for 48 hours, and* ***(C)*** *proliferation of these cells was measured using an MTT assay under 1 μM GSI I (***p<0.0001; n=3).*

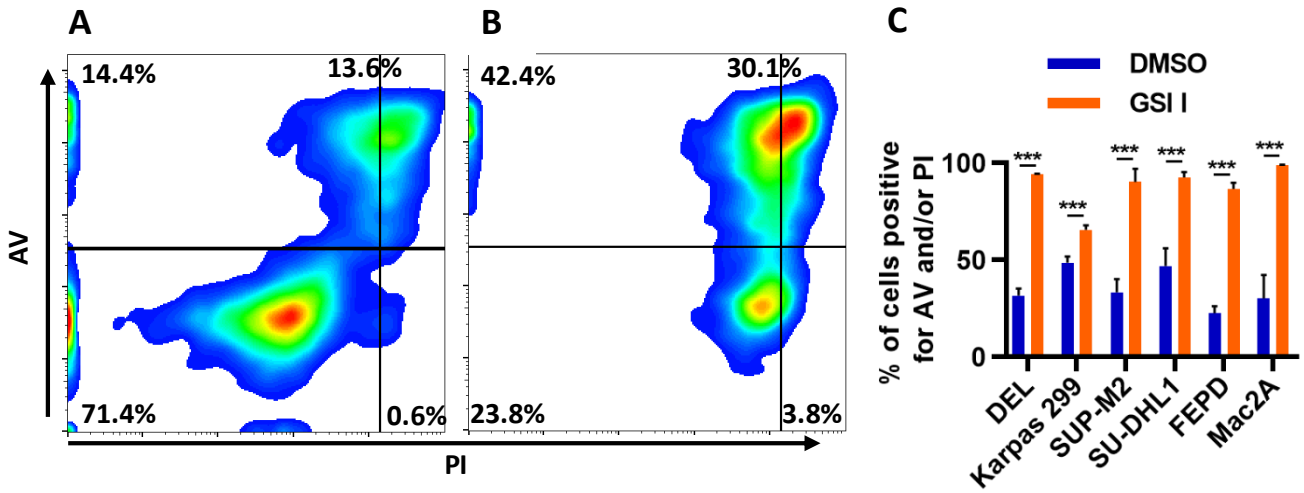

Figure 6.2.3: AV-PI staining of GSI-treated ALCL cell lines. Representative FACS plots of ALCL cells were treated with ***(A)*** *a vehicle control (DMSO) or* ***(B)*** *1 μM of GSI I for 48 hours and stained for AV and PI.* ***(C)*** *Quantification of cells staining for AV and/or PI (***p<0.0001; n=3).*

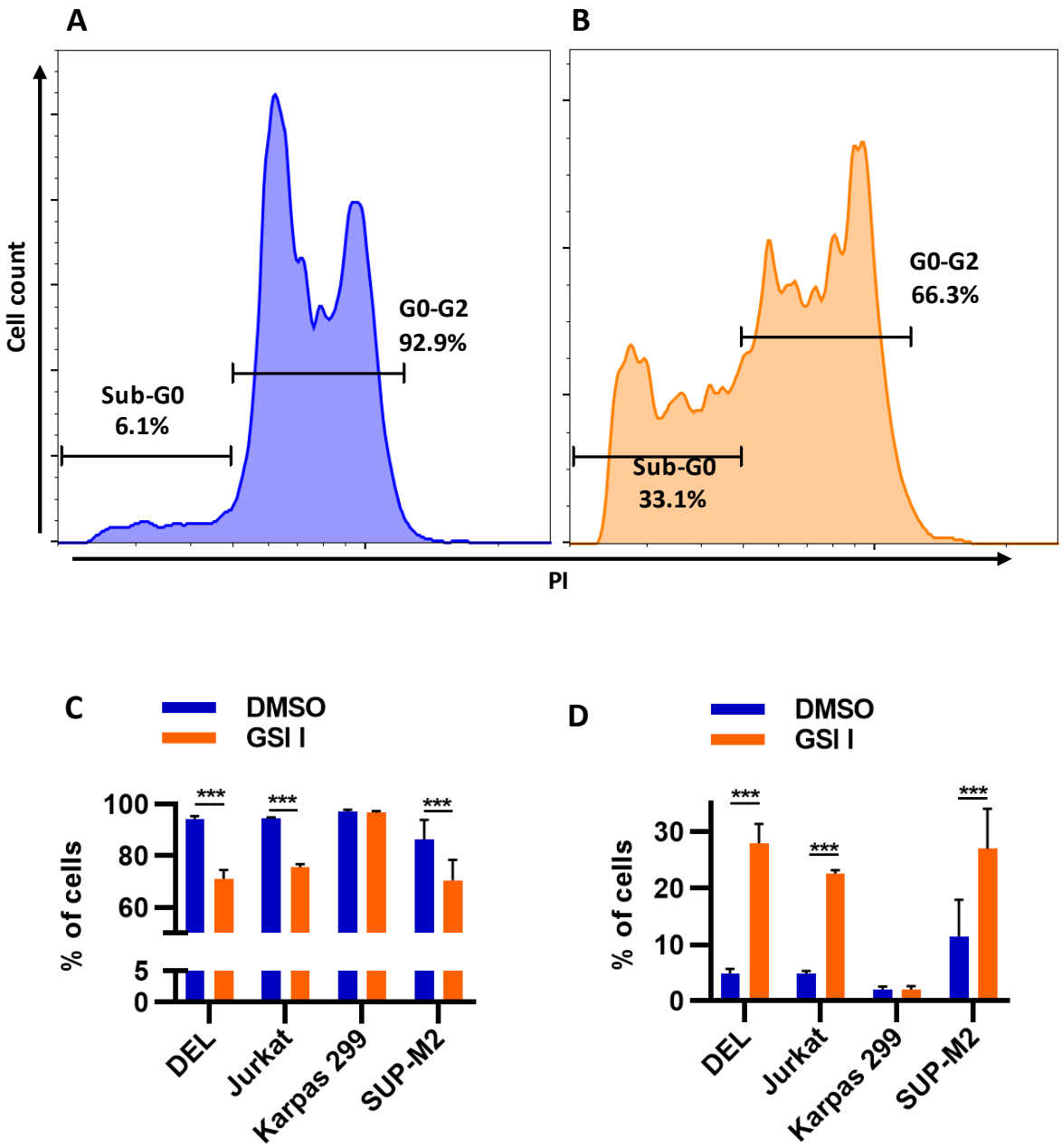

Figure 6.2.4: Intracellular PI staining of ALCL cells treated with 1 µM GSI I. Representative FACS plots of ALCL cells were treated with ***(A)*** *a vehicle control* ***(DMSO)*** *or* ***(B)*** *1 µM of GSI I for 48 hours and stained for intracellular PI. Quantification of cells in either G0 to G2 phases* ***(C)*** *or sub-G0* ***(D)*** *(***p<0.0001; n=3).*

The compounds PF-03084014 (NCT02299635) from Pfizer, and BMS-906024 (NCT03691207) from Bristol-Myers Squibb both currently under study in various clinical trials, including paediatric pre-clinical trials were also assessed for their activity (Papayannidis *et al*, 2015; Messersmith *et al*, 2015; Carol *et al*, 2014; Zweidler-McKay *et al*, 2014). However, there was no growth inhibition of ALCL cell lines even for concentrations up to 10 µM (**Figure 6.2.5**).

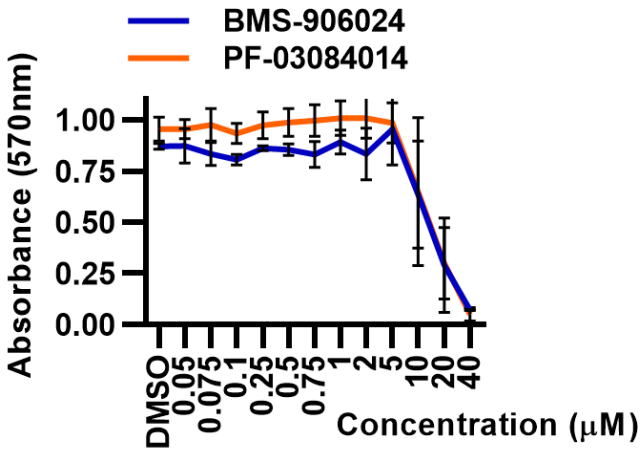

Figure 6.2.5: Proliferation of ALCL cell lines treated with the indicated GSIs. ALK+ and ALK- ALCL cells were treated with varying amounts of the GSIs BMS-906024 or PF-03084014 or a vehicle control (DMSO) for 72 hours, and proliferation of these cells was measured using MTT (n=3).

6.3 Sensitivity of mutated Notch1 to γ-Secretase Inhibitors

To determine whether the Notch1 mutations identified in this study, T349P and T311P modulated sensitivity to GSIs, HEK293FT cell lines expressing either an empty vector, wild-type or mutated Notch1 were treated with GSI I, but no significant difference was found (**Figure 6.3.1**), indicating that response to GSIs is likely independent of these Notch1 mutations.

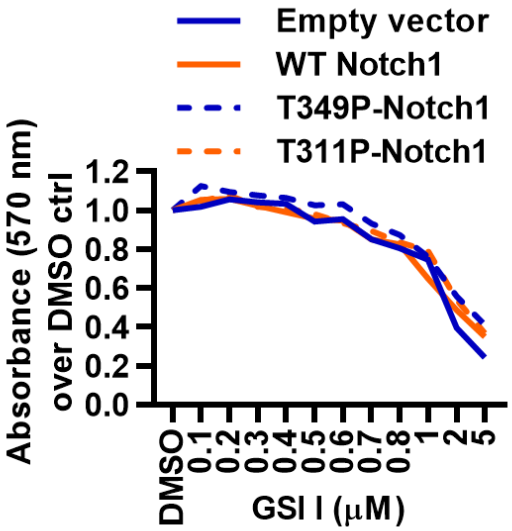

Figure 6.3.1: Proliferation of GSI-treated Notch1-expressing HEK293FT cells. HEK293FT cell lines expressing either an empty vector or wild-type (WT) or T349P or T311P-mutated Notch1 were treated with varying amounts of GSI I or a vehicle control (DMSO) for 48 hours, and proliferation of these cells was measured using MTT (expressed as absorbance over vehicle control; n=3).

6.4 Crizotinib-resistant ALCL cell lines are sensitive to γ-Secretase Inhibitors of Notch1

ALK inhibitors are now being added to frontline therapy (Reviewed by Larose *et al*, 2019) (eg. Trial NCT01979536). Ideally, a single agent ALK inhibitor would provide a less toxic frontline treatment approach in the future although resistance would be expected to develop (Sharma *et al*, 2018; Gambacorti-Passerini *et al*, 2016). Therefore, crizotinib-resistant ALCL cell lines were assessed for their

sensitivity to GSI to test whether inhibition of Notch1 is a potential new second-line treatment for patients relapsing on crizotinib or related TKIs. Four different cell lines were exposed to various quantities of crizotinib to derive TKI-resistant cell lines: K299, resistant to 1 µM, SUP-M2, resistant to 0.3 µM (Ceccon *et al*, 2013), DELs, resistant to 0.2 µM and SU-DHL1, resistant to 0.1 µM crizotinib. No significant difference in the response of these four cell lines to GSI I, as compared to their wild-type counterparts was observed (**Figure 6.4.1**), indicating that patients relapsing on crizotinib would likely still be sensitive to Notch1 inhibition, paving the way for new therapeutic options.

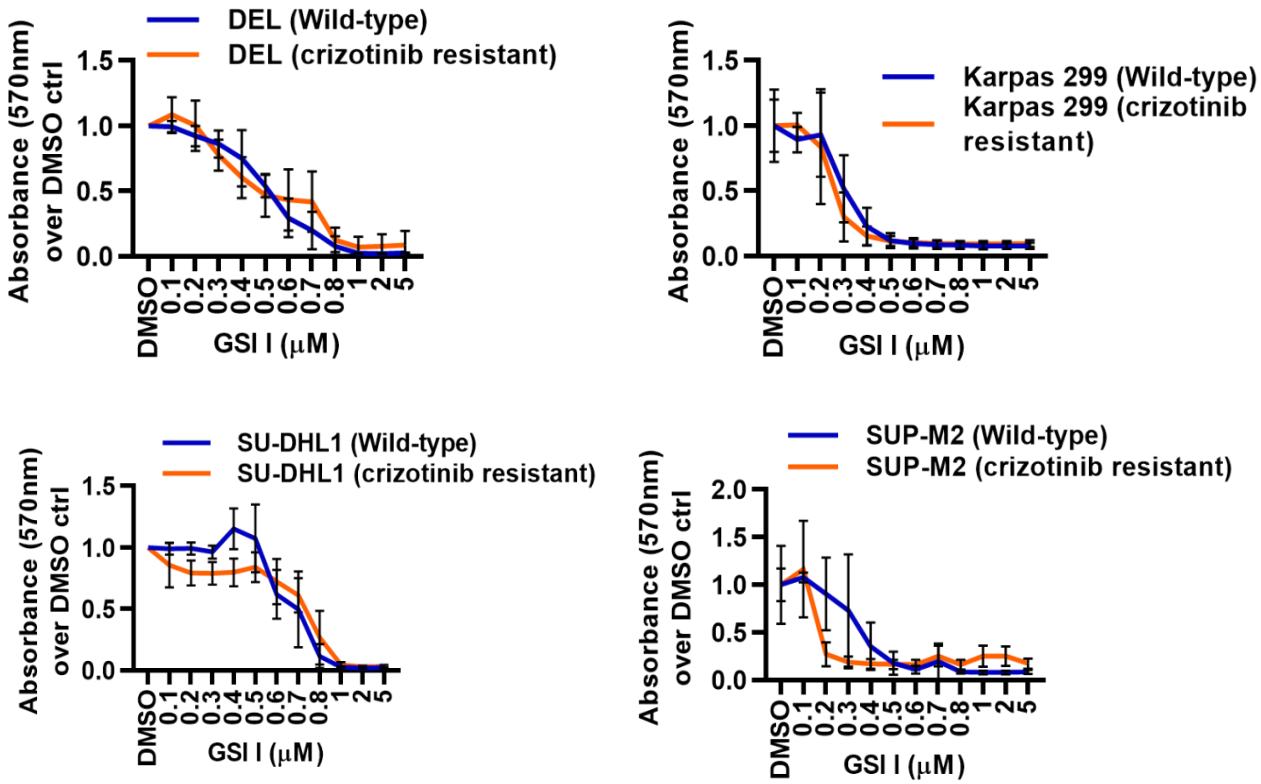

Figure 6.4.1: Proliferation of crizotinib-resistant ALCL cell lines exposed to GSI I. Wild-type and crizotinib-resistant ALK+ ALCL cell lines were treated with varying amounts of GSI I or a vehicle (DMSO) control for 48 hours, and proliferation of these cells was measured using MTT (expressed as absorbance over vehicle control; n=3).

6.5 Synergy between γ-Secretase Inhibitors and Tyrosine Kinase Inhibitors

The combination of TKIs most likely to be approved for use in ALCL with GSIs was investigated. Treating ALCL cell lines with a combination of GSI I and crizotinib led to synergistic activity in reducing cell proliferation as indicated by a Bliss Independence Index of less than 1 across several concentrations and cell lines (**Figure 6.5.1**). Though we only tested one cell line, this synergy is also observed with the combination of GSI I and ceritinib, another ALK TKI, though the synergy was not observed across as many combinations of concentrations (**Figure 6.5.2**). Interestingly, this synergy holds true at concentrations below the IC50 of each respective drug (taken to be IC50 = 30 nM for crizotinib, IC50 = 20 nM for ceritinib and IC50 = 1 µM for GSI I).

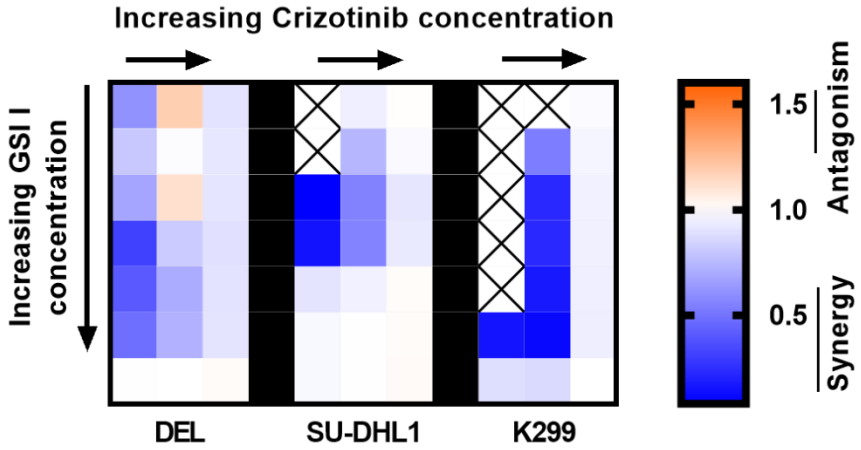

Figure 6.5.1: Combination treatment of GSI I and crizotinib. BLISS matrix showing the calculated combination index obtained on treating the indicated ALK+ ALCL cell lines with crizotinib and GSI I for 72 hours (using a range of concentrations of 10-50 nM for crizotinib, and 10 nM-2 µM GSI I). A combination index of <1 indicates synergy between drugs, 1 indicates additive effects, >1 indicates antagonistic effects (average of n=3). Concentration range were taken to include doses on either side of the IC50.

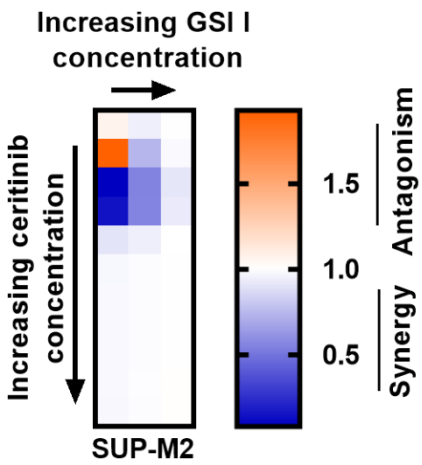

Figure 6.5.2: Combination treatment with GSI I and ceritinib. BLISS matrix showing the combination index on treating the indicated ALK+ ALCL cell lines with ceritinib and GSI I for 72 hours (using a range of concentrations of 5-50 nM for ceritinib, and 500 nM-2 µM GSI I). A combination index of <1 indicates synergy between drugs, 1 indicates additive effects, >1 indicates antagonistic effects (average of n=3). Concentration range were taken to include doses on either side of the IC50.

While Pfizer's compound (PF-03084014) did not affect proliferation or apoptosis on its own in ALCL cell lines, it showed synergistic activity when treating ALK+ ALCL cells in combination with the TKI crizotinib, as shown in the Bliss Matrix (**Figure 6.5.3**). Interestingly, the synergy is less marked when using K299 cell lines, though this can be explained by the mutational burden in these cell lines and crizotinib's significantly higher IC50 in K299. The drug combination also leads to a significant increase in DELs, SUP-M2 and SU-DHL1 staining positive for both AV and PI as well as a significant decrease in cells staining for neither – more so than the effect observed when treating the cells with each drug separately (**Figure 6.5.4**). These data suggest that GSI and ALK inhibitors may lead to a better therapeutic outcome when used in combination than on their own, and may serve as a second-line treatment for ALCL which, at least in children, is currently successfully treated with a combination of traditional chemotherapeutic agents as demonstrated by the ALCL99 trial (Wrobel *et al*, 2011).

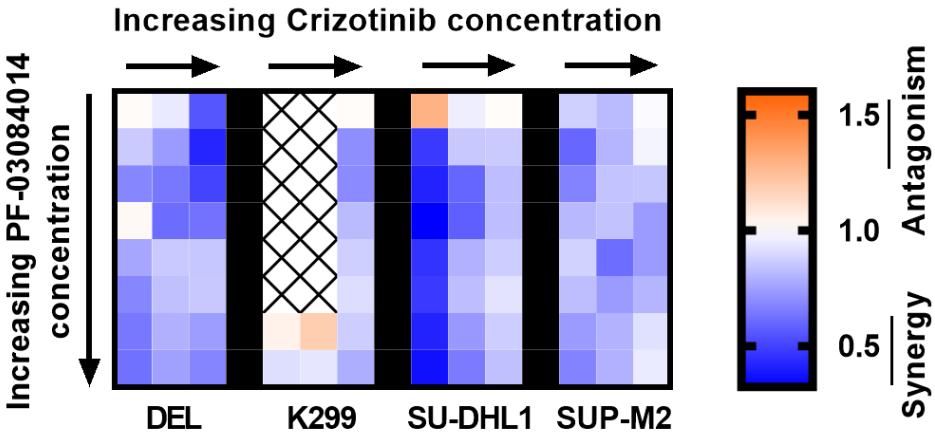

Figure 6.5.3: Combination treatment of crizotinib and PF-03084014. BLISS matrix showing the combination index on treating the indicated ALK+ ALCL cell lines with crizotinib and PF-03084014 for 72 hours (using a range of concentrations of 10-50 nM for crizotinib, and 100 nM-10 µM PF-03084014). A combination index of <1 indicates synergy between drugs, 1 indicates additive effects, >1 indicates antagonistic effects (average of n=3). Concentration range were taken to include doses on either side of the IC50.

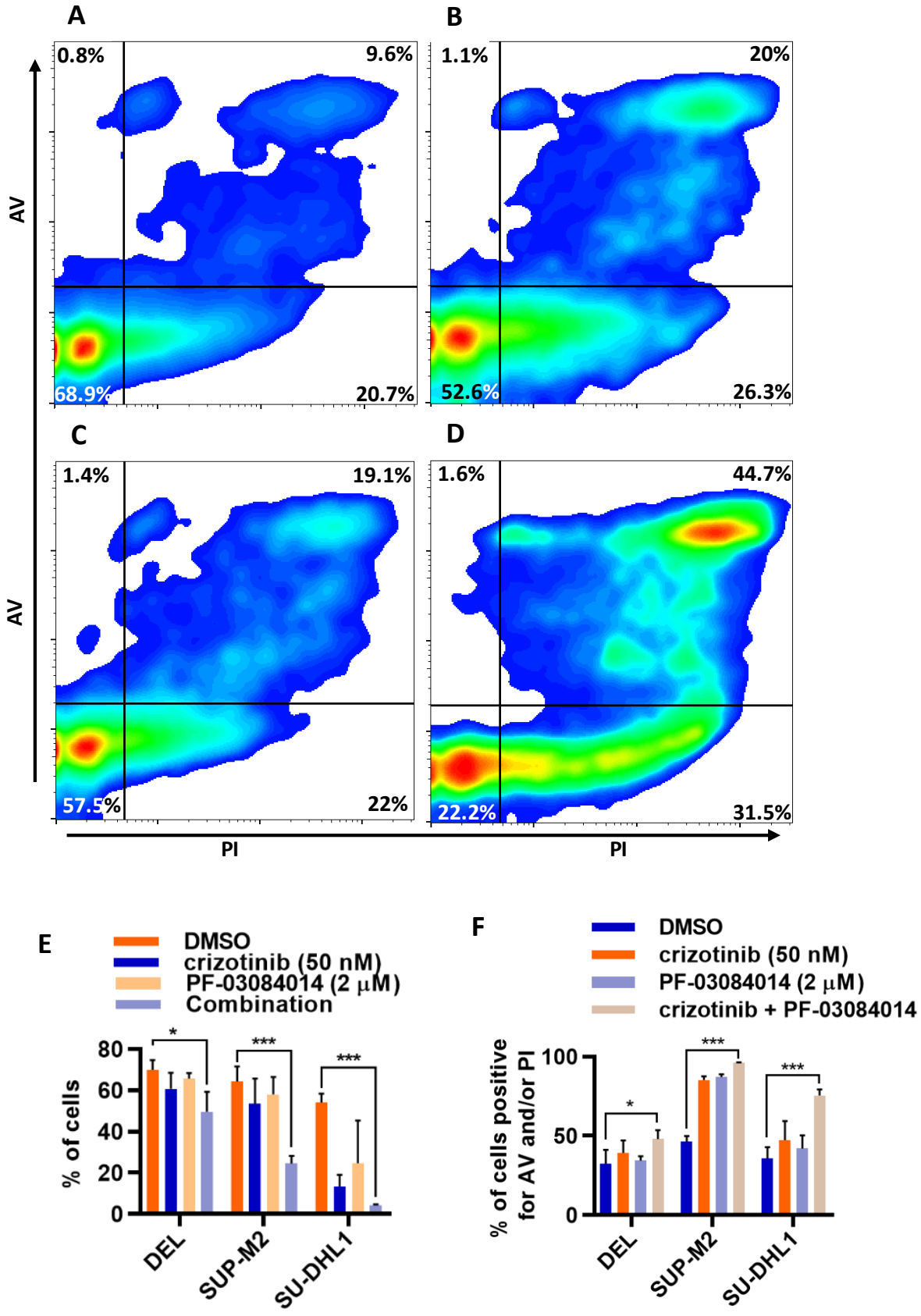

*Figure 6.5.4: AV-PI staining of TKI/GSI combination treatment in ALCL cell lines. Representative FACS plots of ALCL cells were treated with either **(A)** a vehicle control (DMSO), **(B)** 50 nM crizotinib, **(C)** 2 μM PF-03084014 or **(D)** a combination of both for 72 hours and stained for AV and PI. Quantification of cells staining for AV and/or PI **(E)** or neither AV and PI **(F)** (*p<0.05; ***p<0.0001; n=3).*

6.6 Notch1 activation through ligand binding dampens the efficacy of GSIs.

To investigate how cell death induced by GSIs in ALCL is modulated on presentation of the Notch1 ligand, further experiments were conducted. Indeed, as explained in chapter 6.1, the literature suggests that some patient tumours may express Notch1 ligands in the tumour micro-environment, and that this drives Notch1 expression (Jundt *et al*, 2002). Therefore, ALCL cell lines were co-cultured with the OP9 mouse feeder cell line expressing either an empty vector or the Notch1 ligand DLL1 (OP9-DLL1). As expected, ALCL cell lines co-cultured with the OP9 cell line and treated with GSIs showed a significant decrease in expression of *hes1* and *hey1*, but surprisingly, co-culturing them with the OP9-DLL1 cell line rescued *hes1* and *hey1* expression (**Figure 6.6.1**). These data could suggest that Notch1 is already activated and therefore GSIs are less effective, as not able to dampen Notch1 signalling, since the intracellular domain has already been cleaved.

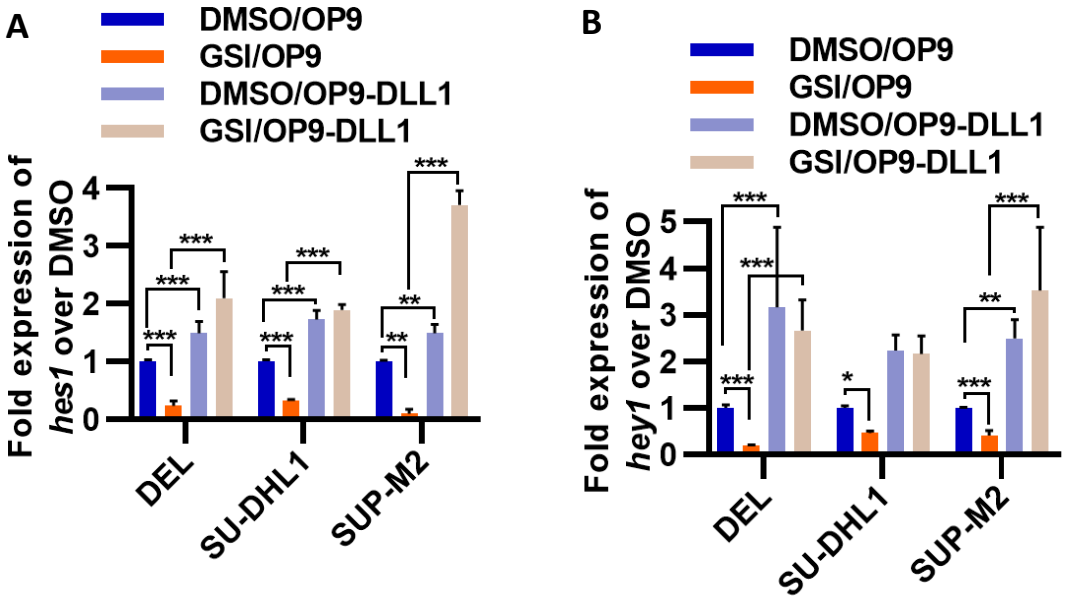

Figure 6.6.1: Expression of Notch1 target genes upon ligand presentation. ALCL cell lines were co-cultured with the OP9 mouse feeder cell line expressing either an empty vector (OP9) or the Notch1 ligand DLL1 (OP9-DLL1) and treated with either 1 µM GSI I or a vehicle control (DMSO). Fold expression of hes1 ***(A)*** *and hey1* ***(B)*** *is displayed, calculated as fold change over expression levels in ALCL cells co-cultured with empty-vector expressing OP9 cells and treated with a vehicle control, and measured by qPCR (*p<0.05; **p<0.01; ***p<0.0001; n=3).*

The proliferation of ALCL cell lines treated with GSI I co-cultured with OP9-DLL1 and presented with the Notch1 ligand resulted in a partial rescue in proliferation (about 75% of the level compared to cells treated with a vehicle control; **Figure 6.6.2A**). Similar results were observed when treating Notch1-expressing HEK293FTs with GSIs (**Figure 6.6.2B**). Again, this suggests that presentation of the Notch1 ligand DLL1 can abrogate some of the effects of GSI in cell lines, though it's unclear as yet whether different Notch1 ligands would have the same effect.

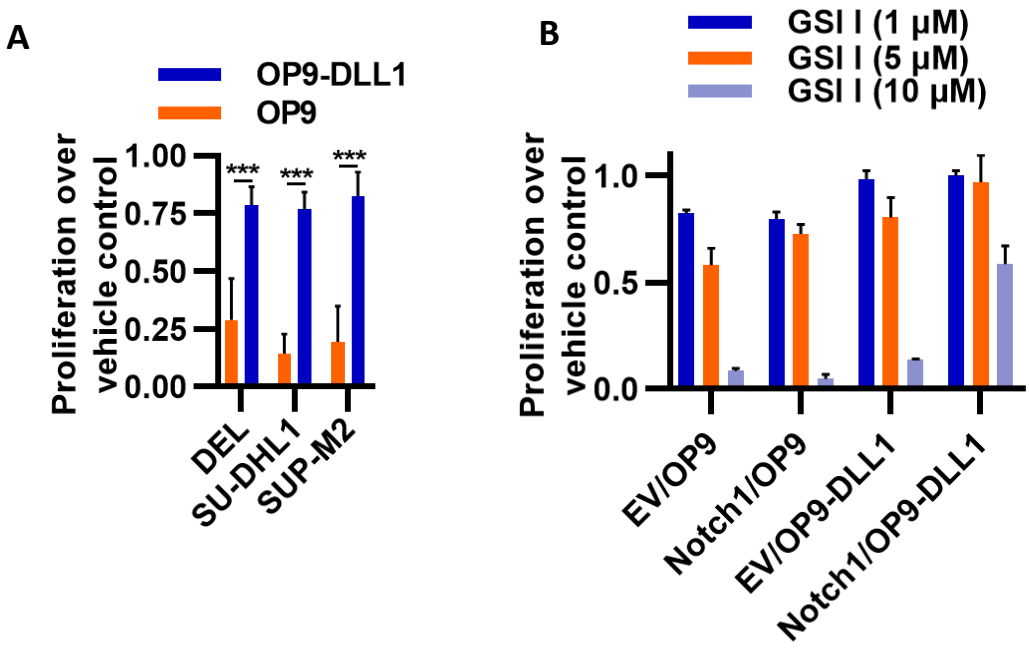

Figure 6.6.2: Proliferation upon Notch1 ligand presentation. ***(A)*** *ALCL cell lines were co-cultured with the OP9 mouse feeder cell line expressing either an empty vector (OP9) or the Notch1 ligand DLL1 (OP9-DLL1) and treated with either 1 µM GSI I or a vehicle control (DSMO) for 48 hours.* ***(B)*** *HEK293FT cells expressing either an empty vector (EV) or Notch1 were co-cultured with the OP9 mouse feeder cell line expressing either an empty vector (OP9) or the Notch1 ligand DLL1 (OP9-DLL1) and treated with either the indicated concentrations of GSI I or a vehicle control (DMSO). Proliferation was measured using an MTT assay, calculated as fold change over cells co-cultured with empty-vector expressing OP9 cells and treated with a vehicle control (***p<0.0001; n=3).*

6.7 Tissue Microarray shows a correlation between Notch1 expression and EFS

A clinically-annotated FFPE tissue microarray of 89 ALK+ ALCL patients, biopsied at initial presentation, was analysed for Notch1 protein expression. Of the 89 patient tumours, 88.8% showed Notch1 staining of varying intensity (**Figure 6.7.1A**). This is consistent with previously published results (Kamstrup *et al*, 2014; Jundt *et al*, 2002). In over half of the patients, the majority of tumour cells stained positive for Notch1, while about a third of patients' tumours presented with either no Notch1 staining or sparse staining (**Figure 6.7.1B**). Interestingly, patients with little or no Notch1 staining have a significantly worse prognosis (p<0.05, **Figure 6.7.2**).

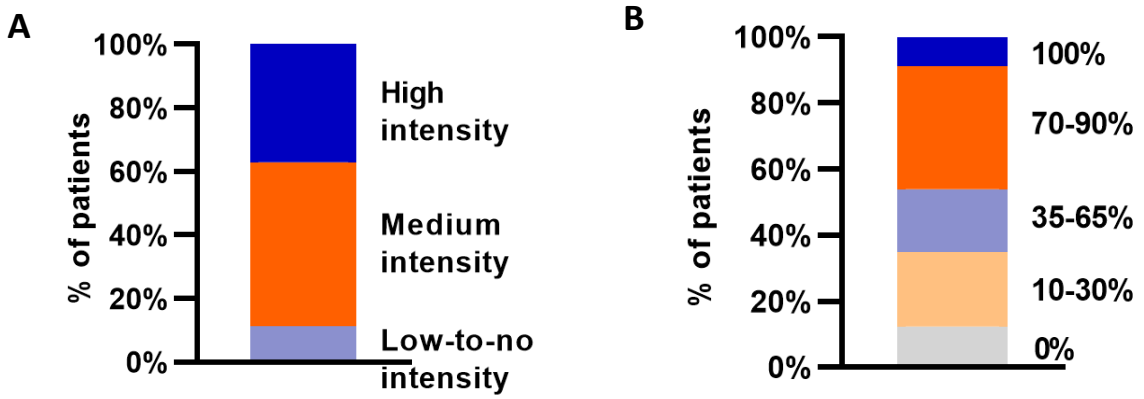

*Figure 6.7.1: Notch1 expression in a wider ALCL patient cohort. A tissue microarray of 89 patient samples was stained for Notch1 by immunohistochemistry and is shown as the percentage of patients presenting with a given Notch1 staining intensity **(A)** or a given percentage of tumour cells staining positive for Notch1 **(B)**.*

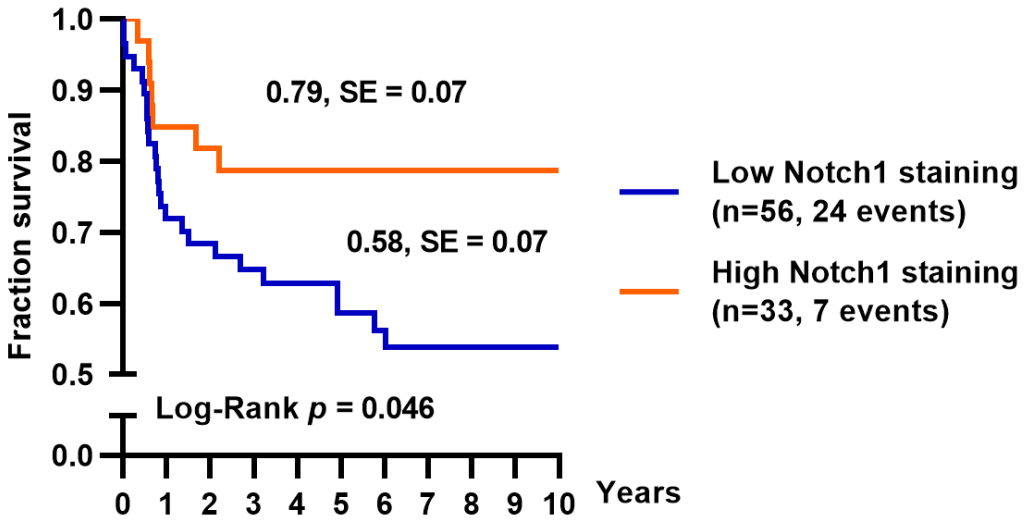

Figure 6.7.2: Notch1 expression and Event-Free Survival of ALCL patients. 10-year Event-Free Survival for ALK+ ALCL patients showing either little or no (n=56), or strong Notch1 expression (n=33).

6.8 Notch1 expression does not correlate with response to GSI exposure in ALCL cell lines

To assess whether the strength of Notch1 expression correlates with the response to mainstream therapies such as Methotrexate (part of the ALCL99 protocol) or GSIs, a CRISPR-activation system (Konermann *et al*, 2015) was employed to increase *notch1* expression in ALCL cell lines: cells were first transduced to express Cas9-VP64 and the MS2 enhancer, which are then recruited to a genomic locus by the sgRNA, produced by a third plasmid transduced into cell lines, binding to the MS2-stem loops, thereby upregulating gene activity. Expression of *notch1* using this approach, as measured by qPCR, was at its highest level 48 hours post selection of sgRNA-expressing cells (**Figure 6.8.1A**). Expression was verified in biological triplicates and two cell lines, as compared to a non-targeting control sgRNA (**Figure 6.8.1B**).

These cells were then treated with increasing concentrations of Methotrexate (the commonly used chemotherapeutic agent of the ALCL99 therapy) or GSI I, but no significant difference in response, when compared to cells transduced with a non-targeting sgRNA was seen (**Figure 6.8.2**): while the ALCL cells that overexpressed *notch1* showed a trend towards being more sensitive to GSI I, this did not reach statistical significance.

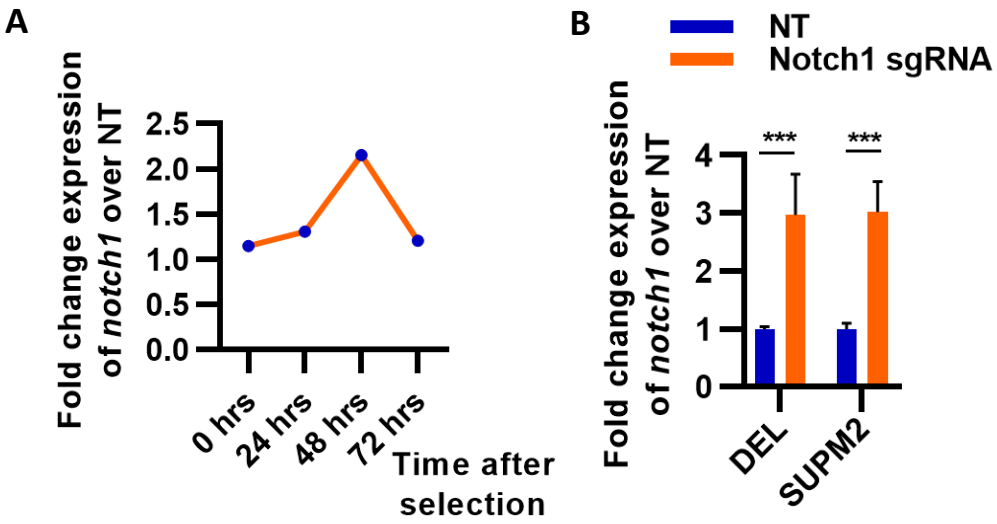

Figure 6.8.1: Validating CRISPR-activation of notch1. Cas9-VP64- and MS2-expressing ALCL cell lines were transduced with sgRNA targeting the notch1 promoter or a non-targeting (NT) control sgRNA. ***(A)*** *Fold expression of notch1 in ALCL cells, calculated as fold change over non-targeting (NT) sgRNA, and measured by qPCR at the indicated times after selection for sgRNA-expressing cells.* ***(B)*** *Fold expression of notch1 in ALCL cells 48 hours post-selection, calculated as fold change over non-targeting (NT) sgRNA, and measured by qPCR (***p<0.0001; n=3).*

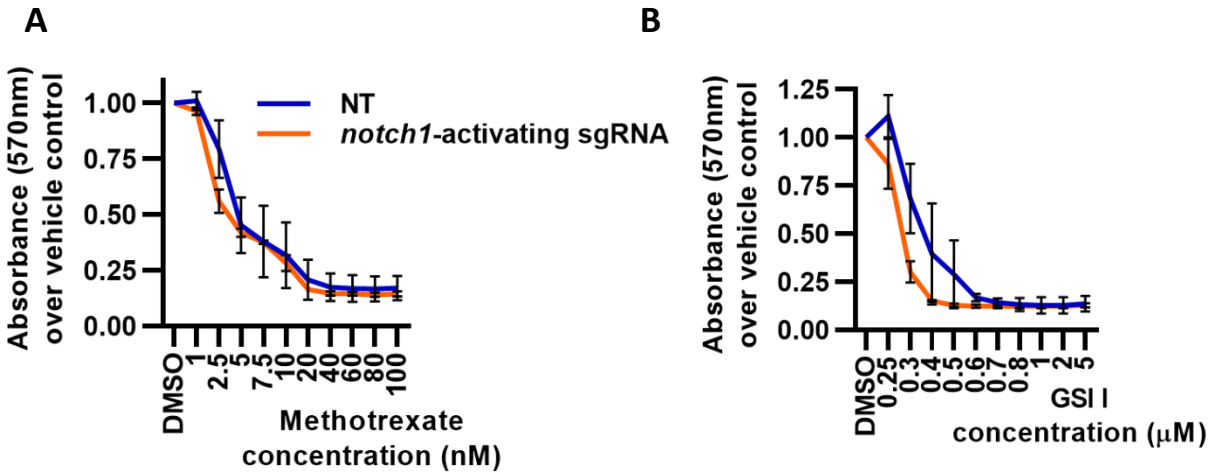

*Figure 6.8.2: Sensitivity of Notch1-overexpressing cells to methotrexate and GSI I. ALCL cell lines were transduced with sgRNA targeting the notch1 promoter or a non-targeting (NT) control and exposed to varying amounts of Methotrexate **(A)** or GSI I **(B)**, or a vehicle control (DSMO) for 48 hours. Proliferation was then measured using MTT and is displayed as fold absorbance over the vehicle control (n=3).*

6.9 Discussion

In this chapter, the potential application of Notch1 as a therapeutic target in ALCL, both ALK+ and ALK- was investigated. Anti-Notch1 drugs, GSIs, showed effectiveness, both in ALK+ ALCL, which has been demonstrated previously (Kamstrup *et al*, 2008), and also in ALK- ALCL, which is a novel finding. Though newer generations of GSIs were also assessed, these proved somewhat less effective. Of course, GSIs inhibit γ-secretase and not Notch1, so by definition are not specific to the Notch1 signalling pathway, although their effectiveness in lymphomas and leukaemia are well-documented, along with the toxic gastrointestinal side-effects (Reviewed in Takebe *et al*, 2014; and Habets *et al*, 2019). In addition, silencing Notch1 more specifically, using shRNA, has by-and-large the same effect as chemical inhibition using GSIs, hence suggesting that the effect observed with GSI is largely due to inhibition of Notch signalling. However, it is likely that the stronger doses required, particularly in the case of PF-03084014, to inhibit ALCL tumour growth is due to its much safer toxicity profile, its higher specificity and non-competitive mechanism of action (Wei *et al*, 2010; Samon *et al*, 2012). Similarly for BMS-069024 (Zweidler-McKay *et al*, 2014). Importantly, the fact that these newer generation GSIs are non-competitive permits a finer tuned targeting, which has allowed pharma companies to design these inhibitors more specifically to the γ-secretase used in T-cells, as opposed to Golgi cells. Regardless, this finding is particularly important in the context of ALK- ALCL, which typically is associated with a much worse prognosis than ALK+ ALCL, and for which the pipeline of potential treatments is not nearly as replete as that of ALK+ ALCL. Indeed, as detailed in the following chapter, this makes a clinical trial of

Notch inhibitors more likely, and easier to recruit for, as the potential pool of eligible patients would be larger once ALK- ALCL patients are included.

Though HEK293FT cells expressing the Notch1 variants T349P or T311P were not more or less sensitive to chemical Notch1 inhibition than cell lines expressing WT Notch1, ALK+ ALCL cell lines resistant to ALK TKIs were just as responsive to GSIs as their wild-type counter-parts. Therefore, Notch1 inhibition is likely a viable strategy for both ALK+ ALCL as ALK- ALCL: indeed, though there is general agreement within the field that ALK TKIs such as crizotinib or ceritinib have a lot of potential to replace the toxic ALCL99 chemotherapy protocol, ultimately resistance is expected to evolve, as with all TKIs (Sharma *et al*, 2018; Gambacorti-Passerini *et al*, 2016). Therefore, Notch1 inhibition constitutes a viable second-line therapeutic strategy, but also has synergistic potential as a combination therapy with ALK TKIs. The concept of combining ALK TKIs with other therapies is not new, synergy has been shown in pre-clinical trials with vascular endothelial growth factor (VEGF) inhibitors in solid tumours (Michaelson *et al*, 2019), with heat-shock protein 90 (HSP90) or epidermal growth factor receptor (EGFR) inhibitors in non-small cell lung cancer (Zhu *et al*, 2019; Courtin *et al*, 2016), or even MYCN and mTOR inhibitors in ALK+ neuroblastoma (Berry *et al*, 2012). Indeed, in ALK+ ALCL more specifically, crizotinib has successfully been combined with the mTOR inhibitor everolimus (Xu *et al*, 2018), while GSI I has been combined with the proteasome inhibitor bortezomib (Dang *et al*, 2019).

Research presented here therefore fits well in a pattern of investigation of combination therapies. The main appeal of combination therapies is to delay – or ideally prevent - emergence of resistance (Courtin *et al*, 2016). Indeed, it is harder for the tumour to select for resistant clones when they would have to resist to both treatments simultaneously. Though this is difficult to prove *in vitro*, anecdotal evidence from our lab shows that adding GSIs, even at very low doses, concentrations of TKIs (such as crizotinib) that would normally induce resistance (Ceccon *et al*, 2013), is enough to ensure complete cell death *in vitro*. Ideally, this would be proven *in vivo*, but there are as of yet few Notch1 inhibitors with satisfyingly low levels of toxicity. In cancer patients – including ALCL - a number of trials have been started which combined different therapies, showing that this strategy one preferred by clinicians and clinical trial committees (Reviewed in Larose *et al*, 2019 and; Prokoph *et al*, 2018). That we show the potential synergy of a combination of various TKIs and GSIs indicates the strength of this combination strategy. Interestingly, this strategy seems least effective in Karpas 299 cells, although this is relatively unsurprising: as detailed earlier, Karpas 299 are different from most other cell lines used in this thesis, due to significant mutations in such important genes as *phosphatase and tensin homolog* (*pten*) and *tp53* (Turturro *et al*, 2001). Unfortunately, the strength of Notch1 expression does not seem to correlate with response to GSIs, and therefore a conclusive biomarker to predict which patients would best react to either GSIs as a stand-alone or GSI and ALK TKIs as a combination therapy is lacking; the example of the cell line Karpas 299 would suggest that such a predictive biomarker would be desirable.

Regardless, Notch1 expression is predictive of prognosis: strength of expression correlates with EFS of patients treated on the ALCL99 protocol or its predecessors (which, it should be said, remain remarkably similar since front-line ALCL therapy has progressed very little since its inception (Reviewed by Larose *et al*, 2019)). Though at first, the fact that high Notch1 expression correlates with an improved EFS over that found for patients with a poorer EFS seems odd, it is important to remember that these patients were treated with the ALCL99 chemotherapy protocol, and as such one would not expect Notch1 expression to correlate with treatment response in any way. Though the statistical significance is slight ($p = 0.046$), the number of patients enrolled (respectively for low and high Notch1 expression n = 56 and n = 33) is large as far as an ALCL study is concerned. Though a number of potential biomarkers predictive of prognosis have been mooted for ALCL (Reviewed in Larose *et al*, 2019), most are more invasive than Notch staining of the biopsy at presentation – although new liquid-biopsy based technologies are also very promising. Unfortunately, however, the data presented here is insufficient to inform future clinical trial biomarkers. Indeed, the effect observed is slight and the functional implications are not clear: why does Notch1 staining intensity correlate with EFS, unless for example this is just a manifestation of another more relevant clinical biomarker? For example, one would imagine that stronger NPM-ALK expression might upregulate Notch1 and therefore lead to the high intensity staining observed, while also increasing the likelihood of the host immune system developing auto-antibodies to NPM-ALK; indeed there is mounting evidence that auto-antibody titre correlates with prognosis (Reviewed by Larose *et al*, 2019). It could therefore be interesting to compare Notch1 staining with NPM-ALK expression and auto-antibody titre.

Notch receptors should ideally not be studied in isolation, indeed in tumours, the microenvironment would play a crucial role in modulating signalling of the Notch pathways, as previously shown in ALCL (Jundt *et al*, 2002), but this is a well-documented fact more broadly (Reviewed in Bray, 2016). To study this, ALCL cells activated by the Notch ligand DLL1 were treated with GSI I, in an attempt to model a more realistic tumour model. The main finding from this experiment was that ligand activation attenuates the effect of γ-secretase inhibition, and reassuringly similar results have been observed previously, albeit in the context of T cell differentiation: presence of the Notch1 ligand DLL1 expressed by OP9 feeder cells reversed the decrease in Notch1 target gene expression caused by γ-secretase inhibition (Zhou *et al*, 2008). However, it is unlikely that the tumour microenvironment would provide the 1:1 ligand-to-receptor ratio simulated here, and thus the effect seen is probably amplified compared to what would be observed in patients. Ideally, GSIs would be tested in a mouse model of ALCL, which is much closer to patient conditions. Nevertheless, this points to an important potential caveat of using GSIs as a stand-alone therapy and reinforces the importance of the combination treatment with ALK TKIs.

To conclude, in this chapter GSIs are shown to be a viable frontline treatment option for ALK+ and ALK- ALCL, and in the former case, in combination with ALK TKIs but also as a second line protocol when resistance to ALK TKIs emerge.

7. Concluding remarks & future work

The genetics underlying ALK+ ALCL remains largely unknown. Being a relatively rare cancer with a common, well-characterised driving oncogenic event, little effort has been made to uncover other genetic alterations. We therefore sequenced 18 ALK+ ALCL tumours and analysed their genome together with 7 previously reported ALK+ cases (Crescenzo *et al*, 2015) in order to uncover mechanisms of pathogenesis, biomarkers and novel therapeutic targets. We revealed that paediatric ALK+ ALCL tumours (≤18 years of age) have fewer variants than adult cases in keeping with age-related increases in mutational load (Gröbner *et al*, 2018). However, overall the genome remains largely silent and devoid of significant insertions, deletions or copy number variations, also in keeping with previous publications (Youssif *et al*, 2009; Salaverria *et al*, 2008). Whilst we detected differences between the genomes at diagnosis of patients who did and did not go on to relapse, our sample size was too small to be able to deduce any firm conclusions as to mutational events that may be predictive of relapse. Analysis of a larger number of samples would be the next step, as it may not only help explain the difference in prognoses between the two different patient groups, but also lead to the discovery of reliable predictive biomarkers to differentiate them, and thus allow tailored, personalized treatment strategies. In addition, as mentioned before, we hold limited numbers of samples with matched constitutive DNA to be able to study of the germline genomic landscape, which is important to identify potential predisposing genetic abnormalities. Therefore, a prospective study would include patient samples with matched constitutional DNA as well as patients with a range of prognoses to allow a full analysis of genetic abnormalities associated with predisposition and/or risk of relapse/recurrence. However, paediatric ALCL is rare and therefore the study described herein utilised all available tumour samples.

To identify pathways that are key to ALCL biology, gene set enrichment analysis was employed revealing a number of pathways commonly affected by mutation in ALK+ ALCL. Unsurprisingly, mutations clustered in genes of the TCR signalling pathway, but another key pathway identified was Notch1. Gain-of-function mutations in Notch1 have previously been identified in a number of other cancers, most notably in approximately 50 to 60% of T cell Acute Lymphoblastic Leukaemia and Lymphoma (Weng *et al*, 2004; Aster *et al*, 2011; Breit *et al*, 2006). However, most of these mutations are in the intracellular domains of the protein, with few in the extracellular domains (Wang *et al*, 2011b; Vollbrecht *et al*, 2015; Athanasakis *et al*, 2014). In contrast, a novel mutation in the 9th EGF-like domain of extracellular Notch1 (T349P) was detected in 9.3% of ALK+ ALCL patient tumours analysed in this study. Whilst variant effect prediction software indicated these variants to be harmful, the functional significance of these mutations was investigated. We showed the positive impact of T349P on Notch1 activity as demonstrated by enhanced cell proliferation when expressed in HEK293FT cells.

We theorize that Notch1 T349P could modulate ligand binding (either directly or through modulation of calcium binding, particularly as calcium signalling is thought to be dysregulated in ALCL and calcium ions play an important role in Notch ligand binding (Rand *et al*, 2000; Rust *et al*, 2005). An interesting next step here would be sequencing the known loci of genomic mutations of the *notch1* gene, as it seems likely that ALCL patients might present with some of the previously identified and characterized mutations of Notch1. As noted previously, this would fit with data from other T cell malignancies, many of which present with Notch1 mutations (Weng *et al*, 2004). Ideally even, the whole exome of the *notch1* gene would be sequenced for further mutations.

Notch1 has been identified on the surface of ALCL cells (Kamstrup *et al*, 2014; Jundt *et al*, 2002), and the genomic location of *notch1* has been shown to be amplified in a significant number of ALCL paediatric patients (10 of 17 patients; Youssif *et al*, 2009). *notch1* also shows strong expression in a great majority of ALK+ ALCL, and about half of ALK- ALCL (Kamstrup *et al*, 2014; Jundt *et al*, 2002), as well as in cutaneous ALCL patients (Kamstrup *et al*, 2008) – this in itself may be a manifestation of the genomic gains identified in ALCL. Strong *notch1* expression has been demonstrated in a number of T-cell and ALCL cell lines (Jundt *et al*, 2002). These data, added to our own, point to the importance of the Notch pathway in ALCL, and led us to investigate the therapeutic potential. Both this study and those cited above suggest however that somewhere around a quarter to a third of ALCL patients present with low Notch1 expression, though it is not clear what separates these tumours from others, with a significantly stronger expression of Notch1. Presumably, this could be caused by reduced NPM-ALK activity; indeed the literature suggests that ALK- ALCL tumours are less likely to present with strong Notch1 expression (Kamstrup *et al*, 2014). However, all 89 patients in our tissue microarray are ALK+ ALCL so it is also likely that there is inter-tumour variability in the expression of Notch1 in ALCL. A combination of NPM-ALK-mediated upregulation of *notch1* and amplification of the genomic locus of *notch1* may explain the variability in expression of *notch1* between the 89 patients samples we studied.

Regardless of the presence of Notch1 mutations, Notch1 constitutes a therapeutic target in ALCL, independent of ALK status. Suppression of Notch1 expression/activity led to an increase in apoptosis in keeping with previous reports, which we replicated in both ALK+ and ALK- cell lines (Jundt *et al*, 2002; Dang *et al*, 2019; Kamstrup *et al*, 2014). Interestingly, in T-ALL the presence of Notch1 mutations has been shown to correlate with response to therapy (Breit *et al*, 2006), whereby patients with activating Notch1 mutations have a more favourable long-term response to treatment (prednisone in this case). How this fits with the data presented here and in other studies pointing to Notch1 as an oncogene is unclear, indeed the role of Notch1 itself in cancers in general has long been unclear, with evidence showing it to be an oncogene while other studies show it to be a tumour suppressor. Ultimately, this likely depends on the tumour type, how Notch1 signalling is regulated, on the types of Notch1 ligands which are used for its activation, and on the interplay with transcription factors in the

nucleus which mediate downstream signalling in combination with the activated, intracellular domain of Notch1.

Efforts to modulate Notch signalling therapeutically have been difficult. Indeed, as highlighted previously, the lack of specificity of most early Notch inhibitors (mostly γ-secretase inhibitors, and not Notch inhibitors *per se*) rendered them too toxic (gastrointestinal issues, mostly) and were therefore discontinued. The main problem stemmed from so-called on-target effects: inhibition of Notch signalling in the epithelial cells of the gut leads progenitor cells to differentiate into goblet cells over enterocytes (Aster, 2009). Considering that these are not off-target effects, the toxicity observed was a major issue, as simply fine-tuning the specificity of Notch inhibitors would not solve the problem.

Fortunately, new, inventive approaches that do not attempt to target γ-secretase have yielded promising new compounds. Recently, CB-103, a pan-Notch protein-protein inhibitor acting to inhibit the Notch transcription factor complex inside the nucleus, thus preventing downstream Notch signalling, has shown its efficacy in a number of tumour types in pre-clinical studies (Lehal *et al*, 2018; Weber *et al*, 2018), and has already progressed to early-phase clinical trials to test its safety profile in patients (Perez Garcia *et al*, 2018; clinical trial IDs NCT03422679 and 2017-001491-35). Another mechanism to inhibit Notch that is being considered is to block the interaction of Notch with its ligand. For example, competitive inhibitors are being investigated, although unfortunately early studies showed little in the way of reduced gastrointestinal toxicity (Briot & Iruela-Arispe, 2015). Different attempts have yielded more promising results, demonstrating an increase in goblet cells in mouse models, while also showing that this approach reduced angiogenesis in addition to reducing tumour growth (Kangsamaksin *et al*, 2015). The latest iterations of such antibodies seem to show ever-decreased toxicity in pre-clinical mouse trials without compromising on anti-tumour activity (Masiero *et al*, 2019). As a result, these newer methods of Notch inhibition raise hope that work such as that laid out in this thesis will have practical use for patients in the clinic, as toxic chemotherapy is phased out from paediatric treatment schedules.

Intriguingly, NPM-ALK has been shown to be sufficient to induce *notch1* expression in mouse thymocytes (Malcolm *et al*, 2016), showing that the two signalling pathways are intricately linked in ALCL. Not only do we confirm this by silencing *npm-alk* in ALCL, but we also show that NPM-ALK acts through STAT3, which binds to *notch1*. This could explain why we observed synergistic effects between crizotinib and γ-secretase inhibitors in inducing cell death. TKIs of NPM-ALK have been a boon for adult ALCL patients, and a potential one for paediatric patients – though unfortunately some patients relapse, as with many small molecule inhibitors (Gambacorti-Passerini *et al*, 2016). For this reason, we show here for the first time that resistance to TKIs such as crizotinib do not significantly impact the sensitivity of ALCL to γ-secretase inhibitors targeting the Notch pathway. In other words, we show the potential of Notch inhibition as a second-line therapy, where TKIs fail (Gambacorti-Passerini *et al*,

2016). In addition, it seems likely that adding a Notch inhibitor to front-line treatment in combination with a TKI such as crizotinib would reduce the chances of relapse or resistance developing, particularly in cases where resistance develops in the form of mutations to *npm-alk* (Prokoph, *et al.*, 2019; in publication). Further work, in the form of pre-clinical studies such as combination treatments in animal models would confirm whether such a therapy schedule does indeed delay relapse significantly.

Importantly, we show the potential of targeting the Notch pathway in the ALK- ALCL setting, which has never been tested before. Given the role we found of NPM-ALK in upregulating *notch1*, it was not clear that Notch1 would be as effective a therapeutic target in tumours lacking the ALK translocation, although as demonstrated, GSIs are just as effective at impeding the growth of ALK- ALCL. Though we did not find that strength of Notch1 expression sensitizes cells to either cytotoxic schedules or GSIs, analysis of a large cohort of 89 ALK+ ALCL patients showed that strength of Notch1 protein expression retrospectively correlates with Event-Free Survival. Given that dose de-escalation in low-risk ALCL patients could reduce toxicity and improve quality of life, as well as decrease long-term risks derived from cytotoxic therapies, these data are particularly important and could inform future trial designs. We also confirm in a significantly larger cohort that Notch1 is strongly expressed in a large majority of ALCL patients. This finding is important in itself as it highlights the potential of Notch inhibitors as a therapy: though we showed that stronger expression does not correlate with increased sensitivity to GSIs, the inverse is unlikely to be true: ALCL cells that do not stably express Notch1 are unlikely to respond to GSIs, thus it is important that a large majority of patients express Notch1 for this treatment strategy to be viable. Since the absolute number of ALCL patients is very small compared to many other cancer types, it is unlikely that any new treatment strategies only targeting a subset of ALCL patients would interest pharmaceutical companies, which typically target larger potential markets. Indeed, the fact that ALK- ALCL patients are a potential market for Notch inhibitors would increase their attractiveness, particularly since they could be trialled more easily in adult patients, who make up a large majority of ALK- ALCL patients, before progressing to paediatric patients.

To conclude, we present here for the first time the genomic landscape of ALK+ ALCL, and use these data to demonstrate the importance of the Notch pathway to ALCL pathobiology, as well as the potential of Notch inhibitors at the bedside.

References

Adzhubei, I.A., Schmidt, S., Peshkin, L., Ramensky, V.E., Gerasimova, A., Bork, P., Kondrashov, A.S. & Sunyaev, S.R. (2010) A method and server for predicting damaging missense mutations. *Nature Methods*, **7,** 248–249.

Ait-Tahar, K., Damm-Welk, C., Burkhardt, B., Zimmermann, M., Klapper, W., Reiter, A., Pulford, K. & Woessmann, W. (2010) Correlation of the autoantibody response to the ALK oncoantigen in pediatric anaplastic lymphoma kinase-positive anaplastic large cell lymphoma with tumor dissemination and relapse risk. *Blood*, **115,** 3314–9.

Alessandri, A.J., Pritchard, S.L., Schultz, K.R. & Massing, B.G. (2002) A population-based study of pediatric anaplastic large cell lymphoma. *Cancer*, **94,** 1830–5.

Alexander, S., Kraveka, J.M., Weitzman, S., Lowe, E., Smith, L., Lynch, J.C., Chang, M., Kinney, M.C., Perkins, S.L., Laver, J., Gross, T.G. & Weinstein, H. (2014) Advanced stage anaplastic large cell lymphoma in children and adolescents: Results of ANHL0131, a randomized phase III trial of APO versus a modified regimen with vinblastine: A report from the children's oncology group. *Pediatric blood & cancer*, **61,** 2236–2242.

Alexandrov, L.B., Nik-Zainal, S., Wedge, D.C., Aparicio, S.A.J.R., Behjati, S., Biankin, A. V., Bignell, G.R., Bolli, N., Borg, A., Børresen-Dale, A.L., Boyault, S., Burkhardt, B., Butler, A.P., Caldas, C., Davies, H.R., Desmedt, C., Eils, R., Eyfjörd, J.E., Foekens, J.A., Greaves, M., et al (2013) Signatures of mutational processes in human cancer. *Nature*, **500,** 415–421.

Ambrogio, C., Martinengo, C., Voena, C., Tondat, F., Riera, L., di Celle, P.F., Inghirami, G. & Chiarle, R. (2009) NPM-ALK oncogenic tyrosine kinase controls T-cell identity by transcriptional regulation and epigenetic silencing in lymphoma cells. *Cancer research*, **69,** 8611–9.

Amin, A.D., Rajan, S.S., Liang, W.S., Pongtornpipat, P., Groysman, M.J., Tapia, E.O., Peters, T.L., Cuyugan, L., Adkins, J., Rimsza, L.M., Lussier, Y.A., Puvvada, S.D. & Schatz, J.H. (2015) Evidence Suggesting That Discontinuous Dosing of ALK Kinase Inhibitors May Prolong Control of ALK+ Tumors. *Cancer research*, **75,** 2916–27.

Amsen, D., Helbig, C. & Backer, R.A. (2015) Notch in T Cell Differentiation: All Things Considered. *Trends in Immunology*, **36,** 802–814.

Andersson, E.R. & Lendahl, U. (2014) Therapeutic modulation of Notch signalling--are we there yet? *Nature reviews. Drug discovery*, **13,** 357–78.

Aster, J.C. (2009) Notch targeting 2.0. *Blood*, **113,** 6044–6045.

Aster, J.C., Blacklow, S.C. & Pear, W.S. (2011) Notch signalling in T-cell lymphoblastic leukaemia/lymphoma and other haematological malignancies. *Journal of Pathology*, **223,** 262–273.

Athanasakis, E., Melloni, E., Rigolin, G.M., Agnoletto, C., Voltan, R., Vozzi, D., Piscianz, E., Segat, L., Dal Monego, S., Cuneo, A., Secchiero, P. & Zauli, G. (2014) The p53 transcriptional pathway is preserved in ATMmutated and NOTCH1mutated chronic lymphocytic leukemias. *Oncotarget*, **5,** 12635–45.

Attarbaschi, A., Mann, G., Rosolen, A., Williams, D., Uyttebroeck, A., Marky, I., Lamant, L., Horibe, K., Wrobel, G., Beishuizen, A., Wössmann, W., Reiter, A., Mauguen, A., Le Deley, M.-C., Brugières, L. & European Intergroup for Childhood Non-Hodgkin Lymphoma (EICNHL) ALCL99 Trial (2011) Limited stage I disease is not necessarily indicative of an excellent prognosis in childhood anaplastic large cell lymphoma. *Blood*, **117,** 5616–9.

Ayaz, F. & Osborne, B.A. (2014) Non-Canonical Notch Signaling in Cancer and Immunity. *Frontiers in Oncology*, **4,** 345.

Bai, R.Y., Dieter, P., Peschel, C., Morris, S.W. & Duyster, J. (1998) Nucleophosmin-anaplastic lymphoma kinase of large-cell anaplastic lymphoma is a constitutively active tyrosine kinase that utilizes phospholipase C-gamma to mediate its mitogenicity. *Molecular and cellular biology*, **18,** 6951–61.

Bai, R.Y., Ouyang, T., Miething, C., Morris, S.W., Peschel, C. & Duyster, J. (2000) Nucleophosmin-anaplastic lymphoma kinase associated with anaplastic large-cell lymphoma activates the phosphatidylinositol 3-kinase/Akt antiapoptotic signaling pathway. *Blood*, **96,** 4319–27.

Barbey, S., Gogusev, J., Mouly, H., Le Pelletier, O., Smith, W., Richard, S., Soulie, J. & Nezelof, C. (1990) Del cell line: A "malignant histiocytosis" CD30 + T(5;6)(Q35;P21) cell line. *International Journal of Cancer*, **45,** 546–553.

Le Beau, M.M., Bitter, M.A., Larson, R.A., Doane, L.A., Ellis, E.D., Franklin, W.A., Rubin, C.M., Kadin, M.E. & Vardiman, J.W. (1989) The t(2;5)(p23;q35): a recurring chromosomal abnormality in Ki-1-positive anaplastic large cell lymphoma. *Leukemia*, **3,** 866–70.

Benharroch, D., Meguerian-Bedoyan, Z., Lamant, L., Amin, C., Brugières, L., Terrier-Lacombe, M.J., Haralambieva, E., Pulford, K., Pileri, S., Morris, S.W., Mason, D.Y. & Delsol, G. (1998) ALK-positive lymphoma: a single disease with a broad spectrum of morphology. *Blood*, **91,** 2076–84.

Berry, T., Luther, W., Bhatnagar, N., Jamin, Y., Poon, E., Sanda, T., Pei, D., Sharma, B., Vetharoy, W.R., Hallsworth, A., Ahmad, Z., Barker, K., Moreau, L., Webber, H., Wang, W., Liu, Q., Perez-Atayde, A., Rodig, S., Cheung, N.-K., Raynaud, F., et al (2012) The ALK(F1174L) mutation potentiates the oncogenic activity of MYCN in neuroblastoma. *Cancer cell*, **22,** 117–30.

Bilsland, J.G., Wheeldon, A., Mead, A., Znamenskiy, P., Almond, S., Waters, K.A., Thakur, M., Beaumont, V., Bonnert, T.P., Heavens, R., Whiting, P., McAllister, G. & Munoz-Sanjuan, I. (2008) Behavioral and neurochemical alterations in mice deficient in anaplastic lymphoma kinase suggest therapeutic potential for psychiatric indications. *Neuropsychopharmacology*, **33,** 685–700.

Bischof, D., Pulford, K., Mason, D.Y. & Morris, S.W. (1997) Role of the nucleophosmin (NPM) portion of the non-Hodgkin's lymphoma-associated NPM-anaplastic lymphoma kinase fusion protein in oncogenesis. *Molecular and cellular biology*, **17,** 2312–25.

Bitter, M.A., Franklin, W.A., Larson, R.A., McKeithan, T.W., Rubin, C.M., Le Beau, M.M., Stephens, J.K. & Vardiman, J.W. (1990) Morphology in Ki-1(CD30)-positive non-Hodgkin's lymphoma is correlated with clinical features and the presence of a unique chromosomal abnormality, t(2;5)(p23;q35). *The American journal of surgical pathology*, **14,** 305–16.

Bonadonna, G. (2000) Historical review of Hodgkin's disease. *British journal of haematology*, **110,** 504–11.

Bonadonna, G., Zucali, R., Monfardini, S., De Lena, M. & Uslenghi, C. (1975) Combination chemotherapy of Hodgkin's disease with adriamycin, bleomycin, vinblastine, and imidazole carboxamide versus MOPP. *Cancer*, **36,** 252–9.

Borggrefe, T. & Oswald, F. (2009) The Notch signaling pathway: Transcriptional regulation at Notch target genes. *Cellular and Molecular Life Sciences*, **66,** 1631–1646.

Bray, S.J. (2016) Notch signalling in context. *Nature Reviews Molecular Cell Biology*, **17,** 722–735.

Breit, S., Stanulla, M., Flohr, T., Schrappe, M., Ludwig, W.D., Tolle, G., Happich, M., Muckenthaler, M.U. & Kulozik, A.E. (2006) Activating NOTCH1 mutations predict favorable early treatment response and long-term outcome in childhood precursor T-cell lymphoblastic leukemia. *Blood*, **108,** 1151–1157.

Briot, A. & Iruela-Arispe, M.L. (2015) Blockade of Specific NOTCH Ligands: A New Promising Approach in Cancer Therapy. *Cancer Discovery*, **5,** 112–114.

Brown, K.L. (1965) Antineoplastic agents derived from the Periwinkle plant: Vinblastine Sulfate (VELBAN). *Journal of the American Medical Association*, **191,** 749–50.

Brugières, L., Le Deley, M.-C., Rosolen, A., Williams, D., Horibe, K., Wrobel, G., Mann, G., Zsiros, J., Uyttebroeck, A., Marky, I., Lamant, L. & Reiter, A. (2009) Impact of the methotrexate administration dose on the need for intrathecal treatment in children and adolescents with anaplastic large-cell lymphoma: results of a randomized trial of the EICNHL Group. *Journal of Clinical Oncology*, **27,** 897–903.

Bruno, A., Boisselier, B., Labreche, K., Marie, Y., Polivka, M., Jouvet, A., Adam, C., Figarella-Branger, D., Miquel, C., Eimer, S., Houillier, C., Soussain, C., Mokhtari, K., Daveau, R. & Hoang-Xuan, K. (2014) Mutational analysis of primary central nervous system lymphoma. *Oncotarget*, **5,** 5065–75.

Burkhardt, B. & Woessmann, W. (2018) Childhood and adolescent NHL survivorship: the BFM perspective. *British Journal of Haematology*, **182,** 5–6.

Camidge, D.R., Bang, Y.-J., Kwak, E.L., Iafrate, A.J., Varella-Garcia, M., Fox, S.B., Riely, G.J., Solomon, B., Ou, S.-H.I., Kim, D.-W., Salgia, R., Fidias, P., Engelman, J.A., Gandhi, L., Jänne, P.A., Costa, D.B., Shapiro, G.I., Lorusso, P., Ruffner, K., Stephenson, P., et al (2012) Activity and safety of crizotinib in patients with ALK-positive non-small-cell lung cancer: updated results from a phase 1 study. *The Lancet. Oncology*, **13,** 1011–9.

Canellos, G.P., Rosenberg, S.A., Friedberg, J.W., Lister, T.A. & Devita, V.T. (2014) Treatment of Hodgkin lymphoma: a 50-year perspective. *Journal of Clinical Oncology*, **32,** 163–8.

Carol, H., Maris, J.M., Kang, M.H., Reynolds, C.P., Kolb, E.A., Gorlick, R., Keir, S.T., Wu, J., Kurmasheva, R.T., Houghton, P.J., Smith, M.A., Lock, R.B. & Lyalin, D. (2014) Initial testing (stage 1) of the notch inhibitor PF-03084014, by the pediatric preclinical testing program. *Pediatric blood & cancer*, **61,** 1493–6.

Ceccon, M., Mologni, L., Bisson, W., Scapozza, L. & Gambacorti-Passerini, C. (2013) Crizotinib-Resistant NPM-ALK Mutants Confer Differential Sensitivity to Unrelated Alk Inhibitors. *Molecular Cancer Research*, **11,** 122–132.

Chiang, M.Y., Wang, Q., Gormley, A.C., Stein, S.J., Xu, L., Shestova, O., Aster, J.C. & Pear, W.S. (2016) High selective pressure for Notch1 mutations that induce Myc in T-cell acute lymphoblastic leukemia. *Blood*, **128,** 2229–2240.

Chiarle, R., Gong, J.Z., Guasparri, I., Pesci, A., Cai, J., Liu, J., Simmons, W.J., Dhall, G., Howes, J., Piva, R. & Inghirami, G. (2003) NPM-ALK transgenic mice spontaneously develop T-cell lymphomas and plasma cell tumors. *Blood*, **101,** 1919–27.

Chiarle, R., Simmons, W.J., Cai, H., Dhall, G., Zamo, A., Raz, R., Karras, J.G., Levy, D.E. & Inghirami, G. (2005) Stat3 is required for ALK-mediated lymphomagenesis and provides a possible therapeutic target. *Nature medicine*, **11,** 623–9.

Chiarle, R., Voena, C., Ambrogio, C., Piva, R. & Inghirami, G. (2008) The anaplastic lymphoma kinase in the pathogenesis of cancer. *Nature Reviews Cancer*, **8,** 11–23.

Chihara, D., Wong, S., Feldman, T., Fanale, M.A., Sanchez, L., Connors, J.M., Savage, K.J. & Oki, Y. (2018) Outcome of patients with relapsed or refractory anaplastic large cell lymphoma who have failed brentuximab vedotin. *Hematological oncology*, **37,** 35–38.

Chillakuri, C.R., Sheppard, D., Lea, S.M. & Handford, P.A. (2012) Notch receptor-ligand binding and activation: Insights from molecular studies. *Seminars in Cell and Developmental Biology*, **23,** 421–428.

Choi, S.H., Severson, E., Pear, W.S., Liu, X.S., Aster, J.C. & Blacklow, S.C. (2017) The common oncogenomic program of NOTCH1 and NOTCH3 signaling in T-cell acute lymphoblastic leukemia.

PLOS ONE, **12,** e0185762.

Choi, Y., Sims, G.E., Murphy, S., Miller, J.R. & Chan, A.P. (2012) Predicting the Functional Effect of Amino Acid Substitutions and Indels. *PLoS ONE*, **7,** e46688.

Chun, S. & Fay, J.C. (2009) Identification of deleterious mutations within three human genomes. *Genome Research*, **19,** 1553–1561.

Chung, I.-H., Lu, P.-H., Lin, Y.-H., Tsai, M.-M., Lin, Y.-W., Yeh, C.-T. & Lin, K.-H. (2017) The long non-coding RNA LINC01013 enhances invasion of human anaplastic large-cell lymphoma. *Scientific reports*, **7,** 295.

Cools, J., Wlodarska, I., Somers, R., Mentens, N., Pedeutour, F., Maes, B., De Wolf-Peeters, C., Pauwels, P., Hagemeijer, A. & Marynen, P. (2002) Identification of novel fusion partners of ALK, the anaplastic lymphoma kinase, in anaplastic large-cell lymphoma and inflammatory myofibroblastic tumor. *Genes, chromosomes & cancer*, **34,** 354–62.

Cordle, J., Redfieldz, C., Stacey, M., van der Merwe, P.A., Willis, A.C., Champion, B.R., Hambleton, S. & Handford, P.A. (2008) Localization of the delta-like-1-binding site in human Notch-1 and its modulation by calcium affinity. *The Journal of biological chemistry*, **283,** 11785–93.

Courtin, A., Smyth, T., Hearn, K., Saini, H.K., Thompson, N.T., Lyons, J.F. & Wallis, N.G. (2016) Emergence of resistance to tyrosine kinase inhibitors in non-small-cell lung cancer can be delayed by an upfront combination with the HSP90 inhibitor onalespib. *British journal of cancer*, **115,** 1069–1077.

Crescenzo, R., Abate, F., Lasorsa, E., Tabbo, F., Gaudiano, M., Chiesa, N., Di Giacomo, F., Spaccarotella, E., Barbarossa, L., Ercole, E., Todaro, M., Boi, M., Acquaviva, A., Ficarra, E., Novero, D., Rinaldi, A., Tousseyn, T., Rosenwald, A., Kenner, L., Cerroni, L., et al (2015) Convergent mutations and kinase fusions lead to oncogenic STAT3 activation in anaplastic large cell lymphoma. *Cancer Cell*, **27,** 516–532.

Cui, Y.X., Kerby, A., McDuff, F.K.E., Ye, H. & Turner, S.D. (2009) NPM-ALK inhibits the p53 tumor suppressor pathway in an MDM2 and JNK-dependent manner. *Blood*, **113,** 5217–27.

Damm-Welk, C., Busch, K., Burkhardt, B., Schieferstein, J., Viehmann, S., Oschlies, I., Klapper, W., Zimmermann, M., Harbott, J., Reiter, A. & Woessmann, W. (2007) Prognostic significance of circulating tumor cells in bone marrow or peripheral blood as detected by qualitative and quantitative PCR in pediatric NPM-ALK-positive anaplastic large-cell lymphoma. *Blood*, **110,** 670–7.

Damm-Welk, C., Zimmermann, M., Attarbaschi, A., Kutscher, N., Schieferstein, J., Oschlies, I., Klapper, W. & Woessmann, W. (2018) Abstract 60: Quantification of minimal disseminated disease in NPM-ALK-positive anaplastic large cell Lymphoma: validation cohort and method. *British Journal of Haematology*, **182,** 42.

Dang, Q., Chen, L., Xu, M., You, X., Zhou, H., Zhang, Y. & Shi, W. (2019) The γ-secretase inhibitor GSI-I interacts synergistically with the proteasome inhibitor bortezomib to induce ALK+ anaplastic large cell lymphoma cell apoptosis. *Cellular signalling*, **59,** 76–84.

Davis, R.L. & Turner, D.L. (2001) Vertebrate hairy and Enhancer of split related proteins: transcriptional repressors regulating cellular differentiation and embryonic patterning. *Oncogene*, **20,** 8342–57.

Davis, T.H., Morton, C.C., Miller-Cassman, R., Balk, S.P. & Kadin, M.E. (1992) Hodgkin's disease, lymphomatoid papulosis, and cutaneous T-cell lymphoma derived from a common T-cell clone. *The New England journal of medicine*, **326,** 1115–22.

Deangelo, D.J., Stone, R.M., Silverman, L.B., Stock, W., Attar, E.C., Dallob, I.F., Matthews, C., Stone, J., Freedman, S.J. & Aster, J. (2006) A phase I clinical trial of the notch inhibitor MK-0752 in patients

with T-cell acute lymphoblastic leukemia/lymphoma (T-ALL) and other leukemias. *Journal of Clinical Oncology*, **24,** 6585.

Deftos, M.L., Huang, E., Ojala, E.W., Forbush, K.A. & Bevan, M.J. (2000) Notch1 signaling promotes the maturation of CD4 and CD8 SP thymocytes. *Immunity*, **13,** 73–84.

Le Deley, M.-C., Reiter, A., Williams, D., Delsol, G., Oschlies, I., McCarthy, K., Zimmermann, M., Brugières, L. & EICNHL (2008) Prognostic factors in childhood anaplastic large cell lymphoma: results of a large European intergroup study. *Blood*, **111,** 1560–6.

Le Deley, M.-C., Rosolen, A., Williams, D.M., Horibe, K., Wrobel, G., Attarbaschi, A., Zsiros, J., Uyttebroeck, A., Marky, I.M., Lamant, L., Woessmann, W., Pillon, M., Hobson, R., Mauguen, A., Reiter, A. & Brugières, L. (2010) Vinblastine in children and adolescents with high-risk anaplastic large-cell lymphoma: results of the randomized ALCL99-vinblastine trial. *Journal of Clinical Oncology*, **28,** 3987–93.

Delsol, G., Al Saati, T., Gatter, K.C., Gerdes, J., Schwarting, R., Caveriviere, P., Rigal-Huguet, F., Robert, A., Stein, H. & Mason, D.Y. (1988) Coexpression of epithelial membrane antigen (EMA), Ki-1, and interleukin-2 receptor by anaplastic large cell lymphomas. Diagnostic value in so-called malignant histiocytosis. *The American journal of pathology*, **130,** 59–70.

Devita, V.T., Serpick, A.A. & Carbone, P.P. (1970) Combination chemotherapy in the treatment of advanced Hodgkin's disease. *Annals of internal medicine*, **73,** 881–95.

Dong, C., Wei, P., Jian, X., Gibbs, R., Boerwinkle, E., Wang, K. & Liu, X. (2015) Comparison and integration of deleteriousness prediction methods for nonsynonymous SNVs in whole exome sequencing studies. *Human molecular genetics*, **24,** 2125–37.

Ducray, S.P., Natarajan, K., Garland, G.D., Turner, S.D. & Egger, G. (2019) The Transcriptional Roles of ALK Fusion Proteins in Tumorigenesis. *Cancers*, **11,** 1074.

Eberth, S., Schneider, B., Rosenwald, A., Hartmann, E.M., Romani, J., Zaborski, M., Siebert, R., Drexler, H.G. & Quentmeier, H. (2010) Epigenetic regulation of CD44 in Hodgkin and non-Hodgkin lymphoma. *BMC cancer*, **10,** 517.

Eckerle, S., Brune, V., Döring, C., Tiacci, E., Bohle, V., Sundström, C., Kodet, R., Paulli, M., Falini, B., Klapper, W., Chaubert, A.B., Willenbrock, K., Metzler, D., Bräuninger, A., Küppers, R. & Hansmann, M.-L. (2009) Gene expression profiling of isolated tumour cells from anaplastic large cell lymphomas: insights into its cellular origin, pathogenesis and relation to Hodgkin lymphoma. *Leukaemia*, **23,** 2129–38.

Ehrhardt, M., Hochberg, J. & Robinson, L. (2018) Childhood and adolescent Non-Hodgkin Lymphoma survivorship: the Childhood Cancer Survivor Study (CCSS) and St Jude Lifetime (SJLIFE) cohorts. *British Journal of Haematology*, **182,** 5.

Ellisen, L.W., Bird, J., West, D.C., Soreng, A.L., Reynolds, T.C., Smith, S.D. & Sklar, J. (1991) TAN-1, the human homolog of the Drosophila notch gene, is broken by chromosomal translocations in T lymphoblastic neoplasms. *Cell*, **66,** 649–61.

Epstein, A.L. & Kaplan, H.S. (1974) Biology of the human malignant lymphomas. I. Establishment in continuous cell culture and heterotransplantation of diffuse histiocytic lymphomas. *Cancer*, **34,** 1851–72.

Fabregat, A., Jupe, S., Matthews, L., Sidiropoulos, K., Gillespie, M., Garapati, P., Haw, R., Jassal, B., Korninger, F., May, B., Milacic, M., Roca, C.D., Rothfels, K., Sevilla, C., Shamovsky, V., Shorser, S., Varusai, T., Viteri, G., Weiser, J., Wu, G., et al (2018) The Reactome Pathway Knowledgebase. *Nucleic acids research*, **46,** D649–D655.

FDA (2011)Brentuximab vedotin: full prescribing information. Maryland, United States.

Feuerstein, N., Chan, P.K. & Mond, J.J. (1988) Identification of numatrin, the nuclear matrix protein associated with induction of mitogenesis, as the nucleolar protein B23. Implication for the role of the nucleolus in early transduction of mitogenic signals. *Journal of Biological Chemistry*, **263,** 10608–10612.

Fischer, P., Nacheva, E., Mason, D.Y., Sherrington, P.D., Hoyle, C., Hayhoe, F.G. & Karpas, A. (1988) A Ki-1 (CD30)-positive human cell line (Karpas 299) established from a high-grade non-Hodgkin's lymphoma, showing a 2;5 translocation and rearrangement of the T-cell receptor beta-chain gene. *Blood*, **72,** 234–40.

Fisher, R.I., Gaynor, E.R., Dahlberg, S., Oken, M.M., Grogan, T.M., Mize, E.M., Glick, J.H., Coltman, C.A. & Miller, T.P. (1993) Comparison of a Standard Regimen (CHOP) with Three Intensive Chemotherapy Regimens for Advanced Non-Hodgkin's Lymphoma. *New England Journal of Medicine*, **328,** 1002–1006.

Forbes, S.A., Bhamra, G., Bamford, S., Dawson, E., Kok, C., Clements, J., Menzies, A., Teague, J.W., Futreal, P.A. & Stratton, M.R. (2008) The Catalogue of Somatic Mutations in Cancer (COSMIC). *Current protocols in human genetics*, **57,** 1–26.

Friedmann, D.R., Wilson, J.J. & Kovall, R.A. (2008) RAM-induced allostery facilitates assembly of a notch pathway active transcription complex. *The Journal of biological chemistry*, **283,** 14781–91.

Fryer, C.J., White, J.B. & Jones, K.A. (2004) Mastermind recruits CycC:CDK8 to phosphorylate the Notch ICD and coordinate activation with turnover. *Molecular cell*, **16,** 509–20.

Gambacorti-Passerini, C., Mussolin, L. & Brugieres, L. (2016) Abrupt Relapse of ALK-Positive Lymphoma after Discontinuation of Crizotinib. *New England Journal of Medicine*, **374,** 95–96.

Gambacorti Passerini, C., Farina, F., Stasia, A., Redaelli, S., Ceccon, M., Mologni, L., Messa, C., Guerra, L., Giudici, G., Sala, E., Mussolin, L., Deeren, D., King, M.H., Steurer, M., Ordemann, R., Cohen, A.M., Grube, M., Bernard, L., Chiriano, G., Antolini, L., et al (2014) Crizotinib in advanced, chemoresistant anaplastic lymphoma kinase-positive lymphoma patients. *Journal of the National Cancer Institute*, **106,** djt378.

Garbin, A., Lovisa, F., Basso, K., Holmes, A., Carraro, E., Pizzi, M., Garaventa, A., Tondo, A., Mura, R., Buffardi, S., Basso, G., D'Amore, E., Pillon, M. & Mussolin, L. (2018) Abstract 61: NPM-ALK expression levels are associated to different miRNA profiles in paediatric anaplastic large cell lymphoma. *British Journal of Haematology*, **182,** 42.

Garces de los Fayos Alonso, I., Kothmayer, M., Schlederer, M., Pusch, O., Tangermann, S., Lagger, S. & Kenner, L. (2018a) Abstract 40: Examining the function of PDGFRB in anaplastic large cell lymphoma. *British Journal of Haematology*, **182,** 29.

Garces de los Fayos Alonso, I., Liang, H.-C., Turner, S.D., Lagger, S., Merkel, O. & Kenner, L. (2018b) The Role of Activator Protein-1 (AP-1) Family Members in CD30-Positive Lymphomas. *Cancers*, **10,**.

Gekas, C., D'Altri, T., Aligué, R., González, J., Espinosa, L. & Bigas, A. (2016) β-Catenin is required for T-cell leukemia initiation and MYC transcription downstream of Notch1. *Leukemia*, **30,** 2002–2010.

Gilbert, L.A., Horlbeck, M.A., Adamson, B., Villalta, J.E., Chen, Y., Whitehead, E.H., Guimaraes, C., Panning, B., Ploegh, H.L., Bassik, M.C., Qi, L.S., Kampmann, M. & Weissman, J.S. (2014) Genome-Scale CRISPR-Mediated Control of Gene Repression and Activation. *Cell*, **159,** 647–61.

Gilbert, R. & Babaiantz, L. (1931) Notre méthode de roentgenthérapie de la lymphogranulomatoses (Hodgkin): Résultats éloignés. *Acta Radiologica*, **12,** 523–529.

Gillis, S. (1980)Biochemical and biological characterization of lymphocyte regulatory molecules - Chapter V: Identification of an interleukin 2-producing human leukemia T cell line. In *Journal of Experimental Medicine* pp 1709–1719.

Goto, S., Bono, H., Ogata, H., Fujibuchi, W., Nishioka, T., Sato, K. & Kanehisa, M. (1997) Organizing and computing metabolic pathway data in terms of binary relations. *Pacific Symposium on Biocomputing.*, 175–86.

Grabher, C., von Boehmer, H. & Look, A.T. (2006) Notch 1 activation in the molecular pathogenesis of T-cell acute lymphoblastic leukaemia. *Nature reviews. Cancer*, **6,** 347–59.

Greenwald, I. (1998) LIN-12/Notch signaling: lessons from worms and flies. *Genes & development*, **12,** 1751–62.

Grigg, C. & Rizvi, N.A. (2016) PD-L1 biomarker testing for non-small cell lung cancer: truth or fiction? *Journal for Immunotherapy of Cancer*, **4,** 48.

Gröbner, S.N., Worst, B.C., Weischenfeldt, J., Buchhalter, I., Kleinheinz, K., Rudneva, V.A., Johann, P.D., Balasubramanian, G.P., Segura-Wang, M., Brabetz, S., Bender, S., Hutter, B., Sturm, D., Pfaff, E., Hübschmann, D., Zipprich, G., Heinold, M., Eils, J., Lawerenz, C., Erkek, S., et al (2018) The landscape of genomic alterations across childhood cancers. *Nature*, **555,** 321–327.

Guan, J., Umapathy, G., Yamazaki, Y., Wolfstetter, G., Mendoza, P., Pfeifer, K., Mohammed, A., Hugosson, F., Zhang, H., Hsu, A.W., Halenbeck, R., Hallberg, B. & Palmer, R.H. (2015) FAM150A and FAM150B are activating ligands for anaplastic lymphoma kinase. *eLife*, **4,** 1–16.

Haapasalo, A. & Kovacs, D.M. (2011) The many substrates of presenilin/γ-secretase. *Journal of Alzheimer's disease*, **25,** 3–28.

Habets, R.A., de Bock, C.E., Serneels, L., Lodewijckx, I., Verbeke, D., Nittner, D., Narlawar, R., Demeyer, S., Dooley, J., Liston, A., Taghon, T., Cools, J. & de Strooper, B. (2019) Safe targeting of T cell acute lymphoblastic leukemia by pathology-specific NOTCH inhibition. *Science translational medicine*, **11,** 6246.

Haines, N. & Irvine, K.D. (2003) Glycosylation regulates Notch signalling. *Nature Reviews Molecular Cell Biology*, **4,** 786–797.

Hassler, M.R., Klisaroska, A., Kollmann, K., Steiner, I., Bilban, M., Schiefer, A.-I., Sexl, V. & Egger, G. (2012) Antineoplastic activity of the DNA methyltransferase inhibitor 5-aza-2'-deoxycytidine in anaplastic large cell lymphoma. *Biochimie*, **94,** 2297–307.

Hebart, H., Lang, P. & Woessmann, W. (2016) Nivolumab for Refractory Anaplastic Large Cell Lymphoma: A Case Report. *Annals of internal medicine*, **165,** 607–608.

Heitzler, P. (2010)Chapter 14 - Biodiversity and Noncanonical Notch Signaling. In pp 457–481.

Helleday, T., Eshtad, S. & Nik-Zainal, S. (2014) Mechanisms underlying mutational signatures in human cancers. *Nature reviews. Genetics*, **15,** 585–98.

Herbst, H., Tippelmann, G., Anagnostopoulos, I., Gerdes, J., Schwarting, R., Boehm, T., Pileri, S., Jones, D.B. & Stein, H. (1989) Immunoglobulin and T-cell receptor gene rearrangements in Hodgkin's disease and Ki-1-positive anaplastic large cell lymphoma: dissociation between phenotype and genotype. *Leukemia research*, **13,** 103–16.

Hernandez Tejada, F.N., Galvez Silva, J.R. & Zweidler-McKay, P.A. (2014) The challenge of targeting notch in hematologic malignancies. *Frontiers in pediatrics*, **2,** 54.

Hildebrand, D., Uhle, F., Sahin, D., Krauser, U., Weigand, M.A. & Heeg, K. (2018) The Interplay of Notch Signaling and STAT3 in TLR-Activated Human Primary Monocytes. *Frontiers in Cellular and Infection Microbiology*, **8,** 241.

Ho, C.C., Mun, K.S. & Naidu, R. (2013) SNP array technology: An array of hope in breast cancer research. *Malaysian Journal of Pathology*, **35,** 33–43.

Hoareau-Aveilla, C., Valentin, T., Daugrois, C., Quelen, C., Mitou, G., Quentin, S., Jia, J., Spicuglia, S.,

Ferrier, P., Ceccon, M., Giuriato, S., Gambacorti-Passerini, C., Brousset, P., Lamant, L. & Meggetto, F. (2015) Reversal of microRNA-150 silencing disadvantages crizotinib-resistant NPM-ALK+ cell growth. *The Journal of clinical investigation*, **125,** 3505–18.

Hodgkin, T. (1832) On some Morbid Appearances of the Absorbent Glands and Spleen. *Medico-chirurgical transactions*, **17,** 68–114.

Hollox, E.J. & Armour, J.A.L. (2008) Directional and balancing selection in human beta-defensins. *BMC evolutionary biology*, **8,** 113.

Holmes, R. & Zúñiga-Pflücker, J.C. (2009) The OP9-DL1 System: Generation of T-Lymphocytes from Embryonic or Hematopoietic Stem Cells In Vitro. *Cold Spring Harbor Protocols*, **2009,** 5156.

Hsu, F.Y.-Y., Johnston, P.B., Burke, K.A. & Zhao, Y. (2006) The expression of CD30 in anaplastic large cell lymphoma is regulated by nucleophosmin-anaplastic lymphoma kinase-mediated JunB level in a cell type-specific manner. *Cancer research*, **66,** 9002–8.

Huang, D.W., Sherman, B.T. & Lempicki, R.A. (2009) Systematic and integrative analysis of large gene lists using DAVID bioinformatics resources. *Nature Protocols*, **4,** 44–57.

Huang, K.-L., Mashl, R.J., Wu, Y., Ritter, D.I., Wang, J., Oh, C., Paczkowska, M., Reynolds, S., Wyczalkowski, M.A., Oak, N., Scott, A.D., Krassowski, M., Cherniack, A.D., Houlahan, K.E., Jayasinghe, R., Wang, L.-B., Zhou, D.C., Liu, D., Cao, S., Kim, Y.W., et al (2018) Pathogenic Germline Variants in 10,389 Adult Cancers. *Cell*, **173,** 355–370.

Hudson, S., Wang, D., Middleton, F., Nevaldine, B.H., Naous, R. & Hutchison, R.E. (2018) Crizotinib induces apoptosis and gene expression changes in ALK+ anaplastic large cell lymphoma cell lines; brentuximab synergizes and doxorubicin antagonizes. *Pediatric blood & cancer*, **65,** e27094.

Iso, T., Kedes, L. & Hamamori, Y. (2003) HES and HERP families: multiple effectors of the Notch signaling pathway. *Journal of cellular physiology*, **194,** 237–55.

Iwahara, T., Fujimoto, J., Wen, D., Cupples, R., Bucay, N., Arakawa, T., Mori, S., Ratzkin, B. & Yamamoto, T. (1997) Molecular characterization of ALK, a receptor tyrosine kinase expressed specifically in the nervous system. *Oncogene*, **14,** 439–449.

Jäger, R., Hahne, J., Jacob, A., Egert, A., Schenkel, J., Wernert, N., Schorle, H. & Wellmann, A. Mice transgenic for NPM-ALK develop non-Hodgkin lymphomas. *Anticancer research*, **25,** 3191–6.

Jiang, P.S. & Yung, B.Y. (1999) Down-regulation of nucleophosmin/B23 mRNA delays the entry of cells into mitosis. *Biochemical and biophysical research communications*, **257,** 865–870.

Joung, J., Konermann, S., Gootenberg, J.S., Abudayyeh, O.O., Platt, R.J., Brigham, M.D., Sanjana, N.E. & Zhang, F. (2017) Genome-scale CRISPR-Cas9 knockout and transcriptional activation screening. *Nature protocols*, **12,** 828–863.

Jundt, F., Anagnostopoulos, I., Förster, R., Mathas, S., Stein, H. & Dörken, B. (2002) Activated Notch1 signaling promotes tumor cell proliferation and survival in Hodgkin and anaplastic large cell lymphoma. *Blood*, **99,** 3398–403.

Kampen, K.R., Fancello, L., Girardi, T., Rinaldi, G., Planque, M., Sulima, S.O., Loayza-Puch, F., Verbelen, B., Vereecke, S., Verbeeck, J., Op de Beeck, J., Royaert, J., Vermeersch, P., Cassiman, D., Cools, J., Agami, R., Fiers, M., Fendt, S.-M. & De Keersmaecker, K. (2019) Translatome analysis reveals altered serine and glycine metabolism in T-cell acute lymphoblastic leukemia cells. *Nature communications*, **10,** 2542.

Kamstrup, M.R., Ralfkiaer, E., Skovgaard, G.L. & Gniadecki, R. (2008) Potential involvement of Notch1 signalling in the pathogenesis of primary cutaneous CD30-positive lymphoproliferative disorders. *British Journal of Dermatology*, **158,** 747–753.

Kamstrup, M.R.R., Biskup, E., Gjerdrum, L.M.R., Ralfkiaer, E., Niazi, O. & Gniadecki, R. (2014) The importance of Notch signaling in peripheral T-cell lymphomas. *Leukemia & Lymphoma*, **55,** 639–644.

Kangsamaksin, T., Murtomaki, A., Kofler, N.M., Cuervo, H., Chaudhri, R.A., Tattersall, I.W., Rosenstiel, P.E., Shawber, C.J. & Kitajewski, J. (2015) NOTCH Decoys That Selectively Block DLL/NOTCH or JAG/NOTCH Disrupt Angiogenesis by Unique Mechanisms to Inhibit Tumor Growth. *Cancer Discovery*, **5,** 182–197.

Kawamata, S., Du, C., Li, K. & Lavau, C. (2002) Overexpression of the Notch target genes Hes in vivo induces lymphoid and myeloid alterations. *Oncogene*, **21,** 3855–63.

Kinney, M.C., Collins, R.D., Greer, J.P., Whitlock, J.A., Sioutos, N. & Kadin, M.E. (1993) A small-cell-predominant variant of primary Ki-1 (CD30)+ T-cell lymphoma. *The American journal of surgical pathology*, **17,** 859–68.

Kircher, M., Witten, D.M., Jain, P., O'Roak, B.J., Cooper, G.M. & Shendure, J. (2014) A general framework for estimating the relative pathogenicity of human genetic variants. *Nature genetics*, **46,** 310–5.

Klimka, A., Barth, S., Matthey, B., Roovers, R.C., Lemke, H., Hansen, H., Arends, J.W., Diehl, V., Hoogenboom, H.R. & Engert, A. (1999) An anti-CD30 single-chain Fv selected by phage display and fused to Pseudomonas exotoxin A (Ki-4(scFv)-ETA') is a potent immunotoxin against a Hodgkin-derived cell line. *British journal of cancer*, **80,** 1214–22.

Knörr, F., Weber, S., Singh, V.K., Pulford, K., Reiter, A., Woessmann, W. & Damm-Welk, C. (2018) Epitope mapping of anti-ALK antibodies in children with anaplastic large cell lymphoma. *Clinical immunology*, **195,** 77–81.

Kohsaka, S., Shukla, N., Ameur, N., Ito, T., Ng, C.K.Y., Wang, L., Lim, D., Marchetti, A., Viale, A., Pirun, M., Socci, N.D., Qin, L.-X., Sciot, R., Bridge, J., Singer, S., Meyers, P., Wexler, L.H., Barr, F.G., Dogan, S., Fletcher, J.A., et al (2014) A recurrent neomorphic mutation in MYOD1 defines a clinically aggressive subset of embryonal rhabdomyosarcoma associated with PI3K-AKT pathway mutations. *Nature genetics*, **46,** 595–600.

Konermann, S., Brigham, M.D., Trevino, A.E., Joung, J., Abudayyeh, O.O., Barcena, C., Hsu, P.D., Habib, N., Gootenberg, J.S., Nishimasu, H., Nureki, O. & Zhang, F. (2015) Genome-scale transcriptional activation by an engineered CRISPR-Cas9 complex. *Nature*, **517,** 583–588.

Krc, I., Macák, J., Krcová, V. & Zahálková, J. (1987) Clinicopathological aspects of Richter's syndrome. *Folia haematologica*, **114,** 367–75.

Krebs, L.T., Deftos, M.L., Bevan, M.J. & Gridley, T. (2001) The Nrarp gene encodes an ankyrin-repeat protein that is transcriptionally regulated by the notch signaling pathway. *Developmental biology*, **238,** 110–9.

Kumar, P., Henikoff, S. & Ng, P.C. (2009) Predicting the effects of coding non-synonymous variants on protein function using the SIFT algorithm. *Nature Protocols*, **4,** 1073–1082.

Laimer, D., Dolznig, H., Kollmann, K., Vesely, P.W., Schlederer, M., Merkel, O., Schiefer, A.-I., Hassler, M.R., Heider, S., Amenitsch, L., Thallinger, C., Staber, P.B., Simonitsch-Klupp, I., Artaker, M., Lagger, S., Turner, S.D., Pileri, S., Piccaluga, P.P., Valent, P., Messana, K., et al (2012) PDGFR blockade is a rational and effective therapy for NPM-ALK-driven lymphomas. *Nature medicine*, **18,** 1699–704.

Lakhtakia, R. & Burney, I. (2015a) A Historical Tale of Two Lymphomas: Part I: Hodgkin lymphoma. *Sultan Qaboos University medical journal*, **15,** 202–206.

Lakhtakia, R. & Burney, I. (2015b) A Historical Tale of Two Lymphomas: Part II: Non-Hodgkin lymphoma.

Sultan Qaboos University medical journal, **15,** 317–321.

Lamant, L., Dastugue, N., Pulford, K., Delsol, G., Mariame, B., Mariamé, B. & Mariame, B. (1999) A new fusion gene TPM3-ALK in anaplastic large cell lymphoma created by a (1;2)(q25;p23) translocation. *Blood*, **93,** 3088–95.

Lamant, L., McCarthy, K., D'Amore, E., Klapper, W., Nakagawa, A., Fraga, M., Maldyk, J., Simonitsch-Klupp, I., Oschlies, I., Delsol, G., Mauguen, A., Brugières, L. & Le Deley, M.-C. (2011) Prognostic impact of morphologic and phenotypic features of childhood ALK-positive anaplastic large-cell lymphoma: results of the ALCL99 study. *Journal of Clinical Oncology*, **29,** 4669–76.

Lamant, L., Meggetto, F., al Saati, T., Brugières, L., de Paillerets, B.B., Dastugue, N., Bernheim, A., Rubie, H., Terrier-Lacombe, M.J., Robert, A., Rigal, F., Schlaifer, D., Shiuta, M., Mori, S. & Delsol, G. (1996) High incidence of the t(2;5)(p23;q35) translocation in anaplastic large cell lymphoma and its lack of detection in Hodgkin's disease. Comparison of cytogenetic analysis, reverse transcriptase-polymerase chain reaction, and P-80 immunostaining. *Blood*, **87,** 284–91.

Landrum, M.J., Lee, J.M., Benson, M., Brown, G., Chao, C., Chitipiralla, S., Gu, B., Hart, J., Hoffman, D., Hoover, J., Jang, W., Katz, K., Ovetsky, M., Riley, G., Sethi, A., Tully, R., Villamarin-Salomon, R., Rubinstein, W. & Maglott, D.R. (2016) ClinVar: public archive of interpretations of clinically relevant variants. *Nucleic acids research*, **44,** 862–868.

Larose, H., Burke, G.A.A., Lowe, E.J. & Turner, S.D. (2019) From bench to bedside: the past, present and future of therapy for systemic paediatric ALCL, ALK+. *British Journal of Haematology*, **185,** 1043–1054.

Larose, H., Mian, S., Nuglozeh, E., Feroze, M., Ahmed, E., Ashankyty, I., Du, M.-Q., Hoefler, G., Pospisilova, S., Woessmann, W., Damm-Welk, C., Federova, A., Lamant, L., Schlederer, M., Merkel, O., Kenner, L. & Turner, S. (2018) Abstract 59: Investigating the functional impact of single nucleotide variatns in anaplastic large cell lymphoma. *British Journal of Haematology*, **182,** 41–42.

Lasorsa, V.A., Formicola, D., Pignataro, P., Cimmino, F., Calabrese, F.M., Mora, J., Esposito, M.R., Pantile, M., Zanon, C., De Mariano, M., Longo, L., Hogarty, M.D., de Torres, C., Tonini, G.P., Iolascon, A. & Capasso, M. (2016) Exome and deep sequencing of clinically aggressive neuroblastoma reveal somatic mutations that affect key pathways involved in cancer progression. *Oncotarget*, **7,** 21840–21852.

Laver, J.H., Kraveka, J.M., Hutchison, R.E., Chang, M., Kepner, J., Schwenn, M., Tarbell, N., Desai, S., Weitzman, S., Weinstein, H.J. & Murphy, S.B. (2005) Advanced-Stage Large-Cell Lymphoma in Children and Adolescents: Results of a Randomized Trial Incorporating Intermediate-Dose Methotrexate and High-Dose Cytarabine in the Maintenance Phase of the APO Regimen: A Pediatric Oncology Group Phase III Trial. *Journal of Clinical Oncology*, **23,** 541–547.

Lehal, R., Urech, C., Vigolo, M., Murone, M. & Radtke, F. (2018)Abstract 5799: Characterization and profiling of CB-103, a novel small-molecule protein-protein interaction inhibitor targeting the NOTCH transcription complex. In *Experimental and Molecular Therapeutics* pp 5799–5799. American Association for Cancer Research.

Lek, M., Karczewski, K.J., Minikel, E. V., Samocha, K.E., Banks, E., Fennell, T., O'Donnell-Luria, A.H., Ware, J.S., Hill, A.J., Cummings, B.B., Tukiainen, T., Birnbaum, D.P., Kosmicki, J.A., Duncan, L.E., Estrada, K., Zhao, F., Zou, J., Pierce-Hoffman, E., Berghout, J., Cooper, D.N., et al (2016) Analysis of protein-coding genetic variation in 60,706 humans. *Nature*, **536,** 285–291.

Letunic, I. & Bork, P. (2018) 20 years of the SMART protein domain annotation resource. *Nucleic acids research*, **46,** 493–496.

Leventaki, V., Drakos, E., Medeiros, L.J., Lim, M.S., Elenitoba-Johnson, K.S., Claret, F.X. & Rassidakis, G.Z. (2007) NPM-ALK oncogenic kinase promotes cell-cycle progression through activation of

JNK/cJun signaling in anaplastic large-cell lymphoma. *Blood*, **110,** 1621–30.

Li, H. & Durbin, R. (2009) Fast and accurate short read alignment with Burrows-Wheeler transform. *Bioinformatics*, **25,** 1754–60.

Li, H., Handsaker, B., Wysoker, A., Fennell, T., Ruan, J., Homer, N., Marth, G., Abecasis, G., Durbin, R. & 1000 Genome Project Data Processing Subgroup (2009) The Sequence Alignment/Map format and SAMtools. *Bioinformatics*, **25,** 2078–9.

Li, H., Lee, J., He, C., Zou, M.-H. & Xie, Z. (2014) Suppression of the mTORC1/STAT3/Notch1 pathway by activated AMPK prevents hepatic insulin resistance induced by excess amino acids. *American Journal of Physiology-Endocrinology and Metabolism*, **306,** 197–209.

Li, K., Li, Y., Wu, W., Gordon, W.R., Chang, D.W., Lu, M., Scoggin, S., Fu, T., Vien, L., Histen, G., Zheng, J., Martin-Hollister, R., Duensing, T., Singh, S., Blacklow, S.C., Yao, Z., Aster, J.C. & Zhou, B.-B.S. (2008) Modulation of Notch signaling by antibodies specific for the extracellular negative regulatory region of NOTCH3. *The Journal of biological chemistry*, **283,** 8046–54.

Liang, H., Prutsch, N., Gurnhofer, E., Timelthaler, G., Eferl, R., Tangermann, S., Horvath, J., Stoiber, D., Mathas, S., Kenner, L. & Merkel, O. (2018) Abstract 63: The AP-1 –BATF and –BATF3 module: divergent roles in tumour growth, invasion and angiogenesis in anaplastic large cell lymphoma. *British Journal of Haematology*, **182,** 43.

Liang, X., Meech, S.J., Odom, L.F., Bitter, M.A., Ryder, J.W., Hunger, S.P., Lovell, M.A., Meltesen, L., Wei, Q., Williams, S.A., Hutchinson, R.N. & McGavran, L. (2004) Assessment of t(2;5)(p23;q35) Translocation and Variants in Pediatric ALK+ Anaplastic Large Cell Lymphoma. *American Journal of Clinical Pathology*, **121,** 496–506.

Lim, M.J. & Wang, X.W. (2006) Nucleophosmin and human cancer. *Cancer Detection and Prevention*, **30,** 481–490.

Ljungström, V., Cortese, D., Young, E., Pandzic, T., Mansouri, L., Plevova, K., Ntoufa, S., Baliakas, P., Clifford, R., Sutton, L.-A., Blakemore, S.J., Stavroyianni, N., Agathangelidis, A., Rossi, D., Höglund, M., Kotaskova, J., Juliusson, G., Belessi, C., Chiorazzi, N., Panagiotidis, P., et al (2016) Whole-exome sequencing in relapsing chronic lymphocytic leukemia: clinical impact of recurrent RPS15 mutations. *Blood*, **127,** 1007–16.

Locatelli, F., Mauz-Koerholz, C., Neville, K., Llort, A., Beishuizen, A., Daw, S., Pillon, M., Aladjidi, N., Klingebiel, T., Landman-Parker, J., Medina-Sanson, A., August, K., Sachs, J., Hoffman, K., Kinley, J., Song, S., Song, G., Zhang, S., Suri, A. & Gore, L. (2018) Brentuximab vedotin for paediatric relapsed or refractory Hodgkin's lymphoma and anaplastic large-cell lymphoma: a multicentre, open-label, phase 1/2 study. *The Lancet. Haematology*, **5,** 450–461.

Lollies, A., Hartmann, S., Schneider, M., Bracht, T., Weiß, A.L., Arnolds, J., Klein-Hitpass, L., Sitek, B., Hansmann, M.-L., Küppers, R. & Weniger, M.A. (2018) An oncogenic axis of STAT-mediated BATF3 upregulation causing MYC activity in classical Hodgkin lymphoma and anaplastic large cell lymphoma. *Leukemia*, **32,** 92–101.

Lovisa, F., Gaffo, E., Bortoluzzi, S., Garbin, A., Di Battista, P., Carraro, E., Faruggia, P., Sala, A., Piglione, M., Vinti, L., D'Amore, E., Basso, G., Pillon, M. & Mussolin, L. (2018) Abstract 39: Comprehensive characterization of plasma-derived exosomes in anaplastic large cell lymphoma of childhood. *British Journal of Haematology*, **182,** 29.

Lowe, E. (2018) Abstract 49: Novel targets and outcome in anaplastic large cell lymphoma. *British Journal of Haematology*, **182,** 35.

Lowe, E.J. & Lim, M.S. (2013) Potential therapies for anaplastic lymphoma kinase-driven tumors in children: progress to date. *Paediatric drugs*, **15,** 163–9.

Lowe, E.J., Sposto, R., Perkins, S.L., Gross, T.G., Finlay, J., Zwick, D., Abromowitch, M. & Children's Cancer Group Study 5941 (2009) Intensive chemotherapy for systemic anaplastic large cell lymphoma in children and adolescents: final results of Children's Cancer Group Study 5941. *Pediatric blood & cancer*, **52,** 335–9.

Lubman, O.Y., Ilagan, M.X.G., Kopan, R. & Barrick, D. (2007) Quantitative dissection of the Notch:CSL interaction: insights into the Notch-mediated transcriptional switch. *Journal of molecular biology*, **365,** 577–89.

Luca, V.C., Kim, B.C., Ge, C., Kakuda, S., Wu, D., Roein-Peikar, M., Haltiwanger, R.S., Zhu, C., Ha, T. & Garcia, K.C. (2017) Notch-Jagged complex structure implicates a catch bond in tuning ligand sensitivity. *Science*, **355,** 1320–1324.

Ma, X., Liu, Y.Y., Liu, Y.Y., Alexandrov, L.B., Edmonson, M.N., Gawad, C., Zhou, X., Li, Y., Rusch, M.C., John, E., Huether, R., Gonzalez-Pena, V., Wilkinson, M.R., Hermida, L.C., Davis, S., Sioson, E., Pounds, S., Cao, X., Ries, R.E., Wang, Z., et al (2018) Pan-cancer genome and transcriptome analyses of 1,699 paediatric leukaemias and solid tumours. *Nature*, **555,** 371–376.

Malcolm, T.I.M., Villarese, P., Fairbairn, C.J., Lamant, L., Trinquand, A., Hook, C.E., Burke, G.A.A.A., Brugières, L., Hughes, K., Payet, D., Merkel, O., Schiefer, A.-I., Ashankyty, I., Mian, S., Wasik, M., Turner, M., Kenner, L., Asnafi, V., Macintyre, E. & Turner, S.D. (2016) Anaplastic large cell lymphoma arises in thymocytes and requires transient TCR expression for thymic egress. *Nature Communications*, **7,** 10087.

Malpighi, M. (1666) De Viscerum Structura Exercitatio Anatomica. *in. J. Montij, Bononiae***,** 125–156.

Martin, D., Abba, M.C., Molinolo, A.A., Vitale-Cross, L., Wang, Z., Zaida, M., Delic, N.C., Samuels, Y., Lyons, J.G. & Gutkind, J.S. (2014) The head and neck cancer cell oncogenome: a platform for the development of precision molecular therapies. *Oncotarget*, **5,** 8906–23.

Marzec, M., Kasprzycka, M., Liu, X., Raghunath, P.N., Wlodarski, P. & Wasik, M.A. (2007) Oncogenic tyrosine kinase NPM/ALK induces activation of the MEK/ERK signaling pathway independently of c-Raf. *Oncogene*, **26,** 813–21.

Marzec, M., Zhang, Q., Goradia, A., Raghunath, P.N., Liu, X., Paessler, M., Wang, H.Y., Wysocka, M., Cheng, M., Ruggeri, B.A. & Wasik, M.A. (2008) Oncogenic kinase NPM/ALK induces through STAT3 expression of immunosuppressive protein CD274 (PD-L1, B7-H1). *Proceedings of the National Academy of Sciences*, **105,** 20852–7.

Masiero, M., Li, D., Whiteman, P., Bentley, C., Greig, J., Hassanali, T., Watts, S., Stribbling, S., Yates, J., Bealing, E., Li, J.-L., Chillakuri, C., Sheppard, D., Serres, S., Sarmiento-Soto, M., Larkin, J., Sibson, N.R., Handford, P.A., Harris, A.L. & Banham, A.H. (2019) Development of therapeutic anti-JAGGED1 antibodies for cancer therapy. *Molecular cancer therapeutics*.

Mason, C.C., Khorashad, J.S., Tantravahi, S.K., Kelley, T.W., Zabriskie, M.S., Yan, D., Pomicter, A.D., Reynolds, K.R., Eiring, A.M., Kronenberg, Z., Sherman, R.L., Tyner, J.W., Dalley, B.K., Dao, K.-H., Yandell, M., Druker, B.J., Gotlib, J., O'Hare, T. & Deininger, M.W. (2016) Age-related mutations and chronic myelomonocytic leukemia. *Leukemia*, **30,** 906–13.

Mason, D.Y., Pulford, K.A., Bischof, D., Kuefer, M.U., Butler, L.H., Lamant, L., Delsol, G. & Morris, S.W. (1998) Nucleolar localization of the nucleophosmin-anaplastic lymphoma kinase is not required for malignant transformation. *Cancer research*, **58,** 1057–62.

McKenna, A., Hanna, M., Banks, E., Sivachenko, A., Cibulskis, K., Kernytsky, A., Garimella, K., Altshuler, D., Gabriel, S., Daly, M. & DePristo, M.A. (2010) The Genome Analysis Toolkit: a MapReduce framework for analyzing next-generation DNA sequencing data. *Genome research*, **20,** 1297–303.

Menotti, M., Ambrogio, C., Cheong, T.-C., Pighi, C., Mota, I., Cassel, S.H., Compagno, M., Wang, Q., Dall'Olio, R., Minero, V.G., Poggio, T., Sharma, G.G., Patrucco, E., Mastini, C., Choudhari, R., Pich,

A., Zamo, A., Piva, R., Giliani, S., Mologni, L., et al (2019) Wiskott-Aldrich syndrome protein (WASP) is a tumor suppressor in T cell lymphoma. *Nature medicine*, **25,** 130–140.

Merkel, O., Hamacher, F., Griessl, R., Grabner, L., Schiefer, A.-I., Prutsch, N., Baer, C., Egger, G., Schlederer, M., Krenn, P.W., Hartmann, T.N., Simonitsch-Klupp, I., Plass, C., Staber, P.B., Moriggl, R., Turner, S.D., Greil, R. & Kenner, L. (2015) Oncogenic role of miR-155 in anaplastic large cell lymphoma lacking the t(2;5) translocation. *The Journal of pathology*, **236,** 445–56.

Merkel, O., Hamacher, F., Laimer, D., Sifft, E., Trajanoski, Z., Scheideler, M., Egger, G., Hassler, M.R., Thallinger, C., Schmatz, A., Turner, S.D., Greil, R. & Kenner, L. (2010) Identification of differential and functionally active miRNAs in both anaplastic lymphoma kinase (ALK)+ and ALK- anaplastic large-cell lymphoma. *Proceedings of the National Academy of Sciences*, **107,** 16228–33.

Messersmith, W.A., Shapiro, G.I., Cleary, J.M., Jimeno, A., Dasari, A., Huang, B., Shaik, M.N., Cesari, R., Zheng, X., Reynolds, J.M., English, P.A., McLachlan, K.R., Kern, K.A. & LoRusso, P.M. (2015) A phase I, dose-finding study in patients with advanced solid malignancies of the oral γ-secretase inhibitor PF-03084014. *Clinical Cancer Research*, **21,** 60–67.

Meurette, O. & Mehlen, P. (2018) Notch Signaling in the Tumor Microenvironment. *Cancer Cell*, **34,** 536–548.

Mi, H., Huang, X., Muruganujan, A., Tang, H., Mills, C., Kang, D. & Thomas, P.D. (2017) PANTHER version 11: Expanded annotation data from Gene Ontology and Reactome pathways, and data analysis tool enhancements. *Nucleic Acids Research*, **45,** 183–189.

Michaelson, M.D., Gupta, S., Agarwal, N., Szmulewitz, R., Powles, T., Pili, R., Bruce, J.Y., Vaishampayan, U., Larkin, J., Rosbrook, B., Wang, E., Murphy, D., Wang, P., Lechuga, M.J., Valota, O. & Shepard, D.R. (2019) A Phase Ib Study of Axitinib in Combination with Crizotinib in Patients with Metastatic Renal Cell Cancer or Other Advanced Solid Tumors. *The Oncologist*, **24,** 1151.

Minard-Colin, V., Brugières, L., Reiter, A., Cairo, M.S., Gross, T.G., Woessmann, W., Burkhardt, B., Sandlund, J.T., Williams, D., Pillon, M., Horibe, K., Auperin, A., Le Deley, M.-C., Zimmerman, M., Perkins, S.L., Raphael, M., Lamant, L., Klapper, W., Mussolin, L., Poirel, H.A., et al (2015) Non-Hodgkin Lymphoma in Children and Adolescents: Progress Through Effective Collaboration, Current Knowledge, and Challenges Ahead. *Journal of Clinical Oncology*, **33,** 2963–74.

Minervini, A., Francesco Minervini, C., Anelli, L., Zagaria, A., Casieri, P., Coccaro, N., Cumbo, C., Tota, G., Impera, L., Orsini, P., Brunetti, C., Giordano, A., Specchia, G. & Albano, F. (2016) Droplet digital PCR analysis of NOTCH1 gene mutations in chronic lymphocytic leukemia. *Oncotarget*, **7,** 86469–86479.

del Mistro, A., Leszl, A., Bertorelle, R., Calabro, M.L., Panozzo, M., Menin, C., D'Andrea, E. & Chieco-Bianchi, L. (1994) A CD30-positive T cell line established from an aggressive anaplastic large cell lymphoma, originally diagnosed as Hodgkin's disease. *Leukemia*, **8,** 1214–9.

Mitchell, A.L., Attwood, T.K., Babbitt, P.C., Blum, M., Bork, P., Bridge, A., Brown, S.D., Chang, H.-Y., El-Gebali, S., Fraser, M.I., Gough, J., Haft, D.R., Huang, H., Letunic, I., Lopez, R., Luciani, A., Madeira, F., Marchler-Bauer, A., Mi, H., Natale, D.A., et al (2019) InterPro in 2019: improving coverage, classification and access to protein sequence annotations. *Nucleic acids research*, **47,** 351–360.

Morgan, R., Smith, S.D., Hecht, B.K., Christy, V., Mellentin, J.D., Warnke, R. & Cleary, M.L. (1989) Lack of involvement of the c-fms and N-myc genes by chromosomal translocation t(2;5)(p23;q35) common to malignancies with features of so-called malignant histiocytosis. *Blood*, **73,** 2155–64.

Morgan, T.H.T. (1917) The Theory of the Gene. *The American Naturalist*, **51,** 513–544.

Mori, T., Fukano, R., Saito, A., Takimoto, T., Sekimizu, M., Nakazawa, A., Tsurusawa, M., Kobayashi, R., Horibe, K. & Japanese Pediatric Leukemia/Lymphoma Study Group (2014) Analysis of Japanese registration from the randomized international trial for childhood anaplastic large cell lymphoma

(ALCL99-R1). *[Rinsho ketsueki] The Japanese journal of clinical hematology*, **55,** 526–33.

Morris, S.W., Kirstein, M.N., Valentine, M.B., Dittmer, K.G., Shapiro, D.N., Saltman, D.L. & Look, a T. (1994) Fusion of a kinase gene, ALK, to a nucleolar protein gene, NPM, in non-Hodgkin's lymphoma. *Science*, **263,** 1281–4.

Mossé, Y.P., Voss, S.D., Lim, M.S., Rolland, D., Minard, C.G., Fox, E., Adamson, P., Wilner, K., Blaney, S.M. & Weigel, B.J. (2017) Targeting ALK With Crizotinib in Pediatric Anaplastic Large Cell Lymphoma and Inflammatory Myofibroblastic Tumor: A Children's Oncology Group Study. *Journal of Clinical Oncology*, **35,** 3215–3221.

Mumm, J.S., Schroeter, E.H., Saxena, M.T., Griesemer, A., Tian, X., Pan, D.J., Ray, W.J. & Kopan, R. (2000) A ligand-induced extracellular cleavage regulates gamma-secretase-like proteolytic activation of Notch1. *Molecular cell*, **5,** 197–206.

Mussolin, L., Damm-Welk, C., Pillon, M., Zimmermann, M., Franceschetto, G., Pulford, K., Reiter, a, Rosolen, a & Woessmann, W. (2013) Use of minimal disseminated disease and immunity to NPM-ALK antigen to stratify ALK-positive ALCL patients with different prognosis. *Leukemia*, **27,** 416–22.

Mussolin, L., Pillon, M., D'Amore, E.S., Santoro, N., Lombardi, A., Fagioli, F., Zanesco, L. & Rosolen, A. (2005) Prevalence and clinical implications of bone marrow involvement in pediatric anaplastic large cell lymphoma. *Leukemia*, **19,** 1643–7.

Mutvei, A.P., Fredlund, E. & Lendahl, U. (2015) Frequency and distribution of Notch mutations in tumor cell lines. *BMC Cancer*, **15,** 311.

Neumann, M., Vosberg, S., Schlee, C., Heesch, S., Schwartz, S., Gökbuget, N., Hoelzer, D., Graf, A., Krebs, S., Bartram, I., Blum, H., Brüggemann, M., Hecht, J., Bohlander, S.K., Greif, P.A. & Baldus, C.D. (2015) Mutational spectrum of adult T-ALL. *Oncotarget*, **6,** 2754–66.

News of Science (1957) *Science*, **125,** 18–22.

Nieborowska-Skorska, M., Slupianek, A., Xue, L., Zhang, Q., Raghunath, P.N., Hoser, G., Wasik, M.A., Morris, S.W. & Skorski, T. (2001) Role of signal transducer and activator of transcription 5 in nucleophosmin/ anaplastic lymphoma kinase-mediated malignant transformation of lymphoid cells. *Cancer Res*, **61,** 6517–6523.

Nishikori, M., Maesako, Y., Ueda, C., Kurata, M., Uchiyama, T. & Ohno, H. (2003) High-level expression of BCL3 differentiates t(2;5)(p23;q35)-positive anaplastic large cell lymphoma from Hodgkin disease. *Blood*, **101,** 2789–96.

Noma, A., Kirino, Y., Ikeuchi, Y. & Suzuki, T. (2006) Biosynthesis of wybutosine, a hyper-modified nucleoside in eukaryotic phenylalanine tRNA. *The EMBO journal*, **25,** 2142–54.

Nowell, C.S. & Radtke, F. (2017) Notch as a tumour suppressor. *Nature Reviews Cancer*, **17,** 145–159.

Oeffinger, K.C., Mertens, A.C., Sklar, C.A., Kawashima, T., Hudson, M.M., Meadows, A.T., Friedman, D.L., Marina, N., Hobbie, W., Kadan-Lottick, N.S., Schwartz, C.L., Leisenring, W., Robison, L.L. & Childhood Cancer Survivor Study (2006) Chronic health conditions in adult survivors of childhood cancer. *The New England journal of medicine*, **355,** 1572–82.

Oh, S.Y., Chen, C.-D. & Abraham, C.R. (2010) Cell-type dependent modulation of Notch signaling by the amyloid precursor protein. *Journal of neurochemistry*, **113,** 262–74.

Osborne, B.A. & Minter, L.M. (2007) Notch signalling during peripheral T-cell activation and differentiation. *Nature Reviews Immunology*, **7,** 64–75.

Pakkiriswami, S., Couto, A., Nagarajan, U. & Georgiou, M. (2016) Glycosylated Notch and Cancer. *Frontiers in Oncology*, **6,** 37.

Pallesen, G. & Hamilton-Dutoit, S.J. (1988) Ki-1 (CD30) antigen is regularly expressed by tumor cells of embryonal carcinoma. *The American journal of pathology*, **133,** 446–50.

Pandurangan, A.P., Ochoa-Montaño, B., Ascher, D.B. & Blundell, T.L. (2017) SDM: a server for predicting effects of mutations on protein stability. *Nucleic acids research*, **45,** 229–235.

Papayannidis, C., DeAngelo, D.J., Stock, W., Huang, B., Shaik, M.N., Cesari, R., Zheng, X., Reynolds, J.M., English, P.A., Ozeck, M., Aster, J.C., Kuo, F., Huang, D., Lira, P.D., McLachlan, K.R., Kern, K.A., Garcia-Manero, G. & Martinelli, G. (2015) A Phase 1 study of the novel gamma-secretase inhibitor PF-03084014 in patients with T-cell acute lymphoblastic leukemia and T-cell lymphoblastic lymphoma. *Blood Cancer Journal*, **5,** 350.

Pasqualucci, L., Flenghi, L., Terenzi, A., Bolognesi, A., Stirpe, F., Bigerna, B. & Falini, B. Immunotoxin therapy of hematological malignancies. *Haematologica*, **80,** 546–56.

Pattanayak, V., Lin, S., Guilinger, J.P., Ma, E., Doudna, J.A. & Liu, D.R. (2013) High-throughput profiling of off-target DNA cleavage reveals RNA-programmed Cas9 nuclease specificity. *Nature biotechnology*, **31,** 839–43.

Pearson, A.D.J., Herold, R., Rousseau, R., Copland, C., Bradley-Garelik, B., Binner, D., Capdeville, R., Caron, H., Carleer, J., Chesler, L., Geoerger, B., Kearns, P., Marshall, L. V, Pfister, S.M., Schleiermacher, G., Skolnik, J., Spadoni, C., Sterba, J., van den Berg, H., Uttenreuther-Fischer, M., et al (2016) Implementation of mechanism of action biology-driven early drug development for children with cancer. *European Journal of Cancer*, **62,** 124–31.

Perez Garcia, J.M., Cortés, J., Stathis, A., Mous, R., López-Miranda, E., Azaro, A., Genta, S., Nuciforo, P., Vivancos, A., Ferrarotto, R., Bertoni, F., Rossi, D., Spardy Burr, N., Schönborn-Kellenberger, O., Jorga, K., Beni, L., Lehal, R., Bauer, M., Weber, D. & Garralda, E. (2018) First-in-human phase 1-2A study of CB-103, an oral Protein-Protein Interaction Inhibitor targeting pan-NOTCH signalling in advanced solid tumors and blood malignancies. *Journal of Clinical Oncology*, **36,** TPS2619–TPS2619.

Peters, M. V. (1950) A study of Survivals in Hodgkin's Disease treated Radiologically. *American Journal of Roentgenology and Radium Therapy*, **63,** 299–311.

Petit, A., St George-Hyslop, P., Fraser, P. & Checler, F. (2002) Gamma-secretase-like cleavages of Notch and beta APP are mutually exclusive in human cells. *Biochemical and biophysical research communications*, **290,** 1408–10.

Piazza, R., Magistroni, V., Mogavero, A., Andreoni, F., Ambrogio, C., Chiarle, R., Mologni, L., Bachmann, P.S., Lock, R.B., Collini, P., Pelosi, G. & Gambacorti-Passerini, C. (2013) Epigenetic silencing of the proapoptotic gene BIM in anaplastic large cell lymphoma through an MeCP2/SIN3a deacetylating complex. *Neoplasia*, **15,** 511–22.

Pileri, S., Falini, B., Delsol, G., Stein, H., Baglioni, P., Poggi, S., Martelli, M., Rivano, M., Mason, D. & Stansfeld, A. (1990) Lymphohistiocytic T-cell lymphoma (anaplastic large cell lymphoma CD30+/Ki-1 + with a high content of reactive histiocytes). *Histopathology*, **16,** 383–91.

Pires, D.E. V, Ascher, D.B. & Blundell, T.L. (2014) mCSM: predicting the effects of mutations in proteins using graph-based signatures. *Bioinformatics*, **30,** 335–42.

Piva, R., Chiarle, R., Manazza, A.D., Taulli, R., Simmons, W., Ambrogio, C., D'Escamard, V., Pellegrino, E., Ponzetto, C., Palestro, G. & Inghirami, G. (2006) Ablation of oncogenic ALK is a viable therapeutic approach for anaplastic large-cell lymphomas. *Blood*, **107,** 689–97.

Prokoph, N., Larose, H., Lim, M., Burke, G. & Turner, S. (2018) Treatment Options for Paediatric Anaplastic Large Cell Lymphoma (ALCL): Current Standard and beyond. *Cancers*, **10,** 99.

Pui, J.C., Allman, D., Xu, L., DeRocco, S., Karnell, F.G., Bakkour, S., Lee, J.Y., Kadesch, T., Hardy, R.R.,

Aster, J.C. & Pear, W.S. (1999) Notch1 expression in early lymphopoiesis influences B versus T lineage determination. *Immunity*, **11,** 299–308.

Pulford, K., Lamant, L., Morris, S.W., Butler, L.H., Wood, K.M., Stroud, D., Delsol, G. & Mason, D.Y. (1997) Detection of anaplastic lymphoma kinase (ALK) and nucleolar protein nucleophosmin (NPM)-ALK proteins in normal and neoplastic cells with the monoclonal antibody ALK1. *Blood*, **89,** 1394–404.

Pusey, W.A. (1902) Cases of Sarcoma and Hodgkin's disease treated by exposures to X-rays - a preliminary report. *Journal of the American Medical Association*, **38,** 166.

Radtke, F., MacDonald, H.R. & Tacchini-Cottier, F. (2013) Regulation of innate and adaptive immunity by Notch. *Nature Reviews Immunology*, **13,** 427–437.

Raimondi, S.C., Pui, C.H., Behm, F.G. & Williams, D.L. (1987) 7q32-q36 translocations in childhood T cell leukemia: cytogenetic evidence for involvement of the T cell receptor beta-chain gene. *Blood*, **69,** 131–4.

Ramensky, V., Bork, P. & Sunyaev, S. (2002) Human non-synonymous SNPs: server and survey. *Nucleic acids research*, **30,** 3894–900.

Rand, M.D., Grimm, L.M., Artavanis-Tsakonas, S., Patriub, V., Blacklow, S.C., Sklar, J. & Aster, J.C. (2000) Calcium Depletion Dissociates and Activates Heterodimeric Notch Receptors. *Molecular and Cellular Biology*, **20,** 1825–1835.

Rangarajan, A., Talora, C., Okuyama, R., Nicolas, M., Mammucari, C., Oh, H., Aster, J.C., Krishna, S., Metzger, D., Chambon, P., Miele, L., Aguet, M., Radtke, F. & Dotto, G.P. (2001) Notch signaling is a direct determinant of keratinocyte growth arrest and entry into differentiation. *The EMBO journal*, **20,** 3427–36.

Rassidakis, G.Z., Feretzaki, M., Atwell, C., Grammatikakis, I., Lin, Q., Lai, R., Claret, F., Medeiros, L.J. & Amin, H.M. (2005) Inhibition of Akt increases p27Kip1 levels and induces cell cycle arrest in anaplastic large cell lymphoma. *Blood*, **105,** 827–9.

Raya, A., Kawakami, Y., Rodríguez-Esteban, C., Ibañes, M., Rasskin-Gutman, D., Rodríguez-León, J., Büscher, D., Feijó, J.A. & Izpisúa Belmonte, J.C. (2004) Notch activity acts as a sensor for extracellular calcium during vertebrate left-right determination. *Nature*, **427,** 121–8.

Rebay, I., Fleming, R.J., Fehon, R.G., Cherbas, L., Cherbas, P. & Artavanis-Tsakonas, S. (1991) Specific EGF repeats of Notch mediate interactions with Delta and serrate: Implications for notch as a multifunctional receptor. *Cell*, **67,** 687–699.

Reed Mendenhall, D. (1902) On the pathological changes in Hodgkin's disease, with special reference to its relation to tuberculosis. *Johns Hopkins Hosp Rep*, **10,** 133–196.

Reizis, B. & Leder, P. (2002) Direct induction of T lymphocyte-specific gene expression by the mammalian Notch signaling pathway. *Genes & development*, **16,** 295–300.

Reva, B., Antipin, Y. & Sander, C. (2011) Predicting the functional impact of protein mutations: application to cancer genomics. *Nucleic Acids Research*, **39,** 118.

Rigaud, C., Abbou, S., Minard-Colin, V., Geoerger, B., Scoazec, J.Y., Vassal, G., Jaff, N., Heuberger, L., Valteau-Couanet, D. & Brugieres, L. (2018) Efficacy of nivolumab in a patient with systemic refractory ALK+ anaplastic large cell lymphoma. *Pediatric blood & cancer*, **65,** 607–608.

Rimokh, R., Magaud, J.P., Berger, F., Samarut, J., Coiffier, B., Germain, D. & Mason, D.Y. (1989) A translocation involving a specific breakpoint (q35) on chromosome 5 is characteristic of anaplastic large cell lymphoma ('Ki-1 lymphoma'). *British journal of haematology*, **71,** 31–6.

Rodrigues, C.H., Pires, D.E. & Ascher, D.B. (2018) DynaMut: predicting the impact of mutations on

protein conformation, flexibility and stability. *Nucleic Acids Research*, **46,** 350–355.

Rolland, D., Prokoph, N., Yu, R., Lowe, E., Sandlund, J., Perkins, S., Pillai, V., Reilly, A., Bollard, C., Turner, S. & Lim, M. (2018) Abstract 143: MDD/MRD and anti-ALK autoantibody titer in patients with ALK+ ALCL: a Children's Oncology Group (COG) study ANHL12P1. *British Journal of Haematology*, **182,** 88.

Röntgen, W. (1896) On a New Kind of Rays. *Nature*, **53,** 274–276.

Rosenberg, S.A. & Kaplan, H.S. (1975) The management of stages I, II, and III Hodgkin's disease with combined radiotherapy and chemotherapy. *Cancer*, **35,** 55–63.

Rosenthal, R., McGranahan, N., Herrero, J., Taylor, B.S. & Swanton, C. (2016) deconstructSigs: delineating mutational processes in single tumors distinguishes DNA repair deficiencies and patterns of carcinoma evolution. *Genome Biology*, **17,** 31.

Rosenwald, A., Ott, G., Pulford, K., Katzenberger, T., Kühl, J., Kalla, J., Ott, M.M., Mason, D.Y. & Müller-Hermelink, H.K. (1999) t(1;2)(q21;p23) and t(2;3)(p23;q21): two novel variant translocations of the t(2;5)(p23;q35) in anaplastic large cell lymphoma. *Blood*, **94,** 362–4.

Ruf, S., Brugieres, L., Pillon, M., Zimmermann, M., Attarbaschi, A., Mellgren, K., Williams, D., Uyttebroeck, A., Wrobel, G., Reither, A. & Woessmann, W. (2015) Abstract 78: Risk-adapted therapy for patients with relapsed or refractory ALCL – final report of the prospective ALCL-relapse trial of the EICNHL. *British Journal of Haematology*, **171,** 45.

Rust, R., Visser, L., Leij, J., Harms, G., Blokzijl, T., Deloulme, J.C., Vlies, P., Kamps, W., Kok, K., Lim, M., Poppema, S. & Berg, A. (2005) High expression of calcium-binding proteins, S100A10, S100A11 and CALM2 in anaplastic large cell lymphoma. *British Journal of Haematology*, **131,** 596–608.

Salaverria, I., Beà, S., Lopez-Guillermo, A., Lespinet, V., Pinyol, M., Burkhardt, B., Lamant, L., Zettl, A., Horsman, D., Gascoyne, R., Ott, G., Siebert, R., Delsol, G. & Campo, E. (2008) Genomic profiling reveals different genetic aberrations in systemic ALK-positive and ALK-negative anaplastic large cell lymphomas. *British journal of haematology*, **140,** 516–26.

Samon, J.B., Castillo-Martin, M., Hadler, M., Ambesi-Impiobato, A., Paietta, E., Racevskis, J., Wiernik, P.H., Rowe, J.M., Jakubczak, J., Randolph, S., Cordon-Cardo, C. & Ferrando, A.A. (2012) Preclinical analysis of the γ-secretase inhibitor PF-03084014 in combination with glucocorticoids in T-cell acute lymphoblastic leukemia. *Molecular cancer therapeutics*, **11,** 1565–75.

San Lucas, F.A., Wang, G., Scheet, P. & Peng, B. (2012) Integrated annotation and analysis of genetic variants from next-generation sequencing studies with variant tools. *Bioinformatics*, **28,** 421–422.

Sanchez-Martin, M., Ambesi-Impiombato, A., Qin, Y., Herranz, D., Bansal, M., Girardi, T., Paietta, E., Tallman, M.S., Rowe, J.M., De Keersmaecker, K., Califano, A. & Ferrando, A.A. (2017) Synergistic antileukemic therapies in NOTCH1-induced T-ALL. *Proceedings of the National Academy of Sciences*, **114,** 2006–2011.

Santoro, A., Bonadonna, G., Valagussa, P., Zucali, R., Viviani, S., Villani, F., Pagnoni, A.M., Bonfante, V., Musumeci, R. & Crippa, F. (1987) Long-term results of combined chemotherapy-radiotherapy approach in Hodgkin's disease: superiority of ABVD plus radiotherapy versus MOPP plus radiotherapy. *Journal of Clinical Oncology*, **5,** 27–37.

Schirrmann, T., Steinwand, M., Wezler, X., ten Haaf, A., Tur, M.K. & Barth, S. (2014) CD30 as a Therapeutic Target for Lymphoma. *BioDrugs*, **28,** 181–209.

Schneider, M., Kumar, V., Nordstrøm, L.U., Feng, L., Takeuchi, H., Hao, H., Luca, V.C., Garcia, K.C., Stanley, P., Wu, P. & Haltiwanger, R.S. (2018) Inhibition of Delta-induced Notch signaling using fucose analogs. *Nature Chemical Biology*, **14,** 65–71.

Schneider, U., Schwenk, H.-U. & Bornkamm, G. (1977) Characterization of EBV-genome negative "null" and "T" cell lines derived from children with acute lymphoblastic leukemia and leukemic transformed non-Hodgkin lymphoma. *International Journal of Cancer*, **19,** 621–626.

Schnell, R., Dietlein, M., Staak, J.O., Borchmann, P., Schomaecker, K., Fischer, T., Eschner, W., Hansen, H., Morschhauser, F., Schicha, H., Diehl, V., Raubitschek, A. & Engert, A. (2005) Treatment of refractory Hodgkin's lymphoma patients with an iodine-131-labeled murine anti-CD30 monoclonal antibody. *Journal of Clinical Oncology*, **23,** 4669–78.

Schwab, U., Stein, H., Gerdes, J., Lemke, H., Kirchner, H., Schaadt, M. & Diehl, V. (1982) Production of a monoclonal antibody specific for Hodgkin and Sternberg-Reed cells of Hodgkin's disease and a subset of normal lymphoid cells. *Nature*, **299,** 65–7.

Schwarz, J.M., Cooper, D.N., Schuelke, M. & Seelow, D. (2014) Mutationtaster2: Mutation prediction for the deep-sequencing age. *Nature Methods*, **11,** 361–362.

Seidemann, K., Tiemann, M., Schrappe, M., Yakisan, E., Simonitsch, I., Janka-Schaub, G., Dörffel, W., Zimmermann, M., Mann, G., Gadner, H., Parwaresch, R., Riehm, H. & Reiter, A. (2001) Short-pulse B-non-Hodgkin lymphoma-type chemotherapy is efficacious treatment for pediatric anaplastic large cell lymphoma: a report of the Berlin-Frankfurt-Münster Group Trial NHL-BFM 90. *Blood*, **97,** 3699–706.

Sekimizu, M., Iguchi, A., Mori, T., Koga, Y., Kada, A., Saito, A.M. & Horibe, K. (2018) Phase I clinical study of brentuximab vedotin (SGN-35) involving children with recurrent or refractory CD30-positive Hodgkin's lymphoma or systemic anaplastic large cell lymphoma: rationale, design and methods of BV-HLALCL study: study protocol. *BMC Cancer*, **18,** 122.

Selkoe, D.J. & Wolfe, M.S. (2007) Presenilin: running with scissors in the membrane. *Cell*, **131,** 215–21.

Serrano-Novillo, C., Capera, J., Colomer-Molera, M., Condom, E., Ferreres, J. & Felipe, A. (2019) Implication of Voltage-Gated Potassium Channels in Neoplastic Cell Proliferation. *Cancers*, **11,** 287.

Sharma, G., Mota, I., Mologni, L., Patrucco, E., Gambacorti-Passerini, C. & Chiarle, R. (2018) Tumor Resistance against ALK Targeted Therapy-Where It Comes From and Where It Goes. *Cancers*, **10,** 62.

Sharma, V.M., Draheim, K.M. & Kelliher, M.A. (2007) The Notch1/c-Myc Pathway in T Cell Leukemia. *Cell Cycle*, **6,** 927–930.

Sherry, S.T. (2001) dbSNP: the NCBI database of genetic variation. *Nucleic Acids Research*, **29,** 308–311.

Shihab, H.A., Gough, J., Cooper, D.N., Stenson, P.D., Barker, G.L.A., Edwards, K.J., Day, I.N.M. & Gaunt, T.R. (2013) Predicting the functional, molecular, and phenotypic consequences of amino acid substitutions using hidden Markov models. *Human mutation*, **34,** 57–65.

Shiramizu, B., Mussolin, L., Woessmann, W. & Klapper, W. (2016) Paediatric non-Hodgkin lymphoma - perspectives in translational biology. *British journal of haematology*, **173,** 617–24.

Shyr, C., Tarailo-Graovac, M., Gottlieb, M., Lee, J.J., van Karnebeek, C. & Wasserman, W.W. (2014) FLAGS, frequently mutated genes in public exomes. *BMC Medical Genomics*, **7,** 64.

Slupianek, A. & Skorski, T. (2004) NPM/ALK downregulates p27Kip1 in a PI-3K-dependent manner. *Exp Hematol*, **32,** 1265–1271.

Smart, S., Vasileiadi, E., Wang, X., DeRyckere, D. & Graham, D. (2018) The Emerging Role of TYRO3 as a Therapeutic Target in Cancer. *Cancers*, **10,** 474.

Spandidos, A., Wang, X., Wang, H. & Seed, B. (2010) PrimerBank: a resource of human and mouse PCR

primer pairs for gene expression detection and quantification. *Nucleic Acids Research*, **38,** 792–799.

Stanley, P. & Okajima, T. (2010) Roles of glycosylation in notch signaling. *Current Topics in Developmental Biology*, **92,** 131–164.

Stein, H., Gerdes, J., Schwab, U., Lemke, H., Mason, D.Y., Ziegler, A., Schienle, W. & Diehl, V. (1982) Identification of Hodgkin and Sternberg-reed cells as a unique cell type derived from a newly-detected small-cell population. *International journal of cancer*, **30,** 445–59.

Steinbuck, M.P., Arakcheeva, K. & Winandy, S. (2018) Novel TCR-Mediated Mechanisms of Notch Activation and Signaling. *Journal of immunology*, **200,** 997–1007.

Stenson, P.D., Mort, M., Ball, E. V, Howells, K., Phillips, A.D., Thomas, N.S. & Cooper, D.N. (2009) The Human Gene Mutation Database: 2008 update. *Genome Medicine*, **1,** 13.

Sternberg, C. (1898) Uber eine eigenartige unter dem Bilde der Pseudoleukamie verlaufende Tuberculose des lymphatischen Apparates. *Ztschr Heilk*, **19,** 21–90.

Suhasini, A.N., Wang, L., Holder, K.N., Lin, A.-P., Bhatnagar, H., Kim, S.-W., Moritz, A.W. & Aguiar, R.C.T. (2016) A phosphodiesterase 4B-dependent interplay between tumor cells and the microenvironment regulates angiogenesis in B-cell lymphoma. *Leukemia*, **30,** 617–626.

Takebe, N., Nguyen, D. & Yang, S.X. (2014) Targeting notch signaling pathway in cancer: clinical development advances and challenges. *Pharmacology & therapeutics*, **141,** 140–9.

Tate, J.G., Bamford, S., Jubb, H.C., Sondka, Z., Beare, D.M., Bindal, N., Boutselakis, H., Cole, C.G., Creatore, C., Dawson, E., Fish, P., Harsha, B., Hathaway, C., Jupe, S.C., Kok, C.Y., Noble, K., Ponting, L., Ramshaw, C.C., Rye, C.E., Speedy, H.E., et al (2019) COSMIC: the Catalogue Of Somatic Mutations In Cancer. *Nucleic Acids Research*, **47,** 941–947.

The 1000 Genomes Project Consortium (2015) A global reference for human genetic variation. *Nature*, **526,** 68–74.

The Gene Ontology Consortium (2019) The Gene Ontology Resource: 20 years and still GOing strong. *Nucleic acids research*, **47,** 330–338.

Trinei, M., Lanfrancone, L., Campo, E., Pulford, K., Mason, D.Y., Pelicci, P.G. & Falini, B. (2000) A new variant anaplastic lymphoma kinase (ALK)-fusion protein (ATIC-ALK) in a case of ALK-positive anaplastic large cell lymphoma. *Cancer research*, **60,** 793–8.

Tsunematsu, R., Nakayama, K., Oike, Y., Nishiyama, M., Ishida, N., Hatakeyama, S., Bessho, Y., Kageyama, R., Suda, T. & Nakayama, K.I. (2004) Mouse Fbw7/Sel-10/Cdc4 is required for notch degradation during vascular development. *The Journal of biological chemistry*, **279,** 9417–23.

Turinsky, A.L., Fanea, E., Trinh, Q., Wat, S., Hallgrímsson, B., Dong, X., Shu, X., Stromer, J.N., Hill, J.W., Edwards, C., Grosenick, B., Yajima, M. & Sensen, C.W. (2008) CAVEman: Standardized anatomical context for biomedical data mapping. *Anatomical Sciences Education*, **1,** 10–18.

Turner, S.D. & Alexander, D.R. (2006) Fusion tyrosine kinase mediated signalling pathways in the transformation of haematopoietic cells. *Leukemia*, **20,** 572–82.

Turner, S.D., Merz, H., Yeung, D. & Alexander, D.R. (2006) CD2 promoter regulated nucleophosmin-anaplastic lymphoma kinase in transgenic mice causes B lymphoid malignancy. *Anticancer Research*, **26,** 3275–3279.

Turner, S.D., Tooze, R., Maclennan, K. & Alexander, D.R. (2003) Vav-promoter regulated oncogenic fusion protein NPM-ALK in transgenic mice causes B-cell lymphomas with hyperactive Jun kinase. *Oncogene*, **22,** 7750–61.

Turner, S.D., Yeung, D., Hadfield, K., Cook, S.J. & Alexander, D.R. (2007) The NPM-ALK tyrosine kinase

mimics TCR signalling pathways, inducing NFAT and AP-1 by RAS-dependent mechanisms. *Cellular signalling*, **19,** 740–7.

Turturro, F., Frist, A.Y., Arnold, M.D., Seth, P. & Pulford, K. (2001) Biochemical differences between SUDHL-1 and KARPAS 299 cells derived from t(2;5)-positive anaplastic large cell lymphoma are responsible for the different sensitivity to the antiproliferative effect of p27(Kip1). *Oncogene*, **20,** 4466–75.

Vaser, R., Adusumalli, S., Leng, S.N., Sikic, M. & Ng, P.C. (2016) SIFT missense predictions for genomes. *Nature protocols*, **11,** 1–9.

Vassal, G., Rousseau, R., Blanc, P., Moreno, L., Bode, G., Schwoch, S., Schrappe, M., Skolnik, J., Bergman, L., Bradley-Garelik, M.B., Saha, V., Pearson, A. & Zwierzina, H. (2015) Creating a unique, multi-stakeholder Paediatric Oncology Platform to improve drug development for children and adolescents with cancer. *European Journal of Cancer*, **51,** 218–224.

Vassallo, J., Lamant, L., Brugieres, L., Gaillard, F., Campo, E., Brousset, P. & Delsol, G. (2006) ALK-positive anaplastic large cell lymphoma mimicking nodular sclerosis Hodgkin's lymphoma: report of 10 cases. *The American journal of surgical pathology*, **30,** 223–9.

Vollbrecht, C., Mairinger, F.D., Koitzsch, U., Peifer, M., Koenig, K., Heukamp, L.C., Crispatzu, G., Wilden, L., Kreuzer, K.-A., Hallek, M., Odenthal, M., Herling, C.D. & Buettner, R. (2015) Comprehensive Analysis of Disease-Related Genes in Chronic Lymphocytic Leukemia by Multiplex PCR-Based Next Generation Sequencing. *PloS one*, **10,** e0129544.

Walden, G. (2017)H.R.2430 FDA Reauthorization Act of 2017 Washington: US Congress.

Wang, H., Zou, J., Zhao, B., Johannsen, E., Ashworth, T., Wong, H., Pear, W.S., Schug, J., Blacklow, S.C., Arnett, K.L., Bernstein, B.E., Kieff, E. & Aster, J.C. (2011a) Genome-wide analysis reveals conserved and divergent features of Notch1/RBPJ binding in human and murine T-lymphoblastic leukemia cells. *Proceedings of the National Academy of Sciences*, **108,** 14908–13.

Wang, K., Li, M. & Hakonarson, H. (2010) ANNOVAR: functional annotation of genetic variants from high-throughput sequencing data. *Nucleic Acids Research*, **38,** 164.

Wang, N.J., Sanborn, Z., Arnett, K.L., Bayston, L.J., Liao, W., Proby, C.M., Leigh, I.M., Collisson, E.A., Gordon, P.B., Jakkula, L., Pennypacker, S., Zou, Y., Sharma, M., North, J.P., Vemula, S.S., Mauro, T.M., Neuhaus, I.M., LeBoit, P.E., Hur, J.S., Park, K., et al (2011b) Loss-of-function mutations in Notch receptors in cutaneous and lung squamous cell carcinoma. *Proceedings of the National Academy of Sciences*, **108,** 17761–17766.

Wang, Y. & Armstrong, S.A. (2007) Genome-Wide SNP Analysis in Cancer: Leukemia Shows the Way. *Cancer Cell*, **11,** 308–309.

Watanabe, M., Ogawa, Y., Itoh, K., Koiwa, T., Kadin, M.E., Watanabe, T., Okayasu, I., Higashihara, M. & Horie, R. (2008) Hypomethylation of CD30 CpG islands with aberrant JunB expression drives CD30 induction in Hodgkin lymphoma and anaplastic large cell lymphoma. *Laboratory Investigation*, **88,** 48–57.

Webb, T.R., Slavish, J., George, R.E., Look, a T., Xue, L., Jiang, Q., Cui, X., Rentrop, W.B. & Morris, S.W. (2009) Anaplastic lymphoma kinase: role in cancer pathogenesis and small-molecule inhibitor development for therapy. *Expert review of anticancer therapy*, **9,** 331–56.

Weber, D., Lehal, R., Frismantas, V., Bourquin, J.-P., Bauer, M., Murone, M. & Radtke, F. (2018) Pharmacological activity of CB-103: An oral pan-NOTCH inhibitor targeting the NOTCH transcription complex. *Annals of Oncology*, **29,**.

Wei, P., Walls, M., Qiu, M., Ding, R., Denlinger, R.H., Wong, A., Tsaparikos, K., Jani, J.P., Hosea, N., Sands, M., Randolph, S. & Smeal, T. (2010) Evaluation of selective gamma-secretase inhibitor PF-

03084014 for its antitumor efficacy and gastrointestinal safety to guide optimal clinical trial design. *Molecular cancer therapeutics*, **9,** 1618–28.

Weilemann, A., Grau, M., Erdmann, T., Merkel, O., Sobhiafshar, U., Anagnostopoulos, I., Hummel, M., Siegert, A., Hayford, C., Madle, H., Wollert-Wulf, B., Fichtner, I., Dörken, B., Dirnhofer, S., Mathas, S., Janz, M., Emre, N.C.T., Rosenwald, A., Ott, G., Lenz, P., et al (2015) Essential role of IRF4 and MYC signaling for survival of anaplastic large cell lymphoma. *Blood*, **125,** 124–132.

Weiss, B. & Winchurch, R.A. (1978) Analyses of cyclic nucleotide phosphodiesterases in lymphocytes from normal and aged leukemic mice. *Cancer research*, **38,** 1274–80.

Weng, A.P., Ferrando, A.A., Lee, W., Morris IV, J.P., Silverman, L.B., Sanchez-Irizarry, C., Blacklow, S.C., Look, A.T., Aster, J.C., Morris, J.P., Silverman, L.B., Sanchez-Irizarry, C., Blacklow, S.C., Look, A.T. & Aster, J.C. (2004) Activating mutations of NOTCH1 in human T cell acute lymphoblastic leukemia. *Science*, **306,** 269–71.

Weng, A.P., Millholland, J.M., Yashiro-Ohtani, Y., Arcangeli, M.L., Lau, A., Wai, C., Del Bianco, C., Rodriguez, C.G., Sai, H., Tobias, J., Li, Y., Wolfe, M.S., Shachaf, C., Felsher, D., Blacklow, S.C., Pear, W.S. & Aster, J.C. (2006) c-Myc is an important direct target of Notch1 in T-cell acute lymphoblastic leukemia/lymphoma. *Genes & development*, **20,** 2096–109.

WHO (2001)Pathology and Genetics of Tumours of Haematopoietic and Lymphoid Tissues 3rd Editio. Jaffes ES Harris NL Stein H & Vardiman JW (eds) International Agency for Cancer Research press.

WHO (2008)WHO Classification of Tumours of Haematopoietic and Lymphoid Tissues 4th Editio. Swerdlow S Campo E Harris N Jaffe E Pileri S Stein H Thiele J & Vardiman J (eds) International Agency for Cancer Research press.

Wilhite, S.E. & Barrett, T. (2012)Strategies to Explore Functional Genomics Data Sets in NCBI's GEO Database. In *Methods in molecular biology* pp 41–53.

Wilson, A., MacDonald, H.R. & Radtke, F. (2001) Notch 1-deficient common lymphoid precursors adopt a B cell fate in the thymus. *The Journal of experimental medicine*, **194,** 1003–12.

Woessmann, W., Brugieres, L., Rosolen, A., Zimmermann, M., Attarbaschi, A., Mellgren, K., Williams, D., Uyttebroeck, A., Wrobel, G. & Reiter, A. (2012) Abstract 74: Risk-adapted therapy for patients with relapsed orrefractory ALCL – interim-results of the prospective EICNHL-Trial ALCL-relapse. *British Journal of Haematology*, **159,** 41.

Woessmann, W., Peters, C., Lenhard, M., Burkhardt, B., Sykora, K.-W., Dilloo, D., Kremens, B., Lang, P., Führer, M., Kühne, T., Parwaresch, R., Ebell, W. & Reiter, A. (2006) Allogeneic haematopoietic stem cell transplantation in relapsed or refractory anaplastic large cell lymphoma of children and adolescents--a Berlin-Frankfurt-Münster group report. *British journal of haematology*, **133,** 176–82.

Woessmann, W., Seidemann, K., Mann, G., Zimmermann, M., Burkhardt, B., Oschlies, I., Ludwig, W.-D., Klingebiel, T., Graf, N., Gruhn, B., Juergens, H., Niggli, F., Parwaresch, R., Gadner, H., Riehm, H., Schrappe, M., Reiter, A. & BFM Group (2005) The impact of the methotrexate administration schedule and dose in the treatment of children and adolescents with B-cell neoplasms: a report of the BFM Group Study NHL-BFM95. *Blood*, **105,** 948–58.

Woessmann, W., Zimmermann, M., Lenhard, M., Burkhardt, B., Rossig, C., Kremens, B., Lang, P., Attarbaschi, A., Mann, G., Oschlies, I., Klapper, W. & Reiter, A. (2011) Relapsed or refractory anaplastic large-cell lymphoma in children and adolescents after Berlin-Frankfurt-Muenster (BFM)-type first-line therapy: a BFM-group study. *Journal of Clinical Oncology*, **29,** 3065–71.

Wrobel, G., Mauguen, A., Rosolen, A., Reiter, A., Williams, D., Horibe, K., Brugières, L., Le Deley, M.-C. & EICNHL (2011) Safety assessment of intensive induction therapy in childhood anaplastic large cell lymphoma: report of the ALCL99 randomised trial. *Pediatric blood & cancer*, **56,** 1071–7.

Wu, C.X., Xu, A., Zhang, C.C., Olson, P., Chen, L., Lee, T.K., Cheung, T.T., Lo, C.M. & Wang, X.Q. (2017) Notch Inhibitor PF-03084014 Inhibits Hepatocellular Carcinoma Growth and Metastasis via Suppression of Cancer Stemness due to Reduced Activation of Notch1–Stat3. *Molecular Cancer Therapeutics*, **16,** 1531–1543.

Wu, R., Ivan, E., Rolland, D., Sahasrabuddhe, A., Elenitoba-Johnson, K. & Lim, M. (2018) Abstract 92: NPM-ALK regulates immune escape through CD48 in ALK+ ALCLs. *British Journal of Haematology*, **182,** 59.

Xu, W., Kim, J.-W., Jung, W.J., Koh, Y. & Yoon, S.-S. (2018) Crizotinib in Combination with Everolimus Synergistically Inhibits Proliferation of Anaplastic Lymphoma Kinase–Positive Anaplastic Large Cell Lymphoma. *Cancer research and treatment*, **50,** 599–613.

Yamamoto, R., Nishikori, M., Tashima, M., Sakai, T., Ichinohe, T., Takaori-Kondo, A., Ohmori, K. & Uchiyama, T. (2009) B7-H1 expression is regulated by MEK/ERK signaling pathway in anaplastic large cell lymphoma and Hodgkin lymphoma. *Cancer science*, **100,** 2093–100.

Ye, K., Schulz, M.H., Long, Q., Apweiler, R. & Ning, Z. (2009) Pindel: a pattern growth approach to detect break points of large deletions and medium sized insertions from paired-end short reads. *Bioinformatics*, **25,** 2865–2871.

Yee, H.T., Ponzoni, M., Merson, A., Goldstein, M., Scarpa, A., Chilosi, M., Menestrina, F., Pittaluga, S., de Wolf-Peeters, C., Shiota, M., Mori, S., Frizzera, G. & Inghirami, G. (1996) Molecular characterization of the t(2;5) (p23; q35) translocation in anaplastic large cell lymphoma (Ki-1) and Hodgkin's disease. *Blood*, **87,** 1081–8.

Youssif, C., Goldenbogen, J., Hamoudi, R., Carreras, J., Viskaduraki, M., Cui, Y.X., Bacon, C.M., Burke, G.A.A. & Turner, S.D. (2009) Genomic profiling of pediatric ALK-positive anaplastic large cell lymphoma: A children's cancer and leukaemia group study. *Genes Chromosomes and Cancer*, **48,** 1018–1026.

Zamo, A., Chiarle, R., Piva, R., Howes, J., Fan, Y., Chilosi, M., Levy, D.E. & Inghirami, G. (2002) Anaplastic lymphoma kinase (ALK) activates Stat3 and protects hematopoietic cells from cell death. *Oncogene*, **21,** 1038–1047.

Zeller, K.I., Haggerty, T.J., Barrett, J.F., Guo, Q., Wonsey, D.R. & Dang, C. V. (2001) Characterization of Nucleophosmin (B23) as a Myc Target by Scanning Chromatin Immunoprecipitation. *Journal of Biological Chemistry*, **276,** 48285–48291.

Zhang, J., Walsh, M.F., Wu, G., Edmonson, M.N., Gruber, T.A., Easton, J., Hedges, D., Ma, X., Zhou, X., Yergeau, D.A., Wilkinson, M.R., Vadodaria, B., Chen, X., McGee, R.B., Hines-Dowell, S., Nuccio, R., Quinn, E., Shurtleff, S.A., Rusch, M., Patel, A., et al (2015) Germline Mutations in Predisposition Genes in Pediatric Cancer. *New England Journal of Medicine*, **373,** 2336–2346.

Zhang, Q., Raghunath, P.N., Xue, L., Majewski, M., Carpentieri, D.F., Odum, N., Morris, S., Skorski, T. & Wasik, M.A. (2002) Multilevel dysregulation of STAT3 activation in anaplastic lymphoma kinase-positive T/null-cell lymphoma. *Journal of immunology*, **168,** 466–74.

Zhang, Q., Wang, H.Y., Liu, X., Bhutani, G., Kantekure, K. & Wasik, M. (2011) IL-2R common gamma-chain is epigenetically silenced by nucleophosphin-anaplastic lymphoma kinase (NPM-ALK) and acts as a tumor suppressor by targeting NPM-ALK. *Proceedings of the National Academy of Sciences*, **108,** 11977–82.

Zhang, Q., Wang, H.Y., Liu, X. & Wasik, M.A. (2007) STAT5A is epigenetically silenced by the tyrosine kinase NPM1-ALK and acts as a tumor suppressor by reciprocally inhibiting NPM1-ALK expression. *Nature medicine*, **13,** 1341–8.

Zhang, Q., Wang, H.Y., Marzec, M., Raghunath, P.N., Nagasawa, T. & Wasik, M.A. (2005) STAT3- and DNA methyltransferase 1-mediated epigenetic silencing of SHP-1 tyrosine phosphatase tumor

suppressor gene in malignant T lymphocytes. *Proceedings of the National Academy of Sciences*, **102,** 6948–53.

Zhang, Q., Wang, H.Y., Woetmann, A., Raghunath, P.N., Odum, N. & Wasik, M.A. (2006) STAT3 induces transcription of the DNA methyltransferase 1 gene (DNMT1) in malignant T lymphocytes. *Blood*, **108,** 1058–64.

Zhang, Q., Wei, F., Wang, H.Y., Liu, X., Roy, D., Xiong, Q. Bin, Jiang, S., Medvec, A., Danet-Desnoyers, G., Watt, C., Tomczak, E., Kalos, M., Riley, J.L. & Wasik, M.A. (2013) The potent oncogene NPM-ALK mediates malignant transformation of normal human CD4+ T lymphocytes. *American Journal of Pathology*, **183,** 1971–1980.

Zhou, L., Li, L.W., Yan, Q., Petryniak, B., Man, Y., Su, C., Shim, J., Chervin, S. & Lowe, J.B. (2008) Notch-dependent control of myelopoiesis is regulated by fucosylation. *Blood*, **112,** 308–319.

Zhu, V.W., Schrock, A.B., Ali, S.M. & Ou, S.-H.I. (2019) Differential response to a combination of full-dose osimertinib and crizotinib in a patient with EGFR-mutant non-small cell lung cancer and emergent MET amplification. *Lung Cancer*, **10,** 21–26.

Zúñiga-Pflücker, J.C. (2004) T-cell development made simple. *Nature Reviews Immunology*, **4,** 67–72.

Zweidler-McKay, P.A., DeAngelo, D.J., Douer, D., Dombret, H., Ottmann, O.G., Vey, N., Thomas, D.A., Zhu, L., Huang, F., Bajaj, G. & Fischer, B.S. (2014) The Safety and Activity of BMS-906024, a Gamma Secretase Inhibitor (GSI) with Anti-Notch Activity, in Patients with Relapsed T-Cell Acute Lymphoblastic Leukemia (T-ALL): Initial Results of a Phase 1 Trial. *Blood*, **124,** 968.

Appendix I

Gene	# Patients	Position	Nucleotide change	Amino Acid change	Type of mutation	COSMIC ID
TYW1B	24	chr7:72728896	G1118A	W373X	stopgain	
DEFB132	20	chr20:257795	17-22 del	6-8 del	nonframeshift deletion	COSM1163662
KCNJ18	20	chr17:21703303	G517A	D173N	nonsynonymous SNV	
MIR1-1HG	18	chr20:62565060	T80C	V27A	nonsynonymous SNV	COSM3758712
ZNF283	17	chr19:43847015	del GGAGAT		frameshift deletion	COSM1394324
NRDC	17	chr1:51840392	462-464 del	154-155 del	nonframeshift deletion	COSM1237693
ZNF720	16	chr16:31759375	381 ins A		frameshift insertion	
PYGL	16	chr14:50911873	del T		splicing variant	
MS4A14	15	chr11:60397880	167-168 del		frameshift deletion	COSM1684267
CLECL1	15	chr12:9733111	153 ins ACTTA		frameshift insertion	
MYO15B	14	chr17:75601463	A3437G	K1146R	nonsynonymous SNV	COSM4130628
RIC8A	13	chr11:209895	621-623 del	207-208 del	nonframeshift deletion	COSM1317342
STK31	13	chr7:23717543	G144C	Q48H	nonsynonymous SNV	COSM3762594
TAAR9	13	chr6:132538470	A181T	K61X	stopgain	
CCDC129	12	chr7:31658299	3097 ins T		frameshift insertion	
IRF5	12	chr7:128947298	502-531 del	168-177 del	nonframeshift deletion	COSM5002496
CYP3A5	12	chr7:99672916	T>C		splicing variant	
ZNF3	11	chr7:100064889	292-295 del		frameshift deletion	COSM5001700
ZNF219	11	chr14:21092594	698-703 del	233-235 del	nonframeshift deletion	COSM248523
PSPH	11	chr7:56019672	T203C	L68P	nonsynonymous SNV	
PSPH	11	chr7:56019681	G194A	R65H	nonsynonymous SNV	
TYRO3	11	chr15:41570603	G>T		splicing variant	COSM1478102

SCRN3	10	chr2:174427853	1212-1224 del		frameshift deletion	COSM253915
CDCP2	10	chr1:54139645	1224 ins C		frameshift insertion	
SYT15	10	chr10:46584599	G927C	E309D	nonsynonymous SNV	COSM4144699
GXYLT1	10	chr12:42087868	G1148A	C383Y	nonsynonymous SNV	
MROH5	10	chr8:141494938	C>T		splicing variant	
PTCHD3	9	chr10:27413327	923 ins G		frameshift insertion	
HOMEZ	9	chr14:23275618	1608-1610 del	536-537del	nonframeshift deletion	COSM954652
POTEE	9	chr2:131264056	G2601T	E867D	nonsynonymous SNV	COSM4303570
PSPH	9	chr7:56019607	G268A	G90S	nonsynonymous SNV	
PDE4DIP	9	chr1:149005097	A4075G	K1359E	nonsynonymous SNV	COSM4590058
TRPT1	9	chr11:64226062	G>C		splicing variant	
TYRO3	8	chr15:41570156	1382 del		frameshift deletion	
RNPC3	8	chr1:103533845	347 del		frameshift deletion	
CELA1	8	chr12:51329814	628 ins C		frameshift insertion	
UBE2N	8	chr12:93411143	C187G	P63A	nonsynonymous SNV	
VWF	8	chr12:6018901	C4517T	S1506L	nonsynonymous SNV	COSM5313831
ACTR2	8	chr2:65261302	C791T	A264V	nonsynonymous SNV	
DNAJC28	7	chr21:33488443	947-951 del		frameshift deletion	
SSPO	7	chr7:149806829	8748 del		frameshift deletion	
CYP4B1	7	chr1:46815075	881-882 del		frameshift deletion	
CHRNA7	7	chr15:32157674	497-498 del		frameshift deletion	COSM5002499
TMEM254	7	chr10:80081665	114 ins A		frameshift insertion	
FSIP2	7	chr2:185738878	252 ins G		frameshift insertion	
ANP32E	7	chr1:150226708	453-458 del	151-153 del	nonframeshift deletion	COSM4770175
THAP11	7	chr16:67842921	367-369 del	123 del	nonframeshift deletion	COSM1479007

ACVR2A	7	chr2:147918575	A621C	K207N	nonsynonymous SNV	COSM132653
RPS3A	7	chr4:151102986	A470C	Q157P	nonsynonymous SNV	COSM328158
NOTCH1	7	chr9:136518645	A1045C	T349P	nonsynonymous SNV	COSM4163567
PPFIA3	7	chr19:49133149	T>G		splicing variant	COSM135843
PTEN	7	chr10:87864104	del T		splicing variant	
MPRIP	7	chr17:17154305	G>T		splicing variant	
OR51F1	6	chr11:4769644	274 del		frameshift deletion	
OR10AD1	6	chr12:48203092	200 dup T		frameshift insertion	
ALOX5AP	6	chr13:30713841	116 ins GTGT		frameshift insertion	
SETBP1	6	chr18:44876699	675 ins TCTC		frameshift insertion	
PSORS1C1	6	chr6:31138723	112 ins C		frameshift insertion	
ZFYVE19	6	chr15:40807701	112 ins GGGGC		frameshift insertion	
FAM205C	6	chr9:34893049	354-355 CC>G-		frameshift substitution	
NUCB2	6	chr11:17330931	1203-1205 del	401-402 del	nonframeshift deletion	COSM1237695
ATN1	6	chr12:6936729	1462-1482 del	488-494 del	nonframeshift deletion	COSM1476884
PLEKHA6	6	chr1:204249206	T1652G	V551G	nonsynonymous SNV	
PLXNA2	6	chr1:208098968	T1609G	C537G	nonsynonymous SNV	
L2HGDH	6	chr14:50283981	T593G	V198G	nonsynonymous SNV	
CAPN5	6	chr11:77084981	T95C	F32S	nonsynonymous SNV	COSM3986477
RPS18	6	chr6:33276005	A230G	Y77C	nonsynonymous SNV	COSM1131899
ERVV-1	6	chr19:53014925	C835G	P279A	nonsynonymous SNV	COSM4132391
PDE4DIP	6	chr1:148931920	G339T	Q113H	nonsynonymous SNV	COSM4593888
PABPC1	6	chr8:100705591	T1685C	L562S	nonsynonymous SNV	
WAS	6	chrX:48685604	A331C	T111P	nonsynonymous SNV	
NPHP4	6	chr1:5875102	T>A		splicing variant	

SLC7A13	5	chr8:86214406	1413-1511 del		frameshift deletion	
PDE4DIP	5	chr1:149010509	4994 del		frameshift deletion	
LFNG	5	chr7:2513247	138-139 ins GATG		frameshift insertion	
WDR73	5	chr15:84643646	944-961 del	315-321 del	nonframeshift deletion	COSM1375060
FOXE1	5	chr9:97854419	505-510 del	169-170 del	nonframeshift deletion	COSM1724903
PAK2	5	chr3:196782706	C60G	S20R	nonsynonymous SNV	COSM1422033
TMTC2	5	chr12:82857341	C415G	R139G	nonsynonymous SNV	COSM1188560
JAG1	5	chr20:10645368	A2101C	T701P	nonsynonymous SNV	
FRMD4A	5	chr10:13657338	A2251C	T751P	nonsynonymous SNV	
KCNJ18	5	chr17:21703568	G782A	R261H	nonsynonymous SNV	
TUBB8	5	chr10:47467	C925T	R309C	nonsynonymous SNV	
PANK3	5	chr5:168561512	G817A	G273R	nonsynonymous SNV	
PABPC1	5	chr8:100704992	G1752A	M584I	nonsynonymous SNV	
EIF4EBP1	5	chr8:38057147	C212T	P71L	nonsynonymous SNV	
WAS	5	chrX:48685610	T337C	F113L	nonsynonymous SNV	
FLNB	5	chr3:58123679	T3713A	I1238K	nonsynonymous SNV	
VPS50	5	chr7:93294638	T>G		splicing variant	
BCAP31	5	chrX:153724015	C>A		splicing variant	
TAS2R19	5	chr12:11021672	A900G	X300W	stoploss	
OR6C76	4	chr12:55427175	922 del		frameshift deletion	
SPATA4	4	chr4:176184859	836-839 del		frameshift deletion	
MSH3	4	chr5:80654881	154-171 del	52-57 del	nonframeshift deletion	COSM3718906
NCL	4	chr2:231460704	774-776 del	258-259 del	nonframeshift deletion	COSM3736247
TSKS	4	chr19:49746676	769-786 del	257-262 del	nonframeshift deletion	COSM5056834

NINL	4	chr20:25476414	2872-2877 del	958-959 del	nonframeshift deletion	COSM1025361
CDSN	4	chr6:31117166	447-449 del	149-150 del	nonframeshift deletion	COSM1077524
RNH1	4	chr11:502130	19-33 del	7-11 del	nonframeshift deletion	COSM927774
POTEE	4	chr2:131263902	G2447A	R816H	nonsynonymous SNV	COSM3836843
POTEI	4	chr2:130462929	G3115A	V1039M	nonsynonymous SNV	
MANEAL	4	chr1:37796745	T662G	V221G	nonsynonymous SNV	COSM4143887
KCNJ18	4	chr17:21703692	G906T	M302I	nonsynonymous SNV	
CHD3	4	chr17:7905953	T4499G	V1500G	nonsynonymous SNV	COSM4130771
CDK11B	4	chr1:1636429	C1202T	A401V	nonsynonymous SNV	
FOXD4L1	4	chr2:113499719	A463G	I155V	nonsynonymous SNV	COSM224838
PABPC3	4	chr13:25096638	C440T	T147I	nonsynonymous SNV	
PABPC1	4	chr8:100704954	T1790C	L597P	nonsynonymous SNV	
DCAF13	4	chr8:103440233	C1504T	R502C	nonsynonymous SNV	COSM3412622
WNT2B	4	chr1:112516325	C313T	R105C	nonsynonymous SNV	
TMPRSS13	4	chr11:117909838	G972T	Q324H	nonsynonymous SNV	
COQ4	4	chr9:128325797	G221A	R74Q	nonsynonymous SNV	COSM5021646
RABL6	4	chr9:136839820	G1888A	G630R	nonsynonymous SNV	
PCDHA5	4	chr5:140822899	A1124T	D375V	nonsynonymous SNV	
PCDHGA5	4	chr5:141365274	A944G	Y315C	nonsynonymous SNV	
RBSN	4	chr3:15090399	G289T	G97C	nonsynonymous SNV	
RNF175	4	chr4:153715537	T756G	C252W	nonsynonymous SNV	
EZR	4	chr6:158787182	C118T	R40W	nonsynonymous SNV	
SLC22A1	4	chr6:160122197	T262C	C88R	nonsynonymous SNV	COSM3928207

SCN7A	4	chr2:166405764	G4865A	R1622Q	nonsynonymous SNV	
ALDH4A1	4	chr1:18883153	G469A	G157S	nonsynonymous SNV	
GATAD2A	4	chr19:19492680	A502G	S168G	nonsynonymous SNV	
NTHL1	4	chr16:2040195	G753C	W251C	nonsynonymous SNV	
GJC2	4	chr1:228158846	C1088T	A363V	nonsynonymous SNV	
CHRND	4	chr2:232531450	C337T	P113S	nonsynonymous SNV	
PYGB	4	chr20:25292528	G2092A	V698M	nonsynonymous SNV	
DMD	4	chrX:31203978	C586T	R196W	nonsynonymous SNV	
DMD	4	chrX:32699119	C800T	S267F	nonsynonymous SNV	
SCUBE3	4	chr6:35239766	C841T	R281C	nonsynonymous SNV	COSM1265091
COL9A2	4	chr1:40314260	A194G	K65R	nonsynonymous SNV	
SPTBN5	4	chr15:41887281	G820A	V274I	nonsynonymous SNV	
CYP4A11	4	chr1:46936786	G388A	G130S	nonsynonymous SNV	
SKOR2	4	chr18:47248873	G311A	R104H	nonsynonymous SNV	COSM4595039
GNG2	4	chr14:51966613	G142T	D48Y	nonsynonymous SNV	COSM1629335
DNAH1	4	chr3:52353415	A3262T	I1088F	nonsynonymous SNV	
ITIH3	4	chr3:52799805	T959C	L320P	nonsynonymous SNV	
SOX17	4	chr8:54458151	G13C	D5H	nonsynonymous SNV	
SOX17	4	chr8:54459282	G532T	G178C	nonsynonymous SNV	
TRIM6	4	chr11:5611169	C769T	R257C	nonsynonymous SNV	COSM429249
PHF3	4	chr6:63691742	T2195C	M732T	nonsynonymous SNV	
MAP3K11	4	chr11:65607491	A1268G	E423G	nonsynonymous SNV	
CLDN3	4	chr7:73769649	C401T	P134L	nonsynonymous SNV	

GOLGA6L10	4	chr15:82344664	T1196C	L399P	nonsynonymous SNV	
FNBP1L	4	chr1:93551055	G1586C	G529A	nonsynonymous SNV	
SLC26A1	4	chr4:989077	T1862A	F621Y	nonsynonymous SNV	
ZFP64	4	chr20:52164759	ins AA		splicing variant	
MTCH2	4	chr11:47622719	G780A	W260X	stopgain	
RETNLB	4	chr3:108757146	39 ins TAATCCCC	L14 ins X	stopgain	
KCNQ2	4	chr20:63407011	C2168A	S723X	stopgain	
TYRO3	3	chr15:41571117	1659-1660 del		frameshift deletion	
OR5B3	3	chr11:58403320	90 del		frameshift deletion	
GRP	3	chr18:59230436	394-397 del		frameshift deletion	
SETBP1	3	chr18:44876700	676-677 del		frameshift deletion	
AP3S1	3	chr5:115866721	121-124 del		frameshift deletion	COSM1319295
PEBP4	3	chr8:22713395	659 del		frameshift deletion	
CNTNAP3	3	chr9:39149858	1597 del		frameshift deletion	
DSPP	3	chr4:87615750	3088-3105 del	1030-1035 del	nonframeshift deletion	COSM5547737
CTBS	3	chr1:84574316	92-100 del	31-34 del	nonframeshift deletion	COSM1290235
FAM109A	3	chr12:111363023	397-405 del	133-135 del	nonframeshift deletion	COSM430328
DSPP	3	chr4:87615391	2729-2737 del	910-913 del	nonframeshift deletion	COSM4603772
NPIPB6	3	chr16:28343070	813-815 del	271-272 del	nonframeshift deletion	COSM5215813
TRAK1	3	chr3:42210086	1842-1844 del	614-615 del	nonframeshift deletion	COSM308433
HRCT1	3	chr9:35906351	64-66 del	22 del	nonframeshift deletion	COSM1490012
PAK2	3	chr3:196803111	A383G	K128R	nonsynonymous SNV	COSM1717568
ZBTB4	3	chr17:7465792	A1010C	Y337S	nonsynonymous SNV	
AK2	3	chr1:33013299	A578T	Y193F	nonsynonymous SNV	

KCNJ18	3	chr17:21703651	G865C	E289Q	nonsynonymous SNV	
PRSS3	3	chr9:33795599	T26C	F9S	nonsynonymous SNV	
CACNA1G	3	chr17:50615426	A4723C	T1575P	nonsynonymous SNV	
CHRNB2	3	chr1:154569495	T98G	V33G	nonsynonymous SNV	COSM3726999
LDLRAD3	3	chr11:36227304	A527C	H176P	nonsynonymous SNV	COSM1285901
SLIT3	3	chr5:168685818	A3445C	T1149P	nonsynonymous SNV	
TFAM	3	chr10:58388704	T326G	V109G	nonsynonymous SNV	COSM5034010
CNTNAP3	3	chr9:39078875	G3488A	G1163D	nonsynonymous SNV	
RBMX	3	chrX:136875541	A586G	R196G	nonsynonymous SNV	
PA2G4	3	chr12:56106718	ins A		splicing variant	
SLC3A1	3	chr2:44301129	del T		splicing variant	
LRRC37A3	3	chr17:64858885	ins A		splicing variant	
IQCK	3	chr16:19717694	G>C		splicing variant	
PIBF1	3	chr13:72835370	ins A		splicing variant	
CSF1	3	chr1:109924191	G>T		splicing variant	
PKD2L2	3	chr5:137936318	A>G		splicing variant	
MAD1L1	3	chr7:2014501	C>A		splicing variant	
PAIP1	3	chr5:43538923	C>T		splicing variant	
DGKZ	3	chr11:46378989	A>C		splicing variant	
PIGQ	3	chr16:582881	A>T		splicing variant	
DOCK8	3	chr9:463655	C5907A	Y1969X	stopgain	COSM3982891
NPIPB15	3	chr16:74391889	G1141T	E381X	stopgain	COSM4592878
BAGE4	3	chr21:10414915	A120C	X40C	stoploss	